



## Status of Thesis

### POWER SYSTEM STATE ESTIMATION IN LARGE-SCALE NETWORKS

I NURSYARIZAL MOHD NOR hereby allow my thesis to be placed at the Information Resource Center (IRC) of Universiti Teknologi Petronas (UTP) with the following conditions:

1. The thesis becomes the property of UTP
2. The IRC of UTP may make copies of the thesis for academic purposes only
3. This thesis is classified as

Confidential

Non-confidential

If this thesis is confidential, please state the reason(s):

---

The contents of the thesis will remain confidential for \_\_\_\_\_ years.

Remarks on disclosure:

---



Nursyarizal Mohd Nor, Author

No. 21, Lapangan Perdana 27

Panorama Lapangan Perdana

31650 Ipoh, Perak

MALAYSIA

Date: 31/12/09

Endorsed by



Professor Dr. Ramiah Jegatheesan,


Supervisor

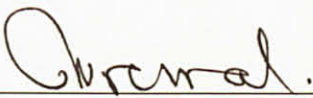
Electrical & Electronic Engineering  
Universiti Teknologi PETRONAS  
Bandar Seri Iskandar 31750 Tronoh  
Perak Darul Ridzuan  
Tel: +605-368 7806 Fax: +605-365 7443  
Website: <http://www.utp.edu.my>

Date: 31/12/09

## Approval by Supervisor

The undersigned certify that they have read, and recommend to the Postgraduate Studies Programme for acceptance, a thesis entitled **“Power System State Estimation in Large-Scale Networks”** submitted by **Nursyarizal Mohd Nor** in fulfillment of the requirements for the degree of Doctor of Philosophy (Ph.D.).

Signature :   
DR. RAMIAH JEGA THEESAN  
Professor  
Electrical & Electronic Engine.  
Universiti Teknologi PETRONAS

Signature :   
Dr. N. Perumal  
Senior Lecturer,  
Electrical & Electronic Engineering  
Academic Block No 22  
Universiti Teknologi PETRONAS  
Bandar Seri Iskandar  
31750 Tronoh, Perak Darul Ridzuan, MALAYSIA

Date : 31/12/09

UNIVERSITI TEKNOLOGI PETRONAS

**POWER SYSTEM STATE ESTIMATION IN LARGE-SCALE NETWORKS**

By

NURSYARIZAL MOHD NOR

Bachelor of Science (Electrical Engineering)  
Universiti Teknologi Malaysia, 1998

Master of Science (Power)  
The University of Manchester Institute of Science and Technology, 2001

A DISSERTATION

Submitted to the Postgraduate Studies Programme  
as a Requirement for the  
Degree of Doctor of Philosophy (Ph.D.)  
(Electrical & Electronics Engineering)

BANDAR SERI ISKANDAR, 31750 TRONOH  
PERAK, MALAYSIA

December, 2009

## Declaration

I hereby declare that the thesis is based on my original work except for quotations and citations which have been duly acknowledged. I also declare that it has not been previously or concurrently submitted for any other degrees at UTP or other institutions.

Signature: 

Name: NURSYARIZAL BIN MOHD NOR

Date: 31/12/09

## DEDICATION

To

my parents, Maimon and Mohd Nor

my wife, Fatimahanizan

sons, Nurafiq and Nurarif

## ACKNOWLEDGEMENTS

First and foremost I would like to thank my supervisor, Professor Dr. Ramiah Jegatheesan for his inspiring guidance, encouragement, and support in bringing this dissertation to completion. His firm grasps and forte on all diverse areas of power systems ensured a steady stream of ideas that spawns gateways for solving the problems at hand. I am forever his student. Special thanks are due to my co-supervisor, Ir. Perumal Nallagownden for his guidance in this endeavor.

Special thanks also goes to the Tenaga Nasional Berhad (TNB) and the Sabah Electricity Sendirian Berhad (SESB) for the support to work on the research.

In this opportunity, I also convey special thanks to technicians and my friends for the invaluable contribution given in knowledge and materials. I also want to extend my gratitude and appreciation to many people who made this dissertation possible.

I gratefully acknowledged Universiti Teknologi PETRONAS (UTP), Malaysia for the financial support.

Finally, I am indebted to my mother, Maimon, my father, Mohd Nor, and my mother-in-law, Aminah, who upbrought me to be what I am today, and who always extend their prayers and best wishes. A special thanks to my wife for allowing this old student to return to school and for taking care of the family. This would not have been possible without her.

## ABSTRACT

Power system state estimation constitutes one of the critical functions that are executed at the control centers. Its optimal performance is required in order to operate the power system in a safe, secure and economic manner. State estimators (SE) process the available measurements by taking into account the information about the network model and parameters. The quality of estimated results will depend on the measurements, the assumed network model and its parameters. Hence, SE requires to use various techniques to ensure validity of the results and to detect and identify sources of errors. The Weighted Least Squares (WLS) method is the most popular technique of SE. This thesis provides solutions to enhance the WLS algorithm in order to increase the performance of SE. The gain and the Jacobian matrices associated with the basic algorithm require large storage and have to be evaluated at every iteration, resulting in more computation time. The elements of the SE Jacobian matrix are processed one-by-one based on the available measurements, and the Jacobian matrix,  $H$  is updated suitably, avoiding all the power flow equations, thus simplifying the development of the Jacobian. The results obtained proved that the suggested method takes lesser computational time compared with the available NRSE method, particularly when the size of the network becomes larger. The uncertainty in analog measurements could occur in a real time system. Thus, the higher weighting factor or wrongly assigned weighting factor to the measurement could lead to flag the measurements as bad. This thesis describes a pre-screening process to identify the bad measurements and the measurement weights before performing the WLS estimation technique employed in SE. The autoregressive (AR) techniques, Burg and Modified Covariance (MC), are used to predict the data and at the same time filtering the logical weighting factors that have been assigned to the identified bad measurements. The results show that AR methods managed to accurately predict the data and filter the weighing factors for the bad measurements. Also the WLS algorithm is modified to include Unified Power Flow Controller (UPFC) parameters. The developed methods are successfully tested on IEEE standard systems and the Sabah Electricity Sdn. Bhd. (SESB) system without and with UPFC. The developed program is suitable either to estimate the UPFC controller parameters or to estimate these parameter values in order to achieve the given control specifications in addition to the power system state variables.



## ABSTRAK

Sistem Kuasa Ramalan Keadaan menjadi salah satu fungsi yang kritikal di dalam pusat-pusat kawalan. Keperluan untuk memastikan prestasinya berada pada tahap yang terbaik adalah penting bagi memastikan sistem kuasa beroperasi pada keadaan yang selamat, tidak merbahaya dan menjimatkan. Peramal keadaan (SE) ini akan memproseskan kesemua pengukuran dengan mengambil kira kesemua maklumat tentang model dan parameter-parameter sistem rangkaian tersebut. Kualiti hasil atau keputusan dari proses ramalan ini bukannya hanya bergantung kepada pengukuran itu sahaja bahkan kepada kesemua parameter-parameter dan andaian yang dibuat atau diperkenalkan kepada model rangkaian tersebut. Justeru itu, beberapa teknik untuk proses ramalan ini diperkenalkan bagi memastikan hasil atau keputusan yang diperolehi dari proses ramalan ini adalah sah dan boleh dipercayai dalam mengesan dan mengenalpasti sumber-sumber kerosakan yang kemungkinan berlaku di dalam proses peramal keadaan ini. Teknik yang paling popular didalam proses ramalan ini adalah teknik Kuasa Dua Beban Terkecil (WLS). Disertasi ini memperkenalkan beberapa penyelesaian di dalam teknik WLS ini dalam usaha untuk mempertingkatkan lagi prestasi SE. Di dalam asas algoritme WLS ini, proses untuk menilai setiap elemen matrik bagi "Gain" dan "Jacobian" yang bersepadu dengan asas algoritme ini memerlukan ruang penyimpanan data yang besar dimana ini akan menyebabkan pemprosesan komputer mengambil masa yang agak panjang. Elemen-elemen di dalam matrik "Jacobian" ini diperolehi daripada pengukuran kuasa aliran di dalam elemen-elemen rangkaian tersebut. Kesemua elemen ini akan diproses dan dikemaskini secara ringkas satu demi satu sehingga kesemua elemen didalam matrik "Jacobian"  $H$  ini dipenuhi. Proses pembinaan matrik "Jacobian"  $H$  ini akan di serapkan kedalam teknik WLS untuk proses meramalkan pembolehubah-pembolehubah keadaan. Keputusan menunjukkan teknik yang dicadangkan dapat mengurangkan masa untuk pemprosesan komputer terutamanya apabila sistem rangkaian bertambah besar. Ketidaktetapan di dalam pengukuran-pengukuran analog sering berlaku di dalam realiti sistem. Hatta, bagi pengukuran yang sebelum ini diletakkan dalam kategori faktor pengaruh kepentingannya tinggi mungkin boleh di kenalpasti sebagai pengukuran yang salah pada bila-bila masa sahaja. Disertasi ini menguraikan satu proses pengimbas untuk memastikan mana-mana pengukuran yang

sebelum ini diletakkan dalam kategori faktor pengaruh kepentingannya tinggi tetapi pengukurannya salah atau tidak berapa tepat. Teknik Autoregresi (AR) diperkenalkan dalam disertasi ini untuk tujuan meramalkan kesemua data dan pada masa yang sama menapis semua faktor pengaruh kepentingan bagi setiap alatan pengukuran yang dikenalpasti sebagai salah atau tidak tepat. Keputusan menunjukkan teknik AR ini berjaya meramalkan kesemua data dan menapis faktor pengaruh kepentingan dengan tepat. Algoritme WLS ini diubahkan dengan memeperkenalkan kesemua nilai bagi Pengatur Aliran Kuasa Penyatuan (UPFC). Teknik yang dicadangkan ini telah berjaya diuji pada semua sistem piawai IEEE dan sistem Sabah Electricity Sdn. Bhd. (SESB). Keputusan menunjukkan algoritme ini berjaya meramal kesemua pengawal parameter UPFC atau meramal kesemua parameter tersebut dalam usaha untuk mencapai kesemua speksifikasi yang diberi sebagai tambahan dalam pembolehubah sistem kuasa.

In compliance with the terms of the Copyright Act 1987 and the IP Policy of the university, the copyright of this thesis has been reassigned by the author to the legal entity of the university,

Institute of Technology PETRONAS Sdn. Bhd.

Due acknowledgement shall always be made of the use of any materials contained in, or derived from this thesis.

© Nursyarizal Mohd Nor, December 2009

Institute of Technology PETRONAS Sdn. Bhd.

All rights reserved.

# TABLE OF CONTENTS

LIST OF TABLES .....	xv
LIST OF FIGURES .....	xvii
LIST OF ABBREVIATIONS .....	xix
LIST OF SYMBOLS .....	xxi
CHAPTER 1 INTRODUCTION .....	1
1.1 Power System State Estimation.....	1
1.2 Components of SE.....	3
1.3 State Estimation Techniques .....	6
1.4 Objectives of Thesis .....	8
1.5 Outline of the Thesis .....	9
CHAPTER 2 THE NEWTON RAPHSON STATE ESTIMATOR .....	12
2.1 Introduction .....	12
2.2 Weight Least Square .....	13
2.2.1 State variables.....	13
2.2.2 Mathematical equations describing ideal measurements.....	13
2.2.3 Analog measurements.....	15
2.2.4 Model of measurement error .....	15
2.2.5 Pseudo-measurements.....	19
2.2.6 WLS criteria.....	20
2.2.7 Solution for AC state estimator .....	21
2.3 Bad Data Processing.....	25
2.3.1 Bad data detection.....	26
2.3.2 Bad data identification and elimination.....	28
2.3.3 Overall algorithm.....	29
2.4 Practical Results of SE in the Malaysian Grid .....	30
2.4.1 Survey findings.....	31
2.4.2 Deficiencies in the existing software .....	36
2.5 Developed Software and the Simulation Results .....	37
2.5.1 Description of simulation .....	37
2.5.2 Bad data simulation .....	41
2.6 Summary .....	45

CHAPTER 3 NEWTON RAPHSON STATE ESTIMATION EMPLOYING SYSTEMATICALLY CONSTRUCTED JACOBIAN MATRIX .....	46
3.1 Introduction .....	46
3.2 General Structure of $H$ Matrix.....	47
3.3 Power Flow Network Elements.....	49
3.4 Construction of SE Jacobian Matrix, $H$ .....	49
3.5 Computing and Recording Only the Required Partial Derivatives Alone .....	52
3.5.1 Application example to illustrate the construction of Jacobian matrix $H$ .....	53
3.6 Simulation Results.....	56
3.7 Summary .....	63
CHAPTER 4 IMPLEMENTATION OF AUTOREGRESSIVE METHOD TO PRE-FILTER THE SET OF MEASUREMENTS .....	65
4.1 Introduction .....	65
4.2 The Autoregressive (AR) .....	66
4.2.1 Linear prediction.....	68
4.2.2 Burg method .....	69
4.2.3 Modified Covariance method .....	70
4.3 Test Results .....	71
4.3.1 Case 1.....	77
4.3.2 Case 2.....	83
4.4 SECJ Method Applied With AR Method.....	85
4.5 Summary .....	88
CHAPTER 5 STATE ESTIMATION OF POWER SYSTEMS EMBEDDED WITH UPFC.....	89
5.1 Introduction .....	89
5.2 Flexible AC Transmission System (FACTS).....	91
5.2.1 Steady state model of Unified Power Flow Controllers .....	91
5.3 Mathematical Representation of UPFC [62, 67].....	93
5.4 Modification of Algorithms of SE with UPFC .....	95
5.5 Power Flow Simulation.....	99
5.5.1 5-bus test system.....	99
5.5.2 IEEE 14-bus system.....	103
5.5.2.1 Case 1 (Power flow analysis without UPFC).....	105

5.5.2.2 Case 5 (Power flow analysis with a UPFC installed at Line 5).....	108
5.5.2.3 Case 6 (Power flow analysis with a UPFC installed at Line 12).....	111
5.6 Simulation Results.....	115
5.6.1 5-bus system embedded with UPFC.....	116
5.6.2 IEEE 14-bus system embedded with UPFC .....	118
5.7 SECJ Method Embedded With UPFC .....	119
5.7.1 Bad data simulation .....	121
5.8 Summary .....	123
CHAPTER 6 CONCLUSIONS.....	124
6.1 Conclusion.....	124
6.2 Summary of Contributions .....	126
6.3 Future Research.....	127
REFERENCES.....	128
LIST OF PUBLICATIONS .....	135
APPENDICES .....	138
Appendix A MATHEMATICAL TERMS AND NOTATIONS.....	139
Appendix B SABAH ELECTRICITY SDN. BHD.....	141
Appendix C REAL AND REACTIVE POWER FLOW IN A NETWORK ELEMENT .....	147

## LIST OF TABLES

Table 2.1	Captured readings which show the large variance of SCADA and SE.... .....	33
Table 2.2	The sample of pair measurements that are suspected as bad measurement.....	34
Table 2.3	Measurement Accuracy Class .....	35
Table 2.4	Sample of data with different weightage of measurements. ....	35
Table 2.5	The summary of description of simulation for all tested system. ....	38
Table 2.6	The summary of computational results. ....	39
Table 2.7	Analysis of State Vector for 5-bus system relative to power flow solutions (true measurements).....	39
Table 2.8	Analysis of State Vector for IEEE 14-bus system relative to power flow solutions (true measurements).....	40
Table 2.9	Performance Indices .....	40
Table 2.10	List of bad measurements.....	41
Table 2.11	Results of normalized residual test for 5-bus system.....	42
Table 2.12	The summarize results of the bad data .....	44
Table 3.1	Partial Derivatives of Line Flows and the Corresponding Partial Derivatives of Bus Powers. ....	52
Table 3.2	Network data for 3-bus system.....	54
Table 3.3	Available measurements for 3-bus system.....	54
Table 3.4	NRSE vs. SECJ methods – computer processing time. ....	58
Table 4.1	Summary of the percentage average error for all measurements in all tested networks. ....	73
Table 4.2	Performance of the AR method on the IEEE 57-bus – Case 1.....	78
Table 4.3	Performance of the AR method on the IEEE 118-bus – Case 1.....	78
Table 4.4	The Measured, Predicted and NRSE values of state variables for IEEE 57-bus network after substituting the bad data with predicted value – Case 1 (1 <sup>st</sup> condition).....	80
Table 4.5	The results of SE process on IEEE 57-bus system – Condition 2.....	83
Table 4.6	The results of SE process on IEEE 118-bus system – Condition 2.....	83
Table 4.7	Analysis of average errors of state vectors between the first condition and second condition. ....	83
Table 4.8	The comparison of the state vectors average errors between Case 1 and Case 2- IEEE 57-bus system. ....	84

Table 4.9	The comparison of the state vectors average errors between Case 1 and Case 2- IEEE 118-bus system. ....	84
Table 4.10	Summary of computational time between NRSE and SECJ for IEEE 57 and IEEE 118-bus systems. ....	86
Table 5.1	IEEE 5-bus power flow results. ....	100
Table 5.2	The result of bus voltages and bus power injections. ....	101
Table 5.3	Reduction in Real and Reactive Power Losses (%) for IEEE 14-bus Test System. ....	105
Table 5.4	Voltage Magnitude, Voltage Phase, Real Power and Reactive Power Profiles at IEEE 14-bus – Bus 6. ....	113
Table 5.5	Line Flows at IEEE 14-bus – Line 5 (Branch 6 – 11). ....	114
Table 5.6	Total Generation, Load and Losses for IEEE 14-bus – Cases 1 and 5. ....	114
Table 5.7	Reduction in Real and Reactive Power Losses (%) for IEEE 14-bus – Case 5. ....	114
Table 5.8	Voltage Magnitude, Voltage Phase, Real Power and Reactive Power Profiles at IEEE 14-bus – Bus 2. ....	114
Table 5.9	Line Flows at IEEE 14-bus – Line 12 (Branch 2 – 3). ....	115
Table 5.10	Total Generation, Load and Losses for IEEE 14-bus – Cases 1 and 6. ....	115
Table 5.11	Reduction in Real and Reactive Power Losses (%) for IEEE 14-bus – Case 6. ....	115
Table 5.12	The summary of available measurements for all tested network. ....	116
Table 5.13	State estimation results. ....	117
Table 5.14	Estimated UPFC variables. ....	118
Table 5.15	Estimated UPFC variables without setting any specific value. ....	118
Table 5.16	State Estimation results. ....	119
Table 5.17	Estimated UPFC variables. ....	119
Table 5.18	Summary of computational time between NRSE and SECJ for IEEE 57 system. ....	120
Table 5.19	List of bad measurements. ....	121
Table 5.20	Results of normalized residual test for 5-bus system. ....	122
Table B1	Bus data and load flow results of 103-bus system. ....	142
Table B2	Line data and power flow results of 103-bus system. ....	144



## LIST OF FIGURES

Figure 1.1	An overview of SCADA configuration.....	2
Figure 1.2	The flow chart of state estimation process. ....	5
Figure 2.1	Transmission Line Model.....	14
Figure 2.2	Gaussian Probability Curve.....	16
Figure 2.3	3-Bus network configuration.....	19
Figure 2.4	Chi-square distribution, $\chi^2_{N_f, \alpha}$ for a small value of $N_f$ degrees of freedom.....	27
Figure 2.5	Regional overview diagram. ....	32
Figure 2.6 (a), (b), (c) & (d)	The Graph of Normalized Residual vs. Measurements for the 1 <sup>st</sup> , 2 <sup>nd</sup> , 3 <sup>rd</sup> and final estimation process of IEEE 300-bus system.....	43
Figure 3.1	Single-line diagram and measurement configuration of a 3-bus power system.....	53
Figure 3.2	NRSE vs. SECJ for total time. ....	59
Figure 3.3	NRSE vs. SECJ for Formation of Gain.....	60
Figure 3.4	NRSE vs. SECJ for formation of H.....	61
Figure 4.1	Average error of the voltage magnitude.....	74
Figure 4.2	Average error of the active power injection.....	74
Figure 4.3	Average error of the reactive power injection.....	75
Figure 4.4	Average error of the active power flow. ....	75
Figure 4.5	Average error of the reactive power flow. ....	76
Figure 4.6	Average error of the reverse active power flow.....	76
Figure 4.7	Average error of the reverse reactive power flow.....	77
Figure 4.8	Active power flow from bus 15 to 23 – relative to power flow solution (actual value). ....	81
Figure 4.9	Active power injected at bus 2 – relative to power flow solution (actual value).....	81
Figure 4.10	Reactive power injected at bus 12 – relative to power flow solution (actual value). ....	82
Figure 4.11	Comparison of NRSE and SECJ for IEEE 57-bus.....	87
Figure 4.12	Comparison of NRSE and SECJ for IEEE 118-bus.....	87
Figure 5.1	A simplified schematic diagram of UPFC. ....	92
Figure 5.2	Steady state model of UPFC [60-62]. ....	93

Figure 5.3	Equivalent circuit of UPFC including transmission line.....	96
Figure 5.4	5-bus –Power System Model.....	100
Figure 5.5	Comparison of active power flow with and without UPFC. ....	102
Figure 5.6	Comparison of active bus power with and without UPFC.....	102
Figure 5.7	Comparison of reactive bus power with and without UPFC.....	103
Figure 5.8	IEEE 14-bus Real Power Losses.....	104
Figure 5.9	IEEE 14-bus Reactive Power Losses. ....	104
Figure 5.10	IEEE 14-bus – Case 1 voltage magnitude profile, without UPFC. ....	106
Figure 5.11	IEEE 14-bus – Case 1 voltage phase angle profile, without UPFC. ..	106
Figure 5.12	IEEE 14-bus – Case 1 real power profile, without UPFC.....	107
Figure 5.13	IEEE 14-bus – Case 1 reactive power profile, without UPFC.....	107
Figure 5.14	IEEE 14-bus – Power System Model with UPFC is connected at line 6 – 11.....	108
Figure 5.15	IEEE 14-bus – Case 5 voltage magnitude profile, with UPFC. ....	109
Figure 5.16	IEEE 14-bus – Case 5 voltage phase angle profile, with UPFC. ....	109
Figure 5.17	IEEE 14-bus – Case 5 real power profile, with UPFC.....	110
Figure 5.18	IEEE 14-bus – Case 5 reactive power profile, with UPFC. ....	110
Figure 5.19	IEEE 14-bus – Case 6 voltage magnitude profile, with UPFC. ....	111
Figure 5.20	IEEE 14-bus – Case 6 voltage phase angle profile, with UPFC. ....	112
Figure 5.21	IEEE 14-bus – Case 6 real power profile, with UPFC.....	112
Figure 5.22	IEEE 14-bus – Case 6 reactive power profile, with UPFC. ....	113
Figure 5.23	The comparison active power flow results between NRSE and power flow result. ....	117
Figure 5.24	The comparison reactive power flow results between NRSE and power flow result.....	117
Figure 5.25	Comparison of NRSE and SECJ for IEEE 57-bus. ....	120
Figure B1	Schematic diagram of SESB captured from SCADA system.....	141

## LIST OF ABBREVIATIONS

A/D	Analog to digital
AC	Alternating Current
AR	Autoregressive
ATWR	Ayer Tawar
BBTU	Bukit Batu
BFLD	Brickfields
BGJH	Batu Gajah
BT	Boosting transformer
BTRK	Bukit Tarek
CPNG	Chuping
CT	Current Transformer
DC	Direct Current
EGAT	Electricity Generating Authority of Thailand
EMS	Energy Management System
EPRI	Electric Power Research Institute
ET	Excitation transformer
FACTS	Flexible Alternate Current Transmission Systems
FASE	Forecasting Aided State Estimation
FDSE	Fast Decoupled State Estimator
GBID	Gebeng Industry
GRNE	Gurun East
GWAY	Galloway
HCOM	Hicom
HVDC	High Voltage Direct Current
IED	Intelligent electronic devices
JMJG	Janamanjung
JURU	Juru
KAWA	Kampung Awah
KNYR	Kenyir
KULE	Kuala Lumpur East
KULN	Kuala Lumpur North
KULS	Kuala Lumpur South

KULW	Kuala Lumpur West
MC	Modified Covariance
NLDC	National Load Dispatch Center
NRSE	Newton Raphson State Estimation
p.d.f	Probability density function
PAKA	Paka
PGPS	Pasir Gudang Power Station
PLTG	Plentong
PT	Potential Transformer
PTAI	Lembah Pantai
RTNET	Real Time Network
RTU	Remote Terminal Unit
SCADA	Supervisory Control and Data Aquisition
SE	State Estimation
SEJ	State Estimation with constructed Jacobian
SESB	Sabah Electricity Sendirian Berhad
SGRI	Segari Power Plant
SIGMA	Number of standard deviations assigned to the maximum possible error for a measurement
SRDG	Serdang Power Station
SVCs	Static Var Compensators
TBIN	Tanjung Bin
TCRs	Thyristor controlled reactors
TCSCs	Thyristor Controlled Series Capacitors
TKLG	Teluk Kalong
TMGR	Temmenggor
TNB	Tenaga Nasional Berhad
UPFC	Unified Power Flow Controller
VSI	Voltage source inverters
WLS	Weight Least Square
XDUCER	Transducer
YGPE	Yong Peng East
YGPN	Yong Peng

## LIST OF SYMBOLS

$+$	$=$	addition
$-$	$=$	subtraction
$\times$ or $\bullet$	$=$	multiplication
$\div$ or $/$ or $—$	$=$	division
$=$	$=$	equal to
$\neq$	$=$	not equal to
$<$	$=$	less than
$>$	$=$	greater than
$\leq$	$=$	less than / equal to
$\geq$	$=$	greater than / equal to
$\therefore$	$=$	therefore
$\forall$	$=$	for all
$\exists$	$=$	there exists
$\in$	$=$	element of
$\subset$	$=$	subset of
$\Rightarrow$	$=$	implies
$\%$	$=$	percent (out of 100)
$\infty$	$=$	infinity
$\sum$	$=$	summation
$\prod$	$=$	Multiplication
$ \cdot $	$=$	denotes the magnitude of a scalar enclosed within
$E[\cdot]$	$=$	expectation operator
$\hat{\phantom{x}}$	$=$	the “estimate” of a scalar, vector or matrix
$x_{ij}$	$=$	to the entry in row $i$ and column $j$ of the matrix $X$
$p_{ij}$	$=$	real power flow from bus $i$ to bus $j$
$q_{ij}$	$=$	reactive power flow from bus $i$ to bus $j$
$P_i$	$=$	active power at bus $i$
$Q_i$	$=$	reactive power at bus $i$
$V$	$=$	voltage magnitude
$\delta$	$=$	phase angle
$N$	$=$	number of buses
$m$	$=$	number of measurements
$\sigma$	$=$	Standard deviation
$W$	$=$	Weightage factor
$H$	$=$	Jacobian matrix
$a$	$=$	tap ratio
$G$	$=$	Gain matrix
$n$	$=$	number of states

$J$	=	the sum of the weighted squared errors
$\chi^2$	=	Chi-square
$r$	=	Normalized residual
$S$	=	Residual sensitivity
$\Omega$	=	Residual covariance
$N_f$	=	degrees of freedom
$Nbr$	=	Number of branches

# CHAPTER 1

## INTRODUCTION

### 1.1 Power System State Estimation

State Estimation (SE) in power systems is considered as the heart of any energy control center. It is responsible for providing a complete and reliable real-time database for analysis, control, and optimization functions [1]. Since electric power system state estimation was introduced by Fred Schweppe *et. al.* [2], it has remained an extremely active and contentious area. Nowadays, state estimation plays an important role in modern Energy Management systems (EMS) providing a complete, accurate, consistent and reliable database for other functions of the EMS system, such as security monitoring, optimal power flow, security analysis, on-line power flow studies, supervisory control, automatic voltage control and economic dispatch control [1-3]. The energy control centers gather information and measurements on the status and state of a power system via Supervisory Control and Data Acquisition System (SCADA).

A typical SCADA system is the network of data links connecting the data center with the remote terminal units (RTUs), as shown in Figure 1.1. It uses RTUs which are located at the substations, to acquire various types of measurements. Today, RTUs are replaced or complemented by intelligent electronic devices (IEDs), which have processing capabilities and hence intelligence. SCADA system is composed of a computer, which has access to the RTUs via a front-end processor, which is responsible for pooling one or more RTUs. This communication link between the control center and the substation, where RTUs are located, can be established in different ways to access their database for post-event analysis. The above mentioned functions are executed by the SCADA server and the results are made available to the EMS operator via user interface. However, the data collected by SCADA are not

immediately useful for the functions of EMS system. These telemetered raw measurements are usually corrupted by different kinds of errors. Small errors

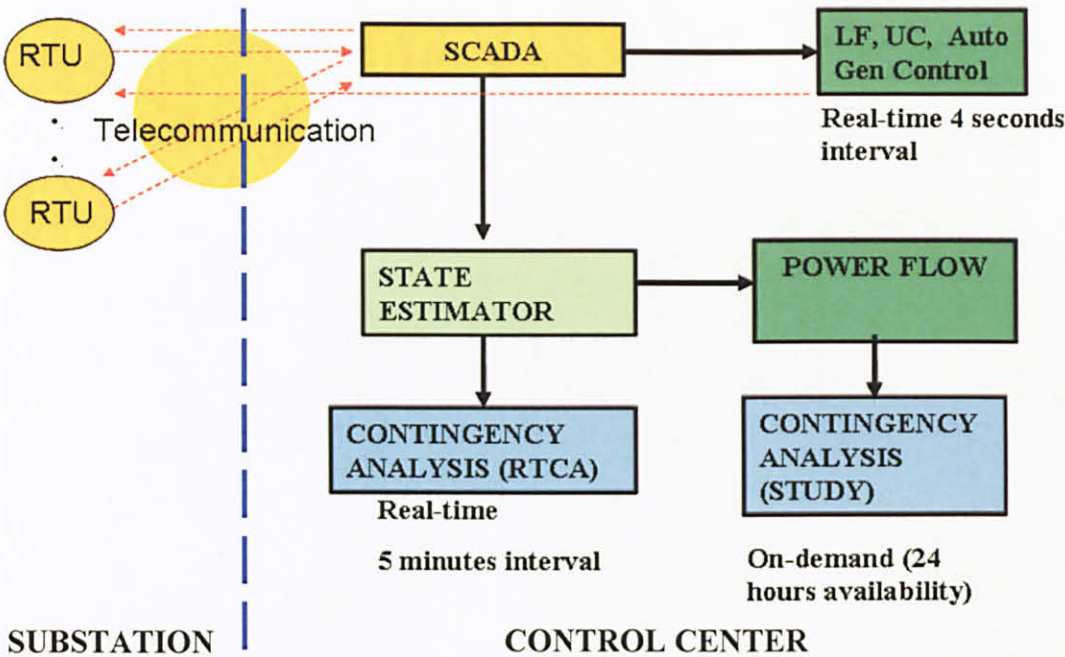


Figure 1.1 An overview of SCADA configuration.

such as meter calibration errors, transducer inaccuracies, analog-digital conversion errors, communication noise and gross errors or bad data such as errors in the network structure due to faulty switch, uncertainties in system parameter values and communication failures are present in the gathered data [4].

In a large power system, it is too expensive and sometimes it is not possible to make all possible measurements to determine the state of the system. If the number of measurements is equal to the number of states of the power system, the situation then corresponds to a real time power flow. In this case, the errors and uncertainties present in the measurements are ignored. Thus, even if one of the measurements is erroneous the power flow results are not accurate anymore. Somehow, if one of the measurements is lost, the states cannot be computed at all. To solve the problems in such situation, the SE is used. State estimator is a digestive system that removes the noises or errors statistically before determining the state of the system. The SE is capable of processing the raw measurements and makes use the available information to establish a reliable and complete data base for on-line monitoring and control. A



power system state estimator makes use of more number of measurements than the number of states to be estimated. The redundancy which is defined as the ratio of the number of measurements to the number of states usually lies in the range of 1.2 to 4.0. Data redundancy is a pre-requisite for the successful SE. This will ensure that the states still can be estimated if some of the measurements are lost. The small random errors can be filtered out by assigning proper weights to the available measurements. An accurate measurement is weighted more, than a less accurate one.

Before computing the states, generally, SE performs two tasks that are filtering of errors inherent to the metering system and the data validation. Moreover, as part of the estimation process, it determines network connectivity and observability [5]. The SE approach relies on the three basic assumptions:

- i. Measurement errors are statistically small;
- ii. Telemetered measurements available in the control centers are large enough not only to run the algorithm but also to achieve redundancy in terms of reducing the impact of eventual large errors;
- iii. Network configuration and parameters are correct;

Practically, these three assumptions are not always true, which has motivated researchers to develop or enhance existing SE algorithms [6]. In formulating power system state estimation problem, the complex bus voltages, i.e. bus voltages magnitudes and phase angles, are commonly used as the state variables. Once system state is determined, the other system quantities such as line power flows and bus power injections can be calculated.

## **1.2 Components of SE**

The SE generally comprises of five general components namely:

- i. Bad data filter (pre-screening process)
- ii. Topology processing
- iii. Observability analysis
- iv. State Estimation Computation
- v. Bad data processing

The complete scheme that involved in SE algorithm is shown in Figure 1.2. The bad data filtering or pre-screening process is used to detect and separate out all measurements with some apparent error in order to avoid any heavy distortion of the estimated network state due to completely wrong measurements. However, in the case of redundancy, this component looks forward to reduce the number of measurements if bad data is detected, which will affect the redundancy as well. Therefore, to avoid such case, Autoregressive (AR) method is proposed in this component. The function of AR method is to calculate one step ahead of the predicted values of the measurements. The predicted value is then compared with measured value for the filtering purposes. If the related measurement shows an error more than 5 % compared with the predicted value, then the related measurement is replaced with predicted value in order to keep the number of measurements same.

Next process after the pre-screening process is topology processing. The function of this process is to deliver an updated consistent model of the system in terms of topology and measurements, based on known system connections and parameters and real-time SCADA input. It must divide the network into electrical islands if necessary, provide the necessary system parameters, and place measurements in their topological locations. It may also serve other important but less essential functions, such as posting warnings for circuit breaker and/or isolator conflicts, or various anomalies in the fields of the SCADA database.

Once the topology of the network is completed, the network is checked for its observability. The function of observability analysis is to identify if there are any unobservable branches and observable islands in the system. It also functions to determine if a SE solution for the entire system can be obtained using the available set of measurements. The power flows in the branches (in megawatts or megavars), the load data (in megawatts or megavars) and the bus voltages are included in the measurement list. Generally, a region of the network is called observable, if the measurements in the system provide sufficient information to estimate the state of that part of the network.

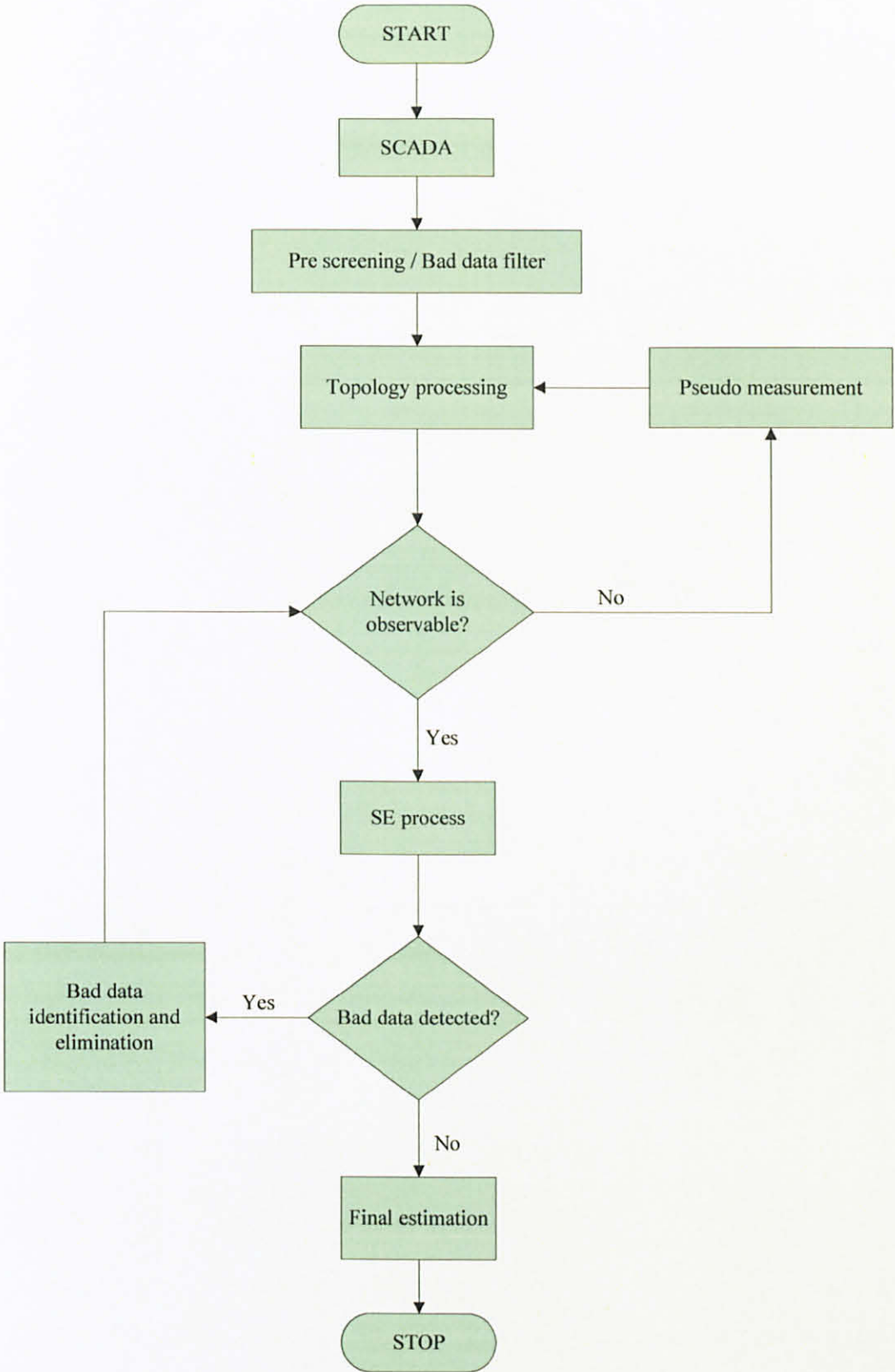


Figure 1.2 The flow chart of state estimation process.

### 1.3 State Estimation Techniques

Although the function of a SE is understandable, there is much freedom of choice in its practical implementation. One of the important options is that of the statistical methodology used to filter the measured data. Various methods for SE have been introduced in the past [1, 2, 7 and 8]. Among those methods, the Weighted Least Squares (WLS) algorithm is the most popular and finds applications in many fields. The basic Newton-Raphson WLS method, when used in power systems, has good convergence, as well as filtering and bad data processing properties, for a given observable meter placement with sufficient redundancy and yields optimum estimates. However, the gain and the Jacobian matrices associated with the basic algorithm require large computer storage and have to be evaluated at every iteration, resulting in very long computing time. The essential requirements for any on-line SE are reliability, speed and less computer storage. The computational burden associated with the basic WLS algorithm makes it unsuitable for on-line implementation in large scale power systems.

Fred Schweppe *et. al.* [9] in their paper had modified the basic WLS algorithm to suit the real time application in large scale power system. In that paper, the constant gain and Jacobian matrices are used in order to reduce the computational time. However, WLS processing could still need a longer time for medium to large networks and becomes even longer in the presence of multiple data with gross error and the procedures for bad data processing. Since then, several different alternatives to the WLS approach have been investigated. Among the algorithms developed and implemented in real time are sequential estimators, orthogonal transformation methods, hybrid method and fast decoupled estimators [8 and 10]. In sequential state estimation, each measurement is processed sequentially, usually one at a time. Processing of the measurement is done by avoiding the matrix procedures. Thus, the objective of sequential state estimation is mainly intended to provide computational efficiency both in terms of computing time and storage requirements. Sequential estimators have so far been found to be practical for small networks, but not for medium to large networks. In orthogonal transformation methods [1, 3, 11 and 12], there is no need to compute the gain matrix. The measurements are transformed into virtual measurements that are functions of the state and of the original measurements. However, the only concern of this method is the need to obtain the orthogonal matrix

which, in spite of being actually expressed as the product of elementary matrices, is much denser than the gain matrix, thus slows the computational time. Some ideas, such as the Hybrid method [13] has been proposed to speed up orthogonal factorization. This method does not require the storage of the orthogonal matrix and it can easily be implemented in the efficient fast decoupled version. However, according to Holten, L *et. al.* [7] and Slutsker *et. al.* [13], this method is less stable than the orthogonal transformation method and also it remains slower compared with the normal equation method. The WLS formulation may be decoupled by separating the measurement set into real and reactive power groups and by using the same simplifying assumptions as used in the fast decoupled load flow [14]. The integrated SE like fast decoupled state estimation may not meet the requirements of on-line state estimation in terms of computer storage and time for very large scale power systems containing thousand or more busses. The reduction of the computation burden that fit with normal equation of SE needs further investigation.

In the case of SE model that is unable to yield estimates within a degree of accuracy compatible with the standard deviations of the quantities estimated, one must conclude either that the measured quantities contain bad data or that the model is unfit to explain the measured quantities. The procedure to identify and solve the former problem is called as bad data analysis [15] while the latter one is topology error detection/identification. Many research papers have been published in the area of bad data analysis [16, 17 and 18]. The bad data have to be detected, identified and eliminated from the measurements. However, in order to maintain or increase the redundancy, the bad measurements are replaced with pseudo-measurements [1 and 19].

Pseudo-measurements can be generated based on typical values, forecasts, historical records, or approximation methods. The main difficulty in generating pseudo-measurements is to get high quality values and assign them proper weighting factor where an accurate measurement is weighted more than a less accurate one. Moreover, the pseudo-measurements generation process has to remain reliable, while the measurement unavailability is present. However, this problem is difficult to deal with, since most of SE commercial applications are static-natured where they do not model the time evolution of the system state. Among the many issues involving marked

improvements in SE, the use of all data available for processing has been pointed out recurrently [20]. In the early 1980s, many published paper reported on how state and measurement forecasting can be used to enhance the SE process [21, 22 and 23]. Since then, after an incubation period, great strides have been made in forecasting aided state estimation (FASE). The method to produce quality pseudo-measurements is not well established and hence needs more investigation.

Pseudo-measurements are also a problem solver for the cases of unobservable system. Generally, a region of the network is called observable, if the measurements in the system provide enough information to estimate the state of that part of the network. The important criterion for an observable system is that the number of available measurements is equal (so-called completely determined system) or larger (so-called over-determined system) than the number of state variables. The entire network is said to be observable if all states can be estimated based on the given measurements. However, the technical challenge in SE is to solve the under-determined systems of equations, that is, systems with lesser number of measurements than the number of state variables. In this case, a unique solution may not exist, that is, it is not solvable. In other words, SE is unobservable. However, this can be solved if more state information is added. Various methods proposed for network observability analysis have been discussed very well in the literature [24, 25 and 26].

#### **1.4 Objectives of Thesis**

The aims of the thesis are to provide solutions to the various problems discussed above. Thus, the objectives of the thesis are:

- i. To develop an SE algorithm that will reduce computational time for large scale power systems.
- ii. To develop a robust SE algorithm with more information and additional features.
- iii. To produce high quality pseudo-measurements that can be used to replace the identified bad measurements.
- iv. To enhance the capability of bad filter mechanism by identifying the bad measurements with high weighting factor.
- v. To extend the use of SE to power systems embedded with UPFC.

## 1.5 Outline of the Thesis

This thesis consists of six chapters and it is organized as follows:

In Chapter 1, preliminaries of the SE and the concept of SE are stated. Further, the objectives of the thesis are presented.

Chapter 2 focuses on the review of WLS state estimator. Newton-Raphson State Estimation (NRSE) method is applied to solve the over-determined set of non-linear power system equations. The mathematical equations of measurements employed in SE and the criterion of WLS is discussed in this chapter. The theory of bad data processing is also presented in this chapter. The full SE package that has been developed is explained in this chapter. Results obtained from the local utility company forms part of this chapter.

Chapter 3 describes the algorithm of constructing the Jacobian matrix,  $H$ . The conventional process of computing the elements of  $H$  matrix is a time consuming step which requires evaluation of large number of trigonometric functions. It is significant, especially in large scale power system networks. In order to reduce the computational time, a simple algorithm to construct the  $H$  matrix is presented in this chapter. It is recognized that each element of the  $H$  matrix is contributed by the partial derivatives of the power flows in the network elements. The elements of the state estimation Jacobian matrix are obtained considering the power flow measurements in the network elements. Network elements are processed one-by-one and the  $H$  matrix is updated in a simple manner. The final  $H$  matrix thus constructed is exactly same as that obtained in available NRSE method. Systematically constructed Jacobian matrix  $H$  is then integrated with WLS method to estimate the state variables. The State Estimation with constructed Jacobian (SECJ) is tested on several power systems. The final estimates and time taken to converge for SECJ method are recorded and compared with results obtained from NRSE method discussed in Chapter 2. It is seen that for large scale power system, SECJ method is very attractive as it takes less than 50 % of the time taken for NRSE method.

Chapter 4 deals with the development of pre-estimation filter using autoregressive (AR) model to identify the gross measurement errors. The identification of the errors is accomplished by making a comparison between the measured values and the

predicted values of the measurements. If the difference exceeds 5 % error, the measured data is assumed to be grossly erroneous and is replaced by its predicted value in the measurement set. Instead of filtering purpose, the output from AR, is effectively used as pseudo-measurements to replace the lost measurement if the network is unobservable. Thus, it is ensured that the network is observable before SE is performed.

Basically, two methods of AR, namely Modified Covariance (MC) and Burg are discussed in this chapter. Both the methods are used to calculate the AR parameters so that the one-step ahead predicted values of state variables can be determined. To investigate the performance of the proposed method, tests are carried out on 5-bus, IEEE 14-bus, IEEE 30-bus, IEEE 57-bus, 103-bus, IEEE 118-bus and IEEE 300-bus systems. It is seen that the AR methods are successful in replacing all the measured data with the predicted values if the difference between the measured data and predicted value exceeds 5 % error. Thus, it makes the proposed AR method offers a measurement pre-screening ability that can complement other post-estimation detection/identification techniques by processing the raw measurements before estimation is performed.

Chapter 5 deals with the modified version of Weight Least Square (WLS) method of state estimation for the power systems embedded with of Flexible Alternate Current Transmission Systems (FACTS) devices. FACTS controllers are invariably incorporated in the present day power system network to control the power flow and enhance system stability. Based on the research done, one device, namely the Unified Power Flow Controller (UPFC) had been selected to be given consideration due to its complexity and versatility in controlling power flows.

This chapter attempts to obtain the state estimation model for the power system embedded with UPFC. A power injection model that transfers the effect of UPFC towards the power flow to the two nodes is presented. This method is integrated to the already developed state estimation program with the consideration of UPFC. The modified state estimation program is successfully tested on several standard networks to prove its validity.



In Chapter 6, highlights of this thesis are briefly reviewed and suggestions for future research are indicated.

## CHAPTER 2

### THE NEWTON RAPHSON STATE ESTIMATOR

#### 2.1 Introduction

The state estimation concept in power systems has developed rapidly from the initial works of F. Schweppe *et. al.* [2] to the present day on line state estimators. Today, the need for the use of power state estimation becomes more important since the power system networks are become larger and more complex. With the world-wide deregulation of the power industry, power system state estimation now becomes a more vital real-time monitoring tool [27]. It is becoming a part of new energy control centres that are being established in large-scale power systems.

The basic structure of power system estimation, based a single phase model, complex power and voltage measurement set, non-simultaneousness measurements and single frequency model, is no longer applicable because of the present interconnected power networks which have become more complex [28]. Various improved versions have been suggested to suit the large scale power systems [7, 11, 12, 15, 29 and 30]. Among the several methods that have been suggested, WLS method is the best method by taking into account of all the considerations such as cost, stability and efficient bad data handling properties. Comprehensive discussion on the state of the art in power system state estimation is discussed in [1, 5 and 31]. Recently, Artificial Intelligent systems such as Fuzzy and Neural Network are being used in SE [32, 33 and 34]. However, testing the techniques on large-scale power systems still a challenging task.

## 2.2 Weight Least Square

Most of the SE programs that are in practical use are formulated as over-determined systems of nonlinear equations and solved as WLS problems. This technique has been extensively discussed in the literature [1-5], [15].

### 2.2.1 State variables

The function of WLS is to find the best estimate of the state variables, where the voltages at all the buses are the most commonly defined state variables. Dependent variables such as power flow can be determined from the state variables. Accurate state variables are needed to ensure that the results obtained from EMS functions are correct.

The vector of the state variables  $\mathbf{x}$  (see APPENDIX A for all mathematical notations and terminologies used throughout the chapters), for an  $N$ -bus network is:

$$\mathbf{x} = \begin{bmatrix} x_1 \\ \vdots \\ x_n \end{bmatrix} = \begin{bmatrix} \delta_2 \\ \vdots \\ \delta_N \\ \text{---} \\ V_1 \\ \vdots \\ V_N \end{bmatrix} \quad (2.1)$$

where  $N$  is number of buses and  $n = 2N-1$  states. One of the buses is taken as the reference or slack bus and its phase angle is assumed to be zero. In equation (2.1), bus number 1 is taken as the slack bus.

### 2.2.2 Mathematical equations describing ideal measurements

The five types of measurements used in power system state estimation are real and reactive line power flows, real and reactive bus power injections, and the bus voltage magnitudes. In order to use these measurements in the state estimator, a mathematical model for the measurements is first developed. Starting with the  $\pi$  model of a transmission line as shown in Figure 2.1, which connects two buses  $i$  and  $j$ , a transmission line is represented by a series impedance  $r_{ij} + jx_{ij}$ . A transformer with

series impedance  $r_{ij} + jx_{ij}$  and off-nominal turns ratio  $a$  with tap setting facility at bus  $i$  is represented by the series admittance  $\frac{1}{a}(g_{ij} + jb_{ij})$  and shunt admittances  $\left(\frac{1-a}{a^2}\right)(g_{ij} + jb_{ij})$  and  $\left(\frac{a-1}{a}\right)(g_{ij} + jb_{ij})$  at buses  $i$  and  $j$ , respectively. Half line charging admittance and external shunt admittance if any, are added together and represented as  $g_{shi} + jb_{shi}$  and  $g_{shj} + jb_{shj}$  at buses  $i$  and  $j$  respectively.

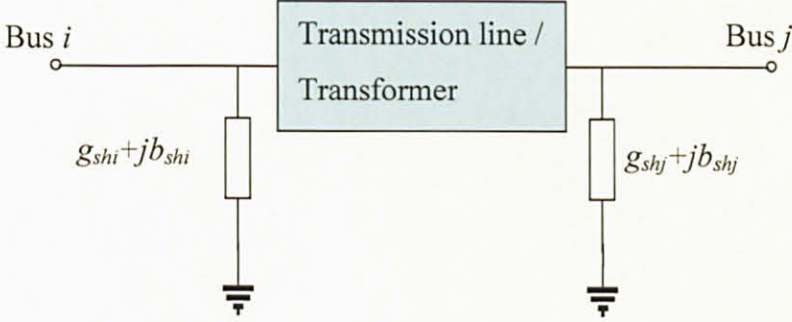


Figure 2.1 Transmission Line Model

Defining

$$g_{ij} = r_{ij} / (r_{ij}^2 + x_{ij}^2) \quad (2.2)$$

$$b_{ij} = -x_{ij} / (r_{ij}^2 + x_{ij}^2) \quad (2.3)$$

$$\delta_{ij} = \delta_i - \delta_j \quad (2.4)$$

the expressions for real and reactive power flows are obtained as follows:

$$p_{ij} = V_i^2 \left( \frac{g_{ij}}{a^2} + g_{shi} \right) - \frac{V_i V_j}{a} (g_{ij} \cos \delta_{ij} + b_{ij} \sin \delta_{ij}) \quad (2.5)$$

$$q_{ij} = -V_j^2 \left( \frac{b_{ij}}{a^2} + b_{shj} \right) - \frac{V_i V_j}{a} (g_{ij} \sin \delta_{ij} - b_{ij} \cos \delta_{ij}) \quad (2.6)$$

$$p_{ji} = V_j^2 (g_{ij} + g_{shj}) - \frac{V_i V_j}{a} (g_{ij} \cos \delta_{ij} - b_{ij} \sin \delta_{ij}) \quad (2.7)$$

$$q_{ji} = -V_j^2 (b_{ij} + b_{shj}) + \frac{V_i V_j}{a} (g_{ij} \sin \delta_{ij} + b_{ij} \cos \delta_{ij}) \quad (2.8)$$

For transmission line,  $a$  is set to 1 and for transformer  $g_{sh}$  and  $b_{sh}$  at bus  $i$  and  $j$  are set to zero.

Taking the general element of bus admittance matrix as  $Y_{ij} = G_{ij} + jB_{ij}$ , the calculated real and reactive powers at bus  $i$  are computed from

$$P_i = V_i^2 G_{ii} + \sum_{j=1, j \neq i}^N V_i V_j (G_{ij} \cos \delta_{ij} + B_{ij} \sin \delta_{ij}) \quad (2.9)$$

$$Q_i = - \left\{ V_i^2 B_{ii} + \sum_{j=1, j \neq i}^N V_i V_j (G_{ij} \sin \delta_{ij} - B_{ij} \cos \delta_{ij}) \right\} \quad (2.10)$$

### 2.2.3 Analog measurements

Analog measurements are made on a given power system and transmitted to the control centre via telecommunication links by making use of SCADA. The analog measurements that are normally included in the state estimator consist of bus voltage magnitudes at generation and load buses, active and reactive generation injections, and active and reactive load powers. Each of these measurements can be written in terms of the state variables. In other words, for a measurement  $z_i$ , the true value of that measurement will be,

$$\hat{z}_i = \mathbf{h}_i(\mathbf{x}) \quad (2.11)$$

For a voltage measurement, the function  $\mathbf{h}_i$  is very simple:

$$\hat{z}_i = V_k \quad (2.12)$$

where measurement  $i$  occurs at bus  $k$ .

For MW and MVAR flows, the function  $\mathbf{h}_i$  is given by the expressions for power flow in line  $i - j$  as given in equation (2.5) to (2.8).

The analog measurements obtained from SCADA normally not are perfect. Small random errors or noise are always present. It is because the data received or displayed at a control center will be passed through transducers, analog-to-digital converter, and transmitted via various communication links to the energy control center. These factors can be the cause for the bad data occurring in the SE.

### 2.2.4 Model of measurement error

The errors  $e_i$  represent the difference between the measured value  $\hat{z}_i$  and the actual measurements  $\mathbf{h}_i(\mathbf{x})$ . The errors are generally small, additive, independent and

statistically well behaved. These small errors are due to meter calibration errors, transducer inaccuracies, analog-digital conversion errors, communication noise. However, gross errors or bad data are the errors due to faulty switch, uncertainties in system parameter values, communication failures and etc. In a real application, the errors and the actual measurements are unknown quantities and the measured values are the known quantities. Thus, it is important to make one of the unknown variables to be available. This can be done by obtaining statistical information from calibration curves of measuring instruments. The vector  $e_i$  is modeled as a random variable with a normal (gaussian) distribution having zero mean, as illustrated in Figure 2.2. This makes sense because a particular measuring instrument, if it is reasonably calibrated, may read a little high (positive error) at times or a little low (negative error) at times, so that the average error is zero. Calibration curves enable determination of the variance  $\sigma_i$ .

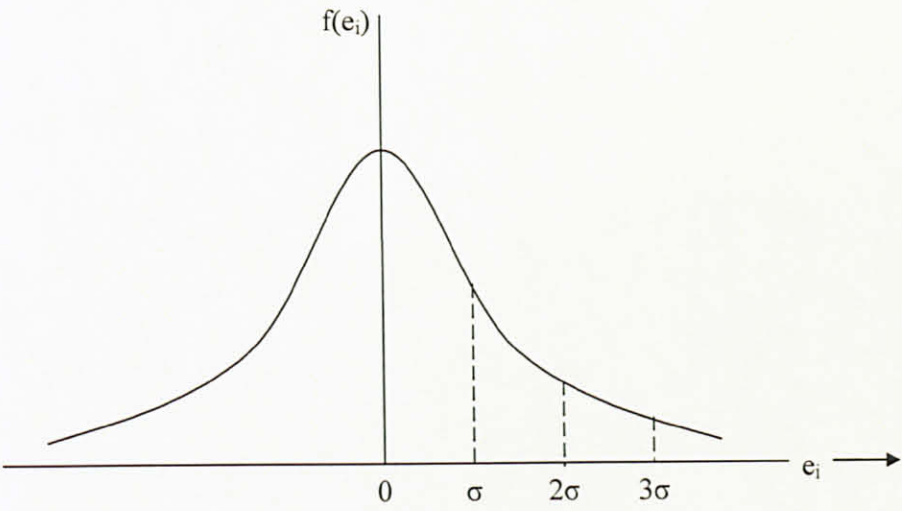


Figure 2.2 Gaussian Probability Curve

Recall the expectation operator, which is denoted as  $E(x)$ . The expected value of  $x$ , is defined as:

$$E(x) = \int_{-\infty}^{\infty} xf(x)dx \tag{2.13}$$

which gives the mean value of a variable  $x$  described by the probability distribution function  $f(x)$ .

Also define variance as:

$$\sigma_x^2 = \text{var}(x) = \int_{-\infty}^{\infty} (x - E(x))^2 f(x) dx \quad (2.14)$$

Then relate variance to mean beginning with equation (2.14).

$$\begin{aligned} \sigma_x^2 = \text{var}(x) &= \int_{-\infty}^{\infty} (x - E(x))^2 f(x) dx = \int_{-\infty}^{\infty} (x^2 - 2xE(x) + (E(x))^2) f(x) dx \\ &= \int_{-\infty}^{\infty} x^2 f(x) dx - 2E(x) \int_{-\infty}^{\infty} xf(x) dx + (E(x))^2 \int_{-\infty}^{\infty} f(x) dx \\ &= E(x^2) - 2(E(x))^2 + (E(x))^2 = E(x^2) - (E(x))^2 \end{aligned} \quad (2.15)$$

From equation (2.15) (which is true for any random variable  $x$ ), it is seen that if the mean is zero ( $E(x)=0$ ), then the last term in equation (2.15) is zero and

$$\sigma_x^2 = E(x^2) \quad (2.16)$$

Thus, for the calibration error characterized by the random variable  $e_i$ ,

- i.  $E(e_i) = 0$  (zero mean)
- ii.  $E(e_i^2) = \sigma_i^2$  (variance)

Note that the larger the variance, accuracy will be lesser in the measuring device.

Due to the multiple measuring instruments, the understanding on how the statistics of one random variable relates to the statistics of another needs clarification.

The covariance measure is effective in doing this and is defined as

$$\sigma_{xy}^2 = \text{cov}(x, y) = \int_{-\infty}^{\infty} (x - E(x))(y - E(y)) f(x, y) dx \quad (2.17)$$

Note that variance is a special case of covariance when  $x=y$ , i.e.,  $\text{var}(x) = \text{cov}(x, x)$ .

It can be shown [35] from equation (2.17) that

- i.  $\sigma_{xy}^2 = \text{cov}(x, y) = E(xy) - E(x)E(y)$  (2.18)
- ii. If  $x$  and  $y$  are independent, then  $E(xy) = E(x)E(y)$ .

Therefore, for two independent random variables, the covariance is:

$$\sigma_{xy}^2 = \text{cov}(x, y) = 0$$

The errors  $e_i$  and  $e_j$  for any two measuring instruments  $i$  and  $j$  are independent. This means that

$$\text{cov}(e_i, e_j) = \begin{cases} 0, & i \neq j \\ \sigma_i^2, & i = j \end{cases} \quad (2.19)$$

Thus, a covariance matrix  $\mathbf{R}$  could be defined where the element in position  $(i, j)$  being  $\text{cov}(e_i, e_j)$ . With the results in equation (2.19), the covariance matrix will appear as:

$$\mathbf{R} = \begin{bmatrix} \sigma_1^2 & 0 & \cdots & 0 \\ 0 & \sigma_2^2 & 0 & 0 \\ \vdots & 0 & \ddots & 0 \\ 0 & 0 & 0 & \sigma_m^2 \end{bmatrix} \quad (2.20)$$

where  $m$  is the number of measuring instruments used.

The determination of proper values for the standard deviation  $\sigma_i$  requires a knowledge of the accuracies of the instruments and instrumentation system, extensive field trials, experience and good engineering judgment. Normally, the  $\sigma_i$  will be derived from the defined instrument errors on potential transformer (PT), current transformer (CT), transducer (XDUCER), Analog to Digital Converters (A/D) and the number of standard deviations assigned to the maximum possible error for a measurement (SIGMA) [36]. Thus,

$$\sigma = \frac{(PT + CT + A/D + XDUCER)}{100 \bullet \text{SIGMA}} \bullet \text{base} \quad (2.21)$$

Typically SIGMA is equivalent to 3.0 which determine that three standard deviations include 99.74 % of the area under a normal distribution curve.

The following are the vectors of measured values, true values and errors.

$$\text{Measured values: } \mathbf{z} = \begin{bmatrix} z_1 \\ \vdots \\ z_m \end{bmatrix} \quad (2.22)$$

$$\text{True values: } \hat{\mathbf{z}} = \begin{bmatrix} \hat{z}_1 \\ \vdots \\ \hat{z}_m \end{bmatrix} \quad (2.23)$$

$$\text{Errors: } \mathbf{e} = \begin{bmatrix} e_1 \\ \vdots \\ e_m \end{bmatrix} \quad (2.24)$$



They are related as

$$z = \hat{z} + e \quad (2.25)$$

Substituting equation (2.11) into (2.25), then:

$$z = h(x) + e \quad (2.26)$$

The number of unknowns is  $n = 2N-1$  (the states in  $x$  are the angle and voltage variables). There will be  $m$  number of measurements. However, the question is which measurements are the best measurements so that the error can be minimized. It is hard to select which are the best for a large scale power system. Due to that it is good to handle the system with more number of measurements,  $m > n$  so-called *over-determined* system According to A. Monticelli, 1999 [1], the equation (2.26) can be solved as follows:

- i. set  $e$  equal to  $\mathbf{0}$
- ii. choose  $m$  number of measurements and from the corresponding  $n$  equations
- iii. Solve for  $x$  (it would need to be non-linear solver but once done, solution is unique).

### 2.2.5 Pseudo-measurements

The greater the redundancy the better will be the accuracy. Over and above the actual measurements pseudo-measurements may be added to increase redundancy. Historical data or non real-time metered types of information, known as pseudo-measurements may be utilized. Pseudo-measurements are not real measurements but are used in the state-estimation algorithm as if they were. If the accuracy of pseudo-measurement is better then it will increase the accuracy of state estimation.

The most common “exact” pseudo-measurement is the bus injection power at a substation that has no generation and load. Figure 2.3 illustrates this aspect.

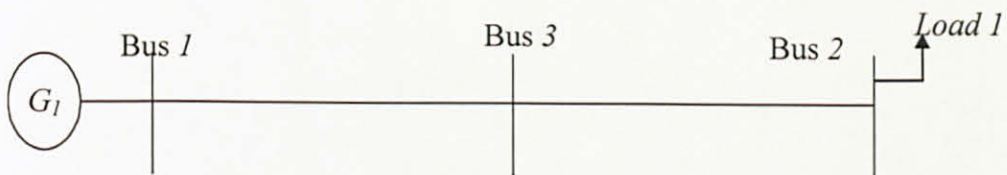


Figure 2.3 3-Bus network configuration.

In Figure 2.3, bus 3 has no generation or load. Therefore, the real and reactive power injections of this bus are exactly zero. So it is possible to add two more measurements to the measurement set that already exists, from equation (2.26),

$$z_{i+1} = h_{i+1}(x) + e_{i+1} \quad (2.27)$$

where:

$$\text{“Measurements”} \left\{ \begin{array}{l} z_i = P_{p,inj} = 0 \\ z_{i+1} = Q_{p,inj} = 0 \end{array} \right. \quad (2.28)$$

$$(2.29)$$

$$h_i(\mathbf{x}) = P_{p,inj} = \sum_{k=1}^N V_p V_k (G_{pk} \cos(\delta_p - \delta_k) + B_{pk} \sin(\delta_p - \delta_k)) = 0 \quad (2.30)$$

$$h_{i+1}(\mathbf{x}) = Q_{p,inj} = \sum_{k=1}^N V_p V_k (G_{pk} \sin(\delta_p - \delta_k) - B_{pk} \cos(\delta_p - \delta_k)) = 0 \quad (2.31)$$

The above two real and reactive power injections are added as pseudo-measurements. For the pseudo-measurements, the terms  $e_i$  and  $e_{i+1}$  are zero-mean Gaussian distributed errors. The fact that these pseudo-measurements are exact can be accounted by letting  $\sigma_i$  and  $\sigma_{i+1}$  to be very small.

### 2.2.6 WLS criteria

With the WLS approach, the state estimate  $\mathbf{x}$  is defined as the value of  $x$  which minimizes the sum of the weighted squared errors. So the strategy now is to choose  $x$  so that it can minimize the sum of the weighted squared errors between the measured values and the actual values.

From equation (2.26), the error is

$$\mathbf{e} = \mathbf{z} - \mathbf{h}(\mathbf{x}) \quad (2.32)$$

The sum of the weighted squared errors can be expressed as

$$J(x) = \frac{1}{2} \sum_{i=1}^m e_i^2 = \frac{1}{2} \mathbf{e}^T \mathbf{e} = \frac{1}{2} (\mathbf{z} - \mathbf{h}(\mathbf{x}))^T (\mathbf{z} - \mathbf{h}(\mathbf{x})) \quad (2.33)$$

In practice, among all the measurement devices available, some are more accurate compared with the others. Therefore, in order to ensure that measurements from meters of greater accuracy are treated more favorably than less accurate

measurements, each term in the sum of the weighted squared errors is multiplied by an appropriate weight factor. Thus, equation (2.33) is modified as

$$J(x) = \frac{1}{2} \sum_{i=1}^m w_i e_i^2 = \frac{1}{2} \sum_{i=1}^m \frac{e_i^2}{\sigma_i^2} \quad (2.34)$$

Larger value of  $\frac{1}{\sigma_i^2}$  represents a greater accuracy measurement, while smaller value of  $\frac{1}{\sigma_i^2}$  represents a lesser accurate measurement.

The covariance matrix given by equation (2.20) is

$$\mathbf{R} = \begin{bmatrix} \sigma_1^2 & 0 & \cdots & 0 \\ 0 & \sigma_2^2 & 0 & 0 \\ \vdots & 0 & \ddots & 0 \\ 0 & 0 & 0 & \sigma_m^2 \end{bmatrix}$$

Its inverse is

$$\mathbf{R}^{-1} = \begin{bmatrix} \frac{1}{\sigma_1^2} & 0 & \cdots & 0 \\ 0 & \frac{1}{\sigma_2^2} & 0 & 0 \\ \vdots & 0 & \ddots & 0 \\ 0 & 0 & 0 & \frac{1}{\sigma_m^2} \end{bmatrix} \quad (2.35)$$

Then express equation (2.34) in matrix form as:

$$J(x) = \frac{1}{2} \sum_{i=1}^m \frac{e_i^2}{\sigma_i^2} = \frac{1}{2} \mathbf{e}^T \mathbf{R}^{-1} \mathbf{e} = \frac{1}{2} (\mathbf{z} - \mathbf{h}(x))^T \mathbf{R}^{-1} (\mathbf{z} - \mathbf{h}(x)) = \frac{1}{2} \sum_{i=1}^m \frac{(z_i - h_i(x))^2}{\sigma_i^2} \quad (2.36)$$

The problem then becomes to find  $\mathbf{x}$  that minimizes  $J(x)$ . Note that  $\mathbf{h}$  is being nonlinear, the solution will necessarily be iterative.

### 2.2.7 Solution for AC state estimator

The problem can be stated as follows:

Mimimize

$$J(x) = \frac{1}{2} \sum_{i=1}^m \frac{e_i^2}{\sigma_i^2} = \frac{1}{2} \mathbf{e}^T \mathbf{R}^{-1} \mathbf{e} = \frac{1}{2} (\mathbf{z} - \mathbf{h}(x))^T \mathbf{R}^{-1} (\mathbf{z} - \mathbf{h}(x)) = \frac{1}{2} \sum_{i=1}^m \frac{(z_i - h_i(x))^2}{\sigma_i^2}$$

For  $J(\mathbf{x})$  to be minimum, all the first derivatives of the objective function with respect to decision variables must be zero. Therefore,

$$\frac{\partial J}{\partial \mathbf{x}} = \begin{bmatrix} \frac{\partial J}{\partial x_1} \\ \vdots \\ \frac{\partial J}{\partial x_n} \end{bmatrix} = \nabla_{\mathbf{x}} J = \begin{bmatrix} 0 \\ \vdots \\ 0 \end{bmatrix} \quad (2.37)$$

For a single element in  $\nabla_{\mathbf{x}} J$ ,

$$J(\mathbf{x}) = \frac{1}{2} \sum_{i=1}^m \frac{(z_i - h_i(\mathbf{x}))^2}{\sigma_i^2} \quad (2.38)$$

$$\begin{aligned} \frac{\partial J}{\partial x_1} &= \frac{1}{2} \sum_{i=1}^m \frac{-2(z_i - h_i(\mathbf{x}))}{\sigma_i^2} \frac{\partial h_i(\mathbf{x})}{\partial x_1} \\ &= \sum_{i=1}^m \frac{-(z_i - h_i(\mathbf{x}))}{\sigma_i^2} \frac{\partial h_i(\mathbf{x})}{\partial x_1} \end{aligned} \quad (2.39)$$

This can be written in matrix form as

$$\frac{\partial J}{\partial x_1} = - \begin{bmatrix} \frac{\partial h_1(\mathbf{x})}{\partial x_1} & \frac{\partial h_2(\mathbf{x})}{\partial x_1} & \dots & \frac{\partial h_m(\mathbf{x})}{\partial x_1} \end{bmatrix} \mathbf{R}^{-1} \begin{bmatrix} z_1 - h_1(\mathbf{x}) \\ z_2 - h_2(\mathbf{x}) \\ \vdots \\ z_m - h_m(\mathbf{x}) \end{bmatrix} \quad (2.40)$$

Extending the above

$$\frac{\partial J}{\partial \mathbf{x}} = - \begin{bmatrix} \frac{\partial h_1(\mathbf{x})}{\partial x_1} & \frac{\partial h_2(\mathbf{x})}{\partial x_1} & \dots & \frac{\partial h_m(\mathbf{x})}{\partial x_1} \\ \frac{\partial h_1(\mathbf{x})}{\partial x_2} & \frac{\partial h_2(\mathbf{x})}{\partial x_2} & \dots & \frac{\partial h_m(\mathbf{x})}{\partial x_2} \\ \vdots & \vdots & \vdots & \vdots \\ \frac{\partial h_1(\mathbf{x})}{\partial x_n} & \frac{\partial h_2(\mathbf{x})}{\partial x_n} & \dots & \frac{\partial h_m(\mathbf{x})}{\partial x_n} \end{bmatrix} \mathbf{R}^{-1} \begin{bmatrix} z_1 - h_1(\mathbf{x}) \\ z_2 - h_2(\mathbf{x}) \\ \vdots \\ z_m - h_m(\mathbf{x}) \end{bmatrix} \quad (2.41)$$

The matrix of partial derivatives shown in equation (2.41) is a sort of Jacobian matrix.

It is a  $n \times m$  rectangular matrix. The matrix  $\mathbf{H}$  is defined as

$$\mathbf{H} = \begin{bmatrix} \frac{\partial h_1(\mathbf{x})}{\partial x_1} & \frac{\partial h_1(\mathbf{x})}{\partial x_2} & \dots & \frac{\partial h_1(\mathbf{x})}{\partial x_n} \\ \frac{\partial h_2(\mathbf{x})}{\partial x_1} & \frac{\partial h_2(\mathbf{x})}{\partial x_2} & \dots & \frac{\partial h_2(\mathbf{x})}{\partial x_n} \\ \vdots & \vdots & \vdots & \vdots \\ \frac{\partial h_m(\mathbf{x})}{\partial x_1} & \frac{\partial h_m(\mathbf{x})}{\partial x_2} & \dots & \frac{\partial h_m(\mathbf{x})}{\partial x_n} \end{bmatrix} \quad (2.42)$$

Note that  $\mathbf{H}$  is  $m \times n$ , and it is the negative transpose of the matrix in equation (2.41). In terms of the above  $\mathbf{H}$  matrix, the optimality condition can be written as:

$$\nabla_{\mathbf{x}} J = \frac{\partial J}{\partial \mathbf{x}} = \begin{bmatrix} \frac{\partial J}{\partial x_1} \\ \vdots \\ \frac{\partial J}{\partial x_n} \end{bmatrix} = -\mathbf{H}^T(\mathbf{x})\mathbf{R}^{-1}[(\mathbf{z} - \mathbf{h}(\mathbf{x}))] = \mathbf{0} \quad (2.43)$$

The solution to equation (2.43) will yield the estimated state vector  $\mathbf{x}$  which minimizes the sum of the weighted squared errors. Because there are  $n$  elements in the partial- $J$  vector on the left, the equation (2.43) gives  $n$  equations. Since there are  $n$  variables in  $\mathbf{x}$ , it is possible to solve equation (2.43) explicitly for  $\mathbf{x}$ .

In order to arrive at a solution procedure for equation (2.43), the left-hand-side of equation (2.43) is defined as  $\mathbf{G}(\mathbf{x})$ , where

$$\mathbf{G}(\mathbf{x}) = -\mathbf{H}^T(\mathbf{x})\mathbf{R}^{-1}[(\mathbf{z} - \mathbf{h}(\mathbf{x}))] = \mathbf{0} \quad (2.44)$$

$\mathbf{G}(\mathbf{x})$  is known as the gain matrix. Noted that the  $\mathbf{G}(\mathbf{x})$  is a  $n \times n$  square matrix.

Performing Taylor series expansion of  $\mathbf{G}(\mathbf{x})$  around a certain solution  $\mathbf{x}_0$ , it gets

$$\mathbf{G}(\mathbf{x}_0 + \Delta\mathbf{x}) = \mathbf{G}(\mathbf{x}_0) + \nabla_{\mathbf{x}} \mathbf{G}(\mathbf{x})|_{\mathbf{x}_0} \Delta\mathbf{x} + h.o.t. = \mathbf{0} \quad (2.45)$$

Note that equation (2.45) indicates that if  $\mathbf{x}_0 + \Delta\mathbf{x}$  is to be a solution, then the right-hand-side of equation (2.45) must be zero.

Recall that in a Taylor series expansion, the higher order terms (h.o.t) contain products of  $\Delta\mathbf{x}$ , and so if  $\Delta\mathbf{x}$  is relatively small, terms containing products of  $\Delta\mathbf{x}$  will be very small, and in fact, negligible. Thus, neglecting the *h.o.t.* in equation (2.45) the new equation is

$$\mathbf{G}(\mathbf{x}_0 + \Delta\mathbf{x}) = \mathbf{G}(\mathbf{x}_0) + \nabla_{\mathbf{x}} \mathbf{G}(\mathbf{x})|_{\mathbf{x}_0} \Delta\mathbf{x} = \mathbf{0} \quad (2.46)$$

Equation (2.46) is a set of nonlinear equation which can be solved using Newton-type algorithm. Initially a good guess,  $\mathbf{x}^{(k)}$  is obtained for the solution of equation (2.46). The difference between our guess and the real solution is relative small. Because it is not the solution,  $\mathbf{G}(\mathbf{x}^{(k)}) \neq \mathbf{0}$ . Denote the better guess as  $\mathbf{x}^{(k+1)}$ . The difference between the old guess  $\mathbf{x}^{(k)}$  and the new guess  $\mathbf{x}^{(k+1)}$  is  $\Delta\mathbf{x}^{(k+1)}$ , i.e.,

$$\mathbf{x}^{(k+1)} = \mathbf{x}^{(k)} + \Delta\mathbf{x} \quad (2.47)$$

or re-writing equation (2.47)

$$\Delta \mathbf{x} = \mathbf{x}^{(k+1)} - \mathbf{x}^{(k)} \quad (2.48)$$

Evaluating  $\mathbf{G}$  at the better guess, yields

$$\mathbf{G}(\mathbf{x}^{(k+1)}) = \mathbf{G}(\mathbf{x}^{(k)} + \Delta \mathbf{x}) = \mathbf{G}(\mathbf{x}^{(k)}) + \nabla_{\mathbf{x}} \mathbf{G}(\mathbf{x}) \Big|_{\mathbf{x}^{(k)}} \Delta \mathbf{x} \quad (2.49)$$

Let that  $\mathbf{G}(\mathbf{x}^{(k+1)}) = \mathbf{0}$ . Under this desired condition, equation (2.49) becomes:

$$\mathbf{G}(\mathbf{x}^{(k+1)}) = \mathbf{G}(\mathbf{x}^{(k)} + \Delta \mathbf{x}) = \mathbf{G}(\mathbf{x}^{(k)}) + \nabla_{\mathbf{x}} \mathbf{G}(\mathbf{x}) \Big|_{\mathbf{x}^{(k)}} \Delta \mathbf{x} = \mathbf{0} \quad (2.50)$$

Solving for  $\nabla_{\mathbf{x}} \mathbf{G}(\mathbf{x}) \Big|_{\mathbf{x}^{(k)}}$ :

$$\nabla_{\mathbf{x}} \mathbf{G}(\mathbf{x}) \Big|_{\mathbf{x}^{(k)}} \Delta \mathbf{x} = -\mathbf{G}(\mathbf{x}^{(k)}) \quad (2.51)$$

In considering equation (2.51), the right-hand-side shows the negative of equation (2.44), evaluated at  $\mathbf{x}^{(k)}$ , i.e.,

$$-\mathbf{G}(\mathbf{x}^{(k)}) = \mathbf{H}^T(\mathbf{x}^{(k)}) \mathbf{R}^{-1} \left[ \mathbf{z} - \mathbf{h}(\mathbf{x}^{(k)}) \right] \quad (2.52)$$

Meanwhile the expression of  $\nabla_{\mathbf{x}} \mathbf{G}(\mathbf{x}) \Big|_{\mathbf{x}^{(k)}}$  from equation (2.51) is the derivatives with respect to each of the  $n$  state variables, of each of the  $n$  functional expressions in equation (2.44). There are  $n$  functional expressions in equation (2.52). Since there are  $n$  functional expressions and  $n$  derivatives are these for each function,  $\mathbf{G}(\mathbf{x})$  will be  $n \times n$ , square matrix.

Based on equation (2.43), it shows that  $\mathbf{G}(\mathbf{x})$  is also the derivatives with respect to each of the  $n$  state variables. Therefore,  $\nabla_{\mathbf{x}} \mathbf{G}(\mathbf{x}) \Big|_{\mathbf{x}^{(k)}}$  are second derivatives of  $J$  with respect to the state variables. The second derivatives is getting started from equation (2.44):

$$\mathbf{G}(\mathbf{x}) = -\mathbf{H}^T(\mathbf{x}) \mathbf{R}^{-1} \left[ \mathbf{z} - \mathbf{h}(\mathbf{x}) \right]$$

So the aim is to get:

$$\nabla_{\mathbf{x}} \mathbf{G}(\mathbf{x}) = \frac{\partial \mathbf{G}(\mathbf{x})}{\partial \mathbf{x}} = \frac{\partial}{\partial \mathbf{x}} \left\{ -\mathbf{H}^T(\mathbf{x}) \mathbf{R}^{-1} \left[ \mathbf{z} - \mathbf{h}(\mathbf{x}) \right] \right\} \quad (2.53)$$

The differentiation of what is inside the brackets of equation (2.53) is formidable. Next, make it easier by assuming that  $\mathbf{H}(\mathbf{x})$  is a constant matrix. This implies  $\mathbf{H}(\mathbf{x} + \Delta \mathbf{x}) \approx \mathbf{H}(\mathbf{x})$ , i.e., the derivatives of the power flow equations do not change.

From equation (2.42),

$$H = \begin{bmatrix} \frac{\partial h_1(\mathbf{x})}{\partial x_1} & \frac{\partial h_1(\mathbf{x})}{\partial x_2} & \dots & \frac{\partial h_1(\mathbf{x})}{\partial x_n} \\ \frac{\partial h_2(\mathbf{x})}{\partial x_1} & \frac{\partial h_2(\mathbf{x})}{\partial x_2} & \dots & \frac{\partial h_2(\mathbf{x})}{\partial x_n} \\ \vdots & \vdots & \ddots & \vdots \\ \frac{\partial h_m(\mathbf{x})}{\partial x_1} & \frac{\partial h_m(\mathbf{x})}{\partial x_2} & \dots & \frac{\partial h_m(\mathbf{x})}{\partial x_n} \end{bmatrix}$$

where the functions  $h_i$  are the expressions for the measurements (voltages, real and reactive power flows) in terms of the states (angles and voltage magnitudes). So  $h_i$  is really a power flow Jacobian matrix. It is well known that the power flow Jacobian is relatively insensitive to relatively small variations in state.

With the above assumption, differentiating the right-hand-side of equation (2.53) and get

$$\begin{aligned} \nabla_x \mathbf{G}(\mathbf{x}) &= \frac{\partial \mathbf{G}(\mathbf{x})}{\partial \mathbf{x}} = \frac{\partial}{\partial \mathbf{x}} \left\{ -\mathbf{H}^T(\mathbf{x})\mathbf{R}^{-1}[(\mathbf{z}-\mathbf{h}(\mathbf{x}))] \right\} \\ &= -\mathbf{H}^T(\mathbf{x})\mathbf{R}^{-1} \left( -\frac{\partial \mathbf{h}(\mathbf{x})}{\partial \mathbf{x}} \right) = \mathbf{H}^T(\mathbf{x})\mathbf{R}^{-1} \frac{\partial \mathbf{h}(\mathbf{x})}{\partial \mathbf{x}} \end{aligned} \quad (2.54)$$

However, from equation (2.42) the term  $\frac{\partial \mathbf{h}(\mathbf{x})}{\partial \mathbf{x}}$  in equation (2.54) is already recognized as  $\mathbf{H}$ . Therefore, equation (2.54) becomes:

$$\nabla_x \mathbf{G}(\mathbf{x}) = \mathbf{H}^T(\mathbf{x})\mathbf{R}^{-1}\mathbf{H}(\mathbf{x}) \quad (2.55)$$

Making this substitution into equation (2.51) results in:

$$\mathbf{H}^T(\mathbf{x})\mathbf{R}^{-1}\mathbf{H}(\mathbf{x}) \Big|_{\mathbf{x}^{(k)}} \Delta \mathbf{x} = -\mathbf{G}(\mathbf{x}^{(k)}) \quad (2.56)$$

Finally, replacing the right-hand-side of equation (2.56) with equation (2.44) evaluated at  $\mathbf{x}^{(k)}$  yields:

$$\begin{aligned} \mathbf{H}^T(\mathbf{x})\mathbf{R}^{-1}\mathbf{H}(\mathbf{x}) \Big|_{\mathbf{x}^{(k)}} \Delta \mathbf{x} &= \mathbf{H}^T(\mathbf{x})\mathbf{R}^{-1}[(\mathbf{z}-\mathbf{h}(\mathbf{x}))] \Big|_{\mathbf{x}^{(k)}} \\ \Delta \mathbf{x} &= \left( \mathbf{H}^T(\mathbf{x})\mathbf{R}^{-1}\mathbf{H}(\mathbf{x}) \Big|_{\mathbf{x}^{(k)}} \right)^{-1} \mathbf{H}^T(\mathbf{x})\mathbf{R}^{-1}[(\mathbf{z}-\mathbf{h}(\mathbf{x}))] \Big|_{\mathbf{x}^{(k)}} \\ \Delta \mathbf{x} &= \mathbf{G}^{-1}(\mathbf{x})\mathbf{H}^T(\mathbf{x})\mathbf{R}^{-1}[(\mathbf{z}-\mathbf{h}(\mathbf{x}))] \Big|_{\mathbf{x}^{(k)}} \end{aligned} \quad (2.57)$$

Equation (2.57) provides a way to solve for  $\Delta \mathbf{x}$ .

### 2.3 Bad Data Processing

The state vector of bus voltage magnitudes and angles is estimated from the set of available measurements. Random noise and gross errors contaminate the final

estimate. Hence, it is important to ensure that the errors present in the measurements are eliminated. Gross measurement errors will result in inaccurate estimate. The measurement errors may occur due to various reasons, such as noise in the communication channels and the noise from electronic parts such as transducer and Analog to Digital Converter (A/D). However, such errors or bad data may be filtered out by state estimator, since one of the fundamental functions of a state estimator is to filter out the measurement errors.

As discussed in the Section 1.2, practical state estimator preprocessing the set of measurements and other available information is carried out to eliminate or replace the obvious bad data. However, pre-filtering process cannot completely eliminate all the bad data and some are bound to enter as the input of SE. Various procedures based on statistical methods of detecting and identifying them are developed [8, 17, 18, 19 and 37]. These methods depend upon analyzing the residuals for smallness in some sense for the detection and identification of bad data.

### 2.3.1 Bad data detection

Processing of the bad data involves three steps namely detection, identification and elimination. The process is started after the estimation algorithm is converged. The detection is the process to indicate the existence of bad data in the set of measurements. This is commonly accomplished using the Chi-square,  $\chi^2$  test. In general there are three steps are involved while implementing this  $\chi^2$  test. First, the SE should complete the estimated process until the final state variables,  $x$  are obtained. Consider the weighted sum squared errors, i.e. as in equation (2.36),

$$J(\mathbf{x}) = \frac{1}{2} \sum_{i=1}^m \frac{e_i^2}{\sigma_i^2} = \frac{1}{2} \sum_{i=1}^m \left( \frac{e_i}{\sigma_i} \right)^2 = \frac{1}{2} \sum_{i=1}^m \left( \frac{e_i}{\sqrt{R_i}} \right)^2 = \frac{1}{2} \sum_{i=1}^m (u_i)^2 \quad (2.58)$$

where  $e_i$  is  $i$ th measurement error,  $R_i$  is the diagonal entry of the measurement error covariance matrix and  $m$  is the total number of measurements. Second, normalize the errors and obtain a new function of  $u_i(x)$  by assuming that  $e_i$ 's are all normally distributed random variables with zero mean and  $u_i$  will follow a standard normal distribution, i.e.  $N(0,1)$ .



$$u_i = \frac{e_i}{\sqrt{R_i}} \quad (2.59)$$

Then, the  $\chi^2$  test statistic is computed with  $N_f$  degrees of freedom, where  $N_f$  is equal to  $m-n$ . A plot of  $p(\chi^2)$  probability density function (p.d.f), shown in Figure 2.4, represents the probability of finding  $J(x)$  in the corresponding region. The dashed line in Figure 2.4 is representing the chi-square distribution,  $\chi^2_{N_f, \alpha}$ , which means the chi-square distribution with  $N_f$  degrees of freedom with probability of false alarm threshold,  $\alpha$ , which represent 5 % probability of error for the most of cases in this thesis. If the  $J(x)$  is above than the set threshold then at least one measurement is detected as a bad measurement. If the  $J(x)$  is less than the set threshold, then the measurement set is free from bad measurement.

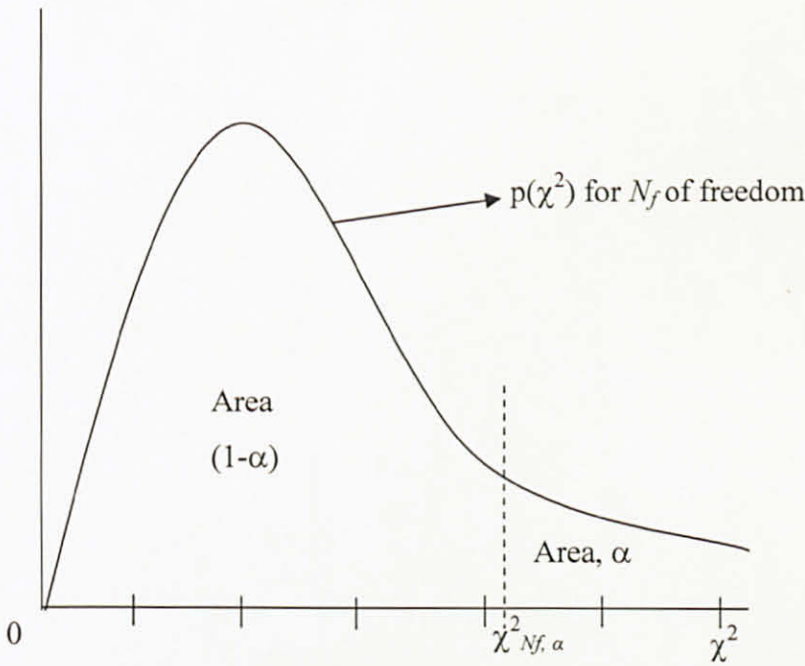


Figure 2.4 Chi-square distribution,  $\chi^2_{N_f, \alpha}$  for a small value of  $N_f$  degrees of freedom.

However, this test only indicates the presence of bad data in the measurement set but unable to identify which one among the measurements is a bad data. Thus, the identification step is required now to identify which specific measurement is incorrect.

### 2.3.2 Bad data identification and elimination

The most common method in power systems SE is the use of the largest normalized residual, or  $r_{\max}^N$  test. This technique will examine the normalized value of the residual for measurement  $i$  and the largest element in  $r^N$  is identified as bad measurement. Due to that, the first step of this technique is to calculate the residual for each measurement as follows:

$$r_i = z_i - h_i(x) \quad \text{where } i=1,2,\dots,m \quad (2.60)$$

Recall equation (2.57), the updated state for  $x$  in WLS is

$$\Delta x = G^{-1}(x)H^T(x)R^{-1}(z - h(x)) = G^{-1}(x)H^T(x)R^{-1}\Delta z$$

On solving for  $\Delta z$ , the following equation is obtained

$$\Delta \hat{z} = H\Delta \hat{x} = HG^{-1}H^T R^{-1}\Delta z = K\Delta z \quad (2.61)$$

where  $K$  is called the hat matrix, for putting hat on  $\Delta z$ . Referring to the authors Ali Abur *et. al.* [3], the  $K$  has the following properties

$$K \cdot K \cdot K \cdots K = K \quad (2.62)$$

$$K \cdot H = H \quad (2.63)$$

$$(I - K) \cdot H = 0 \quad (2.64)$$

Now, the relationship between the residuals and the measurement errors can be obtained as:

$$\begin{aligned} r &= \Delta z - \Delta \hat{z} = (I - K)\Delta z \\ &= (I - K)(H\Delta x + e) \\ &= H\Delta x - KH\Delta x + (I - K)e \quad [\text{use property of } K \text{ in equation (2.64)}] \\ &= (I - K)e = Se \end{aligned} \quad (2.65)$$

where  $S$  is called residual sensitivity matrix, which represents the sensitivity of measurement residual to measurement error. Normalized value of the residual for measurement  $i$  can be obtained by simply dividing its absolute value by the corresponding diagonal entry in the residual covariance matrix, where the residual covariance matrix is given by

$$\text{Cov}(r) = \Omega = E[rr^T] = S \cdot E[ee^T] \cdot S^T = SRS^T = SR \quad (2.66)$$

Thus, the normalized value of the residual for measurement  $i$  is

$$r_i^N = \frac{|r_i|}{\sqrt{\Omega_i}} \quad (2.67)$$

The normalized residual vector  $r^N$  will then have a standard normal distribution, i.e.  $r_i^N \sim N(0,1)$ . Thus, the largest element in  $r^N$  can be compared against a statistical threshold to decide on the existence of bad data. Normally the threshold is set to 4. Furthermore, the measurement with the largest  $r^N$  will be identified as bad data in most of the cases. If bad data is identified, the corresponding measurement is deleted and the SE is run again.

### 2.3.3 Overall algorithm

As a conclusion for a given measurements  $z$ , i.e.  $[z_1, \dots, z_m]$ , standard deviations  $\sigma_1, \dots, \sigma_m$  and the network, the state estimate,  $x$ , i.e. all voltage magnitudes and all voltage angles except for swing bus angle, can be computed by executing the following steps.

- Step 1 Form measurement expressions  $h(x)$
- Step 2 Form derivative expressions  $H = \frac{\partial h(x)}{\partial x}$
- Step 3 Form  $R$
- Step 4 Let  $k = 0$ . Guess solution  $x^{(k)}$ .
- Step 5 Compute  $H(x)$ ,  $h(x)$
- Step 6 Compute the gain  $G = H^T(x)R^{-1}H(x)\Big|_{x^{(k)}}$
- Step 7 Solve  $\Delta x$  using equation (2.57)
- Step 8 Compute  $x^{(k+1)} = x^{(k)} + \Delta x$
- Step 9 If  $|\Delta x^{(k)}| > \varepsilon$  then, setting  $k = k+1$  go to Step 5. Else go to Step 10
- Step 10 The weighted sum of squares of the final errors is calculated using equation (2.58) and is compared with the data from the Chi-square distribution
- Step 11 If the weighted sum of squares is greater than the data from Chi square distribution, then the measurement having highest normalized residual is

deleted from the measurement set and the state estimation is repeated; otherwise the states estimated are taken as the final estimates.

## **2.4 Practical Results of SE in the Malaysian Grid**

Realizing the importance of the accuracies needed in the data taken from SCADA for the power system operation and control, Tenaga Nasional Berhad (TNB) has decided to incorporate the SCADA system with EMS. Therefore, in the year 1995, in conjunction with the life cycle, typically 10 – 15 years, the existing SCADA system is changed to SCADA/EMS systems supplied by WESTINGHOUSE Company. At present the SCADA/EMS in TNB is operated with the number of stations and substations increasing from time to time. Until August 2007, about 381 out of 440 substations are monitored by SCADA/EMS systems. While 353 are linked with supervisory switching and resulting 2193 number of breakers is on supervisory. These numbers are expected to growth up increase in the future. Meanwhile, the total numbers of transformers are 1029 with total MVA of 76,216.50. The subsidiary of TNB such as Sabah Electricity Sdn. Bhd. (SESB) also now has installed SCADA/EMS in their stations.

Malaysia grid has been divided into four main regions namely as North, Central, South and East. The total maximum demand for the peninsular of Malaysia is about 13,000 MW. Figure 2.5 shows the regional overview diagram. The National Load Dispatch Center (NLDC) of TNB is functioning as operating, reporting and monitoring center for the network. It will provide access to real-time and historical data for analysis and reporting purposes. The data will be updated and stored in every 10 minutes. The type of data that can be obtained at NLDC is network data, transformer data, topology network, generation data, system data, voltage data, hydro data and also the status of circuit breakers and isolators.

The software used by NLDC is a good package including contingency analysis and optimal power flow. The other software used in NLDC is the Power System Software for Engineers, which is capable of performing contingency analysis and power flow analysis.

### *2.4.1 Survey findings*

The observation mainly focused on the effect of assigning weightage to the individual measurements, redundancy of the measurement, the margin errors of actual and estimated value and bad data. All these information can be found via Real time Network (RTNET) window, which is provided in the software package. During the observation period, of three days, a variety of data are taken at different times. The peak load data are taken in the morning while the normal load data are taken in the afternoon.

In each region, certain stations are taken for the purpose of survey. The substations such as Temmenggor (TMGR), Segari Power Plant (SGRI), Batu Gajah (BGJH), Juru (JURU), Gurun East (GRNE), Chuping (CPNG), Ayer Tawar (ATWR) and Janamanjung (JMJG) are considered for the North region. Meanwhile for the Central region the selected substations are Kuala Lumpur East (KULE), Kuala Lumpur West (KULW), Kuala Lumpur North (KULN), Galloway (GWAY), Kuala Lumpur South (KULS), Brickfields (BFLD), Serdang Power Station (SRDG), Hicom (HCOM), Lembah Pantai (PTAI) and Bukit Tarek (BTRK). In the South region, the selected substations are Tanjung Bin (TBIN), Bukit Batu (BBTU), Yong Peng (YGPN), Pasir Gudang Power Station (PGPS), Yong Peng East (YGPE) and Plentong (PLTG). Lastly, substations like Paka (PAKA), Gebeng Industry (GBID), Kampung Awah (KAWA), Teluk Kalong (TKLG) and Kenyir (KNYR) are identified for the East region. Those substations are selected due to the several criteria such as interface substations in between region, critical substations in terms of maximum load demand and substations that are connected with tie-line.

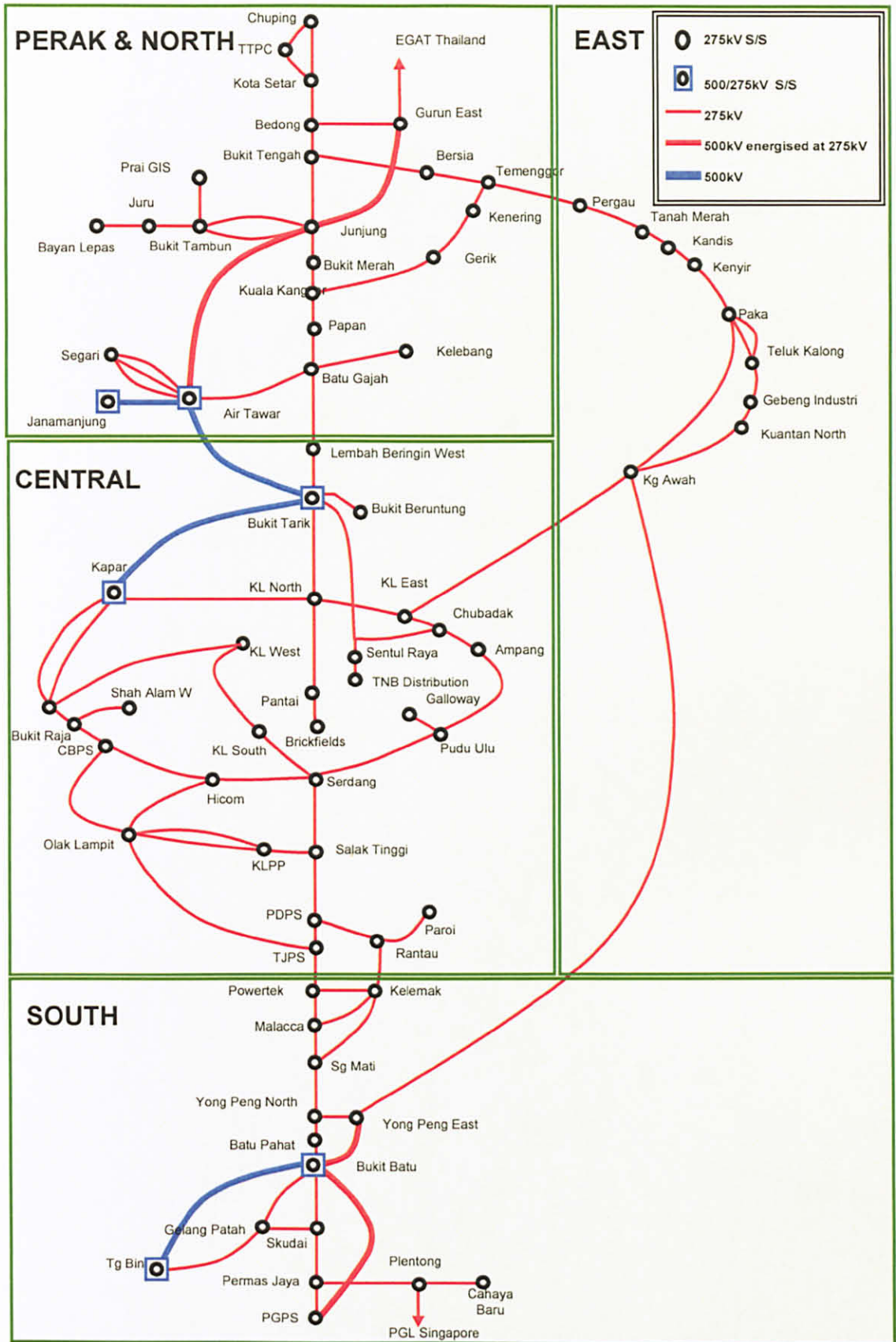


Figure 2.5 Regional overview diagram.

Table 2.1 shows the sample of data which have large variance of errors between actual and estimated values. The large variances will affect the performance of SE if these reading are taken as the input of the SE. However, all those values captured are considered as most trusted measurements of SE since the assigned accuracy is high. The large variance can influence the meter bias which will end up with big standard deviation. Because of this, the accuracy of SE is badly affected.

The measurement of load flow is categorized as pair measurements in the package of the software used by NLDC, which means that when either active power flow or reactive power flow is bad, both measurements are considered bad. This is not a good practice as one of them normally provides a good data as shown in Table 2.2.

Table 2.1 Captured readings which show the large variance of SCADA and SE

LOCATION	CLASS	SCADA	SE	Error
BUS 572 ND ID MB2	MEA1	283.41	288.9	5.49
BUS 572 ND ID RB2	MEAS	291.79	288.9	2.89
UNIT HY01	UMR2	34.03	34.21	0.18
	UMR2	26.52	26.61	0.09
UNIT HY02	MEAS	34.54	34.66	0.12
	MEAS	25.11	25.17	0.06
UNIT HY03	UMR2	34.49	34.67	0.18
	UMR2	27.99	28.07	0.08
UNIT HY04	UMR2	34.47	34.64	0.17
	UMR2	26.64	26.73	0.09
XF2 WT2	MEA7	0	10	10
LN2 275KKSRTMGR1 SEG (S2)	MEA3	36.63	31.96	4.67
	MEA3	65.93	-0.66	65.27
LN2 275PGAUTMGR2 SEG (S1)	MEAS	-107.84	-95.41	12.43
	MEAS	38.75	55.78	17.03
BUS 1059 ND ID MB2A	MEAS	286.17	291.22	5.05
BUS 1059 ND ID RB2A	MEA2	283.28	291.22	7.94
UNIT BLK3	MEAS	634.14	0	634.14
	MEAS	42.95	0	42.95
UNIT BNG3	MEA3	-645.08	0	645.08
	MEA3	0	0	0
UNIT BLK1	UMR2	589.91	589.91	0
	UMR2	27.47	27.47	0

Most of the problems are due to the MVAR readings. As seen from Table 2.2, for transformer 1 the MVAR measurement is in reverse direction therefore the MVAR is considered bad but the MW reading is good. Same goes to the transformer 2, due to the large variance of MVAR reading between SCADA and SE, the measurement is suspected as bad, although the MW reading is good. Thus, it will be more beneficial if both of the measurements are separated from each other so that the number of available good measurements will increase.

Table 2.2 The sample of pair measurements that are suspected as bad measurement.

Location	Unit	RTNET available	Suspect bad	Accuracy Class	SCADA	SE
XF2 WT1	MW	y	y	MEAS	-25.91	-23.61
	MVAR			MEAS	-11.5	11.83
XF2 WT2	MW	y	y	MEAS	-25.91	-26.73
	MVAR			MEAS	-11.77	-35.5

In practice, the individual measurement is assigned with their own weight factor based on technical experience of the engineers. However, uncertainty in analog measurements could occur in a real time system. Those measurements that are assigned with high weighting factor need not be a good data. In TNB, the weight factor or accuracy class is calculated using equation (2.21). Table 2.3 depicted the accuracy class that is used in TNB to differentiate which measurement is trusted more or less. The accuracy class with less percentage error of PT, CT, XDUCER and A/D is counted as trusted measurement. Meanwhile, the accuracy class with high percentage error of PT, CT, XDUCER and A/D such as MEA7 is countered as untrusted measurement.

Wrongly assigning the accuracy class to the individual measurement also can affect the performance of SE. As shown in Table 2.4, most of the less trusted measurements also could possibly produce a good reading (such as BUS 383 with accuracy class is MEA1 and line LN2132BKHMCPNG1, with accuracy class is MEA3) and if these measurements are not considered as trusted measurement the SE will lose one trusted



measurement. Table 2.4 also shows that the measurement with first class accuracy (MEAS) such as line, LN2132CPNGKGAR2 is also not giving consistently good result.

Table 2.3 Measurement Accuracy Class

Accuracy Class	Percentage of error			
	PT	CT	XDUCER	A/D
MEAS	1.0	1.0	1.0	1.0
UMW1	1.0	1.0	1.0	1.0
UMW2	1.0	1.0	1.0	3.0
UMR1	1.0	1.0	1.0	3.0
UMR2	1.0	1.0	1.0	2.0
MEA1	1.0	1.0	1.0	3.0
MEA2	1.0	1.0	1.0	4.0
MEA3	1.0	1.0	1.0	5.0
MEA4	1.0	1.0	1.0	6.0
MEA5	1.0	1.0	10.0	10.0
MEA6	1.0	1.0	25.0	25.0
MEA7	55.0	25.0	25.0	25.0

Table 2.4 Sample of data with different weightage of measurements.

LOCATION	MEASURE	CLASS	SCADA	SE	Error
BUS 383 ND ID MB1	KV	MEA1	134.65	134.53	0.12
BUS 383 ND ID RB1	KV	MEA1	135.6	134.53	1.07
LN2 132CPNGKGAR1 SEG (S1)	MW FMVAR	MEAS MEAS	-34.46 -15.05	-29.96 -9.15	4.5 5.9
LN2 132CPNGKGAR2 SEG (S1)	MW FMVAR	MEAS MEAS	-1.27 0.2	-29.96 -9.15	28.69 8.95
LN2 132BKTRCPNG1 SEG (S1)	MW TMVAR	MEAS MEAS	13.25 2.14	16.98 7.92	3.73 5.78
LN2 132BKTRCPNG2 SEG (S1)	MW FMVAR	MEAS MEAS	14.22 4.58	16.98 7.92	2.76 3.34
LN2 132BKHMCPNG1 SEG (S1)	MW FMVAR	MEA3 MEA3	12.76 2.14	10.67 12.28	2.09 10.14
LN2 132CPNGPAUH1 SEG (S1)	MW FMVAR	MEAS MEAS	44.23 16.65	45.14 18.21	0.91 1.56

#### *2.4.2 Deficiencies in the existing software*

The five types of conventional measurements used in power system state estimation are real and reactive line power flows, real and reactive bus power injections, and the bus voltage magnitudes. However, the real and reactive bus power injections are not available as inputs of SE provided in NLDC. Lack of those measurements will certainly reduce the accuracy of SE since redundancy rate is reduced [1-3].

The software considers the measurement of power flows as pair measurements, which means that if one of the measurements, either the real or reactive power flows, is bad then both the real and reactive power flows are identified as non priority measurement. However, it is not a good practice to follow pair measurements. It is proven from the observations that the real power flows always gave a good reading but end up with less confidence because of bad measurement of the reactive power flows.

The margin of errors between the SCADA and RTNET reading are large. The big margin of the errors most probably can influence the meter bias which will end up with big standard deviation as shown in Table 2.1. The increase of standard deviation will cause the weightage to reduce and the measurement will be classified as less trusted measurement. All of the said factors will affect the performance or accuracy of SE.

Assigning constant weightage or accuracy class to the measurement is not advisable for the dynamic system. However, from the observations the weightage or accuracy class given is unchangeable which means that the weightage or accuracy class is always constant regardless of either the reading is good or bad. The SE will be affected if the measurement with a good accuracy class is in bad condition. The SE will somehow use that measurement as an input because a good accuracy class was assigned to the related measurement.

Based on the above discussions, it can conclude that the existing software in NLDC needs improvement.

## 2.5 Developed Software and the Simulation Results

Thus, there is a need for developing and improved SE software which will yield more accurate estimate. The software must be robust and reliable. It must be well suited for large scale power systems. With these objectives in mind a new SE software package is developed. The developed software is written in MATLAB. NR method of solving equations and WLS method of optimization are the backbone of this software. This SE software package is tested on the IEEE 5, IEEE 14, IEEE 30, IEEE 57, 103-bus, IEEE 118 and IEEE 300 bus systems. The bus data and line data together with load flow results for the 103-bus system are given in APPENDIX B. The load flow computation was carried out using the load and generation data obtained via load curve and generation participation factor. Its output results served as the true values of measurements. The superior performances of this software are presented in the next section.

### 2.5.1 Description of simulation

In order to simulate the NRSE algorithm, the data obtained from power flow studies, as attached in APPENDIX B are used. The measurements used for the different test systems are shown in Table 2.5. The initial states of voltage vectors are commonly assumed to have a flat profile that means all the voltage phasors are of 1 p.u and in phase with each other, i.e. 0 degree. The convergence of the algorithm is tested using the following criteria:

$$\max |\Delta x_k| = \varepsilon \quad (2.69)$$

where  $\varepsilon$  is given by user, in most of the cases it is set to 0.001.

Table 2.5 The summary of description of simulation for all tested system.

System Bus	Measurements					Redundancy <i>m/n</i>
	<i>V</i>	<i>P</i>	<i>Q</i>	<i>p<sub>ij</sub> &amp; p<sub>ji</sub></i>	<i>q<sub>ij</sub> &amp; q<sub>ji</sub></i>	
5	4	4	3	4	4	2.11
IEEE 14	6	10	8	16	13	1.96
IEEE 30	22	2	0	57	37	2.00
IEEE 57	55	33	33	122	62	2.70
103	100	52	51	287	289	3.80
IEEE 118	113	95	61	209	48	2.24
IEEE 300	297	212	48	655	343	2.59

The performance of the algorithm in the simulation studies is assessed by comparing the estimated values,  $\hat{z}$  and the measured values,  $z$  with the true values,  $z^t$ . The following indices are used for this comparison.

$$J_{meas} = \frac{1}{m} \sum_{i=1}^m \left( \frac{z_i - z_i^t}{\sigma_i} \right)^2 \quad (2.70)$$

$$J_{est.} = \frac{1}{m} \sum_{i=1}^m \left( \frac{\hat{z}_i - z_i^t}{\sigma_i} \right)^2 \quad (2.71)$$

$$R_{ave.} = \frac{1}{m} \sum_{i=1}^m \left( \frac{|\hat{z}_i - z_i^t|}{\sigma_i} \right) \quad (2.72)$$

$$R_{max} = \max \left[ \frac{|\hat{z}_i - z_i^t|}{\sigma_i} \right] \text{ for } i = 1, 2, \dots, m \quad (2.73)$$

The level of uncertainty in the measurements is indicated by the performance index  $J_{meas}$ . While the performance index of  $J_{est.}$  shows how close are the estimated values to the measured value. The filtering process is good if the ratio of  $J_{est.}/J_{meas}$  is less than one. The performance indices  $R_{ave.}$  and  $R_{max}$  indicate the average and the maximum values of weighted residuals from the true values to compliment the general information of the indices  $J_{meas}$  and  $J_{est.}$ .

On the other hand, the true and the estimated values of the state variables are compared by the error index,

$$E_x = \left( \frac{|\hat{x}_i - x_i^t|}{x_i^t} \right) \times 100\% \quad (2.74)$$

Table 2.6 shows the summary of the general computational results for the tested networks. The convergence tolerance of 0.001 p.u. and the margin of error 5 % are assigned to all tested network. In the tested network no bad data is detected since the value of the objective function  $J$  is found less than the Chi-square value.

Table 2.6 The summary of computational results.

System Bus	Degrees of freedom $N_f = m - n$	Chi-Square $\chi^2_{N_f, \alpha}$	Objective function, $J$	Number of iterations
5	10	1.83E+01	4.37E-03	3
IEEE 14	26	3.89E+01	1.19E+01	4
IEEE 30	59	7.79E+01	7.45E+01	4
IEEE 57	192	2.25E+02	1.92E+02	7
103-bus	574	6.31E+02	4.60E+02	6
IEEE 118	291	3.32E+02	3.00E+02	7
IEEE 300	956	1.03E+03	1.00E+03	8

Tables 2.7 and 2.8 depict the analysis of state vector  $x$  for 5-bus and IEEE 14-bus system respectively.

Table 2.7 Analysis of State Vector for 5-bus system relative to power flow solutions (true measurements).

Bus no.	Voltage magnitude (p.u.)		Voltage phase (degree)		$E_x$ (%)	
	TRUE $ V ^t$	Estimated $ \hat{V} $	TRUE $\delta^t$	Estimated $\hat{\delta}$	$\Delta V $	$\Delta\delta$
1	1.06	1.06	0	0	0	0
2	1	1	-2.061	-2.06115	0	0.00728
3	0.987	0.98725	-4.64	-4.6366	0.02533	0.07328
4	0.984	0.98413	-4.96	-4.95691	0.01321	0.0623
5	0.972	0.9717	-5.76	-5.76476	0.03086	0.08264

Table 2.8 Analysis of State Vector for IEEE 14-bus system relative to power flow solutions (true measurements).

Bus no.	Voltage magnitude (p.u.)		Voltage phase (degree)		$E_x$ (%)	
	TRUE $ V ^t$	Estimated $ \hat{V} $	TRUE $\delta^t$	Estimated $\hat{\delta}$	$\Delta V $	$\Delta\delta$
1	1.06	1.06071	0	0	0.06698	0
2	1.045	1.04551	-4.98	-4.99057	0.0488	0.21225
3	1.01	1.0105	-12.72	-12.75775	0.0495	0.29678
4	1.019	1.01249	-10.33	-10.2318	0.63886	0.95063
5	1.02	1.0165	-8.78	-8.75767	0.34314	0.25433
6	1.07	1.07042	-14.22	-14.4546	0.03925	1.64979
7	1.062	1.05997	-13.37	-13.25646	0.19115	0.84921
8	1.09	1.09076	-13.36	-13.25655	0.06972	0.77433
9	1.056	1.05337	-14.94	-14.83789	0.24905	0.68347
10	1.051	1.05239	-15.1	-15.04667	0.13225	0.35318
11	1.057	1.05759	-14.79	-14.87054	0.05582	0.54456
12	1.055	1.05389	-15.07	-15.30079	0.10521	1.53145
13	1.05	1.04744	-15.16	-15.33827	0.24381	1.17592
14	1.036	1.03124	-16.04	-16.08195	0.45946	0.26153

Overall, these two networks show that the performance of NRSE is good since the average error for state vector is less than 1 % for both the networks as shown in Tables 2.7 and 2.8. To support the reliability of NRSE, the performance of indices for all tested network are shown in Table 2.9. It can be concluded that the filtering process of the NRSE is acceptable since the ratio of  $J_{est}/J_{meas}$  is less than one.

Table 2.9 Performance Indices

System Bus	$J_{meas}$	$J_{est}$	$R_{ave}$	$R_{max}$	$J_{est}/J_{meas}$
5	0.0115	0.0088	0.0274	0.3861	0.7638
IEEE 14	0.5713	0.2257	0.0881	1.5950	0.3952
IEEE 30	1.0942	0.6221	0.0668	2.0470	0.5685
IEEE 57	1.00E+05	4.76E+04	0.8214	1.65E+03	0.4748
103	1.1473	0.7844	0.0413	6.3426	0.6837
IEEE 118	1.1174	0.5694	0.0006	3.9587	0.5096
IEEE 300	1.0861	0.6455	0.0309	4.6512	0.5943

### 2.5.2 Bad data simulation

The capability of NRSE method is also tested by introducing bad measurements in the measurement set. For each tested network, certain true measurements are randomly selected and are made as bad measurements either by changing the power flow direction or increasing the value of voltage magnitude intentionally as shown in Table 2.10.

To analyze the process of the bad data, the 5-bus system is considered. Three of the 19 measurements are made as bad measurements. At the end of first run of estimation, the measurement with the largest normalized error ( $p_{1-2}$ ) was flagged as a gross error with the normalized residual  $r^N = 124.954$ . After removing  $p_{1-2}$  from the measurement set, a new estimate and  $r^N$  is obtained as shown in Table 2.11. In the second run, the measurement  $P_3$  presenting the largest normalized residual was flagged as bad data since  $r^N > 4$ . The measurement  $P_3$  is deleted from the measurement set. The procedure is repeated and in the final run, the largest normalized residual corresponds to  $P_2$  and is equal to 0.03643. This is less than the threshold 4, meaning that all the bad data has already been eliminated.

Table 2.10 List of bad measurements

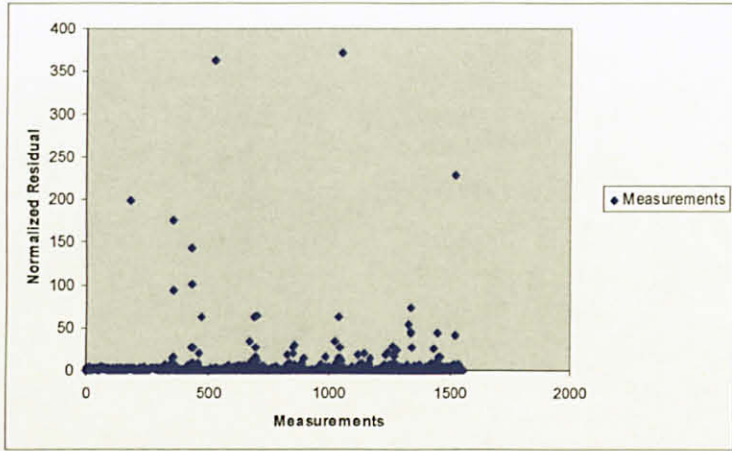
System Bus	Measurements	Measured value	Bad value
5	$p_{1-2}$	0.8933	-0.8933
	$P_3$	-0.45	0.45
	$Q_5$	-0.1	0.1
IEEE 14	$p_{2-3}$	0.7345	-0.7345
	$q_{4-7}$	-0.0656	0.0656
	$V_2$	1.045	2.045
IEEE 30	$q_{14-16}$	0.01628	-0.01628
	$V_2$	1.043	2.043
	$p_{10-17}$	0.07206	-0.07206
IEEE 57	$p_{24-26}$	-0.1018	0.1018
	$q_{30-25}$	-0.0453	0.0453
	$P_{33}$	-0.038	0.038
103	$q_{33-47}$	-0.247	0.247
	$V_{13}$	1.0258	2.0258
	$V_{28}$	1.0148	2.0148
IEEE 118	$P_{96}$	-0.38	0.38
	$p_{80-98}$	0.2895	-0.2895
	$V_{93}$	0.985	1.985
IEEE 300	$p_{235-88}$	-0.247	0.247
	$Q_{192}$	0.4408	-0.4408
	$V_{187}$	0.999	1.999

Table 2.11 Results of normalized residual test for 5-bus system.

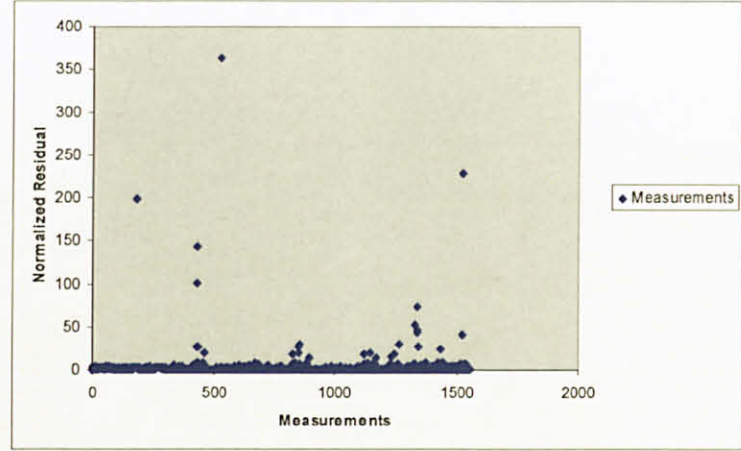
1st. estimation			2nd. estimation			3rd. estimation			4th. estimation		
No.	Meter	$r_i^N$	No.	Meter	$r_i^N$	No.	Meter	$r_i^N$	No.	Meter	$r_i^N$
1	$V_1$	2.83637	1	$V_1$	0.46088	1	$V_1$	0.25838	1	$V_1$	0.00031
2	$V_2$	0.49857	2	$V_2$	0.88274	2	$V_2$	0.49844	2	$V_2$	8.9E-05
3	$V_4$	2.03985	3	$V_4$	0.6918	3	$V_4$	0.16795	3	$V_4$	0.00028
4	$V_5$	1.2611	4	$V_5$	0.21895	4	$V_5$	0.46131	4	$V_5$	0.0002
5	$P_2$	26.0154	5	$P_2$	14.561	5	$P_2$	0.09303	5	$P_2$	0.03643
6	$P_3$	6.8886	6	$P_3$	<b>130.705</b>	6	$P_4$	0.03628	6	$P_4$	0.00921
7	$P_4$	10.3103	7	$P_4$	36.1985	7	$P_5$	0.21779	7	$P_5$	0.00041
8	$P_5$	15.7062	8	$P_5$	25.7285	8	$Q_3$	5.23865	8	$Q_3$	0.00772
9	$Q_3$	6.8911	9	$Q_3$	3.92686	9	$Q_4$	5.33838	9	$Q_4$	0.00353
10	$Q_4$	2.94337	10	$Q_4$	4.37978	10	$Q_5$	<b>5.64828</b>	10	$p_{2-3}$	0.00057
11	$Q_5$	9.31402	11	$Q_5$	5.08892	11	$p_{2-3}$	0.12212	11	$p_{2-1}$	0.0219
12	$p_{1-2}$	<b>124.954</b>	12	$p_{2-3}$	22.4187	12	$p_{2-1}$	0.03992	12	$p_{4-2}$	0.00017
13	$p_{2-3}$	25.1729	13	$p_{2-1}$	21.4039	13	$p_{4-2}$	0.09846	13	$q_{1-3}$	0.00016
14	$p_{2-1}$	111.403	14	$p_{4-2}$	13.9433	14	$q_{1-3}$	0.73014	14	$q_{4-5}$	4.1E-05
15	$p_{4-2}$	20.6225	15	$q_{1-3}$	1.42059	15	$q_{4-5}$	3.44295	15	$q_{3-1}$	0.00029
16	$q_{1-3}$	9.15492	16	$q_{4-5}$	2.07546	16	$q_{3-1}$	0.61621	16	$q_{5-4}$	5.5E-05
17	$q_{4-5}$	4.0057	17	$q_{3-1}$	2.42974	17	$q_{5-4}$	3.35333			
18	$q_{3-1}$	3.14029	18	$q_{5-4}$	3.8929						
19	$q_{5-4}$	3.80776									

The same procedure is applied to other tested systems. Figure 2.6 shows the normalized residual of measurement in IEEE 300-bus system. At the end of first estimation, the measurement with the largest normalized error ( $p_{235-88}$ ) was flagged as a gross error, as seen from Figure 2.6 (a). After removing  $p_{235-88}$  from the measurement set, a new estimate and  $r^N$  is obtained as shown in Figure 2.6 (b). The largest normalized residual measurement on the second estimation is detected on measurement  $Q_{192}$ . Meanwhile in the third estimation it is obvious that only one measurement where the normalized residual is too large compared with the others (see Figure 2.6 (c)), which is  $V_{187}$ . Figure 2.6 (d) shows that no measurements are considered as bad measurement since  $r^N > 4$ . The summarized results of all the tested networks are tabulated in Table 2.12. In this way, the  $\chi^2$ -test and normalized residual test method are followed to detect, to identify and to eliminate the all the bad data in the measurement set.





(a)



(b)

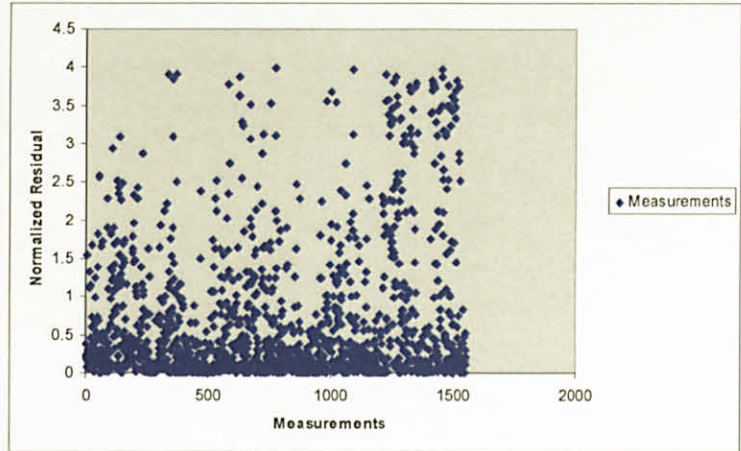
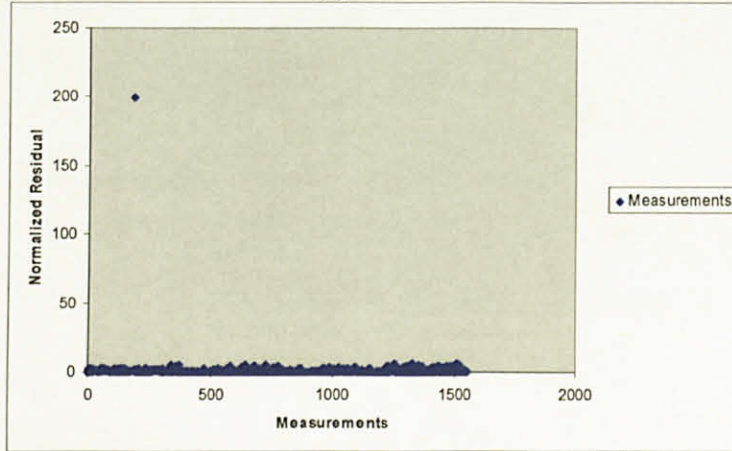


Figure 2.6 (a), (b), (c) &amp; (d)

The Graph of Normalized Residual vs Measurements for the 1<sup>st</sup>, 2<sup>nd</sup>, 3<sup>rd</sup> and final estimation process of IEEE 300-bus system

Table 2.12 The summarized results of the bad data.

System Bus	1st. estimation				2nd. estimation				3rd. estimation				4th. estimation		
	Bad	$r_i^N$	$J(x)$	$\chi^2$	Bad	$r_i^N$	$J(x)$	$\chi^2$	Bad	$r_i^N$	$J(x)$	$\chi^2$	Bad	$J(x)$	$\chi^2$
5	$P_{1-2}$ $P_3$ $Q_5$	124.9537 6.888602 9.314016	17081.1	18.307	$P_3$ $Q_5$	130.705 5.08892	1434.31	16.919	$Q_5$	5.64828	31.9545	15.5073	None	0.00026	14.0671
IEEE 14	$P_{2-3}$ $q_{4-7}$ $V_2$	376.3426 298.04 200.2217	263413	38.8851	$q_{4-7}$ $V_2$	298.807 203.739	121843	37.6525	$V_2$	181.165	32836.9	36.415	None	11.7089	35.1725
IEEE 24	$P_{2-6}$ $P_8$ $V_9$	366.4456 357.8881 204.8949	302830	66.3386	$P_8$ $V_9$	358.097 200.933	168525	65.1708	$V_9$	200.604	40291.6	64.0011	None	42.3958	62.8296
IEEE 30	$Q_{19}$ $q_{26-25}$ $P_{10}$	348.9799 325.243 100.3271	237962	174.101	$q_{26-25}$ $P_{10}$	325.238 100.767	116120	173.004	$P_{10}$	100.836	10265.8	171.907	None	155.689	170.809
IEEE 57	$q_{30-25}$ $p_{24-26}$ $P_{33}$	382.3044 281.5742 334.573	337607	225.329	$P_{33}$ $p_{24-26}$	333.295 282.07	191533	224.245	$p_{24-26}$	282.978	80267.3	223.16	None	190.912	222.076
103	$V_{13}$ $V_{28}$ $q_{33-47}$	100.8082 95.79497 17.54758	20095.3	630.845	$V_{28}$ $q_{33-47}$	95.795 17.5393	9932.93	629.796	$q_{33-47}$	17.5714	755.097	628.748	None	445.529	627.699
IEEE 118	$P_{96}$ $P_{80-98}$ $V_{93}$	341.1776 335.0865 203.4906	283363.2	331.786	$P_{80-98}$ $V_{93}$	355.7137 202.304	166958.06	330.717	$V_{93}$	200.3235	40424.044	329.649	None	294.120	328.580
IEEE 300	$p_{235-88}$ $Q_{192}$ $V_{187}$	371.2231 363.5065 198.4898	310765.4	1029.042	$Q_{192}$ $V_{187}$	363.3409 198.3559	172954.31	1028.005	$V_{187}$	199.825	40928.742	1026.967	None	999.056	1025.929

## 2.6 Summary

The SE software currently used in a local utility company is studied and the findings are discussed in this chapter. Some of the drawbacks of this software can result in inaccurate final estimate. Thus, there is a dire need for developing an improved SE software. A more efficient SE package is developed in this thesis using Matlab 7.0 and the programs are run on a Pentium-III processor.

The NRSE package thus developed is tested on several IEEE systems up to a size of 300-bus, in addition to 103-bus SESB system. Since the final estimates obtained on the test systems are close to the actual values, the accuracy of the developed NRSE package is considered acceptable. From the performance indices computed for different tested systems, it is shown that the filtering process incorporated in this NRSE package is also quite acceptable. It is demonstrated that the normalized residual test in this NRSE package is capable of detecting and identifying the bad data correctly. Thus, the developed package is found robust, more efficient and suitable for conducting SE on large power systems. In the chapters to come, while illustrating certain new techniques developed, the results obtained through this NRSE method are used for the purpose of comparison.

In spite of several advantages of NRSE method, the computational effort required still remains as a hurdle, particularly while dealing with the large power networks. More computer time is required due to enormous amount of calculations involved in computing the Jacobian matrix. Alternate method of getting the Jacobian matrix, with the aim of reducing computer time, is attempted in the next chapter.

## CHAPTER 3

# NEWTON RAPHSON STATE ESTIMATION EMPLOYING SYSTEMATICALLY CONSTRUCTED JACOBIAN MATRIX

### 3.1 Introduction

In SE, the process of creating and updating the Jacobian matrix is a significantly time consuming step which requires a large number of floating point multiplication, especially in large scale power system networks. Due to that, Fred Schweppe *et. al.* had modified the basic WLS algorithm for real time application in large scale power system [9]. In that paper, the constant gain and Jacobian matrices are used in order to reduce the computational time. However, WLS processing could still need a longer time for medium to large networks and becomes even longer in the presence of multiple data with gross error and bad data processing. Since then, several different alternatives to the WLS approach have been investigated. Among the algorithms developed and implemented in real time are sequential estimators, orthogonal transformation methods, hybrid method and fast decoupled estimators [8, 10 and 38]. Almost all the algorithms are mainly developed to provide computational efficiency both in terms of computing time and storage requirements.

Fast Decoupled State Estimator (FDSE) [1, 8 and 15] is based on the assumptions that in practical power system networks, under steady-state, real power flows are less sensitive to voltage magnitudes and are more sensitive to voltage phase angles, while reactive power flows are less sensitive to voltage phase angles and are more sensitive to voltage magnitudes. Using these properties, the sub-matrices  $\mathbf{H}_{P,V}$ ,  $\mathbf{H}_{Pij,V}$ ,  $\mathbf{H}_{Pji,V}$ ,  $\mathbf{H}_{Q,\delta}$ ,  $\mathbf{H}_{Qij,\delta}$  and  $\mathbf{H}_{Qji,\delta}$  are neglected. Because of the approximations made, the corrections on the voltages computed in each iteration are less accurate. This results in poor convergence characteristic. Nowadays, with the advent of fast computers,

even huge amount of complex calculations can be carried out very efficiently in much lesser time. Therefore, there is no need to go for approximate models.

Newton-Raphson State Estimator (NRSE) method [3, 15, 39 and 40] is more popular because of exact problem formulation and very good convergence characteristic. In NRSE method, elements of Jacobian matrix are computed from the standard expressions which are functions of bus voltages, bus powers and elements of bus admittance matrix. For on-line SE, particularly for large scale power systems, the computational time is very crucial. The reduction of the computation burden that fit with normal equation of SE needs further investigation.

A simple algorithm to construct the  $H$  matrix is presented in this chapter. This algorithm can be easily fit into the Newton Raphson State Estimation (NRSE) method. In the proposed algorithm, the network elements are processed one-by-one and the  $H$  matrix is updated in a simple manner. The final  $H$  matrix, thus constructed is exactly the same as that obtained in the available NRSE method. The details of the proposed algorithm are discussed in the following sections. The SE method presented in this chapter makes use of the constructed Jacobian matrix and hence called as the State Estimation using constructed Jacobian (SECJ).

### 3.2 General Structure of $H$ Matrix

The SE Jacobian  $H$ , is not a square matrix. The  $H$  matrix always has  $(2N - 1)$  columns, where  $N$  is equal to the number of buses. The number of rows in  $H$  matrix is equal to number of measurements available. For full measurement set, number of rows will be equal to  $(3N + 4B)$  where  $B$  is number of lines. The elements of  $H$  are the partial derivatives of bus voltage magnitudes, bus powers and line flows with respect to state variables  $\delta$  and  $V$ . The general structure of  $H$  matrix is as in equation (3.1). In equation (3.1) the  $H_{V,\delta}$ ,  $H_{V,V}$ ,  $H_{Pij,\delta}$ ,  $H_{Pij,V}$ ,  $H_{Pji,\delta}$ ,  $H_{Pji,V}$ ,  $H_{Qij,\delta}$ ,  $H_{Qij,V}$ ,  $H_{Qji,\delta}$ ,  $H_{Qji,V}$ ,  $H_{P,\delta}$ ,  $H_{P,V}$ ,  $H_{Q,\delta}$  and  $H_{Q,V}$  are the sub-matrices of the Jacobian matrix. The first suffix indicates the available measurement and the second suffix indicates the variable on which the partial derivatives are obtained. The constructional details of the SE sub-matrices are discussed in Section 3.4.

$$\begin{array}{c}
\begin{array}{c}
\delta_2 \quad \delta_3 \quad \dots \quad \delta_N \quad V_1 \quad V_2 \quad \dots \quad V_N \\
\left[ \begin{array}{ccc|ccc}
\frac{\partial |V_1|}{\partial \delta_2} & \frac{\partial |V_1|}{\partial \delta_3} & \dots & \frac{\partial |V_1|}{\partial \delta_N} & \frac{\partial |V_1|}{\partial V_1} & \frac{\partial |V_1|}{\partial V_2} & \dots & \frac{\partial |V_1|}{\partial V_N} \\
\frac{\partial |V_2|}{\partial \delta_2} & \frac{\partial |V_2|}{\partial \delta_3} & \dots & \frac{\partial |V_2|}{\partial \delta_N} & \frac{\partial |V_2|}{\partial V_1} & \frac{\partial |V_2|}{\partial V_2} & \dots & \frac{\partial |V_2|}{\partial V_N} \\
\vdots & \vdots & \dots & \vdots & \vdots & \vdots & \dots & \vdots \\
\frac{\partial |V_N|}{\partial \delta_2} & \frac{\partial |V_N|}{\partial \delta_3} & \dots & \frac{\partial |V_N|}{\partial \delta_N} & \frac{\partial |V_N|}{\partial V_1} & \frac{\partial |V_N|}{\partial V_2} & \dots & \frac{\partial |V_N|}{\partial V_N}
\end{array} \right] & \mathbf{H}_{V,\delta} & \mathbf{H}_{V,V} \\
\hline
\begin{array}{c}
\vdots \\
\dots \quad \frac{\partial p_{ij}}{\partial \delta_i} \quad \dots \quad \frac{\partial p_{ij}}{\partial \delta_j} \quad \dots \\
\vdots
\end{array} & \mathbf{H}_{p_{ij},\delta} & \mathbf{H}_{p_{ij},V} \\
\hline
\begin{array}{c}
\vdots \\
\dots \quad \frac{\partial p_{ji}}{\partial \delta_i} \quad \dots \quad \frac{\partial p_{ji}}{\partial \delta_j} \quad \dots \\
\vdots
\end{array} & \mathbf{H}_{p_{ji},\delta} & \mathbf{H}_{p_{ji},V} \\
\hline
\begin{array}{c}
\vdots \\
\dots \quad \frac{\partial q_{ij}}{\partial \delta_i} \quad \dots \quad \frac{\partial q_{ij}}{\partial \delta_j} \quad \dots \\
\vdots
\end{array} & \mathbf{H}_{q_{ij},\delta} & \mathbf{H}_{q_{ij},V} \\
\hline
\begin{array}{c}
\vdots \\
\dots \quad \frac{\partial q_{ji}}{\partial \delta_i} \quad \dots \quad \frac{\partial q_{ji}}{\partial \delta_j} \quad \dots \\
\vdots
\end{array} & \mathbf{H}_{q_{ji},\delta} & \mathbf{H}_{q_{ji},V} \\
\hline
\begin{array}{ccc|ccc}
\frac{\partial P_1}{\partial \delta_2} & \frac{\partial P_1}{\partial \delta_3} & \dots & \frac{\partial P_1}{\partial \delta_N} & \frac{\partial P_1}{\partial V_1} & \frac{\partial P_1}{\partial V_2} & \dots & \frac{\partial P_1}{\partial V_N} \\
\frac{\partial P_2}{\partial \delta_2} & \frac{\partial P_2}{\partial \delta_3} & \dots & \frac{\partial P_2}{\partial \delta_N} & \frac{\partial P_2}{\partial V_1} & \frac{\partial P_2}{\partial V_2} & \dots & \frac{\partial P_2}{\partial V_N} \\
\vdots & \vdots & \dots & \vdots & \vdots & \vdots & \dots & \vdots \\
\frac{\partial P_N}{\partial \delta_2} & \frac{\partial P_N}{\partial \delta_3} & \dots & \frac{\partial P_N}{\partial \delta_N} & \frac{\partial P_N}{\partial V_1} & \frac{\partial P_N}{\partial V_2} & \dots & \frac{\partial P_N}{\partial V_N}
\end{array} & \mathbf{H}_{P,\delta} & \mathbf{H}_{P,V} \\
\hline
\begin{array}{ccc|ccc}
\frac{\partial Q_1}{\partial \delta_2} & \frac{\partial Q_1}{\partial \delta_3} & \dots & \frac{\partial Q_1}{\partial \delta_N} & \frac{\partial Q_1}{\partial V_1} & \frac{\partial Q_1}{\partial V_2} & \dots & \frac{\partial Q_1}{\partial V_N} \\
\frac{\partial Q_2}{\partial \delta_2} & \frac{\partial Q_2}{\partial \delta_3} & \dots & \frac{\partial Q_2}{\partial \delta_N} & \frac{\partial Q_2}{\partial V_1} & \frac{\partial Q_2}{\partial V_2} & \dots & \frac{\partial Q_2}{\partial V_N} \\
\vdots & \vdots & \dots & \vdots & \vdots & \vdots & \dots & \vdots \\
\frac{\partial Q_N}{\partial \delta_2} & \frac{\partial Q_N}{\partial \delta_3} & \dots & \frac{\partial Q_N}{\partial \delta_N} & \frac{\partial Q_N}{\partial V_1} & \frac{\partial Q_N}{\partial V_2} & \dots & \frac{\partial Q_N}{\partial V_N}
\end{array} & \mathbf{H}_{Q,\delta} & \mathbf{H}_{Q,V}
\end{array}
\end{array} \tag{3.1}$$

### 3.3 Power Flow Network Elements

A transmission network usually consists of transmission lines, transformers and shunt parameters. In the NRSE method, the transmission network is represented by the bus admittance matrix and the elements of the  $H$  matrix are computed using the elements of bus admittance matrix. The formula for Jacobian matrix formulation indicates that each element of the Jacobian matrix is contributed by the partial derivatives of the power flows in the network elements [41-42].

Consider a general transmission network element between buses  $i$  and  $j$ , as shown in Figure 2.1. For such a general transmission network element, the real and reactive power flows are given as in equation (2.5) to (2.8) in Chapter 2. All the line flows computed from equation (2.5) to (2.8) are stored in the real power and reactive power matrix as in equation (3.2) and (3.3) from which bus powers can be calculated.

$$\mathbf{P} = \begin{bmatrix} 0 & p_{12} & p_{13} & \cdots & p_{1N} \\ p_{21} & 0 & p_{23} & \cdots & p_{2N} \\ p_{31} & p_{32} & 0 & \cdots & p_{3N} \\ \vdots & \vdots & \vdots & \vdots & \vdots \\ p_{N1} & p_{N2} & p_{N3} & \cdots & 0 \end{bmatrix} \quad (3.2)$$

$$\mathbf{Q} = \begin{bmatrix} 0 & q_{12} & q_{13} & \cdots & q_{1N} \\ q_{21} & 0 & q_{23} & \cdots & q_{2N} \\ q_{31} & q_{32} & 0 & \cdots & q_{3N} \\ \vdots & \vdots & \vdots & \vdots & \vdots \\ q_{N1} & q_{N2} & q_{N3} & \cdots & 0 \end{bmatrix} \quad (3.3)$$

The real and reactive power flows in line  $i$ - $j$  depend on  $\delta_i$ ,  $\delta_j$ ,  $V_i$  and  $V_j$ . The partial derivatives of  $p_{ij}$ ,  $p_{ji}$ ,  $q_{ij}$  and  $q_{ji}$  with respect to  $\delta_i$ ,  $\delta_j$ ,  $V_i$  and  $V_j$  can be derived from equations (2.5) to (2.8).

### 3.4 Construction of SE Jacobian Matrix, $H$

All the elements of  $H$  matrix are partial derivatives of available measurements with respect to  $\delta$  and  $V$ . The elements of sub-matrices  $H_{V,\delta}$ ,  $H_{V,V}$  are given by

$$\mathbf{H}_{V_i, \delta_j} = \frac{\partial V_i}{\partial \delta_j} = 0 \quad \left| \text{for all } i \text{ and } j \right. \quad (3.4)$$

$$\left. \begin{aligned} \mathbf{H}_{V_i, V_j} &= \frac{\partial V_i}{\partial V_j} = 0 & \left| i \neq j \right. \\ \mathbf{H}_{V_i, V_i} &= \frac{\partial V_i}{\partial V_i} = 1 \end{aligned} \right\} \quad (3.5)$$

If at particular bus, the voltmeter is not available, the row corresponding to that particular bus will be deleted.

Using equation (2.5) to (2.8) the expression for the partial derivatives of  $p_{ij}$ ,  $p_{ji}$ ,  $q_{ij}$  and  $q_{ji}$  with respect to  $\delta_i$ ,  $\delta_j$ ,  $V_i$  and  $V_j$  are obtained. Thus

$$\frac{\partial p_{ij}}{\partial \delta_i} = \frac{V_i V_j}{a} (g_{ij} \sin \delta_{ij} - b_{ij} \cos \delta_{ij}) \quad (3.6)$$

$$\frac{\partial p_{ij}}{\partial \delta_j} = -\frac{V_i V_j}{a} (g_{ij} \sin \delta_{ij} - b_{ij} \cos \delta_{ij}) \quad (3.7)$$

$$\frac{\partial p_{ij}}{\partial V_i} = 2V_i \left( \frac{g_{ij}}{a^2} + g_{shi} \right) - \frac{V_j}{a} (g_{ij} \cos \delta_{ij} + b_{ij} \sin \delta_{ij}) \quad (3.8)$$

$$\frac{\partial p_{ij}}{\partial V_j} = -\frac{V_i}{a} (g_{ij} \cos \delta_{ij} + b_{ij} \sin \delta_{ij}) \quad (3.9)$$

$$\frac{\partial p_{ji}}{\partial \delta_i} = \frac{V_i V_j}{a} (g_{ij} \sin \delta_{ij} + b_{ij} \cos \delta_{ij}) \quad (3.10)$$

$$\frac{\partial p_{ji}}{\partial \delta_j} = -\frac{V_i V_j}{a} (g_{ij} \sin \delta_{ij} + b_{ij} \cos \delta_{ij}) \quad (3.11)$$

$$\frac{\partial p_{ji}}{\partial V_i} = -\frac{V_j}{a} (g_{ij} \cos \delta_{ij} - b_{ij} \sin \delta_{ij}) \quad (3.12)$$

$$\frac{\partial p_{ji}}{\partial V_j} = 2V_j (g_{ij} + g_{shj}) - \frac{V_i}{a} (g_{ij} \cos \delta_{ij} - b_{ij} \sin \delta_{ij}) \quad (3.13)$$

$$\frac{\partial q_{ij}}{\partial \delta_i} = -\frac{V_i V_j}{a} (g_{ij} \cos \delta_{ij} + b_{ij} \sin \delta_{ij}) \quad (3.14)$$

$$\frac{\partial q_{ij}}{\partial \delta_j} = \frac{V_i V_j}{a} (g_{ij} \cos \delta_{ij} + b_{ij} \sin \delta_{ij}) \quad (3.15)$$



$$\frac{\partial q_{ij}}{\partial V_i} = -2V_i \left( \frac{b_{ij}}{a^2} + b_{sh_i} \right) - \frac{V_j}{a} (g_{ij} \sin \delta_{ij} - b_{ij} \cos \delta_{ij}) \quad (3.16)$$

$$\frac{\partial q_{ij}}{\partial V_j} = -\frac{V_i}{a} (g_{ij} \sin \delta_{ij} - b_{ij} \cos \delta_{ij}) \quad (3.17)$$

$$\frac{\partial q_{ji}}{\partial \delta_i} = \frac{V_i V_j}{a} (g_{ij} \cos \delta_{ij} - b_{ij} \sin \delta_{ij}) \quad (3.18)$$

$$\frac{\partial q_{ji}}{\partial \delta_j} = -\frac{V_i V_j}{a} (g_{ij} \cos \delta_{ij} - b_{ij} \sin \delta_{ij}) \quad (3.19)$$

$$\frac{\partial q_{ji}}{\partial V_i} = \frac{V_j}{a} (g_{ij} \sin \delta_{ij} + b_{ij} \cos \delta_{ij}) \quad (3.20)$$

$$\frac{\partial q_{ji}}{\partial V_j} = -2V_j (b_{ij} + b_{sh_j}) + \frac{V_i}{a} (g_{ij} \sin \delta_{ij} + b_{ij} \cos \delta_{ij}) \quad (3.21)$$

To construct the  $\mathbf{H}$  matrix, initially all its elements are set to zero. Network elements are considered one-by-one. For the element between buses  $i$ - $j$ , the partial derivatives of line flows with respect to  $\delta_i$ ,  $\delta_j$ ,  $V_i$  and  $V_j$  are computed using equations (3.6) to (3.21). These values are simply added to the corresponding elements of sub-matrices  $\mathbf{H}_{pij, \delta_i}$ ,  $\mathbf{H}_{pij, \delta_j}$ ,  $\mathbf{H}_{pij, V_i}$ ,  $\mathbf{H}_{pij, V_j}$ ,  $\mathbf{H}_{pji, \delta_i}$ ,  $\mathbf{H}_{pji, \delta_j}$ ,  $\mathbf{H}_{pji, V_i}$ ,  $\mathbf{H}_{pji, V_j}$ ,  $\mathbf{H}_{qij, \delta_i}$ ,  $\mathbf{H}_{qij, \delta_j}$ ,  $\mathbf{H}_{qij, V_i}$ ,  $\mathbf{H}_{qij, V_j}$ ,  $\mathbf{H}_{qji, \delta_i}$ ,  $\mathbf{H}_{qji, \delta_j}$ ,  $\mathbf{H}_{qji, V_i}$  and  $\mathbf{H}_{qji, V_j}$ .

Sub-matrices  $\mathbf{H}_{P, \delta}$ ,  $\mathbf{H}_{P, V}$ ,  $\mathbf{H}_{Q, \delta}$  and  $\mathbf{H}_{Q, V}$  are now considered. Partial derivatives of bus powers can be expressed in terms of partial derivatives of line flows. To illustrate this, let  $i$ - $j$ ,  $i$ - $k$  and  $i$ - $m$  be the elements connected at bus  $i$ . Then the bus powers  $P_i$  and  $Q_i$  are given by

$$P_i = p_{ij} + p_{ik} + p_{im} \quad (3.22)$$

$$Q_i = q_{ij} + q_{ik} + q_{im} \quad (3.23)$$

Therefore

$$\frac{\partial P_i}{\partial \delta_i} = \frac{\partial p_{ij}}{\partial \delta_i} + \frac{\partial p_{ik}}{\partial \delta_i} + \frac{\partial p_{im}}{\partial \delta_i} \quad (3.24)$$

$$\frac{\partial Q_i}{\partial \delta_i} = \frac{\partial q_{ij}}{\partial \delta_i} + \frac{\partial q_{ik}}{\partial \delta_i} + \frac{\partial q_{im}}{\partial \delta_i} \quad (3.25)$$

Similar expressions can be written for other partial derivatives of  $P_i$  and  $Q_i$  with respect to  $\delta_j$ ,  $V_i$  and  $V_j$ . Likewise, considering bus powers  $P_j$  and  $Q_j$ , partial derivatives of  $P_j$  and  $Q_j$  can also be obtained in terms of partial derivatives of line flows in the lines connected to bus  $j$ . It is to be noted that the partial derivatives of the line flows contribute to the partial derivatives of bus powers. Table 3.1 shows a few partial derivatives of line flows and the corresponding partial derivative of bus powers to which it contributes.

Table 3.1 Partial Derivatives of Line Flows and the Corresponding Partial Derivatives of Bus Powers.

Partial Derivatives of	
Line flows	Bus Power
$\frac{\partial p_{ij}}{\partial \delta_i}, \frac{\partial p_{ji}}{\partial \delta_j}, \frac{\partial q_{ij}}{\partial V_i}, \frac{\partial q_{ji}}{\partial V_j}$	$\frac{\partial P_i}{\partial \delta_i}, \frac{\partial P_j}{\partial \delta_j}, \frac{\partial Q_i}{\partial V_i}, \frac{\partial Q_j}{\partial V_j}$

The partial derivatives of  $\frac{\partial p_{ij}}{\partial \delta_i}, \frac{\partial p_{ij}}{\partial \delta_j}, \frac{\partial p_{ij}}{\partial V_i}, \frac{\partial p_{ij}}{\partial V_j}$  will contribute to

$\frac{\partial P_i}{\partial \delta_i}, \frac{\partial P_i}{\partial \delta_j}, \frac{\partial P_i}{\partial V_i}, \frac{\partial P_i}{\partial V_j}$  respectively. Similar results are true for  $p_{ji}$ ,  $q_{ij}$  and  $q_{ji}$ . Those

values will be added to the corresponding elements of  $H_{P,\delta}$ ,  $H_{P,V}$ ,  $H_{Q,\delta}$  and  $H_{Q,V}$ . This process is repeated for all the network elements. Once all the network elements are added, the final  $H$  matrix is completed.

### 3.5 Computing and Recording Only the Required Partial Derivatives Alone

The  $H$  matrix will have  $3N+4B$  number of rows if all possible measurements are available in the network. However, in practice, number of available measurements will be much less. Instead of computing elements of rows corresponding to unavailable measurements and then deleting them, proper logics can be adopted to compute and record only the required partial derivatives alone. When line  $i-j$  is processed, it may not be always necessary to compute all the 16 partial derivatives

given by equation (3.6) to (3.21). The partial derivatives  $\frac{\partial p_{ij}}{\partial \delta_i}, \frac{\partial p_{ij}}{\partial \delta_j}, \frac{\partial p_{ij}}{\partial V_i}$  and  $\frac{\partial p_{ij}}{\partial V_j}$

are to be computed only when  $p_{ij}$  or  $P_i$  or both  $p_{ij}$  and  $P_i$  are in the available

measurement list. Thus, the following three cases are possible.

**CASE 1:**  $p_{ij}$  is an available measurement. The four partial derivatives are entered in the row corresponding to  $p_{ij}$ .

**CASE 2:**  $P_i$  is an available measurement. The four partial derivatives are added to previous values in the row corresponding to  $P_i$ .

**CASE 3:**  $p_{ij}$  and  $P_i$  are available measurements. The four partial derivatives are entered in the row corresponding to  $p_{ij}$  and added to previous values in the row corresponding to  $P_i$ .

Such logics are to be followed for  $\frac{\partial p_{ji}}{\partial \delta_i}, \frac{\partial p_{ji}}{\partial \delta_j}, \frac{\partial p_{ji}}{\partial V_i}, \frac{\partial p_{ji}}{\partial V_j}; \frac{\partial q_{ij}}{\partial \delta_i}, \frac{\partial q_{ij}}{\partial \delta_j}, \frac{\partial q_{ij}}{\partial V_i}, \frac{\partial q_{ij}}{\partial V_j}$

and  $\frac{\partial q_{ji}}{\partial \delta_i}, \frac{\partial q_{ji}}{\partial \delta_j}, \frac{\partial q_{ji}}{\partial V_i}, \frac{\partial q_{ji}}{\partial V_j}$  also.

### 3.5.1 Application example to illustrate the construction of Jacobian matrix $H$

The three bus power system [3], shown in Figure 3.1, is used to illustrate the construction of Jacobian matrix  $H$ . In this system, bus 1 is the slack bus and the tap setting “ $a$ ” for all lines are 1. With the network data as listed in Table 3.2 and the available measurements as listed in Table 3.3, the Jacobian matrix  $H$  is constructed as discussed in Section 3.4, taking the initial bus voltages as  $V_1 = V_2 = V_3 = 1.0 \angle 0^\circ$ .

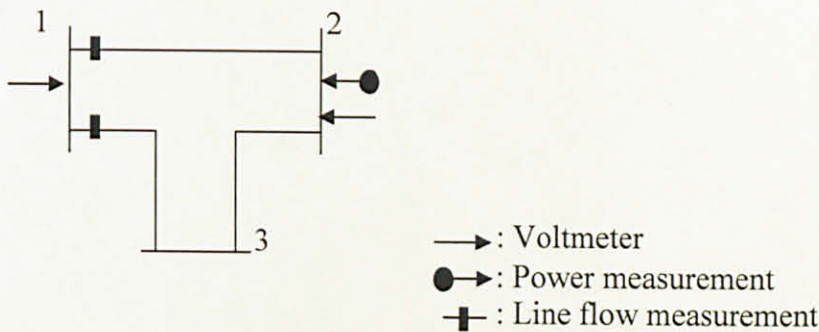


Figure 3.1 Single-line diagram and measurement configuration of a 3-bus power system.

Table 3.2 Network data for 3-bus system

Line		R (p.u.)	X (p.u.)	Total Line Charging Susceptance B (p.u.)
From Bus	To Bus			
1	2	0.01	0.03	0
1	3	0.02	0.05	0
2	3	0.03	0.08	0

Table 3.3 Available measurements for 3-bus system

Measurements	Value (p.u.)	Weightage
$V_1$	1.006	62500
$V_2$	0.968	62500
$p_{12}$	0.888	15625
$p_{13}$	1.173	15625
$q_{12}$	0.568	15625
$q_{13}$	0.663	15625
$P_2$	-0.501	10000
$Q_2$	-0.286	10000

Noting that  $V_1$  and  $V_2$  are available measurements, the sub-matrices of  $H_{V,\delta}$ ,  $H_{V,V}$  are obtained as

$$\begin{bmatrix} H_{V_1,\delta} & H_{V_1,V} \\ H_{V_2,\delta} & H_{V_2,V} \end{bmatrix} = \begin{bmatrix} 0 & 0 & 0 & 1 & 0 & 0 \\ 0 & 0 & 0 & 0 & 1 & 0 \end{bmatrix}$$

where  $\delta$  spans from  $\delta_1, \delta_2$  to  $\delta_3$  and  $V$  spans from  $V_1, V_2$  to  $V_3$ .

To illustrate all the stages of constructing the other sub-matrices of the network elements are added one by one as shown below:-

#### Iteration 1

**Element 1-2 is added.** The line flow measurements corresponding to this element are  $p_{12}, p_{21}, q_{12}$  and  $q_{21}$ . All these measurements are categorized according to the three different cases as in Section 3.5. The  $p_{12}$  will be categorized as CASE 1 since this measurement is one of the available measurements and  $P_1$  is not an available measurement. Similarly,  $q_{12}$  is also categorized as CASE 1. However,  $p_{21}$  and  $q_{21}$  are categorized as CASE 2 since these measurements will contribute to  $P_2$  and  $Q_2$  respectively; but they are not listed as the available measurements. The new constructed sub-matrices are:

The final  $H$  matrix will be the combination of all the sub-matrices with the column corresponding to slack bus being deleted. Thus the constructed Jacobian matrix  $H$  in the first iteration is

$$H = \begin{bmatrix} 0 & 0 & 1 & 0 & 0 \\ 0 & 0 & 0 & 1 & 0 \\ -30 & 0 & 10 & -10 & 0 \\ 0 & -17.24 & 6.89 & 0 & -6.89 \\ 10 & 0 & 30 & -30 & 0 \\ 0 & 6.89 & 17.24 & 0 & -17.24 \\ 40.96 & -10.96 & -10 & 14.11 & -4.11 \\ -14.11 & 4.11 & -30 & 40.96 & -10.96 \end{bmatrix}$$

Using the above  $H$  matrix, state variables are updated as  $V_1 = 0.9997 \angle 0^\circ$ ;  $V_2 = 0.9743 \angle -1.20^\circ$ ;  $V_3 = 0.9428 \angle -2.58^\circ$ .

All the above stages are repeated until the convergence is obtained in iteration 3 with the final state variables values as  $V_1 = 0.9996 \angle 0^\circ$ ;  $V_2 = 0.9741 \angle -1.25^\circ$ ;  $V_3 = 0.9439 \angle -2.75^\circ$ . These estimates are the same as obtained in the NRSE method [3].

The suggested procedure is also tested on several other standard systems, the largest being the IEEE 300-bus system. The final estimates obtained for the system agree with those obtained by NRSE method. The details are discussed in the following section.

### 3.6 Simulation Results

The proposed SECJ method is successfully tested on 5-bus, IEEE 14-bus, IEEE 30-bus, IEEE 57-bus, 103-bus, IEEE 118-bus and IEEE 300-bus system. The required Jacobian matrices are constructed using the algorithm discussed earlier. In order to prove the superiority of the SECJ method, the test results are compared with results obtained using NRSE method.

The final estimates of the SECJ method are compared with the actual values from power flow solution and the final estimates obtained from the NRSE method for the 5-bus system, IEEE 14-bus, IEEE 30-bus, IEEE 57-bus, 103-bus, IEEE 118-bus and IEEE 300-bus system. It is to be noticed that the final estimates of the SECJ method are exactly the same as those obtained in the NRSE method. The SECJ method deviates from the NRSE method only in the procedure of getting the SECJ Jacobian matrix,  $H$ . Therefore, the performance indices of the overall SECJ method are exactly the same as discussed in Chapter 2.

On the other hand, it is to be seen that the SECJ method is significantly advantageous in terms of computer processing time. Table 3.4 shows the computer time for different stages of computation process. Noted that the overall algorithm is developed using Matlab 7.0 and the program run on computer with the CPU time is 504 MB of Ram and the speed of CPU is Pentium(R) 3.40 GHz. For the sake of analysis, the tabulated data in Table 3.4 are converted in terms of graphical figure as shown in Figure 3.2 to 3.4. It is clearly seen that processor time increases considerably when size of network become larger. This is true for the both methods. However, comparing the two methods, the SECJ method needs significantly less processor time than that of the NRSE method in particular when the size of network becomes larger.

Table 3.4 NRSE vs SECJ methods – computer processing time

System bus	NRSE method			SECJ method		
	<i>H</i> time sec	<i>G</i> time sec	Completed Process sec	<i>H</i> time sec	<i>G</i> time sec	Completed Process sec
5	0.0313	0.1875	0.3281	0.1563	0.5156	0.6563
IEEE 14	0.0313	0.2188	0.3750	0.2656	0.6563	0.7969
IEEE 30	0.0313	0.3281	0.5625	0.2813	0.7656	0.9844
IEEE 57	0.1094	0.9844	1.3750	0.4844	1.3281	1.7188
103	1.2188	8.1563	13.7031	0.5000	3.3125	7.8438
IEEE 118	1.5156	11.2500	15.3750	0.2969	4.5625	7.4375
IEEE 300	25.1719	227.7969	303.2500	4.2500	83.3281	137.0781

**Note :** *H* time is the time taken to build Jacobian Matrix; *G* time is the time taken to build the Gain Matrix.

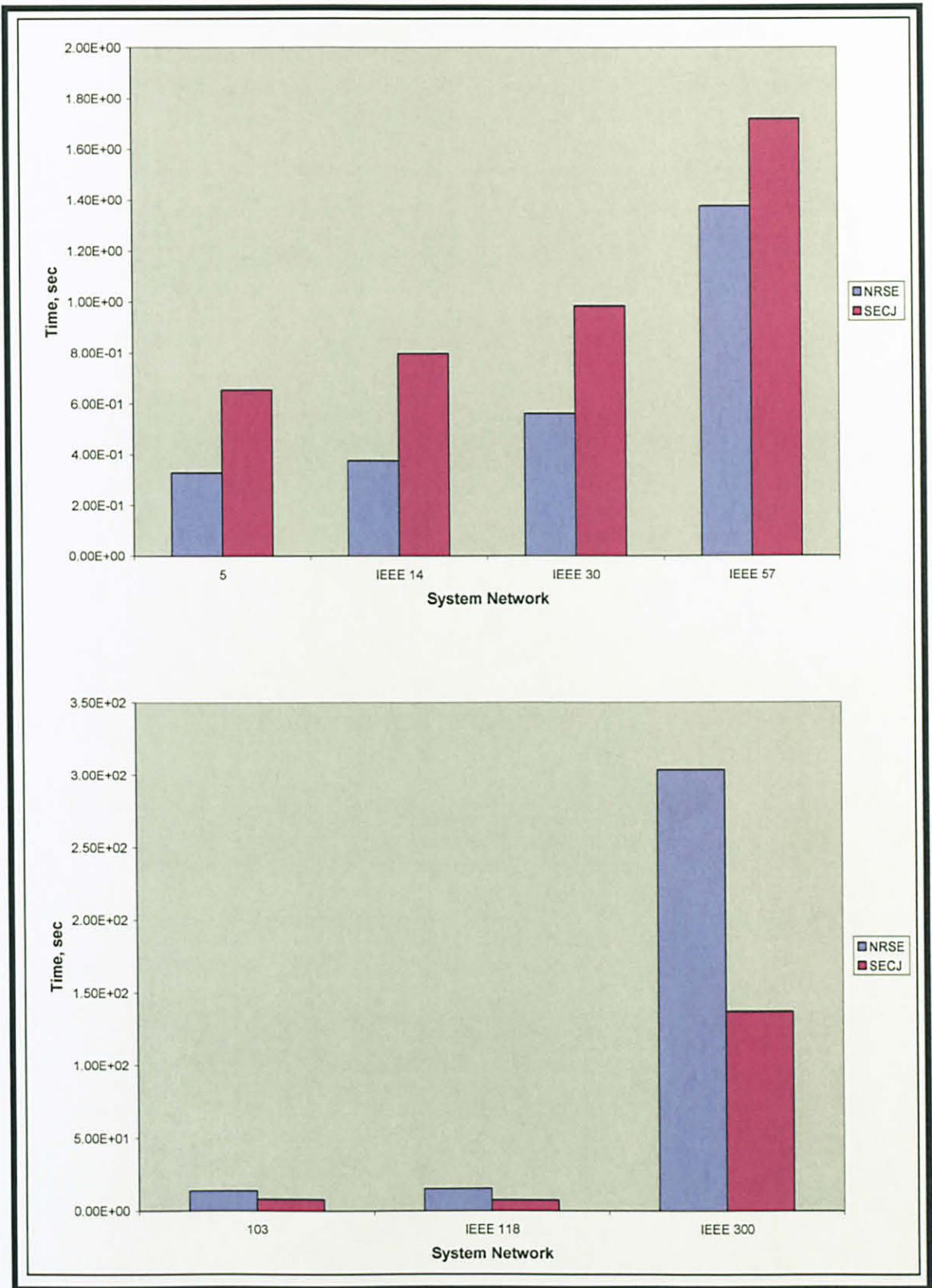


Figure 3.2 NRSE vs. SECJ for total time.



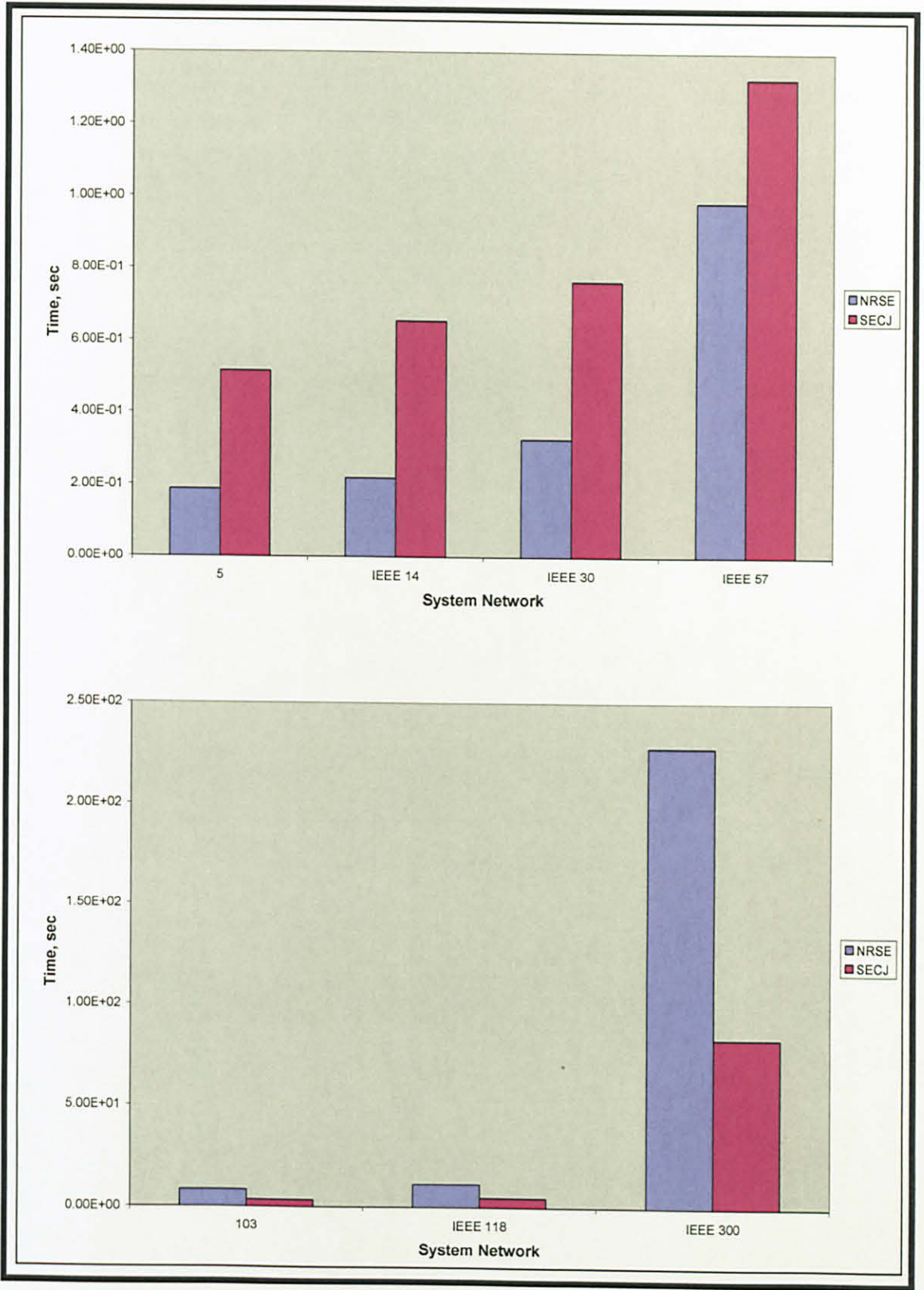


Figure 3.3 NRSE vs. SECJ for Formation of Gain.

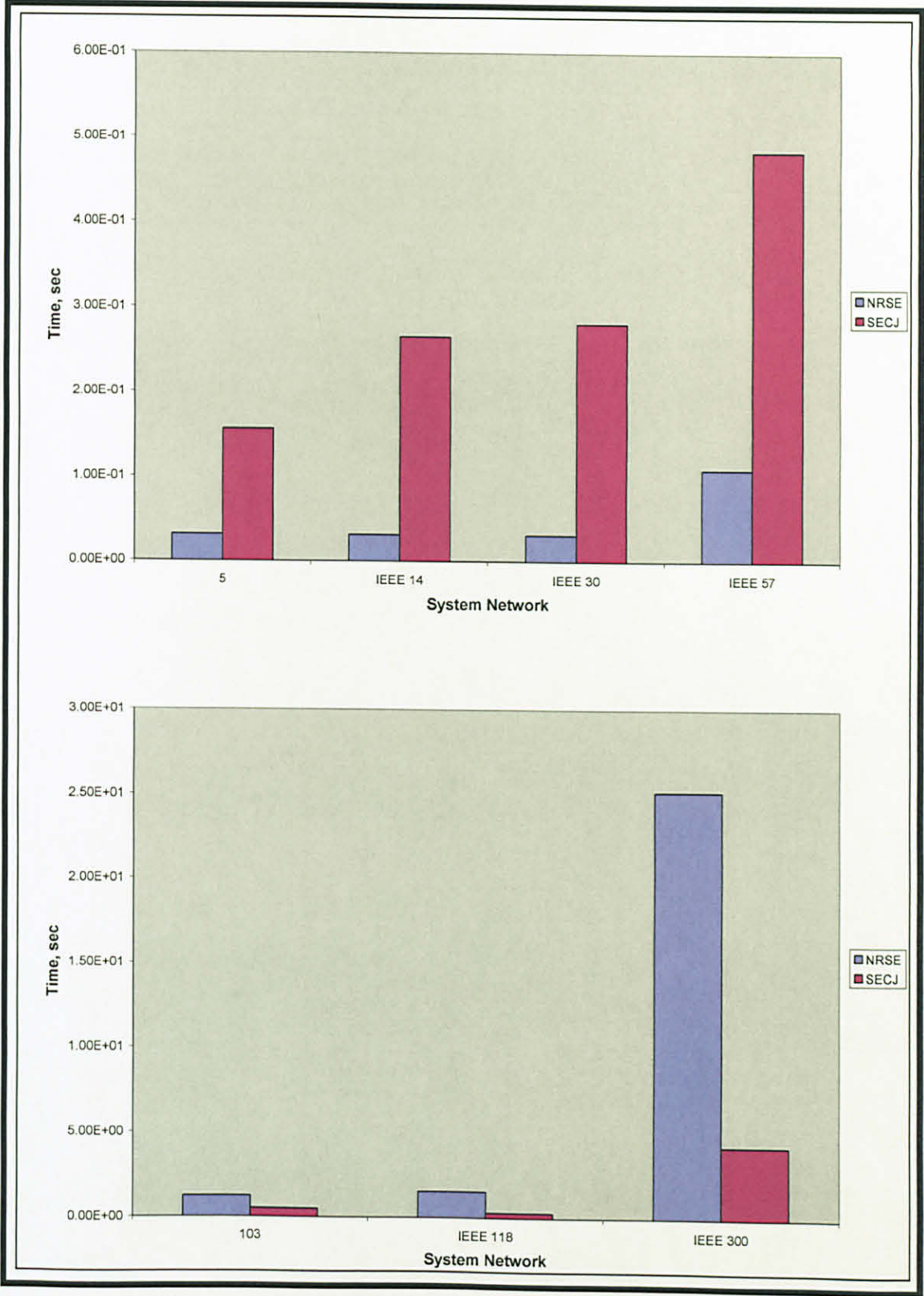


Figure 3.4 NRSE vs. SECJ for formation of H.

It has been illustrated in Figures 3.2 through 3.4 that the SECJ method does not provide any advantage when applied to a small network. However, the advantages of the SECJ method can be seen when it is applied to a large network. Processing time reduction is achieved when the network size is large. To understand this phenomenon, an  $N$ -bus network with a maximum number of measurements is examined, where  $N$  is number of buses and  $Nbr$  is number of branches. The assumptions made for the case of full measurements are as follows:

- i. All active power ( $P$ ) and reactive power ( $Q$ ) are measured at the sending and receiving end of each transmission line
- ii. Active and reactive power injection, as well as voltage magnitude are measured at each bus in the system
- iii. The number of states ( $2N - 1$ ) is approximately equal to  $2N$ .

In NRSE method, the sub-matrix  $\mathbf{H}_V$ , shown in equation (3.4) and equation (3.5), is constant, i.e. 0 or 1. It does not require to be computed at each iteration and this resulting in very small computation time. The sub-matrices of  $\mathbf{H}_{p_{ij}}$ ,  $\mathbf{H}_{p_{ji}}$ ,  $\mathbf{H}_{q_{ij}}$  and  $\mathbf{H}_{q_{ji}}$  have exactly the same zero and nonzero structures as the network branches. This is because each line flow is incident to its two terminal buses. Thus, these sub-matrices are sparse and may not take longer time to compute. On the other hand, the sub-matrices of  $\mathbf{H}_P$  and  $\mathbf{H}_Q$  involve derivatives of real and reactive power injections into the buses. When the measurement set is full, the sub matrix in matrix  $\mathbf{H}_P$  and  $\mathbf{H}_Q$  will be of size  $N \times N$ . Each sub-matrix will have  $N$  diagonal terms and  $N^2$  off-diagonal terms. For each diagonal term,  $N$  numbers of trigonometric functions are to be evaluated and for each off-diagonal term, one trigonometric function is to be evaluated. Therefore,

$$\text{the total number of trigonometric functions that are to be evaluated} = 8 N^2 \quad (3.26)$$

In the SECJ method, the sub-matrix of  $\mathbf{H}_V$  is the same as in NRSE method. However, the rest of the sub-matrices totally depend on 16 numbers of partial derivatives of line flows, shown in equation (3.6) through equation (3.21). For each partial derivative of line flow, 2 trigonometric functions are to be evaluated. Meanwhile, to compute the calculated powers, 4 numbers of line flows, shown in equation (2.5) through

equation (2.8) are to be computed. For each calculated power, 2 trigonometric functions are to be evaluated. Therefore the number of trigonometric functions that are to be evaluated is equal to  $32 Nbr + 8 Nbr$ . Taking  $Nbr = 1.4 N$ ,

$$\text{the total number of trigonometric functions that are to be evaluated} = 56 N \quad (3.27)$$

Based on equation (3.26) and equation (3.27), it can conclude that the SECJ method uses significantly less number of mathematical operations and hence takes less CPU time particularly for larger networks compared to the NRSE method.

### 3.7 Summary

The Newton-Raphson State Estimation (NRSE) method using the bus admittance matrix remains as an efficient and most popular method to estimate the state variables. In the NRSE method, the elements of the Jacobian matrix are computed from standard expressions which lack physical significance. The process of computing the elements of the Jacobian matrix is a significantly time consuming step which requires evaluation of large number of trigonometric functions. In this chapter, elements of the state estimation Jacobian matrix are obtained considering the power flow measurements in the network elements. These elements are processed one-by-one and the Jacobian matrix,  $H$  is updated suitably in a simple manner. The constructed Jacobian matrix,  $H$  is integrated with the WLS method to estimate the state variables. The suggested procedure, SECJ is successfully tested on the 5-bus, IEEE 14-bus, IEEE 30-bus, IEEE 57-bus, 103-bus, IEEE 118-bus and IEEE 300-bus system. The merit of the proposed SECJ is the reduction in computer time. It is significant, especially in large scale power system networks, where the reduction in computer time of about 50 % compared to the NRSE method.

Reduction in computational speed will not yield the full benefit if the final estimates are not accurate. One of the major points to ensure the accuracy is the redundancy of the measurements. The bad data filtering or pre-screening process is used to detect and separate out all measurements with some apparent error in order to avoid any heavy distortion of the estimated network state due to completely wrong measurements. However, in the case of redundancy, this process looks forward to

reduce the number of measurements if bad data is detected, which will affect the redundancy as well. This problem is answered in the Autoregressive (AR) method that is discussed in the next chapter.

## CHAPTER 4

# IMPLEMENTATION OF AUTOREGRESSIVE METHOD TO PRE-FILTER THE SET OF MEASUREMENTS

### 4.1 Introduction

In a modern power system control center, SE is responsible for providing a complete and reliable real-time data-base for analysis, control, and optimization functions [62]. Realizing on the importance of SE, it has remained as an extremely active and contentious area. Conventionally, power system state estimators implemented in EMS are static-natured. This means that the state at the present time is determined exactly from the network inputs at the current time regardless of the previous state value. In other words, state estimates are extracted from a single scan of measurements, which corresponds to a situation of concentrated redundancy. Thus, high redundancy levels are required for adequate performance of the SE function.

Generally, SE is performed to complete two tasks, i.e. filtering of errors inbuilt to the telemetering measurements and data validation. Redundancy is a requirement for the success of any data validation scheme. Therefore, highly redundant telemetering systems are always desirable. However, the ideal redundancy level of information is not monitored in power systems since the cost involving to install the measurements are too costly [43]. Thus, additional data or pseudo-measurements are introduced to increase the data redundancy and improve the accuracy of the calculated state.

SE is based on the assumption that measurement errors are statistically distributed with zero mean. The sources of such errors are mainly contributed by the instrument transformers, the cables connecting the instrument transformers to the sensors or A/D converters and the sensors or A/D converters themselves [37]. Furthermore,

integration between different sensors introduces an additional uncertainty in the measurements. Thus, some measurements in the data set can become critical, in the sense that without any one of them, the system is unobservable or can reduce the data redundancy for SE to critical levels. Critical measurements in this chapter are defined as a group of measurements in which the removal of any measurement from this group makes the system unobservable. In bad data processing algorithms, once a certain measurement is detected and eliminated there is a possibility of another measurement becoming critical where the estimation residual is zero, i.e. measured and estimated values are identical. Therefore, bad critical measurements can not be detected by SE residual analysis. Also, all measurements of a critical set present equal normalized residuals. This implies that a detectable error in any of such measurements can not be correctly identified by residual analysis. In order to solve the above problems, state forecasting and estimation has been proposed [21 and 30] as a powerful alternative in place of static SE, especially regarding real-time bad data processing [23, 44, 45 and 46]. The main objective of the state forecasting and estimation is that the data can be checked and validated before filtering step is performed by calculating the differences between telemetered and forecasted quantities. Indeed, most of the existing commercial software performs a pre-screening process to check whether the measured values are within the reasonable limit or not. The margin of the limitations set in the SCADA subsystem is typically around 15 % [47]. However, this pre-screened process is not fully screened or filtered in large power system network. The later problem is identified during the author's industrial attachment at Tenaga Nasional Berhad (TNB).

In the Autoregressive (AR) method introduced by [22] the linear prediction method is used to calculate the reflection coefficients. However, in this chapter, two different methods known as Burg and Modified Covariance (MC) are proposed to calculate the reflection coefficients. The details of both methods are discussed in the following sections.

## **4.2 The Autoregressive (AR)**

As for as SE is concerned, research works are concentrated more to improve the bad data processing and observability. Among them, state forecasting has emerged as an

important tool. The method of state forecasting and estimation had its early developments in 1970s [30] where the Kalman filtering proposed by Debs *et. al.* [48] is recognized as the initial work for dynamic state estimator. Since then, the concept of tracking state estimation is extended further as in [48-49]. With the aim of improving model performance of state estimation tracking, invariant parameters exponential smoothing describing the state transition equations is used by Leite da Silva [21 and 49]. These methods used various dynamic models that ignored the power flow constraints and also did not use the load forecast to predict the state transition. Thus, they become inappropriate for exploiting the state forecasting benefits.

The basic function of AR method is to predict the one-step ahead expected value of a measurement from immediate past measurement. The predicted value of the measurement is then compared with its measured value for the same instant of time.

Under normal operating conditions, the difference should not exceed a certain pre-determined threshold. If it is not meeting the requirement, the measurement is identified as a bad data. If bad measurements are initially assigned with high weight factor, the predicted value that obtained from AR algorithm is substituted and the SE is carried out. The main step in AR algorithm is the establishment of a mathematical model for describing the system state time evolution.

An autoregressive process of order  $m$  is a linear stochastic process with outcome depending on the only  $m$  previous outcomes. AR model is given by:

$$E_{AR\ m}(n) = e(n) + \sum_{k=1}^m a_m(k)E_{AR}(n-k) \quad (4.1)$$

where

- $a_m(k)$  are the prediction coefficients with  $0 \leq k \leq m-1$
- $m$  is the number of past measurements/observations
- $n$  is the instant of time
- $E_{AR\ m}(n)$  is an observed sequence
- $e(n)$  is unobservable sequence
- $E_{AR}(n-k)$  is equal to  $(E_{AR}(n-1), E_{AR}(n-2), \dots, E_{AR}(n-k))$



The above is called an autoregressive model of order  $m$  or, in short,  $AR(m)$ . When an observed sequence  $E_{AR}(n)$  is to be estimated via  $AR(m)$  modeling, the coefficients  $a(k)$  are chosen so that the AR model correctly represents the signal. A variety of methods to find the prediction coefficients of the model,  $a(k)$  are found in [26]. However, the Burg and MC are selected as the AR methods in this chapter due to their ability to minimize the sum of backward and forward prediction errors. The objective of both methods is to minimize the sum of squares of prediction errors.

$$\mathcal{E}_m = \mathcal{E}_{f_m} + \mathcal{E}_{b_m} \quad (4.2)$$

where,

$\mathcal{E}_m$  is the sum of squares of prediction errors

$\mathcal{E}_{f_m}$  is the forward error

$\mathcal{E}_{b_m}$  is the backward error

In real-time applications, each time a measurement  $m$  passes the above test, it replaces the most recent measurement in the vector of past measurements,  $\mathbf{x}(n)$ . The AR parameters are then calculated using Burg or MC, and the one-step ahead predicted value of variable,  $m$ , is determined so that, when the next snapshot is available, the filtering procedure can be repeated.

#### 4.2.1 Linear prediction

The  $n$ th sample of an autoregressive process linearly depends on its  $m$  previous values, shown in equation (4.1). Hence, for a complex sequence that may be modeled by an  $AR(m)$  signal, in the forward prediction filter, an estimate of its sample  $x(n)$  can be found as a linear combination of  $\{x(n-m), \dots, x(n-1)\}$  using coefficients  $\{a_1, \dots, a_m\}$ , as:

$$\hat{x}(n) = -\sum_{k=1}^m a_m(k)x(n-k) \quad (4.3)$$

The forward prediction differs from the observed value by the prediction error  $\varepsilon_{fm}(n)$ . This error  $\varepsilon_{fm}(n)$  is a measure for the accuracy of the prediction.

$$\varepsilon_{f_m}(n) = x(n) - \hat{x}(n) = x(n) - \sum_{k=1}^m a_m(k)x(n-k) \quad (4.4)$$

The AR parameter estimation through linear prediction consists of finding the set of coefficients  $\{a_1, \dots, a_m\}$  such that the power of the prediction error is minimized. This is the least square solution for the linear prediction as in equation (4.3).

## 4.2.2 Burg method

The Burg method for estimating the AR parameters can be viewed as an order-recursive least-squares lattice method, based on the minimization of the forward and backward errors in linear predictors, with the constraint that the AR parameters satisfy the Levinson-Durbin recursion [50, 51 and 52]. Forward prediction consists of predicting the sample of  $x(n)$  from the  $m$  previous observations  $\{x(n-m), \dots, x(n-1)\}$ . Alternatively, if  $\{x(n+1), \dots, x(n+m)\}$  are known, it may be possible to guess the value of the previous data sample  $x(n)$ , where this procedure is known as backward prediction. While prediction of the past may not seem to be very relevant, backward prediction is of great help when the purpose is to estimate the AR parameters of the sample  $x(n)$ . The backward linear prediction of  $x(n)$  with prediction coefficients  $\{a_1^*, \dots, a_m^*\}$  is expressed as:

$$\hat{x}(n-m) = -\sum_{k=1}^m a_m^*(k)x(n+k-m) \quad (4.5)$$

The corresponding forward and backward errors  $\varepsilon_{f_m}(n)$  and  $\varepsilon_{b_m}(n)$  are defined as in equation (4.4) and equation (4.6).

$$\varepsilon_{b_m}(n) = x(n-m) - \hat{x}(n-m) \quad (4.6)$$

The least square error is

$$E_m = \sum_{n=m}^{N-1} \left[ |\varepsilon_{f_m}(n)|^2 + |\varepsilon_{b_m}(n)|^2 \right] \quad (4.7)$$

This error is to be minimized by selecting the prediction coefficients, subject to Levinson-Durbin constraint given by

$$a_m(k) = a_{m-1}(k) + K_m a_{m-1}^*(m-k), \quad 1 \leq k \leq m-1 \\ 1 \leq m \leq p \quad (4.8)$$

where  $K_m = a_m(m)$  is the  $m$ th reflection coefficient in the lattice filter realization of the predictor. Substitution of the equation (4.7) into the expressions for  $\varepsilon_{f_m}(n)$  and  $\varepsilon_{b_m}(n)$ , results in the pair of order-recursive equations for the forward and backward prediction errors given by

$$\varepsilon_{f_m}(n) = \varepsilon_{f_{m-1}}(n) + K_m \varepsilon_{b_{m-1}}(n-1), \quad m = 1, 2, \dots, p \\ \varepsilon_{b_m}(n) = K_m^* \varepsilon_{f_{m-1}}(n) + \varepsilon_{b_{m-1}}(n-1), \quad m = 1, 2, \dots, p \quad (4.9)$$

The minimization of  $\varepsilon_m$  with respect to the complex-valued reflection coefficient  $K_m$  is performed by substituting equation (4.8) into (4.7) as shown in equation (4.10).

$$\hat{K}_m = \frac{-\sum_{n=m}^{N-1} \varepsilon_{f_{m-1}}(n) \varepsilon_{b_{m-1}}(n-1)}{\frac{1}{2} \sum_{n=m}^{N-1} \left[ |\varepsilon_{f_{m-1}}(n)|^2 + |\varepsilon_{b_{m-1}}(n-1)|^2 \right]} \quad m = 1, 2, \dots, p \quad (4.10)$$

The term in the numerator of equation (4.10) is an estimate of the cross correlation between the forward and backward prediction errors. With the normalization factors in the denominator of equation (4.10), it is obvious that  $K_m < 1$ , so that the all-pole model obtained from the data is stable. The denominator in equation (4.10) is simply the least-squares estimate of the forward and backward errors  $E_{m-1}^f$  and  $E_{m-1}^b$ , respectively [50]. Hence equation (4.10) can be expressed as

$$\hat{K}_m = \frac{-\sum_{n=m}^{N-1} \varepsilon_{f_{m-1}}(n) \varepsilon_{b_{m-1}}(n-1)}{\frac{1}{2} [\hat{E}_{m-1}^f + \hat{E}_{m-1}^b]} \quad m = 1, 2, \dots, p \quad (4.11)$$

where  $\hat{E}_{m-1}^f + \hat{E}_{m-1}^b$  is an estimate of the total squared error,  $E_m$ . The denominator term of equation (4.11) can be computed in an order-recursive approach according to the relation [50],

$$\hat{E}_m = \left(1 - |\hat{K}_m|^2\right) \hat{E}_{m-1} + |\varepsilon_{f_{m-1}}(m-1)|^2 - |\varepsilon_{b_{m-1}}(m-2)|^2 \quad (4.12)$$

where  $\hat{E}_m \equiv \hat{E}_m^f + \hat{E}_m^b$  is the total squared error.

### 4.2.3 Modified Covariance method

Consider the data  $x(n)$ ,  $n=0,1,\dots, N-1$ . Similar to the Burg method, equation from (4.3) to (4.5) is used. To find the prediction coefficients that minimize  $\varepsilon_m$ , the derivative of  $\varepsilon_m$  with respect to  $a_m^*(l)$  is set to zero for  $l=1,2,\dots,m$  [50]. Hence

$$\begin{aligned} \frac{\partial E_m}{\partial a_m^*(l)} &= \sum_{n=m}^{N-1} \left[ \varepsilon_{f_m}(n) \frac{\partial [\varepsilon_{f_m}(n)]^*}{\partial a_m^*(l)} + [\varepsilon_{b_m}(n)]^* \frac{\partial \varepsilon_{b_m}(n)}{\partial a_m^*(l)} \right] \\ &= \sum_{n=m}^{N-1} \left[ \varepsilon_{f_m}(n) x^*(n-l) + [\varepsilon_{b_m}(n)]^* x(n-m+l) \right] = 0 \end{aligned} \quad (4.13)$$

Substituting equation (4.3) to (4.5) into (4.13) and simplifying, the normal equations

for the MC method are obtained as

$$\begin{aligned} & \sum_{k=1}^m [c_x(l, k) + c_x(m - k, m - l)] a_m(k) \\ & = -[c_x(l, 0) + c_x(m, m - l)] \end{aligned} \quad (4.14)$$

where  $c_x(l, k) = \sum_{n=m}^{N-1} x(n-k)x^*(n-l)$  that are known as autocorrelation coefficients, which dependent only on the absolute value of the difference between  $l$  and  $k$ , i.e.  $c_x(l, k) = c_x(|l - k|)$ . However, the autocorrelation matrix is not Toeplitz but it is symmetric [50].

### 4.3 Test Results

The performance of the AR methods is tested on the 5-bus, IEEE 14-bus, IEEE 30-bus, IEEE 57-bus, 103-bus, IEEE 118-bus and IEEE 300-bus systems. The historical data are executed through successive power flow programs to record different types of measurements for all the IEEE tested networks. The simulations are carried out for 24 time samples. Meanwhile for the 103-bus network, the data are recorded in every 10 minutes. Results of the average errors for all system states relative to power flow solution are tabulated in Table 4.1. For the sake of analysis, the tabulated data in Table 4.1 is converted and shown graphically as in Figures 4.1 to 4.7. It is clearly seen that average errors of all system states in both methods are less than 4 %. The accuracy of the Burg and MC methods is obviously illustrated when it is implemented in the IEEE 118-bus and IEEE 300-bus system. The average error of all system states in the both networks are less than 1 % error. The capability of Burg and MC methods to predict a step ahead of the system states with less than 4 % error can be the platform for producing a high quality of pseudo-measurements. The later statement is strengthened by testing the Burg and MC methods under the following two case studies.

**Case 1:** The system is tested for detecting the weighting factor for erroneous measurements assigned with higher weighting factor. The standard variation is calculated using

$$\sigma = 0.005 \cdot |z^f| + 1 \times 10^{-10} \quad (4.13)$$

where  $z^f$  is the measured value.

Meanwhile, the weighting factor  $W$  is calculated from the respective standard deviation,  $\sigma$ , as follows:

$$W = \frac{1}{\sigma^2} \quad (4.14)$$

Any weighting factor that exceeds  $W$  value calculated in equation (4.14) is considered high.

**Case 2:** The system is considering a non-convergent system due to the incorrect assigning of weighting factor.

Table 4.1 Summary of the percentage average error for all measurements in all tested networks.

	AR method	Meas.	System Bus							
			5	IEEE 14	IEEE 24	IEEE 30	IEEE 57	103	IEEE 118	IEEE 300
Percentage of average error	Burg	$V$	0.0286	0.0239	0.0313	0.0278	0.0288	0.0669	0.0103	0.0109
		$P$	0.0035	0.1566	0.0056	0.3708	0.3381	0.3411	0.0362	0.0698
		$Q$	0.2108	0.2923	0.0357	1.0490	0.8640	0.2850	0.0957	0.2178
		$p_{ij}$	0.1332	0.1868	0.0199	4.0692	0.1819	1.1247	0.2954	0.0446
		$q_{ij}$	0.6601	0.4137	0.0394	0.1951	0.1101	0.2636	0.0179	0.6170
		$p_{ji}$	0.1373	0.1838	0.0203	54.1420	0.0929	0.0419	0.0014	0.0454
		$q_{ji}$	2.6183	1.7980	0.5049	0.4567	0.4307	0.4193	0.0091	0.5038
	MC	$V$	0.0283	0.0229	0.0272	0.0275	0.0285	0.0694	0.0103	0.0109
		$P$	0.0035	0.1548	0.0055	0.3666	0.3341	0.2183	0.0361	0.0694
		$Q$	0.2083	0.2886	0.0365	1.0375	0.8535	0.2899	0.0953	0.2143
		$p_{ij}$	0.1317	0.1847	0.0195	4.1452	0.1789	1.0969	0.2967	0.0448
		$q_{ij}$	0.6538	0.4098	0.0389	0.1951	0.1049	0.2618	0.0203	0.6210
		$p_{ji}$	0.1357	0.1816	0.0199	56.2867	0.0924	0.1246	0.0028	0.0449
		$q_{ji}$	2.5843	1.7711	0.5013	0.4506	0.4188	0.4194	0.0113	0.5122

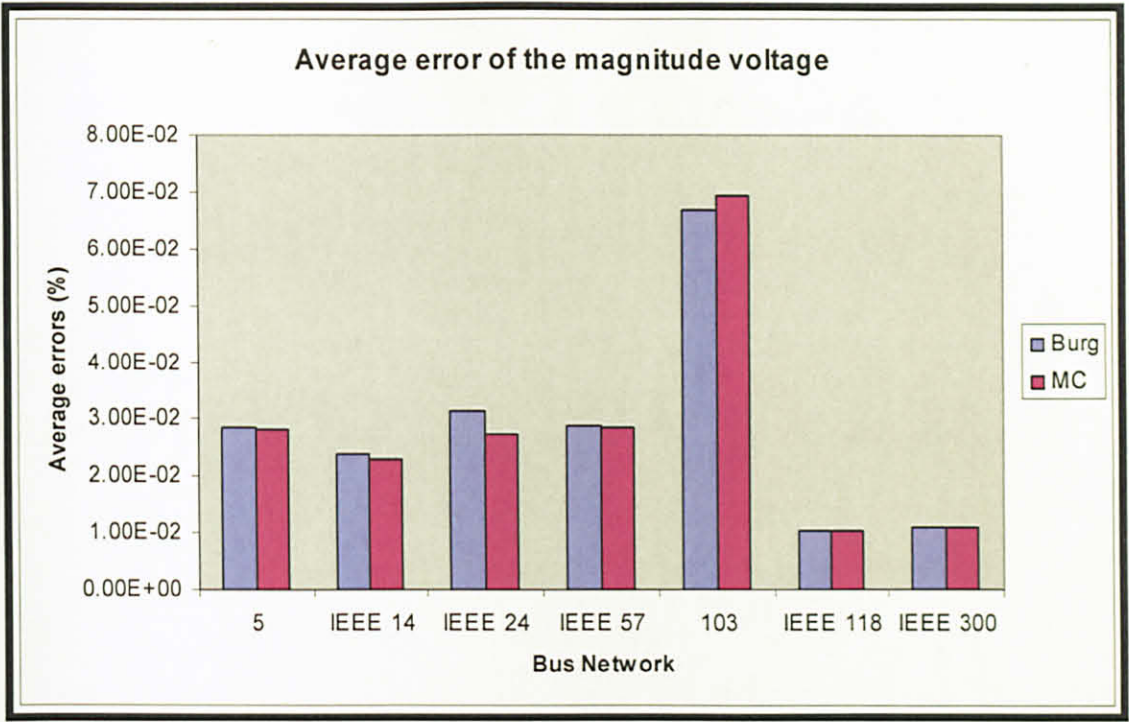


Figure 4.1 Average error of the voltage magnitude.

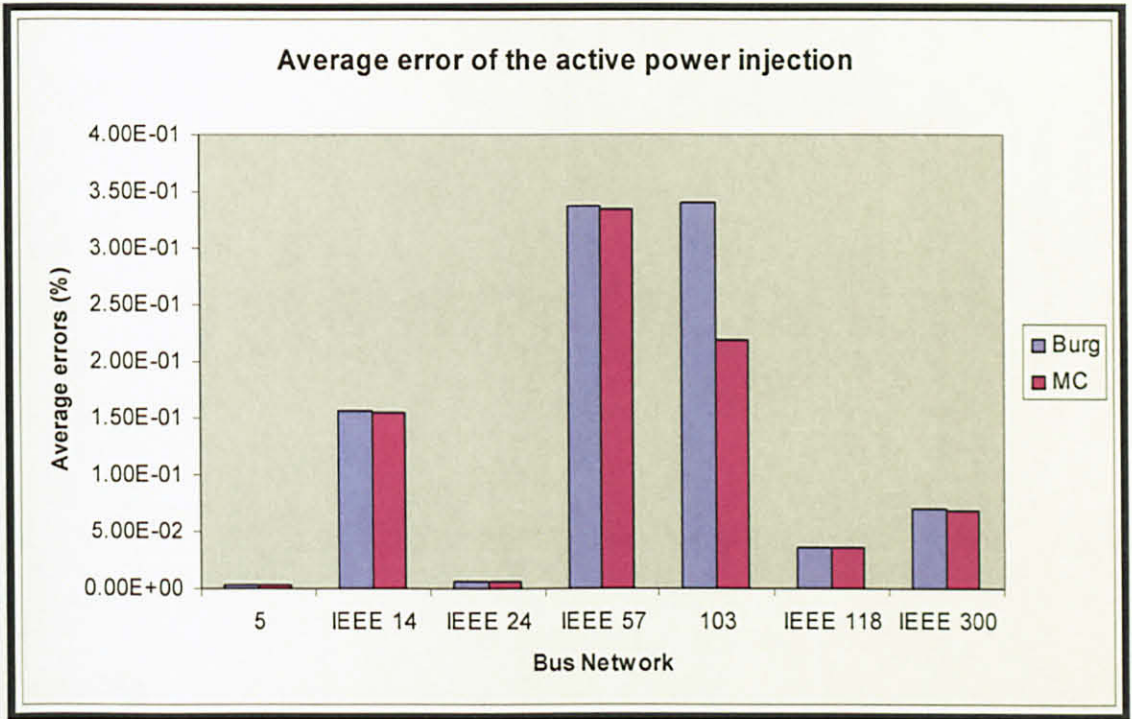


Figure 4.2 Average error of the active power injection.

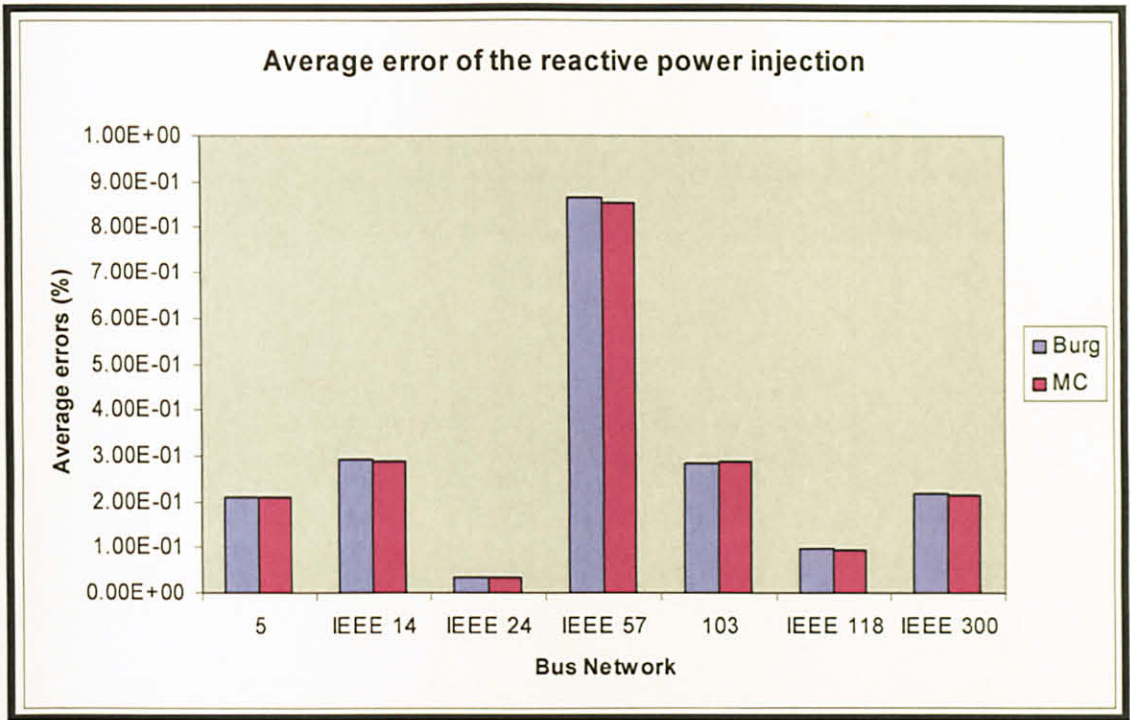


Figure 4.3 Average error of the reactive power injection.

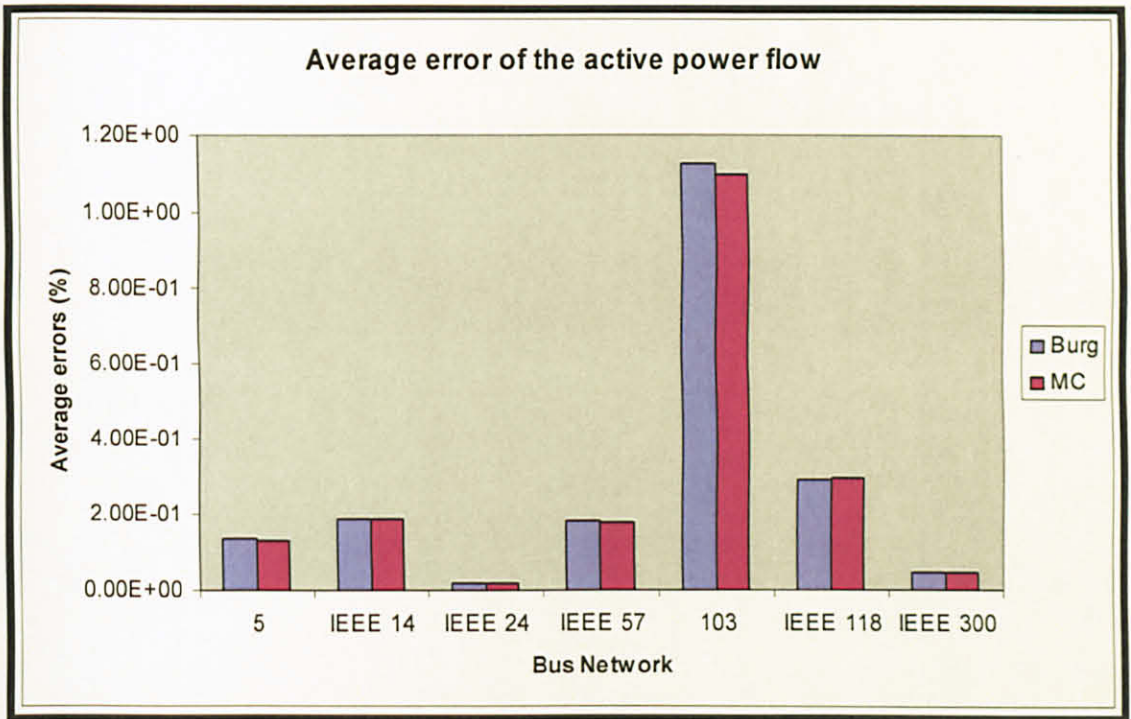


Figure 4.4 Average error of the active power flow.



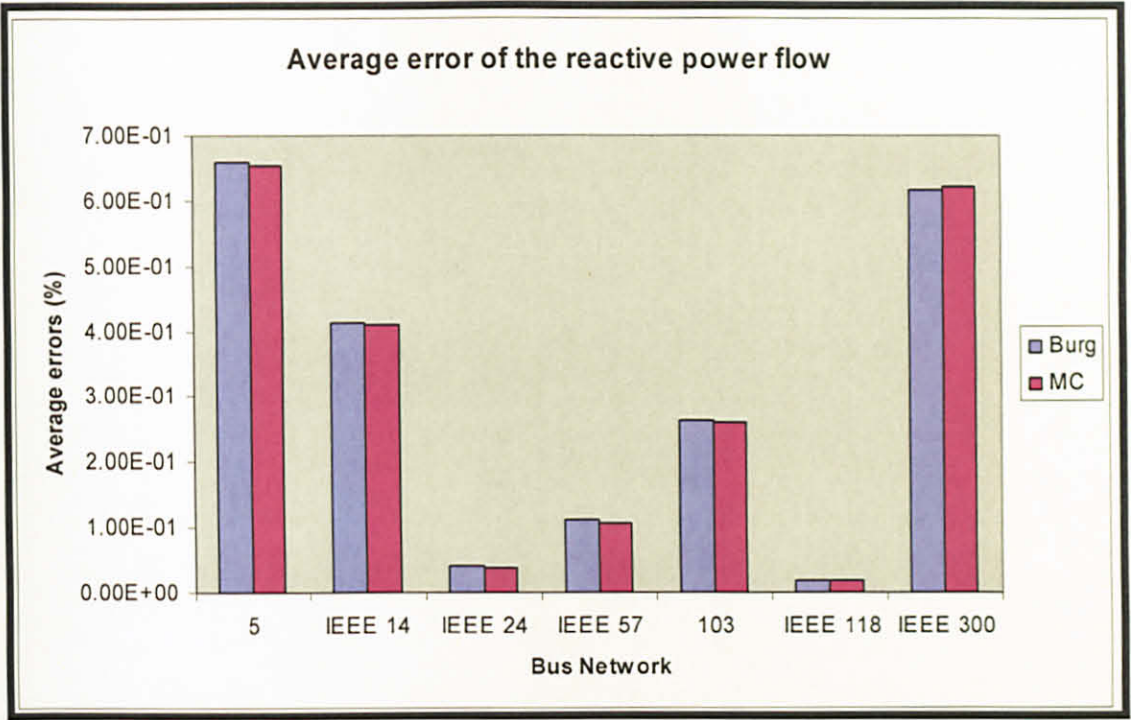


Figure 4.5 Average error of the reactive power flow.

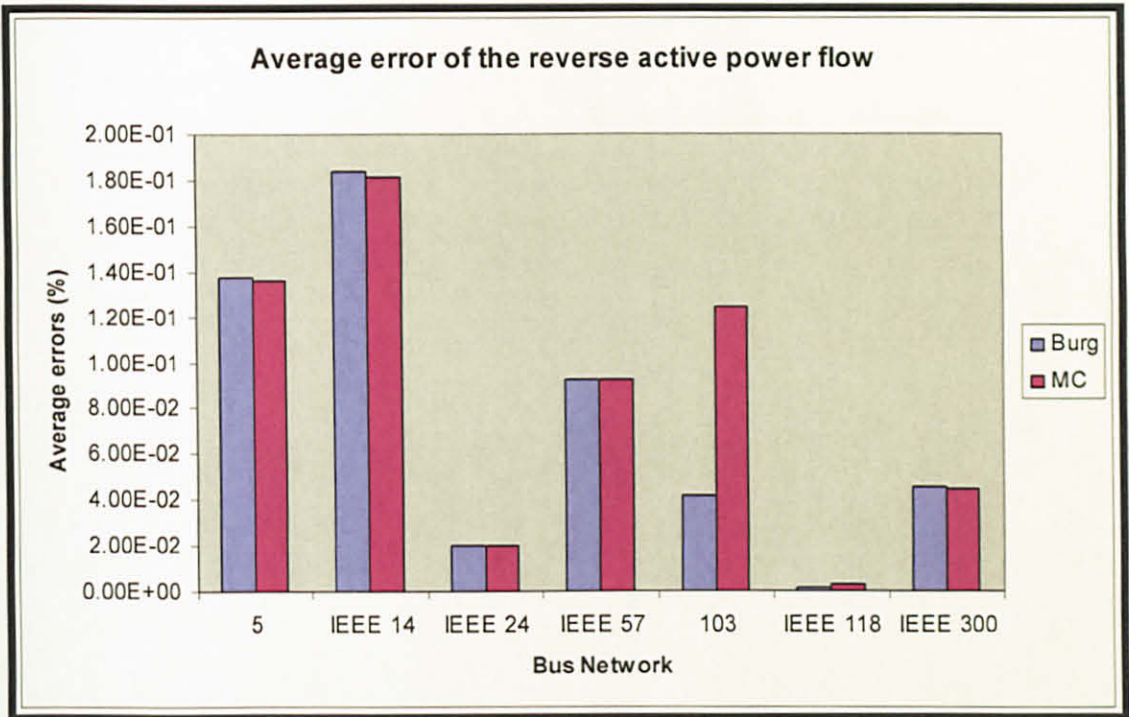


Figure 4.6 Average error of the reverse active power flow.

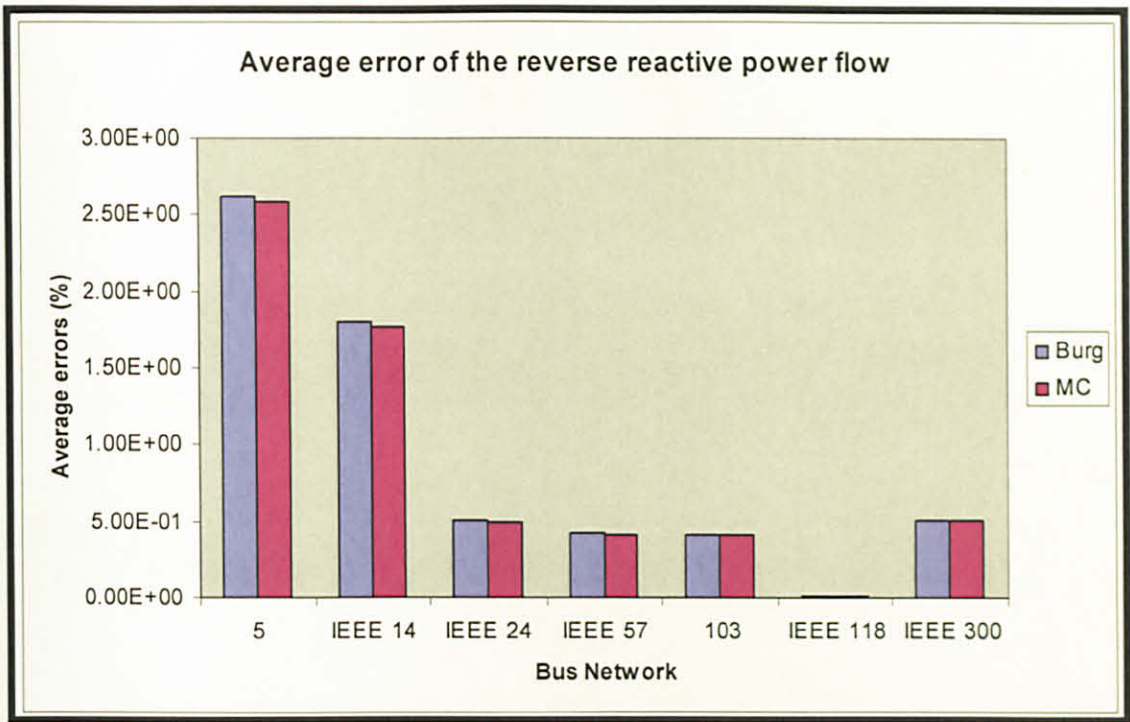


Figure 4.7 Average error of the reverse reactive power flow.

#### 4.3.1 Case 1

The analysis of IEEE 24-bus and SESB system are furnished in the earlier publication [52]. Due to space limitation, only details on the IEEE 57-bus and IEEE 118-bus systems are presented. In this case study, two and five bad measurements are introduced in the IEEE 57-bus and IEEE 118-bus network, respectively. In the IEEE 57-bus network, the directions of  $Q_8$  and active power flow from bus 13 to 49,  $p_{13-49}$  are reversed. The weighting factor of measurement,  $p_{13-49}$ , is purposely reduced below the calculated value of  $W$  as in equation (4.14). The five bad measurements introduced in the IEEE 118-bus network are  $V_{22}$ ,  $Q_{14}$ ,  $P_{47}$ ,  $p_{16-17}$  and  $q_{81-68}$ . Only measurement,  $V_{22}$ , is set with a low weighting factor while the rest of the measurements are purposely set with a high weighting factor. Table 4.2 and Table 4.3 summarize the results of AR after introducing bad data to several measurements at time step 23 for both networks.

Table 4.2 Performance of the AR method on the IEEE 57-bus – Case 1

Measurement	Measured	Forecasted Burg	Forecasted MC	Identified bad data with more than 5% error
$Q_8$	0.40078	0.39878	0.39878	-0.40078
$p_{13-49}$	0.32961	0.32850	0.32850	-0.32961
Analog measurement considered bad and the weighting factor is high.			$Q_8$	

Table 4.3 Performance of the AR method on the IEEE 118-bus – Case 1

Measurement	Measured	Forecasted Burg	Forecasted MC	Identified bad data with more than 5% error
$Q_{14}$	-0.00970	-0.00969	-0.00969	-0.10970
$V_{22}$	0.97030	0.97044	0.97044	1.97030
$P_{47}$	-0.33970	-0.33956	-0.33956	0.33970
$p_{16-17}$	-0.17480	-0.17620	-0.17620	-0.27480
$q_{81-68}$	-0.75380	-0.73723	-0.73743	0.75380
Analog measurements considered bad and the weighting factor is high.			$Q_{14}, P_{47}, p_{16-17}$ and $q_{81-68}$	

It should be noted that the predicted values depend on the past historical data. In the first run of SE, the Burg and MC algorithms detected a few analog measurements with wrong readings compared with predicted values, typically more than 5 % error, as depicted in Table 4.2 and Table 4.3. The results based on two different conditions are presented as follows:

- i. The identified bad measurements are replaced with the predicted values obtained from the AR algorithm and then the SE is carried out.
- ii. All the higher weighting factor for the identified bad measurements are set to 20 % lower than the values of  $W$  computed from equation (4.14) meaning that the measurements are not trusted, and then the SE is carried out.

**Condition 1:** The result of IEEE 57-bus is summarized in Table 4.4. All the measurements that are identified by AR methods as bad measurements, are replaced with the predicted values obtained in AR methods. After SE is carried out, the final

output shows that no bad data is present in the system even though at the first place two bad measurements are introduced in the system. With the accuracy of predicted values provided by both AR methods, as shown in Table 4.1, it is seen that the bad data is eliminated without reducing the number of available measurements. This will retain the accuracy of normal SE since the measurement redundancy is maintained same. For the IEEE 118-bus system, the average errors of all variables are low or in other words, the accuracy of both AR methods are high. This can be illustrated in the curve of the predicted value and measured value for measurements  $p_{15-23}$ ,  $P_2$  and  $Q_{12}$ . The results are shown in Figure 4.8 to 4.10.

Figure 4.8 to 4.10 depict the final output of SE for measurements  $p_{15-23}$ ,  $P_2$  and  $Q_{12}$  respectively after the bad measurements detected by AR methods (see Table 4.3) are replaced with predicted results obtained in AR method. The average errors of the measurements  $p_{15-23}$ ,  $P_2$  and  $Q_{12}$  are 0.41 %, 0.15 % and 0.037 % respectively. With the errors below than 1 %, it is established that both the AR methods are able to produce high quality of prediction values. Hence, it is guaranteed that the SE will produce an accurate final estimate with no reduction in the number of measurements and at the same time maintaining the redundancy.

Table 4.4 The Measured, Predicted and NRSE values of state variables for IEEE 57-bus network after substituting the bad data with predicted value – Case 1 (1<sup>st</sup> condition)

<i>V</i> (p.u.)				$\delta$ (deg)			
<i>Measured</i>	<i>Burg</i>	<i>MC</i>	<i>NRSE</i>	<i>Measured</i>	<i>Burg</i>	<i>MC</i>	<i>NRSE</i>
1.040	1.040	1.040	1.042	0	0	0	0
1.010	1.010	1.010	1.011	-1.180	-1.180	-1.180	-1.124
0.985	0.985	0.985	0.986	-5.970	-5.970	-5.970	-5.909
0.981	0.981	0.981	0.982	-7.320	-7.320	-7.320	-7.210
0.976	0.976	0.976	0.978	-8.520	-8.520	-8.520	-8.439
0.980	0.980	0.980	0.981	-8.650	-8.650	-8.650	-8.577
0.984	0.984	0.984	0.985	-7.580	-7.580	-7.580	-7.520
1.005	1.005	1.005	1.007	-4.450	-4.450	-4.450	-4.441
0.980	0.980	0.980	0.982	-9.560	-9.560	-9.560	-9.551
0.986	0.986	0.986	0.988	-11.430	-11.430	-11.430	-11.431
0.974	0.974	0.974	0.976	-10.170	-10.170	-10.170	-10.175
1.015	1.015	1.015	1.017	-10.460	-10.460	-10.460	-10.452
0.979	0.979	0.979	0.981	-9.790	-9.790	-9.790	-9.786
0.970	0.970	0.970	0.972	-9.330	-9.330	-9.330	-9.338
0.988	0.988	0.988	0.990	-7.180	-7.180	-7.180	-7.167
1.013	1.013	1.013	1.016	-8.850	-8.850	-8.850	-8.842
1.017	1.017	1.017	1.020	-5.390	-5.390	-5.390	-5.393
1.001	1.001	1.001	0.992	-11.710	-11.710	-11.710	-14.681
0.970	0.970	0.970	0.970	-13.200	-13.200	-13.200	-15.218
0.964	0.964	0.964	0.968	-13.410	-13.410	-13.410	-14.805
1.008	1.008	1.008	1.011	-12.890	-12.890	-12.890	-13.268
1.010	1.010	1.010	1.010	-12.840	-12.840	-12.840	-12.946
1.008	1.008	1.008	1.009	-12.910	-12.910	-12.910	-12.992
0.990	0.990	0.990	1.000	-13.250	-13.250	-13.250	-13.028
0.982	0.982	0.982	0.957	-18.130	-18.130	-18.130	-21.733
0.959	0.959	0.959	0.960	-12.950	-12.950	-12.950	-12.728
0.982	0.982	0.982	0.983	-11.480	-11.480	-11.480	-11.357
0.997	0.997	0.997	0.998	-10.450	-10.450	-10.450	-10.360
1.010	1.010	1.010	1.011	-9.750	-9.750	-9.750	-9.673
0.962	0.962	0.962	0.939	-18.680	-18.680	-18.680	-22.039
0.936	0.936	0.936	0.918	-19.340	-19.340	-19.340	-22.045
0.949	0.949	0.949	0.943	-18.460	-18.460	-18.460	-20.109
0.947	0.947	0.947	0.941	-18.500	-18.500	-18.500	-20.149
0.959	0.959	0.959	0.954	-14.100	-14.100	-14.100	-14.465
0.966	0.966	0.966	0.963	-13.860	-13.860	-13.860	-14.155
0.976	0.976	0.976	0.974	-13.590	-13.590	-13.590	-13.844
0.985	0.985	0.985	0.984	-13.410	-13.410	-13.410	-13.616
1.013	1.013	1.013	1.013	-12.710	-12.710	-12.710	-12.803
0.983	0.983	0.983	0.982	-13.460	-13.460	-13.460	-13.654
0.973	0.973	0.973	0.972	-13.620	-13.620	-13.620	-13.866
0.996	0.996	0.996	0.998	-14.050	-14.050	-14.050	-14.103
0.966	0.966	0.966	0.969	-15.500	-15.500	-15.500	-15.600
1.010	1.010	1.010	1.012	-11.330	-11.330	-11.330	-11.348
1.017	1.017	1.017	1.018	-11.830	-11.830	-11.830	-11.905
1.036	1.036	1.036	1.038	-9.250	-9.250	-9.250	-9.279
1.060	1.060	1.060	1.061	-11.090	-11.090	-11.090	-11.131
1.033	1.033	1.033	1.035	-12.490	-12.490	-12.490	-12.549
1.027	1.027	1.027	1.029	-12.570	-12.570	-12.570	-12.656
1.036	1.036	1.036	1.038	-12.920	-12.920	-12.920	-12.964
1.023	1.023	1.023	1.025	-13.390	-13.390	-13.390	-13.423
1.052	1.052	1.052	1.055	-12.520	-12.520	-12.520	-12.520
0.980	0.980	0.980	0.982	-11.470	-11.470	-11.470	-11.402
0.971	0.971	0.971	0.972	-12.230	-12.230	-12.230	-12.159
0.996	0.996	0.996	0.998	-11.690	-11.690	-11.690	-11.643
1.031	1.031	1.031	1.033	-10.780	-10.780	-10.780	-10.759
0.968	0.968	0.968	0.969	-16.040	-16.040	-16.040	-16.130
0.965	0.965	0.965	0.965	-16.560	-16.560	-16.560	-16.656

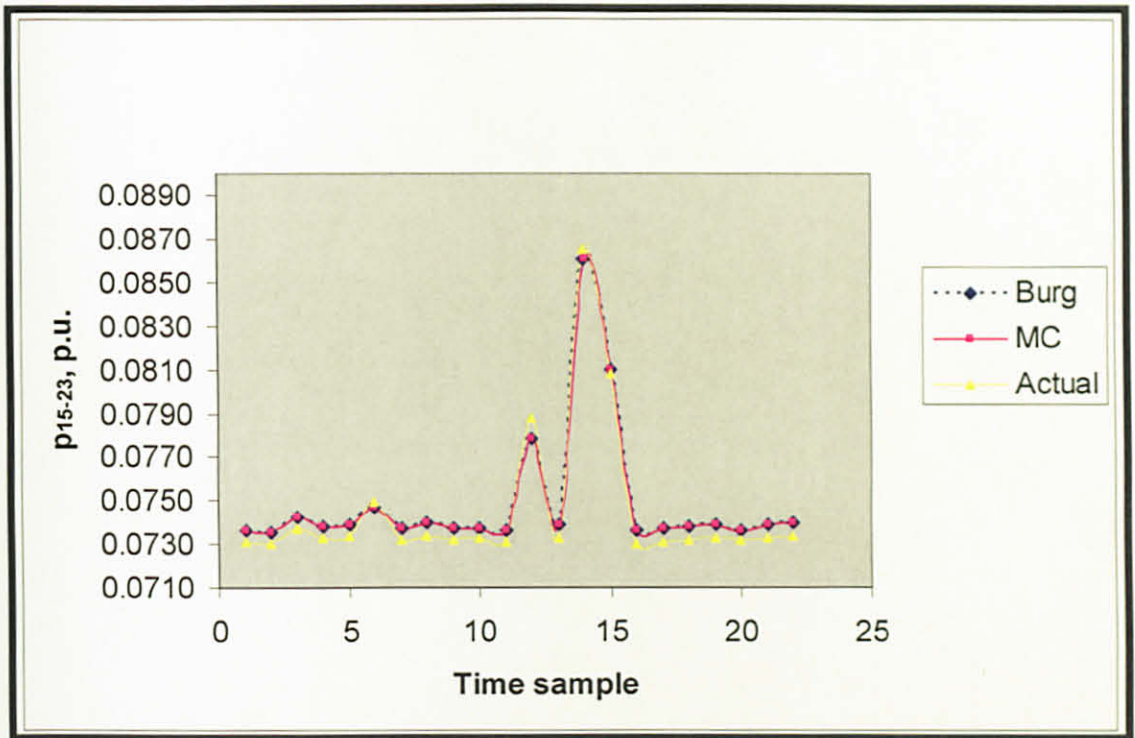


Figure 4.8 Active power flow from bus 15 to 23 – relative to power flow solution (actual value).

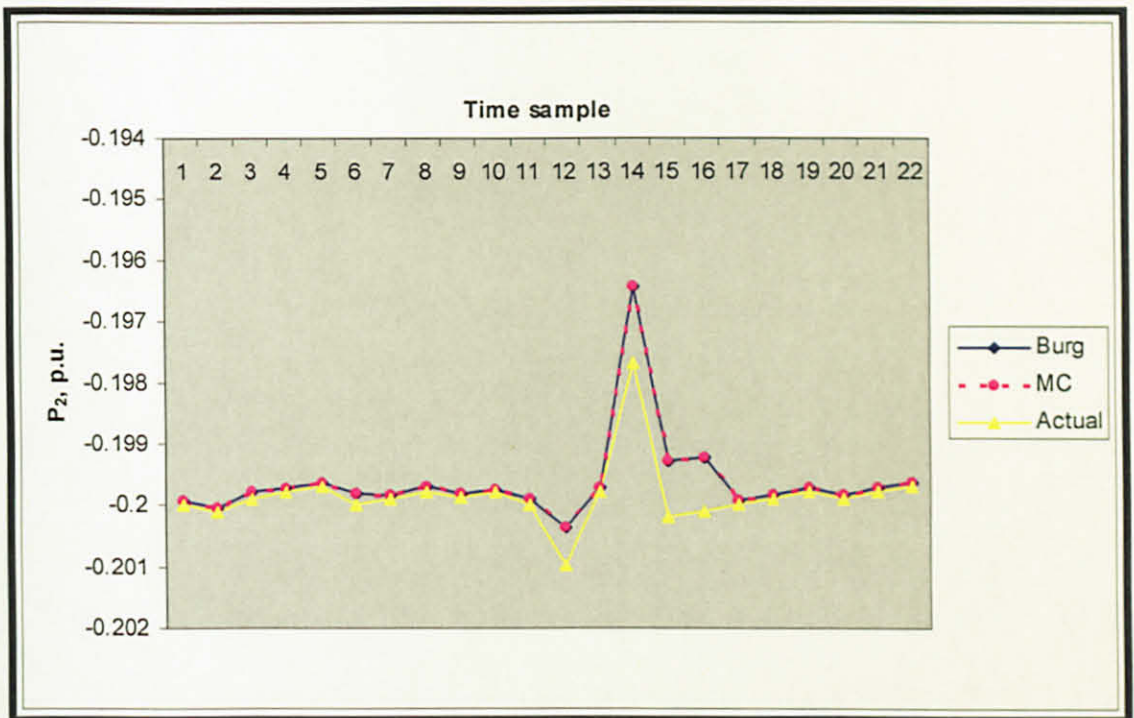


Figure 4.9 Active power injected at bus 2 – relative to power flow solution (actual value).

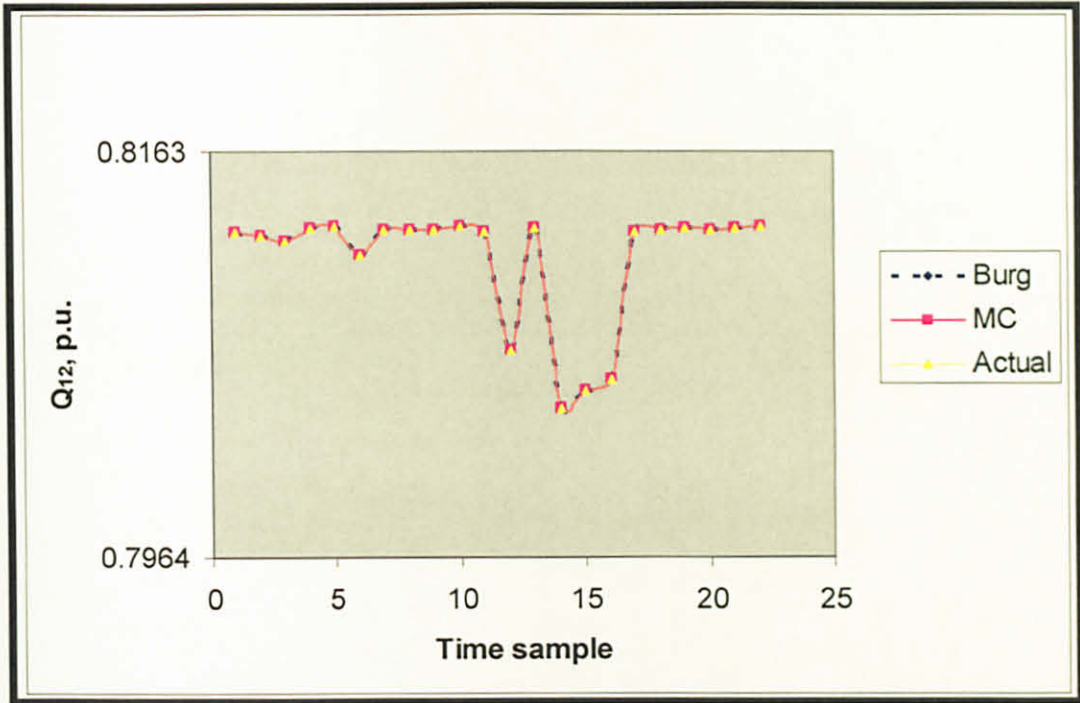


Figure 4.10 Reactive power injected at bus 12 – relative to power flow solution (actual value).

**Condition 2:** Table 4.5 and Table 4.6 show the summarized results corresponding to the second condition, for IEEE 57-bus and IEEE 118-bus system, respectively. As shown in Table 4.2 and Table 4.3, the bad measurements with higher weighting factor are identified as  $Q_8$  for IEEE 57-bus and  $Q_{14}$ ,  $P_{47}$ ,  $p_{16-17}$  and  $q_{81-68}$  for IEEE 118-bus system. The SE program is carried out after the higher weighting factor of the bad measurements are reduced. The bad measurements are eliminated one by one. The final estimation will end up in reduced number of measurements from 305 to 303 for IEEE 57-bus and 526 to 521 for IEEE 118-bus system. As a result, the redundancy of the measurement is reduced and it will affect to the accuracy of final estimated state variables as shown in Table 4.7. The average error between the final state estimation and measured data of second condition is increased due to the reduction of redundancy or number of measurements.

redundancy also increased in line with the number of measurements. Thus, the accuracy of the final estimated values of the state variables are also increased as compared with the final estimated of the state variables when number of measurement is 305 as in Case 1. The results are shown in Table 4.8.

Table 4.8 The comparison of the state vectors average errors between Case 1 and Case 2- IEEE 57-bus system.

Case Study	Number of measurements	Average error for the voltage magnitude	Average error for the phase of angle
Case 1	305	0.32 %	2.83 %
Case 2-Output from Burg	491	0.019 %	1.08 %
Case 2-Output from MC	491	0.019 %	1.08 %

Similarly, after SE is carried out by changing the weighting factor for a few of measurements in IEEE 118-bus system, the result obtained is not converging for the tolerance, number of measurements and maximum number of iteration are 0.001, 526 and 50, respectively. In the second run, the output from Burg and MC are taken as the input to SE and it successfully converged when the tolerance, number of measurements and maximum number of iteration are 0.001, 1098 and 50, respectively. The comparison of the average error of the state variables between Case 1 and Case 2 is shown in Table 4.9.

Table 4.9 The comparison of the state vectors average errors between Case 1 and Case 2- IEEE 118-bus system.

Case Study	Number of measurements	Average error for the voltage magnitude	Average error for the phase of angle
Case 1	526	0.43 %	7.43 %
Case 2-Output from Burg	1098	0.013 %	0.561 %
Case 2-Output from MC	1098	0.013 %	0.561 %

Apart from these two case studies, the output from the Burg and MC, also can be effectively used as pseudo-measurements to replace the lost measurement in the network in case of the network is unobservable. Network observability is important to be ensured first, before a SE can be performed. The analysis of Case 1 and Case 2



also can be classified as analysis of unobservable system for IEEE 57-bus and IEEE 118-bus system. It is applied when the condition of number of measurements is less than number of state ( $m < n$ ), also known as under-determined system. Thus, to overcome the problem of insufficient number of measurements, the output of AR method is used as pseudo-measurements to replace or to add more measurements in the system.

Details of the simulated results on network observability have been discussed in [53] and [54] for Burg and MC, respectively. In reference [53], it is claimed that SE is successful in converging after it is run twice on IEEE 14-bus system where for the first estimate, the output does not converge. The second estimate processes the input of SE taken from Burg's output. It is observed that SE is successful in getting the results converged in 3 iterations with a tolerance of 0.001 and  $m$  of 82. Similarly, the SE is run twice on IEEE 24-bus system [54] where for the first estimate the output does not converge. For the second estimate processes, the input of SE is taken from MC's output. The results obtained are shown to converge in 3 iterations with a tolerance of 0.001 and  $m$  of 148.

#### **4.4 SECJ Method Applied With AR Method**

The performance of the AR method is also tested on the SECJ method. It is already discussed in Chapter 3, that SECJ method is significantly beneficial in terms of computer processing time especially when the size of network becomes larger. Table 4.10 shows the summary of computational time for NRSE and SECJ methods when both AR methods are applied. In this case, IEEE 57 and IEEE 118-bus networks are discussed. For the sake of analysis, the results shown in Table 4.10 are represented by graphical as shown in Figures 4.11 and 4.12.

Table 4.10 Summary of computational time between NRSE and SECJ for IEEE 57 and IEEE 118-bus systems.

System	SE method	AR method	Time, sec		
			<i>H</i>	<i>G</i>	Completed Process
IEEE 57	NRSE	Burg	0.219	1.80	3.25
		MC	0.172	1.67	3.08
	SECJ	Burg	0.0625	1.38	2.73
		MC	0.0469	1.30	2.59
IEEE 118	NRSE	Burg	3.44	69.4	85.7
		MC	3.09	65.4	81.0
	SECJ	Burg	0.234	18.3	31.6
		MC	0.219	18.3	31.2

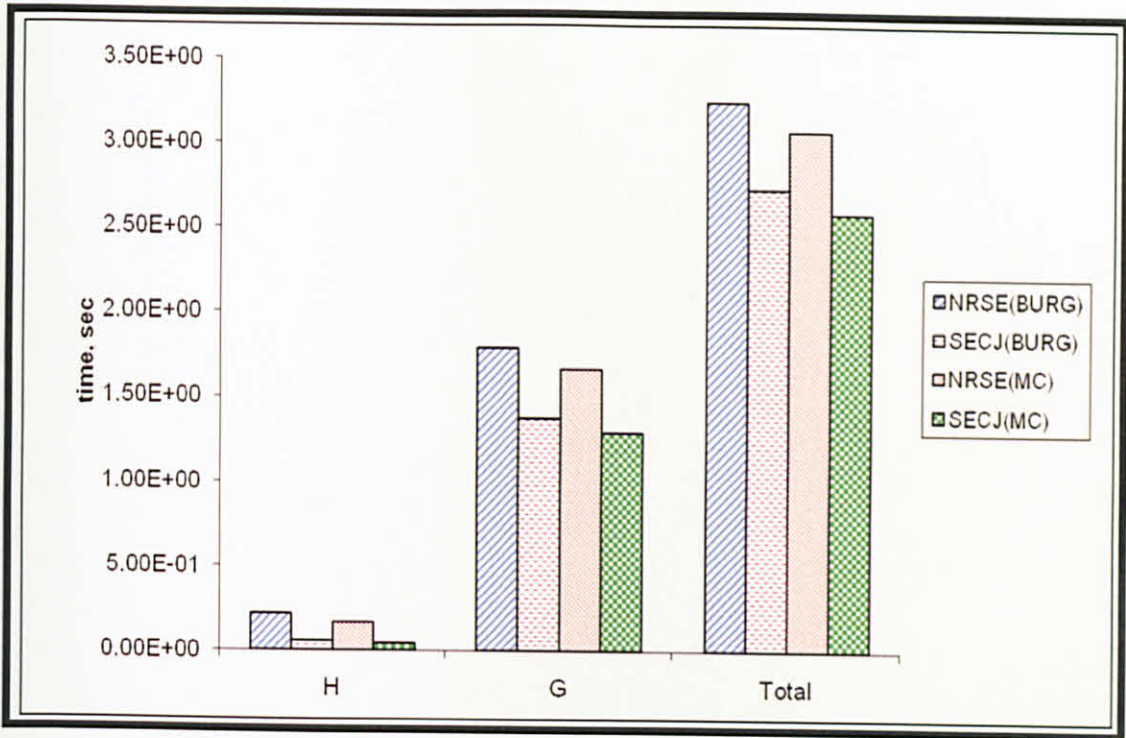


Figure 4.11 Comparison of NRSE and SECJ for IEEE 57-bus.

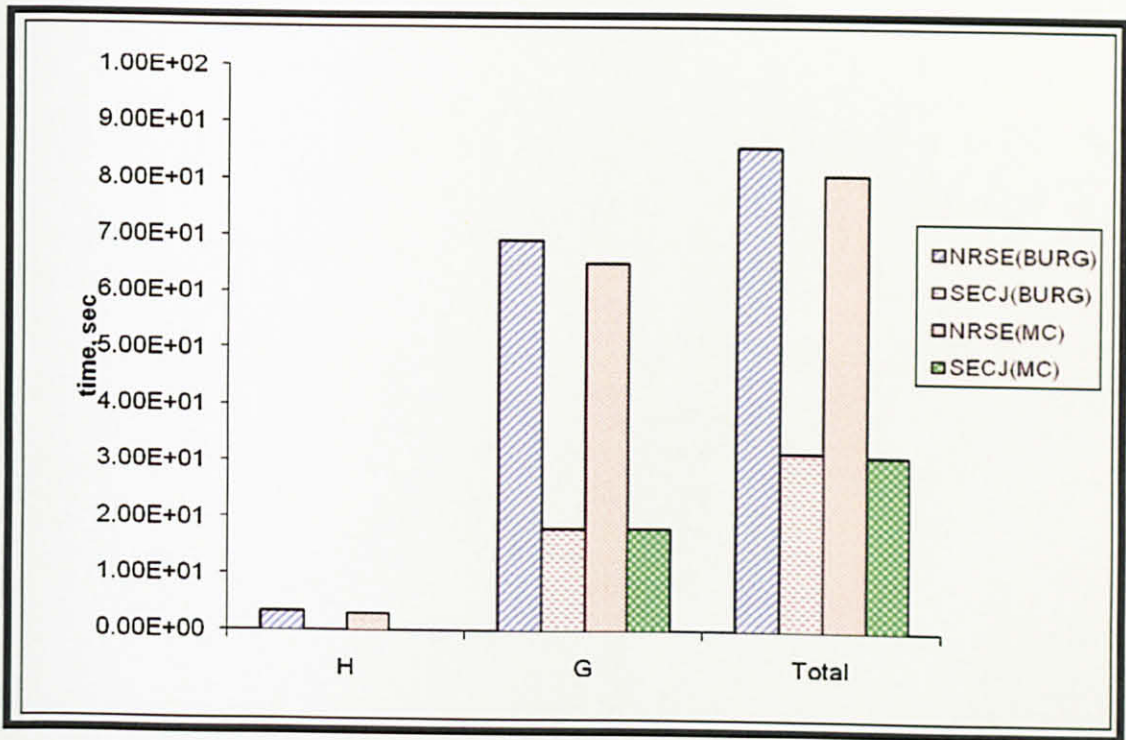


Figure 4.12 Comparison of NRSE and SECJ for IEEE 118-bus.

It has been illustrated through Figures 4.11 and 4.12 that the SECJ method again proved to be faster in term of computational time as compared to NRSE method. The reduction in processing time is significant when the network size is large.

## 4.5 Summary

While carrying out SE, the individual measurement is assigned with its own weighting factor based on technical experience of the engineers. However, uncertainty in analog measurements can occur in a real time system. Thus, the high weighting factor or wrongly assigned weighting factor to the measurement can lead to flag the measurement as bad. This chapter describes a pre-screening process to identify the bad measurements and the measurement weights before WLS estimation method, employed in SE, is performed. The AR method proposed in this chapter is used to predict the data and at the same time filtering the logical weighting factors that have been assigned to the identified bad measurements. The AR algorithms known as Burg and Modified Covariance (MC) are used to calculate the one-step-ahead of the predicted values of the state variables. The performance of the AR filter is tested on several standard systems where the largest being IEEE 300-bus system. Simulation results are presented and compared with the actual values to validate the proposed method. The simulation results show that the proposed methods are able to accurately predict the behavior of the system variables given that the states of the system are within their normal variation. The simulation results also show that both AR methods are capable of identifying bad measurements assigned with the high weight factor. Also the AR methods will provide the necessary pseudo-measurements for those measurements that are identified as bad data.

Further, the SECJ method is also tested by incorporating the AR methods. The SECJ method shows a significant advantage especially in large scale power system networks, where the total computational time reduces to about 50 % when compared with the NRSE method. Thus, the strength of Burg and MC algorithms in the field of SE is established.

## CHAPTER 5

# STATE ESTIMATION OF POWER SYSTEMS EMBEDDED WITH UPFC

### 5.1 Introduction

Congestion that occurs throughout the network grid resulted in serious operational problems in today's large scale power systems. It may make the electricity grid unreliable and subject to blackouts. Therefore, it is necessary to have a good interconnection technology that can improve the capability of power delivery and efficiently controlling the power flows across specified lines. There are several alternative technologies suitable to power system interconnection such as, Alternating Current (AC), High Voltage Direct Current (HVDC) and Hybrid AC/HVDC interconnection systems.

Alternating Current (AC) interconnections are more popular. In Malaysia, the grid is connected to Singapore's transmission system at Senoko via 2 x 230 kV AC submarine cables with a firm transmission capacity of 200 MW each. Large interconnected systems will pose several operational problems major one being inter-area oscillations that can cause instability of the system.

High Voltage Direct Current (HVDC) transmission system, whose advantages are in bulk power transmission over long distances, enhancement of the performance of connected AC system during voltage dips, connection of AC systems with different frequencies, is developed to overcome the problem of AC technology. In HVDC, power is taken from one point in an AC network and converted to Direct Current (DC) in a converter station (rectifier) and transmitted over a line and converted back to AC again in another converter station (inverter) before it is injected into the

receiving AC network. HVDC interconnection could contribute better to both technical and economic advantages of interconnection system. However, HVDC has some disadvantages such as the cost of converter station of HVDC is much expensive compared with AC substation, requires a large reactive power controllers to be installed in the converter station in order to support its normal operation and can cause instability in the system if the controllers are not properly set. In Malaysia, the grid is interconnected to Thailand's transmission system operated by the Electricity Generating Authority of Thailand (EGAT) in the North via a HVDC interconnection with a transmission capacity of 300 MW plus a 132 kV AC overhead line with maximum capacity of 80 MW.

Hybrid AC/HVDC interconnection system is then developed purposely for exchanging the HVDC power between neighbouring systems over a direct and shorter AC interconnection route as well as to use HVDC for transmission of large power networks over long distances. With this combination of AC/DC systems, the interconnected systems become more stable since HVDC can damp oscillations by its fast control. Furthermore, a weak AC interconnection (small power exchange) can then be allowed to exchange increased power between interconnected systems supported by HVDC control. Beside the shortcomings given by the HVDC and AC, the cost to install the Hybrid AC/HVDC is too expensive, thus, it may be unworthy to implement this technology.

All the conventional technologies discussed above may need to improve especially in terms of controllability of power flows and voltages, enhancing the utilization and stability of existing systems. Due to that, new developments in the field of power electronic devices led the Electric Power Research Institute (EPRI) to introduce a new technology known as Flexible Alternating Current Transmission Systems (FACTS) in the late 1980s. The objectives of FACTS technology are to enhance the system controllability and to increase the power transfer limit by introducing power electronic devices at the proper places of the existing AC systems. Such kind of technology can improve system dynamic behavior and enhance system transfer limit that is desirable in interconnected system. Some interesting application of FACTS devices can be found in economic dispatch, optimal power flow and transmission

congestion management [55-56]. The details of networks with FACTS controllers are discussed in the following section.

## **5.2 Flexible AC Transmission System (FACTS)**

FACTS devices are used for dynamic control of voltage, impedance and phase angle of high voltage AC transmission lines [55]. With the improvements in current and voltage handling capabilities of power electronic devices that have allowed for the development of FACTS, the possibility has arisen using different types of controllers for efficient shunt and series compensation. Thus, FACTS controllers based on thyristor controlled reactors (TCRs), such as Static Var Compensators (SVCs) and Thyristor Controlled Series Capacitors (TCSCs), are being used by several utilities to compensate their systems. More recently, various types of controllers for shunt and series compensation, based on voltage source inverters (VSIs), i.e., Shunt and Series Static Synchronous Compensators (STATCOMs and SSSCs) and Unified Power Flow Controllers (UPFCs) have been proposed and developed [57]. However, due to the versatility in controlling active power flow, reactive power flow and voltage magnitude, UPFC [58] is selected for the work presented in this chapter.

### **5.2.1 Steady state model of Unified Power Flow Controllers**

Among the converter based FACTS-devices, the UPFC [59-60] is a versatile FACTS device, which can simultaneously control a local bus voltage and power flows of a transmission line and make it possible to control circuit impedance, voltage angle and power flow for optimal operation of power systems. In recent years, there has been increasing interest in computer modeling of the UPFC in power flow and on optimal power flow analysis [55-61]. However, in most recent research work, the UPFC is primarily used to control a local bus voltage and active and reactive power flows of a transmission line. As reported in [62], in practice, the UPFC series converter may have other control modes such as direct voltage injection, phase angle shifting and impedance control modes, etc.

The steady-state model of UPFC developed in [59-61] consists of an excitation transformer (ET), a boosting transformer (BT) and two voltage-source converters, i.e. series and shunt converters, connected to a dc link capacitor. The losses associated

congestion management [55-56]. The details of networks with FACTS controllers are discussed in the following section.

## **5.2 Flexible AC Transmission System (FACTS)**

FACTS devices are used for dynamic control of voltage, impedance and phase angle of high voltage AC transmission lines [55]. With the improvements in current and voltage handling capabilities of power electronic devices that have allowed for the development of FACTS, the possibility has arisen using different types of controllers for efficient shunt and series compensation. Thus, FACTS controllers based on thyristor controlled reactors (TCRs), such as Static Var Compensators (SVCs) and Thyristor Controlled Series Capacitors (TCSCs), are being used by several utilities to compensate their systems. More recently, various types of controllers for shunt and series compensation, based on voltage source inverters (VSIs), i.e., Shunt and Series Static Synchronous Compensators (STATCOMs and SSSCs) and Unified Power Flow Controllers (UPFCs) have been proposed and developed [57]. However, due to the versatility in controlling active power flow, reactive power flow and voltage magnitude, UPFC [58] is selected for the work presented in this chapter.

### ***5.2.1 Steady state model of Unified Power Flow Controllers***

Among the converter based FACTS-devices, the UPFC [59-60] is a versatile FACTS device, which can simultaneously control a local bus voltage and power flows of a transmission line and make it possible to control circuit impedance, voltage angle and power flow for optimal operation of power systems. In recent years, there has been increasing interest in computer modeling of the UPFC in power flow and on optimal power flow analysis [55-61]. However, in most recent research work, the UPFC is primarily used to control a local bus voltage and active and reactive power flows of a transmission line. As reported in [62], in practice, the UPFC series converter may have other control modes such as direct voltage injection, phase angle shifting and impedance control modes, etc.

The steady-state model of UPFC developed in [59-61] consists of an excitation transformer (ET), a boosting transformer (BT) and two voltage-source converters, i.e. series and shunt converters, connected to a dc link capacitor. The losses associated



with UPFC operation are typically neglected and under this assumption the UPFC will neither inject nor absorb any real power from the system while operating in steady state. This assumption translates into a constant voltage across the DC link capacitor. Thus, the steady-state model can be built by using a voltage source and its source impedance inserted in series with the line and another voltage source and its source impedance connected in shunt at the bus where the excitation transformer is connected. A simplified schematic representation of the UPFC is given in Figure 5.1, together with its equivalent circuit, in Figure 5.2. The series ( $V_p$ ) and shunt ( $V_q$ ) voltage sources allow independent control of the voltage magnitude, as well as the real and reactive power flows along a given transmission line [59-62].

The active power demanded by the series converter is drawn by the shunt converter from the AC network and supplied to bus  $m$  through the DC link. The output voltage of the series converter is added to the nodal voltage, at say bus  $k$ , to boost the nodal voltage at bus  $m$ . The voltage magnitude of the output voltage  $V_p$  provides voltage regulation, and the phase angle  $\delta_p$  determines the mode of power flow control [63].

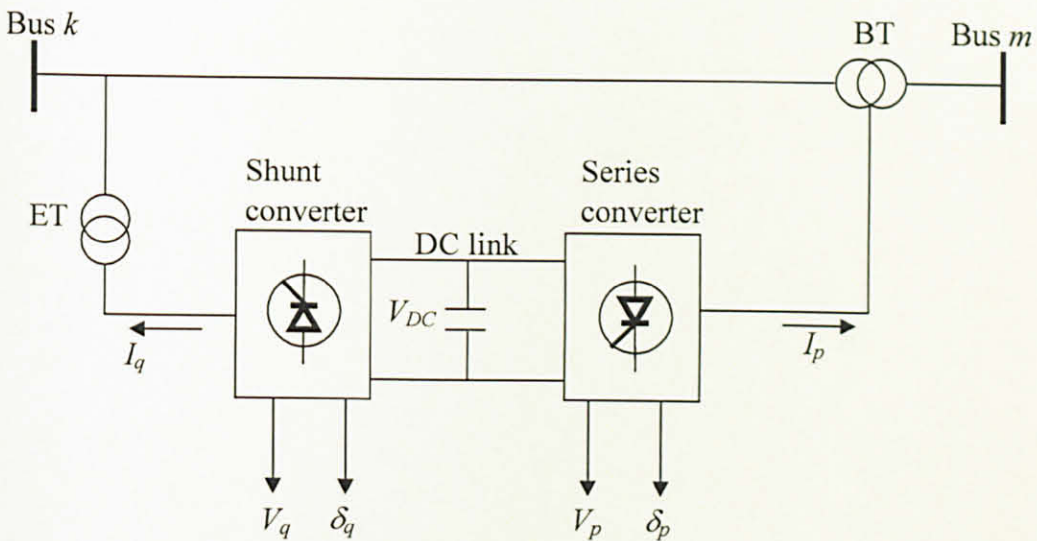


Figure 5.1 A simplified schematic diagram of UPFC.

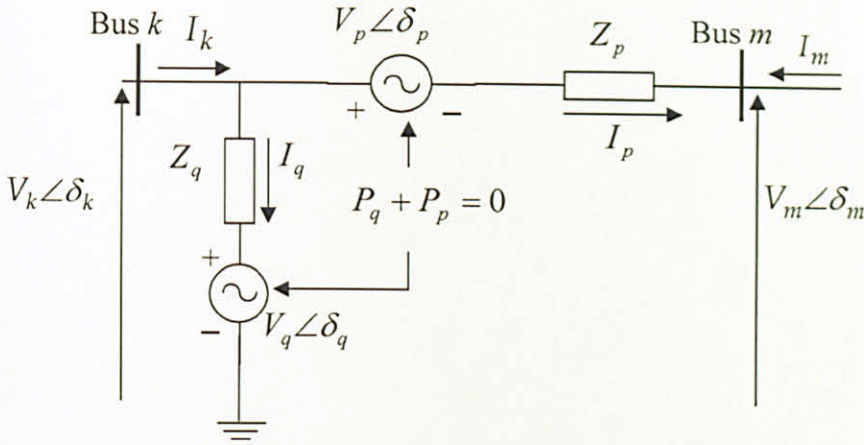


Figure 5.2 Steady state model of UPFC [60-62].

### 5.3 Mathematical Representation of UPFC [62, 67]

The two ideal voltage sources of the UPFC can be mathematically represented as:

$$E_q = V_q (\cos \delta_q + j \sin \delta_q) \quad (5.1)$$

$$E_p = V_p (\cos \delta_p + j \sin \delta_p) \quad (5.2)$$

where the output of shunt voltage source,  $V_q$  and  $\delta_q$  are controllable with the magnitude and phase angle between the limits of  $V_{q \max} \leq V_q \leq V_{q \min}$  and  $0 \leq \delta_q \leq 2\pi$ , respectively and the output of series voltage source,  $V_p$  and  $\delta_p$  are controllable with the magnitude and phase angle between the limits of  $V_{p \max} \leq V_p \leq V_{p \min}$  and  $0 \leq \delta_p \leq 2\pi$ , respectively. The behavior of these two voltage sources is independent from each other, but rather, they satisfy a common active power exchange with the external network.

Applying the Kirchhoff's current and voltage laws for the equivalent circuit shown in Figure 5.2, gives

$$\begin{bmatrix} I_k \\ I_m \end{bmatrix} = \begin{bmatrix} (Y_p + Y_q) & -Y_p & -Y_p & -Y_q \\ -Y_p & Y_p & Y_p & 0 \end{bmatrix} \begin{bmatrix} V_k \\ V_m \\ V_p \\ V_q \end{bmatrix} \quad (5.3)$$

where the  $Y_p = \frac{1}{Z_p}$  and  $Y_q = \frac{1}{Z_q}$

The element of the transfer admittance equation can be written as

$$\left. \begin{aligned} Y_{kk} &= G_{kk} + j B_{kk} = Y_p + Y_q \\ Y_{mm} &= G_{mm} + j B_{mm} = Y_p \\ Y_{km} &= Y_{mk} = G_{km} + j B_{km} = -Y_p \\ Y_{sh} &= G_{sh} + j B_{sh} = -Y_q \end{aligned} \right\} \quad (5.4)$$

The injected active and reactive powers at bus  $k$  and bus  $m$  may be derived using the complex power equation as follows:

$$\begin{aligned} \begin{bmatrix} S_k \\ S_m \end{bmatrix} &= \begin{bmatrix} V_k & 0 \\ 0 & V_m \end{bmatrix} \begin{bmatrix} I_k^* \\ I_m^* \end{bmatrix} \\ &= \begin{bmatrix} V_k & 0 \\ 0 & V_m \end{bmatrix} \begin{bmatrix} (Y_p^* + Y_q^*) & -Y_p^* & -Y_p^* & -Y_q^* \\ -Y_p^* & Y_p^* & Y_p^* & 0 \end{bmatrix} \begin{bmatrix} V_k^* \\ V_m^* \\ V_p^* \\ V_q^* \end{bmatrix} \end{aligned} \quad (5.5)$$

Substituting equation (5.4) into equation (5.5),

$$\begin{bmatrix} S_k \\ S_m \end{bmatrix} = \begin{bmatrix} V_k & 0 \\ 0 & V_m \end{bmatrix} \begin{bmatrix} G_{kk} - j B_{kk} & G_{km} - j B_{km} & G_{km} - j B_{km} & G_{sh} - j B_{sh} \\ G_{km} - j B_{km} & G_{mm} - j B_{mm} & G_{mm} - j B_{mm} & 0 \end{bmatrix} \begin{bmatrix} V_k^* \\ V_m^* \\ V_p^* \\ V_q^* \end{bmatrix} \quad (5.6)$$

Deriving for the active and reactive powers at bus  $k$  and bus  $m$  [62-64], (see APPENDIX C)

$$\begin{aligned} P_k &= V_k^2 (G_{kk}) + V_k V_m [G_{km} \cos(\delta_k - \delta_m) + B_{km} \sin(\delta_k - \delta_m)] \\ &\quad + V_k V_p [G_{km} \cos(\delta_k - \delta_p) + B_{km} \sin(\delta_k - \delta_p)] \\ &\quad + V_k V_q [G_{sh} \cos(\delta_k - \delta_q) + B_{sh} \sin(\delta_k - \delta_q)] \end{aligned} \quad (5.7)$$

$$\begin{aligned} Q_k &= -V_k^2 (B_{kk}) + V_k V_m [G_{km} \sin(\delta_k - \delta_m) - B_{km} \cos(\delta_k - \delta_m)] \\ &\quad + V_k V_p [G_{km} \sin(\delta_k - \delta_p) - B_{km} \cos(\delta_k - \delta_p)] \\ &\quad + V_k V_q [G_{sh} \sin(\delta_k - \delta_q) - B_{sh} \cos(\delta_k - \delta_q)] \end{aligned} \quad (5.8)$$

$$\begin{aligned} P_m &= V_m^2 (G_{mm}) + V_m V_k [G_{mk} \cos(\delta_m - \delta_k) + B_{mk} \sin(\delta_m - \delta_k)] \\ &\quad + V_m V_p [G_{mm} \cos(\delta_m - \delta_p) + B_{mm} \sin(\delta_m - \delta_p)] \end{aligned} \quad (5.9)$$

$$Q_m = -V_m^2 (B_{mm}) + V_m V_k [G_{mk} \sin(\delta_m - \delta_k) - B_{mk} \cos(\delta_m - \delta_k)] \\ + V_m V_p [G_{mp} \sin(\delta_m - \delta_p) - B_{mp} \cos(\delta_m - \delta_p)] \quad (5.10)$$

Also, the active and reactive powers for the series converter can be derived as follows:

$$S_p = P_p + jQ_p = V_p I_m^* = V_m [Y_{mk}^* V_k^* + Y_{mm}^* V_m^* + Y_{mp}^* V_p^*] \quad (5.11)$$

$$P_p = V_p^2 (G_{pp}) + V_p V_k [G_{pk} \cos(\delta_p - \delta_k) + B_{pk} \sin(\delta_p - \delta_k)] \\ + V_p V_m [G_{pm} \cos(\delta_p - \delta_m) + B_{pm} \sin(\delta_p - \delta_m)] \quad (5.12)$$

$$Q_p = -V_p^2 (B_{pp}) + V_p V_k [G_{pk} \sin(\delta_p - \delta_k) - B_{pk} \cos(\delta_p - \delta_k)] \\ + V_p V_m [G_{pm} \sin(\delta_p - \delta_m) - B_{pm} \cos(\delta_p - \delta_m)] \quad (5.13)$$

Further, the active and reactive powers for the shunt converter can be derived as follows:

$$S_q = P_q + jQ_q = V_q I_q^* = V_q Y_{sh}^* [V_q^* - V_k^*] \quad (5.14)$$

$$P_q = -V_q^2 (G_{sh}) + V_q V_k [G_{sh} \cos(\delta_q - \delta_k) + B_{sh} \sin(\delta_q - \delta_k)] \quad (5.15)$$

$$Q_q = V_q^2 (B_{sh}) + V_q V_k [G_{sh} \sin(\delta_q - \delta_k) - B_{sh} \cos(\delta_q - \delta_k)] \quad (5.16)$$

Assuming lossless voltage sources model implies that there is no absorption or generation of active power by the two converters with respect to the AC system. Hence, the active power supplied to the shunt converter  $P_q$  must be equal to the active power demanded by the series converter  $P_p$  at the DC link. Then the following equality constraint has to be guaranteed.

$$P_{bb} = P_q + P_p = 0 \quad (5.17)$$

#### 5.4 Modification of Algorithms of SE with UPFC

Compared with the WLS state estimation, the measurement equations for the bus injected powers of the UPFC buses should be modified. Figure 5.3 shows the four possible measurements on line  $k - m$  embedded with UPFC.

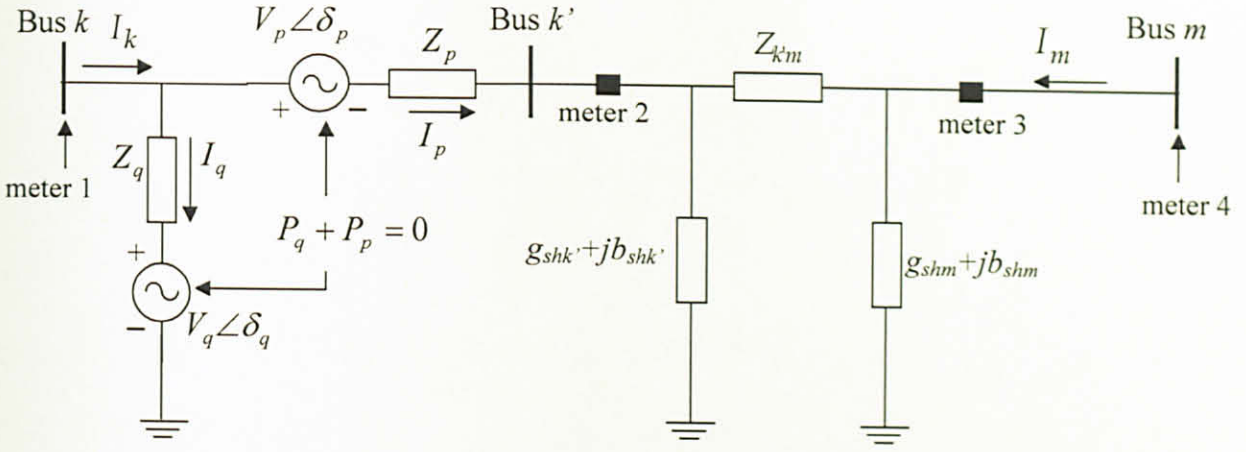


Figure 5.3 Equivalent circuit of UPFC including transmission line.

Suppose a UPFC is installed on line  $k - m$ . To include the UPFC in the network an additional bus (bus  $k'$ ) is introduced as shown. Measurements 1, 2, 3, 4 are the measurements that can be placed on line  $k - m$ .

Power measurement at meter 1 are given by,

$$P_k = V_k^2 (G_{kk} + G_{km}) + V_k \sum_{j=1, j \neq k, m}^N V_j (G_{kj} \cos(\delta_{kj}) + B_{kj} \sin(\delta_{kj})) + V_k V_p B_p \sin(\delta_{kp}) - V_k V_{k'} B_p \sin(\delta_{kk'}) - V_k V_q B_q \sin(\delta_{kq}) \quad (5.18)$$

$$Q_k = -V_k^2 (B_{kk} + B_{km} + B_p + B_q) + V_k \sum_{j=1, j \neq k, m}^N V_j (G_{kj} \sin(\delta_{kj}) - B_{kj} \cos(\delta_{kj})) - V_k V_p B_p \cos(\delta_{kp}) + V_k V_{k'} B_p \cos(\delta_{kk'}) + V_k V_q B_q \cos(\delta_{kq}) \quad (5.19)$$

Power measurement at meter 2 are given by,

$$P_{km} = V_{k'}^2 G_{km} + V_{k'} V_m (G_{km} \cos(\delta_{k'} - \delta_m) + B_{km} \sin(\delta_{k'} - \delta_m)) \quad (5.20)$$

$$Q_{km} = -V_{k'}^2 (B_{km} + b_{sh_{k'}}) - V_{k'} V_m (G_{km} \sin(\delta_{k'} - \delta_m) - B_{km} \cos(\delta_{k'} - \delta_m)) \quad (5.21)$$

Power measurement at meter 3 are given by,

$$P_m = V_m^2 (G_{km} + g_{sh_m}) - V_m V_k (G_{km} \cos(\delta_k - \delta_m) - B_{km} \sin(\delta_k - \delta_m)) + V_m V_p (G_{km} \cos(\delta_m - \delta_p) + B_{km} \sin(\delta_m - \delta_p)) \quad (5.22)$$

$$Q_{mk} = -V_m^2 (B_{km} - b_{sh_m}) + V_m V_k (G_{km} \sin(\delta_k - \delta_m) + B_{km} \cos(\delta_k - \delta_m)) \\ + V_m V_p (G_{km} \sin(\delta_m - \delta_p) - B_{km} \cos(\delta_m - \delta_p)) \quad (5.23)$$

Power measurement at meter 4 are given by,

$$P_m = V_m^2 (G_{mm} + G_{km} + g_{sh_m}) + V_m \sum_{j=1, j \neq k, m}^N V_j (G_{mj} \cos(\delta_m - \delta_j) + B_{mj} \sin(\delta_m - \delta_j)) \\ + V_m V_k (G_{km} \cos(\delta_m - \delta_k) + B_{km} \sin(\delta_m - \delta_k)) + V_m V_p (G_{km} \cos(\delta_m - \delta_p) + B_{km} \sin(\delta_m - \delta_p)) \quad (5.24)$$

$$Q_m = -V_m^2 (B_{mm} + B_{km} + b_{sh_m}) + V_m \sum_{j=1, j \neq k, m}^N V_j (G_{mj} \sin(\delta_m - \delta_j) - B_{mj} \cos(\delta_m - \delta_j)) \\ + V_m V_k (G_{km} \sin(\delta_m - \delta_k) - B_{km} \cos(\delta_m - \delta_k)) + V_m V_p (G_{km} \sin(\delta_m - \delta_p) - B_{km} \cos(\delta_m - \delta_p)) \quad (5.25)$$

From the above equations (5.18 through 5.25), it can conclude that by connecting any FACTS devices in a line, the original equations need to be modified. The increase in the dimensions of the Jacobian, compared with the case when there are no power system controllers, is proportional to the number and type of such controllers. In very general terms, the structure of the modified Jacobian is shown in equation (5.26). In this case, the estimated state variables vector takes into account the nodal voltage magnitudes and angles,  $\hat{x}$ , excluding the reference nodal angle, as well as the FACTS controllers state variables,  $\hat{x}_{upfc}$ , i.e.  $\hat{x} = [\hat{x}, \hat{x}_{upfc}]$ . Hence, the Jacobian matrix  $H(\hat{x})$  is extended as follows,

$$H(\hat{x}, \hat{x}_{upfc}) = \begin{bmatrix} \frac{\partial h(\hat{x}, \hat{x}_{upfc})}{\partial \hat{x}} & \frac{\partial h(\hat{x}, \hat{x}_{upfc})}{\partial \hat{x}_{upfc}} \\ \frac{\partial h_{upfc}(\hat{x}, \hat{x}_{upfc})}{\partial \hat{x}} & \frac{\partial h_{upfc}(\hat{x}, \hat{x}_{upfc})}{\partial \hat{x}_{upfc}} \end{bmatrix} \quad (5.26)$$

where  $h(\hat{x}, \hat{x}_{upfc}) \in \mathfrak{R}^M$  is the measured vector and  $h_{upfc}(\hat{x}, \hat{x}_{upfc}) \in \mathfrak{R}^{UPFC}$  is the measurement associated with the mismatch equation as in equation (5.17). For example if full measurements are available in the system as in Figure 5.2, the contribution of the UPFC to the Jacobian matrix,  $H$ , in equation (5.26) is given by,

$$\begin{bmatrix}
0 & 0 & \frac{\partial V_k}{\partial V_k} & 0 & 0 & 0 & 0 & 0 \\
0 & 0 & 0 & \frac{\partial V_m}{\partial V_m} & 0 & 0 & 0 & 0 \\
\frac{\partial P_k}{\partial \delta_k} & \frac{\partial P_k}{\partial \delta_m} & \frac{\partial P_k}{\partial V_k} & \frac{\partial P_k}{\partial V_m} & \frac{\partial P_k}{\partial \delta_p} & \frac{\partial P_k}{\partial V_p} & \frac{\partial P_k}{\partial \delta_q} & \frac{\partial P_k}{\partial V_q} \\
\frac{\partial P_m}{\partial \delta_k} & \frac{\partial P_m}{\partial \delta_m} & \frac{\partial P_m}{\partial V_k} & \frac{\partial P_m}{\partial V_m} & \frac{\partial P_m}{\partial \delta_p} & \frac{\partial P_m}{\partial V_p} & 0 & 0 \\
\frac{\partial Q_k}{\partial \delta_k} & \frac{\partial Q_k}{\partial \delta_m} & \frac{\partial Q_k}{\partial V_k} & \frac{\partial Q_k}{\partial V_m} & \frac{\partial Q_k}{\partial \delta_p} & \frac{\partial Q_k}{\partial V_p} & \frac{\partial Q_k}{\partial \delta_q} & \frac{\partial Q_k}{\partial V_q} \\
\frac{\partial Q_m}{\partial \delta_k} & \frac{\partial Q_m}{\partial \delta_m} & \frac{\partial Q_m}{\partial V_k} & \frac{\partial Q_m}{\partial V_m} & \frac{\partial Q_m}{\partial \delta_p} & \frac{\partial Q_m}{\partial V_p} & 0 & 0 \\
\frac{\partial p_{km}}{\partial \delta_k} & \frac{\partial p_{km}}{\partial \delta_m} & \frac{\partial p_{km}}{\partial V_k} & \frac{\partial p_{km}}{\partial V_m} & \frac{\partial p_{km}}{\partial \delta_p} & \frac{\partial p_{km}}{\partial V_p} & \frac{\partial p_{km}}{\partial \delta_q} & \frac{\partial p_{km}}{\partial V_q} \\
\frac{\partial p_{mk}}{\partial \delta_k} & \frac{\partial p_{mk}}{\partial \delta_m} & \frac{\partial p_{mk}}{\partial V_k} & \frac{\partial p_{mk}}{\partial V_m} & \frac{\partial p_{mk}}{\partial \delta_p} & \frac{\partial p_{mk}}{\partial V_p} & 0 & 0 \\
\frac{\partial q_{km}}{\partial \delta_k} & \frac{\partial q_{km}}{\partial \delta_m} & \frac{\partial q_{km}}{\partial V_k} & \frac{\partial q_{km}}{\partial V_m} & \frac{\partial q_{km}}{\partial \delta_p} & \frac{\partial q_{km}}{\partial V_p} & \frac{\partial q_{km}}{\partial \delta_q} & \frac{\partial q_{km}}{\partial V_q} \\
\frac{\partial q_{mk}}{\partial \delta_k} & \frac{\partial q_{mk}}{\partial \delta_m} & \frac{\partial q_{mk}}{\partial V_k} & \frac{\partial q_{mk}}{\partial V_m} & \frac{\partial q_{mk}}{\partial \delta_p} & \frac{\partial q_{mk}}{\partial V_p} & 0 & 0 \\
\frac{\partial P_{bb}}{\partial \delta_k} & \frac{\partial P_{bb}}{\partial \delta_m} & \frac{\partial P_{bb}}{\partial V_k} & \frac{\partial P_{bb}}{\partial V_m} & \frac{\partial P_{bb}}{\partial \delta_p} & \frac{\partial P_{bb}}{\partial V_p} & \frac{\partial P_{bb}}{\partial \delta_q} & \frac{\partial P_{bb}}{\partial V_q}
\end{bmatrix} \quad (5.27)$$

Prior to simulation the proposed algorithm, Power System Analysis Toolbox (PSAT) [65] is used in order to evaluate the performance of the UPFC placed at various PV buses. For each test network in SE simulation, the results obtained in the PSAT analysis will be taken as the reference. The UPFC's constraints which should be added to the estimation equations are as follows: [60-64]

$$\text{Shunt Power Constraints: } \sqrt{P_q^2 + Q_q^2} \leq S_{q,\max} \quad (5.28)$$

$$\text{Series Power Constraints: } \sqrt{P_p^2 + Q_p^2} \leq S_{p,\max} \quad (5.29)$$

$$\text{Series Voltage Constraints: } |V_p| \leq V_{p,\max} \quad (5.30)$$

$$\text{Shunt Voltage Constraints: } |V_q| \leq V_{q,\max} \quad (5.31)$$

The parameters of UPFC are considered to be successfully estimated if all the constraints in equation (5.17) and equations (5.28) through (5.31) are met.

## 5.5 Power Flow Simulation

Due to space limitation, the result of simulation study was carried out only on two different test systems. The power system networks are modeled based on the bus and line data furnished in Chapter 2. For each test case, the power system network without the UPFC is taken as the reference.

### 5.5.1 5-bus test system

The 5-bus network is modified to include one UPFC to compensate the transmission line linking bus 3 and bus 4. The modified network is shown in Figure 5.4. The UPFC is used to maintain active and reactive powers leaving the UPFC, towards bus 4, at 0.4 p.u. and 0.02 p.u., respectively. Moreover, the UPFC shunt converter is set to regulate the nodal voltage magnitude at bus 3 at 1 p.u.

The starting values of the UPFC voltage sources are taken to be  $V_p = 0.04$  p.u.,  $\delta_p = 87.13^\circ$ ,  $V_q = 1$  p.u., and  $\delta_q = 0^\circ$ . The source impedances have values of  $X_p = X_q = 0.1$  p.u. Convergence is obtained in five iterations to a power mismatch tolerance of  $1e-12$ . The UPFC upheld its target values. The power flow results are shown in Table 5.1, and the bus voltages are given in Table 5.2. Power flow analysis has been performed according to suitable location of UPFC as proposed in [66]. The PSAT software is used to run the power flow analysis.



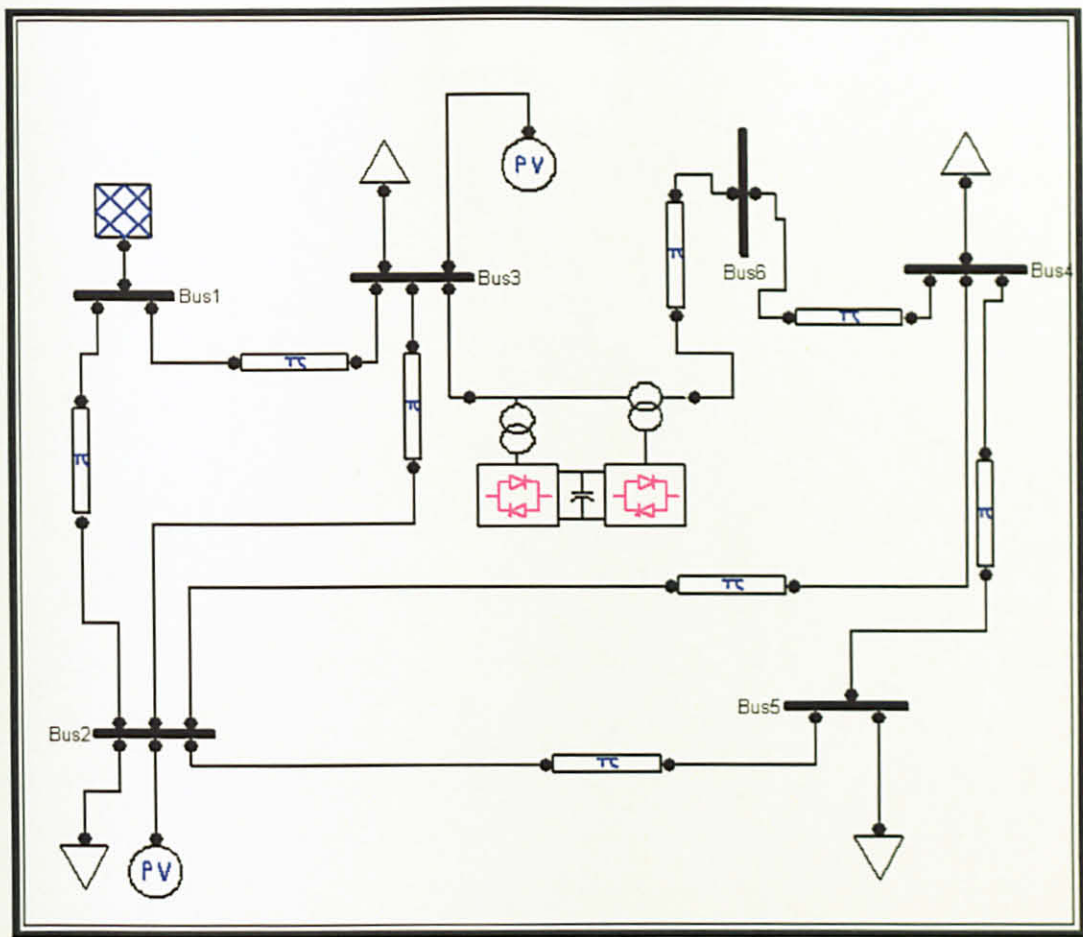


Figure 5.4 5-bus –Power System Model.

Table 5.1 IEEE 5-bus power flow results.

Branch no.	From Bus	To Bus	From Bus Injection		To Bus Injection		Loss	
			P (p.u.)	Q (p.u.)	P (p.u.)	Q (p.u.)	P (p.u.)	Q (p.u.)
1	1	2	0.81143	0.76424	-0.78838	0.75879	0.023053	0.005452
2	1	3	0.50341	0.093432	-0.48431	0.089238	0.019095	0.004194
3	2	3	0.37484	0.12969	-0.36569	0.11715	0.009152	0.012543
4	2	4	0.13739	0.0178	-0.13626	0.01847	0.001133	0.036269
5	2	5	0.47614	0.051405	-0.4669	0.052915	0.009245	0.00151
6	3	4	0.4	0.02	-0.39838	0.034904	0.00162	0.014904
7	4	5	0.13464	0.0033731	-0.1331	0.047085	0.001538	0.043712

Table 5.2 The result of bus voltages and bus power injections.

Bus	Voltage		PQ Bus	
	$ V $ (p.u.)	$\delta$ (deg.)	$P$ (p.u.)	$Q$ (p.u.)
1	1.0600	0	1.3148	0.85767
2	1.0000	-1.7693	0.4	0.75487
3	1.0000	-6.0161	-0.85	0.027912
4	0.9917	-3.1906	-0.4	0.05
5	0.9745	-4.9741	-0.6	0.1
6 (additional)	0.9965	-2.5122	0.4	0.02

The power flows in the network embedded with UPFC are different from the results without UPFC as in Chapter 2. The most noticeable changes are the active power flowing towards bus 3 through branch 3 and 4 as shown in Figure 5.5. The increase is in response to the large amount of active power demanded by the UPFC series converter. The maximum amount of active power exchanged between the UPFC and the AC system will depend on the robustness of the UPFC shunt bus, bus 3. Since the UPFC generates its own reactive power, the generator at bus 1 decreases its reactive power generation by 5.6 %, and the generator connected at bus 2 increases its absorption of reactive power by 22.6 % as illustrated in Figure 5.6 and 5.7 respectively. Later, these power flow results are used to verify the SE results in the next section.

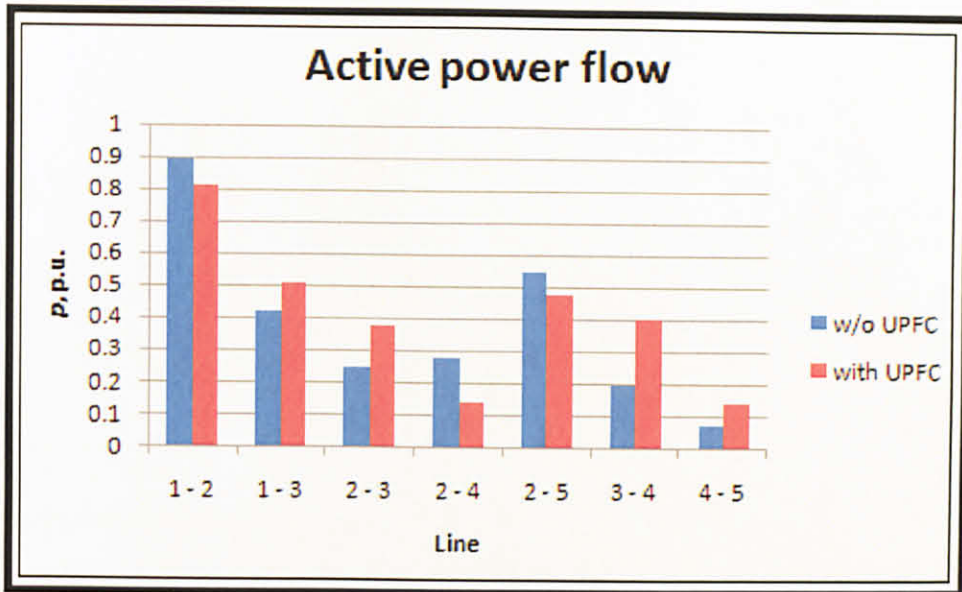


Figure 5.5 Comparison of active power flow with and without UPFC.

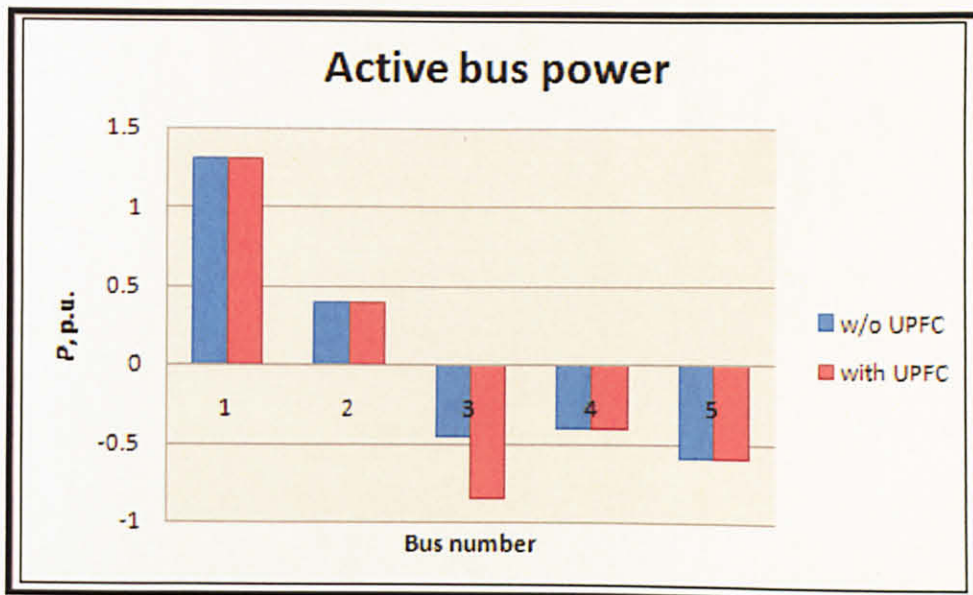


Figure 5.6 Comparison of active bus power with and without UPFC.

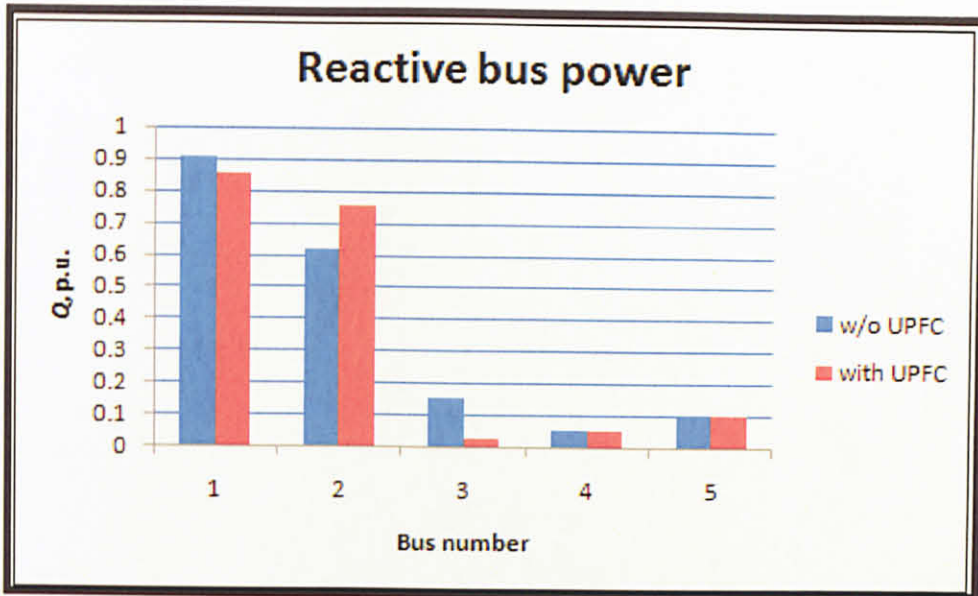


Figure 5.7 Comparison of reactive bus power with and without UPFC.

### 5.5.2 IEEE 14-bus system

In the IEEE 14-bus test system, eight test cases are conducted. Case 1 functions as the base case in which the system network is not incorporated with any FACTS controller. For the other 7 test cases, the UPFC has been installed at all the allowed PV buses (Bus 2, Bus 3 and Bus 6). The test cases are presented as follows:

- i. Case 1: Power flow analysis without FACTS controller.
- ii. Case 2: Power flow analysis with a UPFC installed at line 1
- iii. Case 3: Power flow analysis with a UPFC installed at line 2
- iv. Case 4: Power flow analysis with a UPFC installed at line 4
- v. Case 5: Power flow analysis with a UPFC installed at line 5
- vi. Case 6: Power flow analysis with a UPFC installed at line 12
- vii. Case 7: Power flow analysis with a UPFC installed at line 13
- viii. Case 8: Power flow analysis with a UPFC installed at line 16

Power flow analysis has been performed on all the test cases. The real and reactive power losses for all the cases are then evaluated and the percentage reduction is tabulated in Table 5.3. The power flow results of these cases are shown in Figures 5.8 and 5.9.

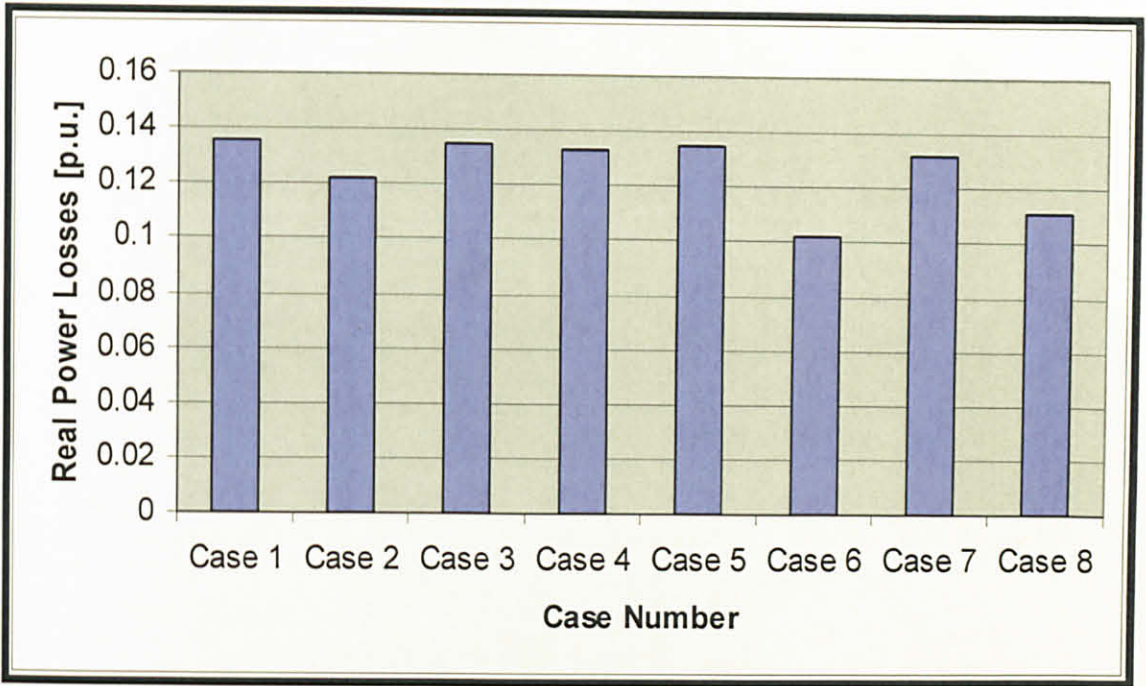


Figure 5.8 IEEE 14-bus Real Power Losses.

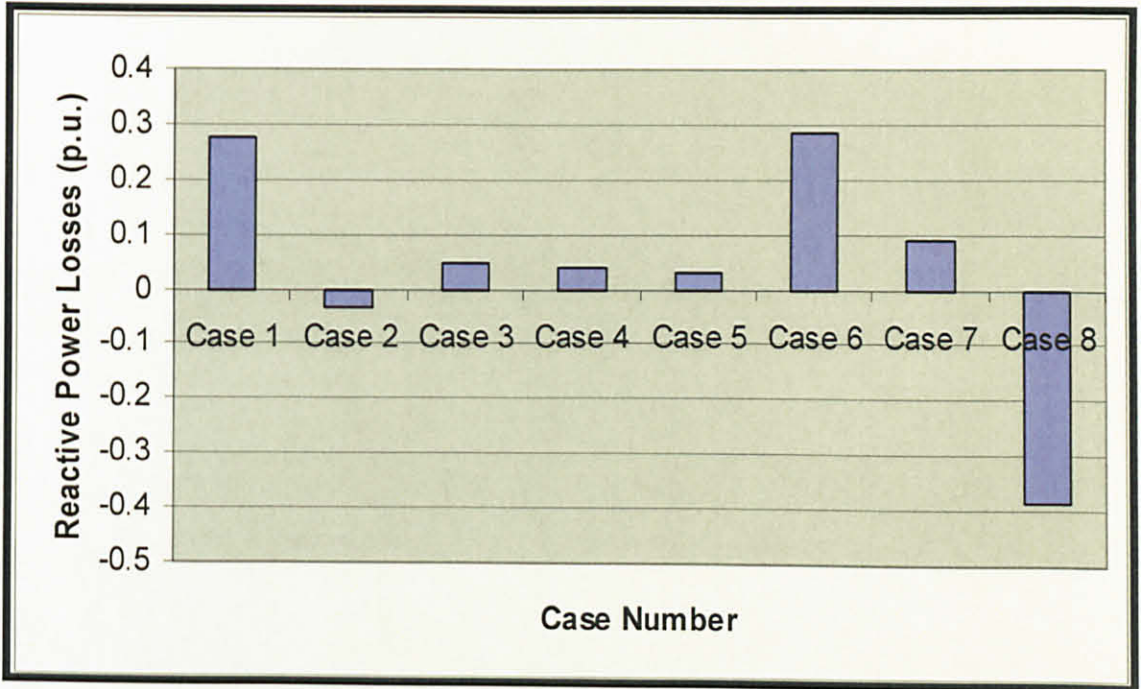


Figure 5.9 IEEE 14-bus Reactive Power Losses.

Table 5.3 Reduction in Real and Reactive Power Losses (%) for IEEE 14-bus Test System.

Test Case	Reduction in Real Power Losses (%)	Reduction in Reactive Power Losses (%)
Case 2	9.97	87.52
Case 3	0.76	82.71
Case 4	2.28	86.43
Case 5	0.84	<b>88.56</b>
Case 6	<b>24.65</b>	4.41
Case 7	3.08	67.43
Case 8	18.31	40.48

For the Real Power Losses, the largest reduction is found by incorporating the UPFC at Line 12 (case 6: Branch 2 – 3). It has been reduced by 24.65 %. The range of the real power losses reduction is in between 0.76 % to 24.65 %. The least amount of reduction in real power losses occurred for case 3 (UPFC incorporated at Branch 6 – 13).

The negative sign in the reactive power losses indicates that the reactive losses are capacitive. For the Reactive Power Losses, the greatest amount of total losses reduced, occurred at Line 5, by 88.56 %. The range of the reactive power losses reduction is in between 4.41 % to 88.56 %. The least amount of reduction in reactive power losses occurred for case 6 (UPFC incorporated at Branch 2 – 3).

Further analysis has been conducted on the test cases with the greatest reduction in the real and reactive power losses. Analysis is conducted on voltage magnitude, voltage phase angle, real power and reactive power profiles at all the buses for cases 5 and 6, using case 1 as the reference.

#### 5.5.2.1 Case 1 (Power flow analysis without UPFC)

In case 1, power flow analysis is performed on the IEEE 14-bus test system without the UPFC. Figures 5.10 to 5.13 present the voltage magnitude, voltage phase angle, real power and reactive power profiles at all the buses for case 1.

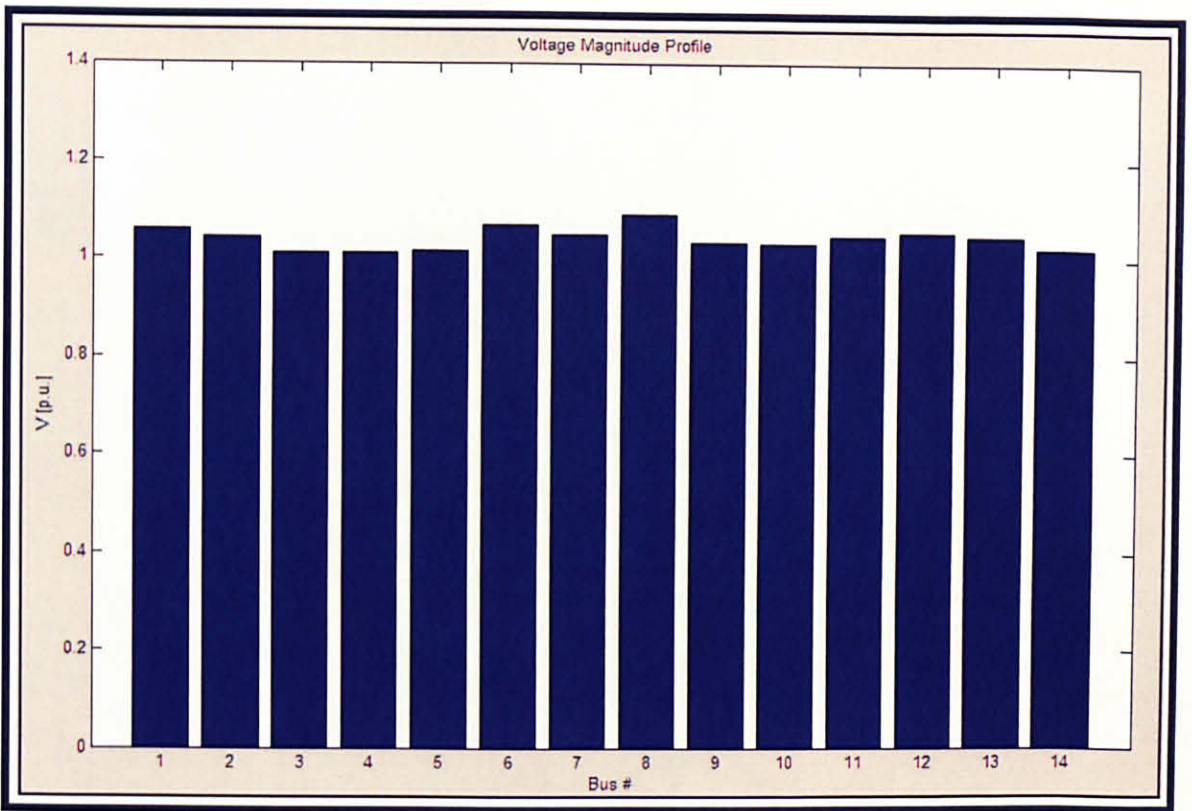


Figure 5.10 IEEE 14-bus – Case 1 voltage magnitude profile, without UPFC.

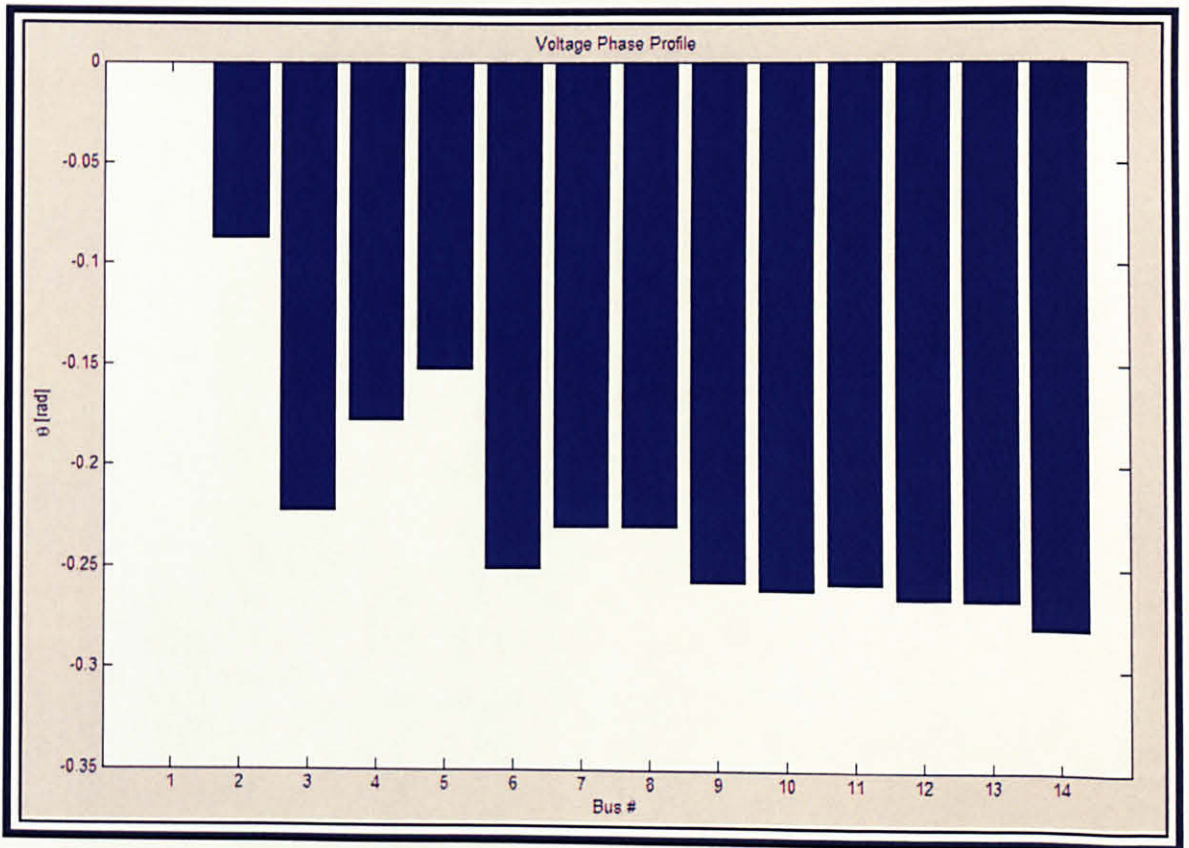


Figure 5.11 IEEE 14-bus – Case 1 voltage phase angle profile, without UPFC.

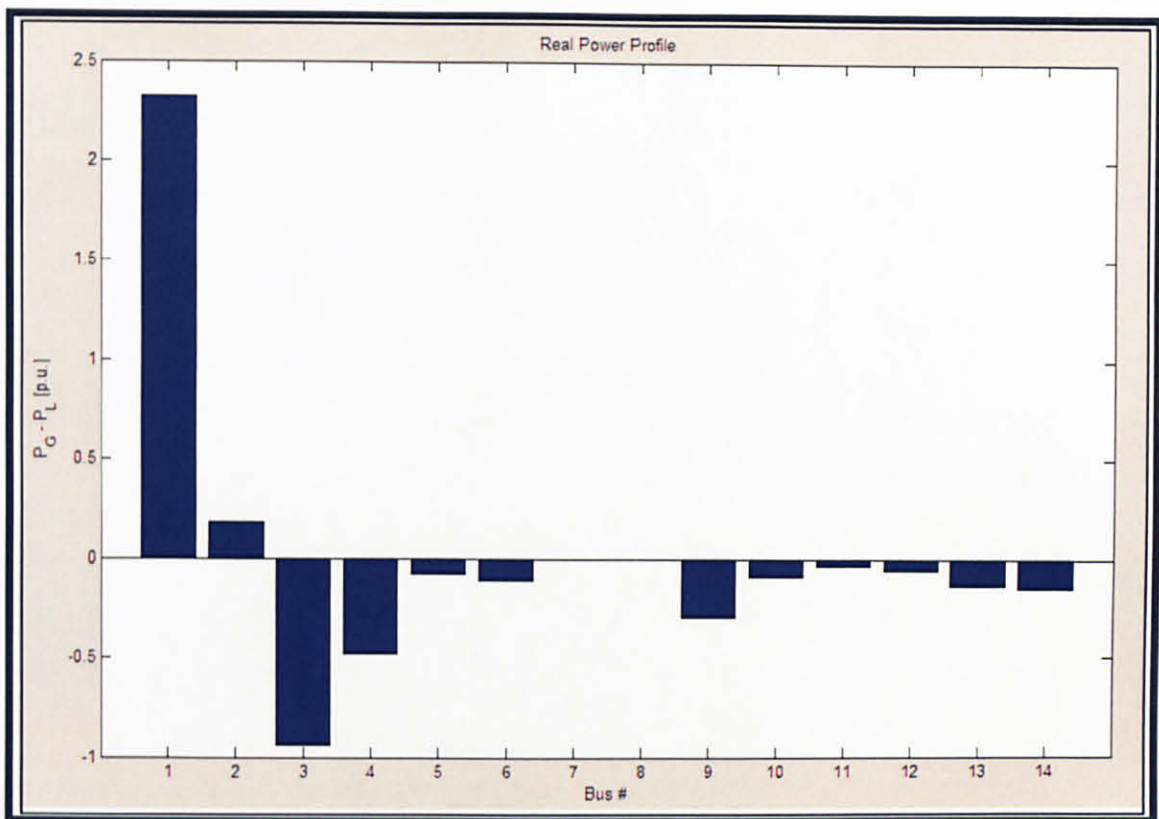


Figure 5.12 IEEE 14-bus – Case 1 real power profile, without UPFC.

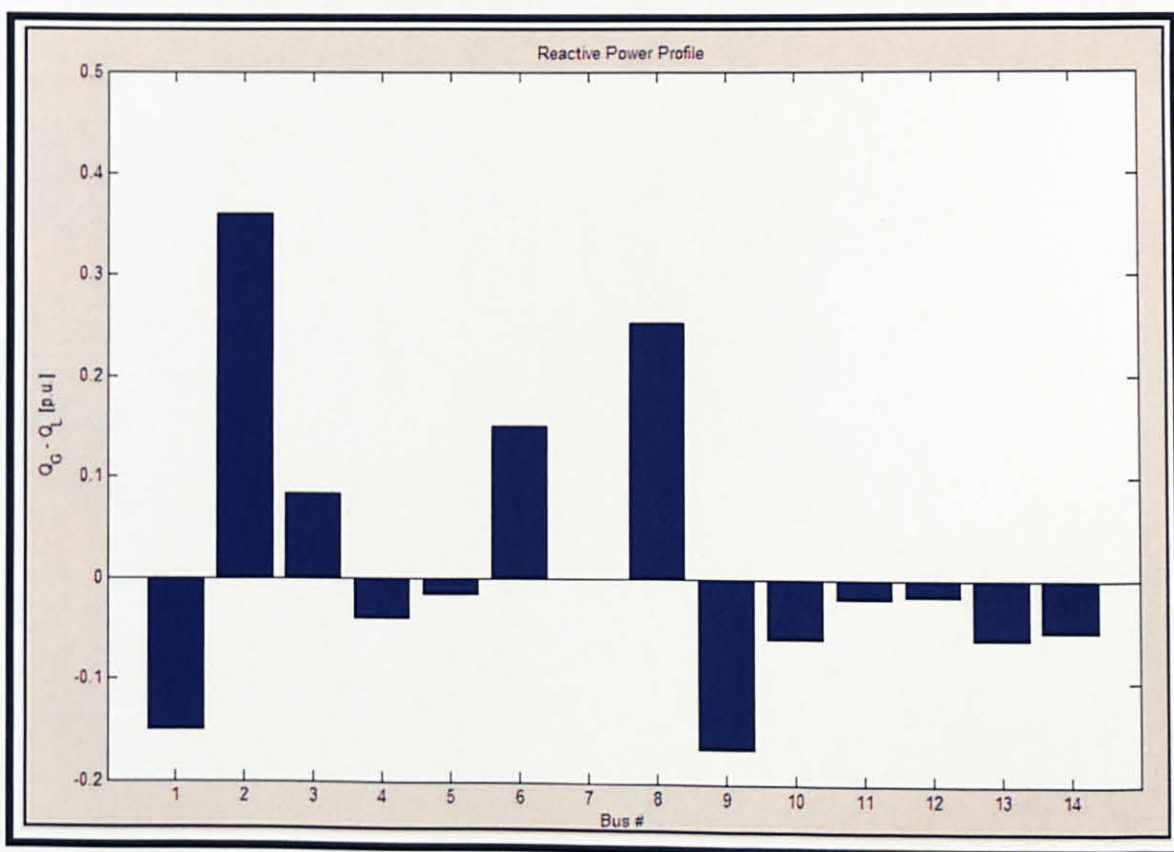


Figure 5.13 IEEE 14-bus – Case 1 reactive power profile, without UPFC.



5.5.2.2 Case 5 (Power flow analysis with a UPFC installed at Line 5)

In case 5, power flow analysis is performed on the IEEE 14-bus test system with a UPFC installed a Line 5 (Branch 6 – 11), as shown in Figure 5.14. Figures 5.15 to 5.18 present the voltage magnitude, voltage phase, real power and reactive power profiles at all the buses for case 5.

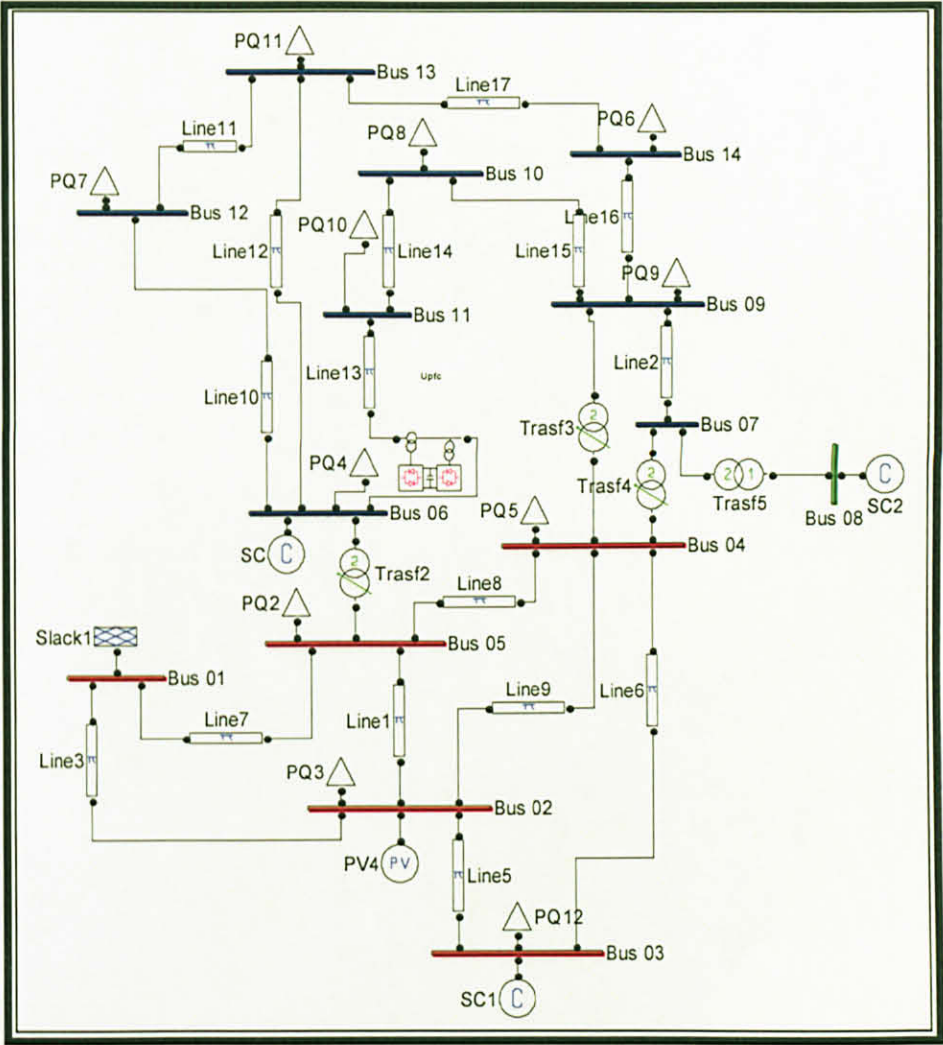


Figure 5.14 IEEE 14-bus – Power System Model with UPFC is connected at line 6 – 11.

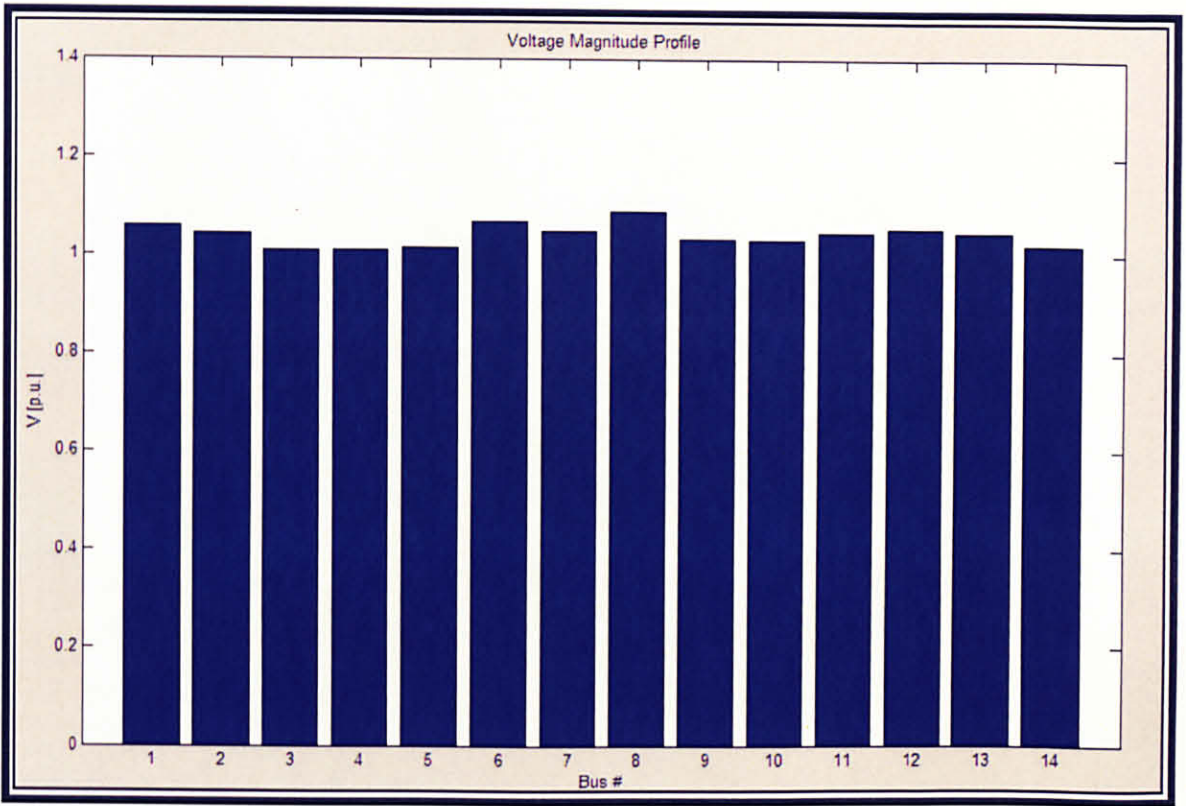


Figure 5.15 IEEE 14-bus – Case 5 voltage magnitude profile, with UPFC.

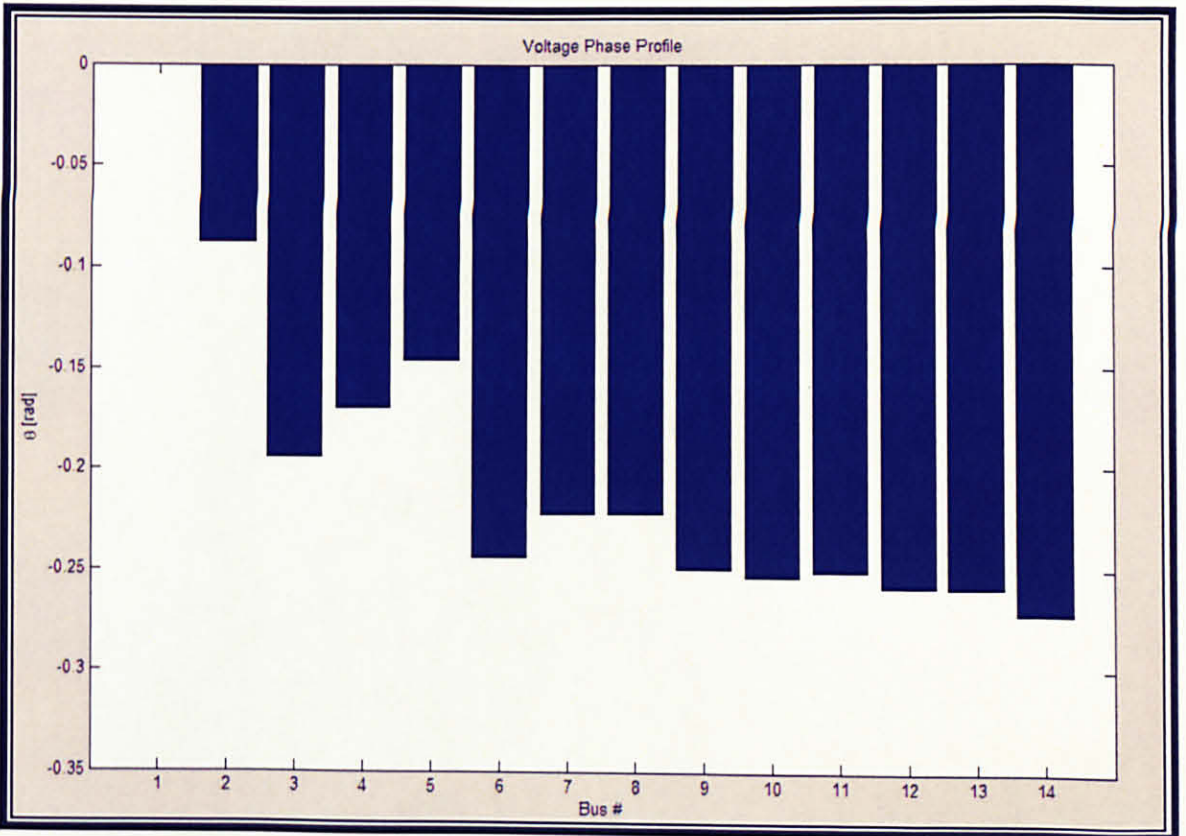


Figure 5.16 IEEE 14-bus – Case 5 voltage phase angle profile, with UPFC.

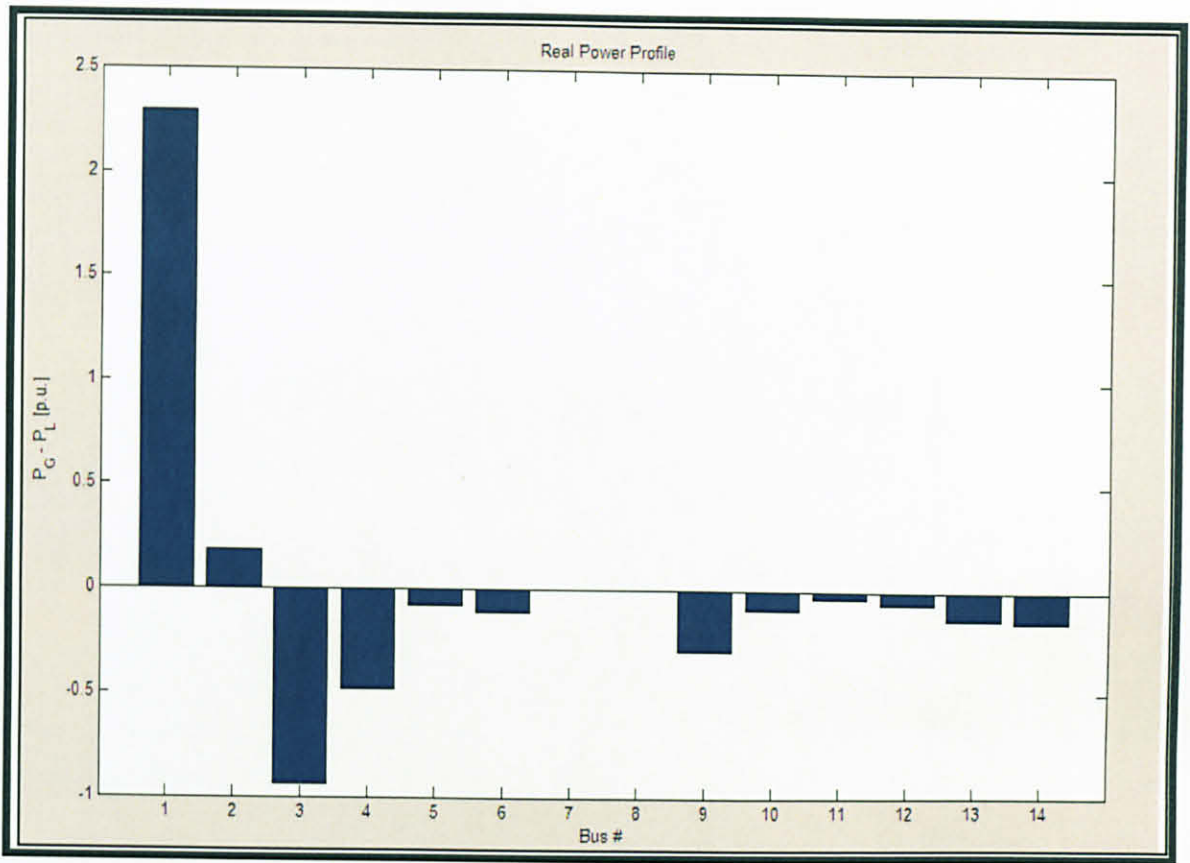


Figure 5.17 IEEE 14-bus – Case 5 real power profile, with UPFC.

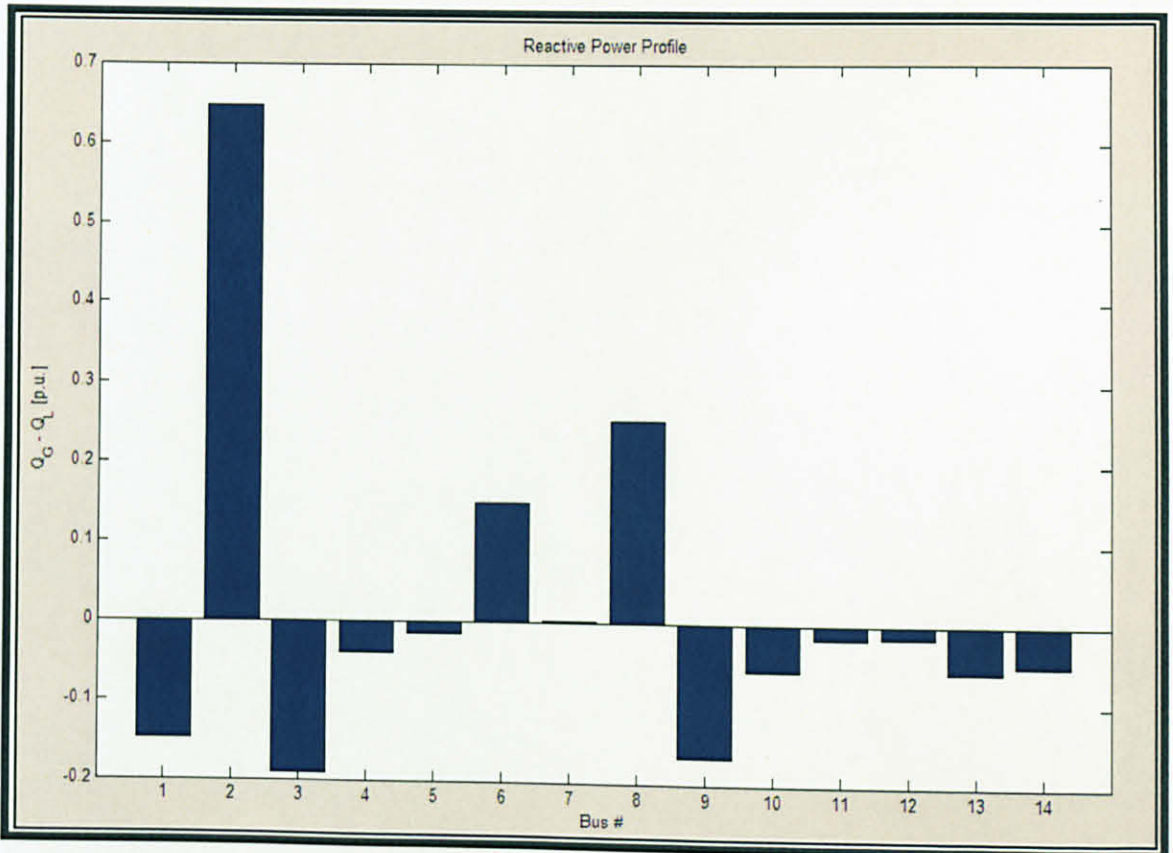


Figure 5.18 IEEE 14-bus – Case 5 reactive power profile, with UPFC.

### 5.5.2.3 Case 6 (Power flow analysis with a UPFC installed at Line 12)

In case 6, power flow analysis is performed on the IEEE 14-bus test system with a UPFC installed at Line 12 (Branch 2 – 3). Figures 5.19 to 5.22 present the voltage magnitude, voltage phase, real power and reactive power profiles at all the buses for case 6.

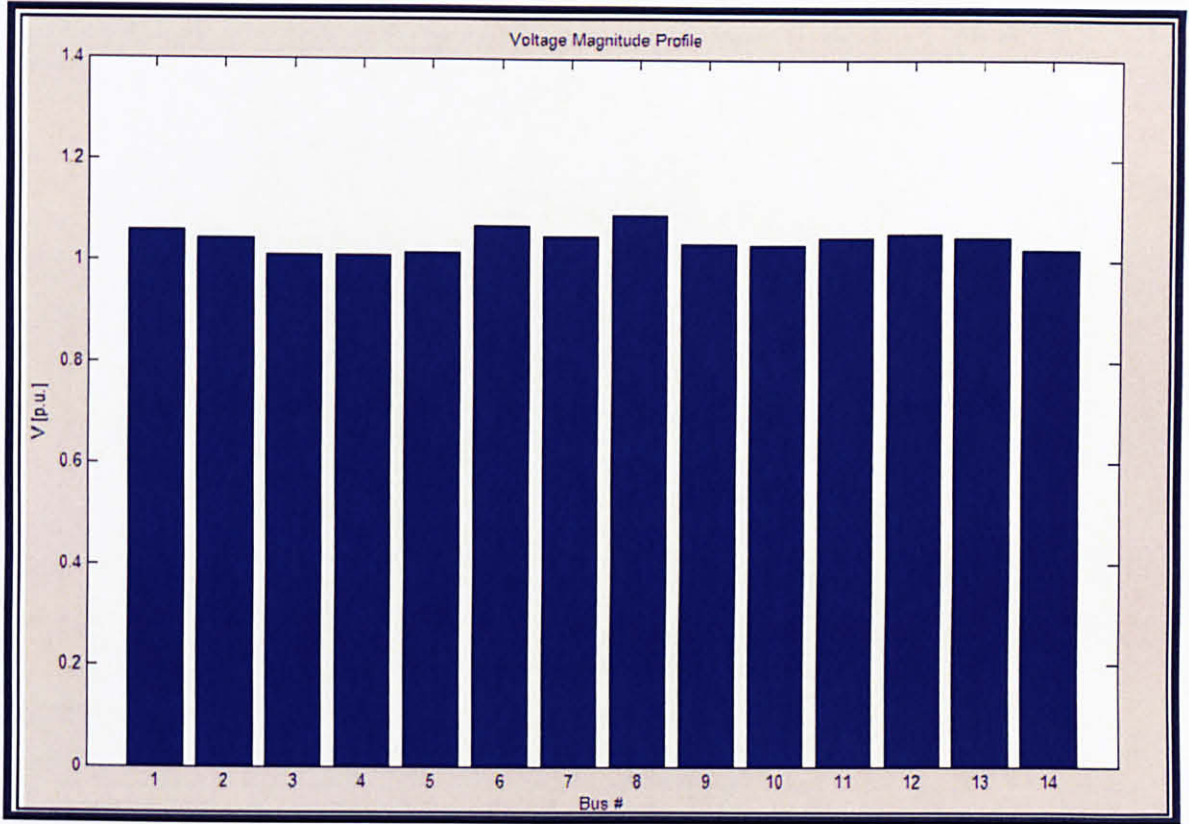


Figure 5.19 IEEE 14-bus – Case 6 voltage magnitude profile, with UPFC.

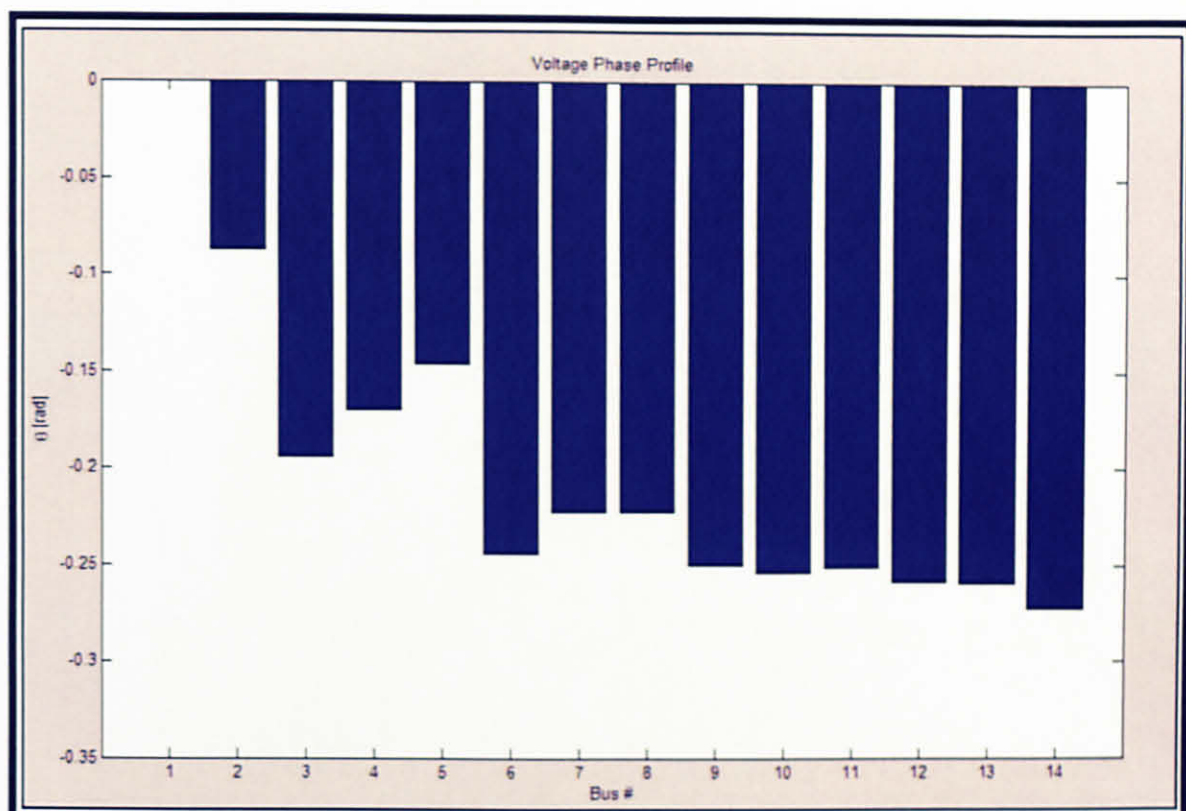


Figure 5.20 IEEE 14-bus – Case 6 voltage phase angle profile, with UPFC.

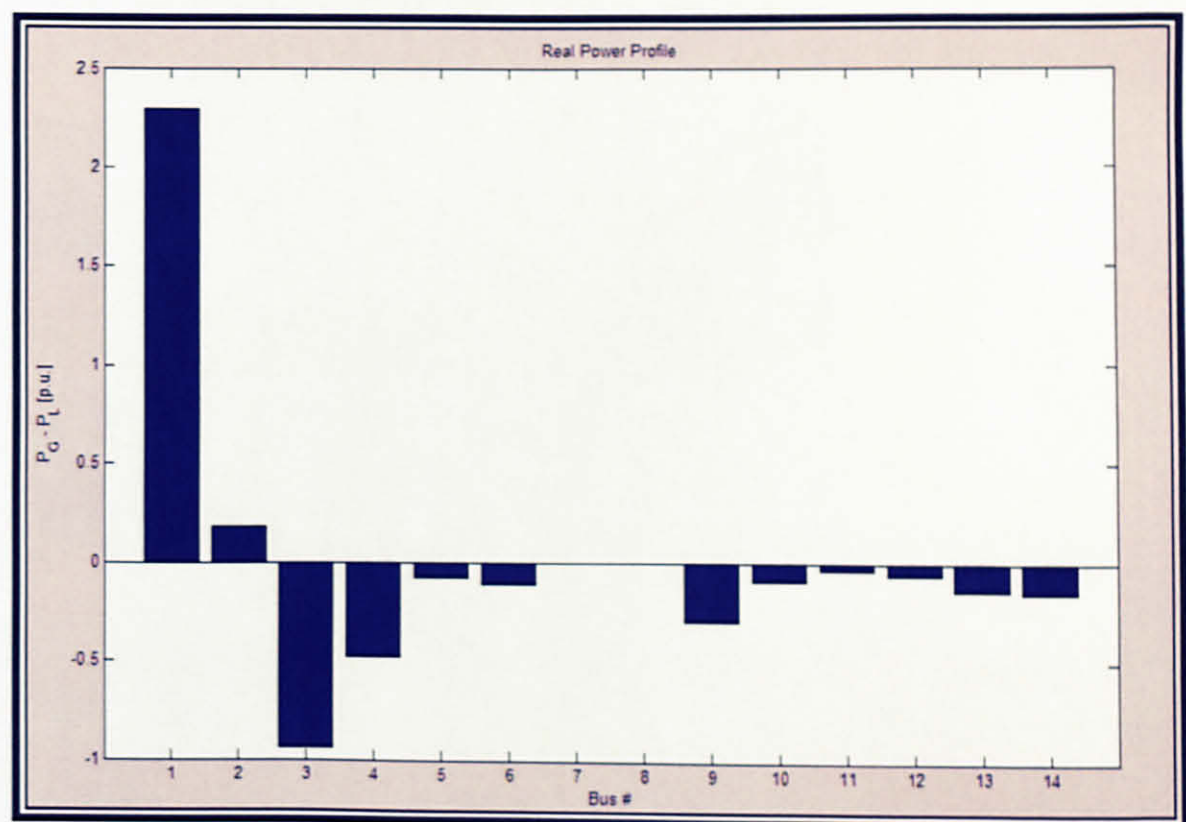


Figure 5.21 IEEE 14-bus – Case 6 real power profile, with UPFC.

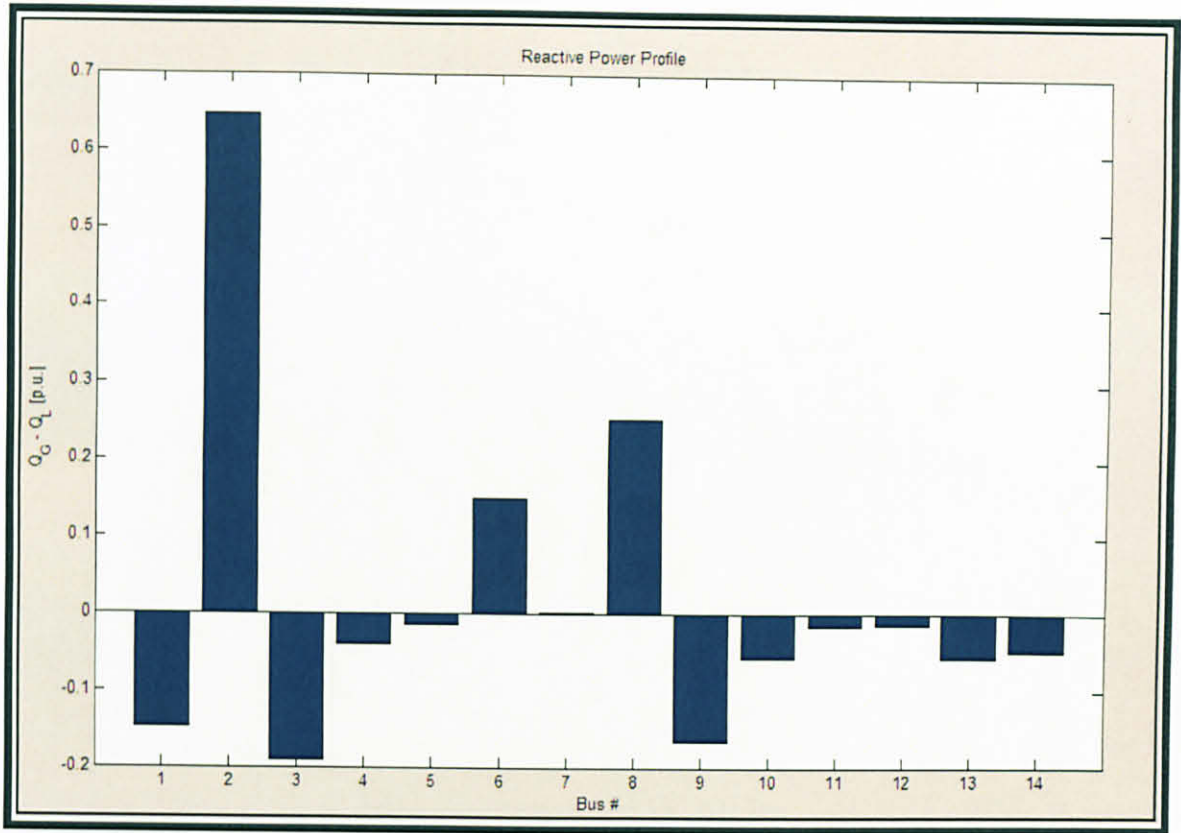


Figure 5.22 IEEE 14-bus – Case 6 reactive power profile, with UPFC.

The effect of the reactive power losses is observed from Case 5. Tables 5.4 to 5.7 tabulate the power flow results for cases 1 and 5, analyzed at Line 5 (Branch 6 – 11).

Table 5.4 Voltage Magnitude, Voltage Phase, Real Power and Reactive Power Profiles at IEEE 14-bus – Bus 6.

Test Cases	$ V $	$\delta$	$P$	$Q$
Case 1	1.070000	-0.251580	-0.112000	0.149691
Case 5	1.070000	-0.251110	-0.112000	0.166780

In case 5,  $|V|$  is kept unchanged, therefore  $P$  would also remain unchanged.

$|V|$  remains  $\therefore P$  remains

A change in  $\delta$  would affect  $Q$ . When  $\delta$  is increased, therefore  $Q$  would also increase.

$\delta \uparrow \therefore Q \uparrow$

Table 5.5 Line Flows at IEEE 14-bus – Line 5 (Branch 6 – 11).

Test Cases	<i>P</i> Flow (p.u.)	<i>Q</i> Flow (p.u.)	<i>P</i> Loss (p.u.)	<i>Q</i> Loss (p.u.)
Case 1	0.081372	-0.134830	0.000000	-0.239580
Case 5	0.236704	-0.482910	0.000000	-0.843019

Table 5.6 Total Generation, Load and Losses for IEEE 14-bus – Cases 1 and 5.

Test Cases	Total Generation		Total Load		Total Losses	
	<i>P</i> (p.u.)	<i>Q</i> (p.u.)	<i>P</i> (p.u.)	<i>Q</i> (p.u.)	<i>P</i> (p.u.)	<i>Q</i> (p.u.)
Case 1	2.725808	1.088962	2.590000	0.814000	0.135808	0.274962
Case 5	2.724665	1.087233	2.590000	0.814000	0.134665	0.031452

From equation (5.32), it is observed that when the total losses ( $P_{LOSS}$ ) have been reduced, the total generation ( $P_G$ ) is also reduced; as the total load ( $P_L$ ) remains unchanged (no extra loads have been added to the network).

$$\therefore P_G \downarrow - P_L = P_{LOSS} \downarrow \quad (5.32)$$

Table 5.7 Reduction in Real and Reactive Power Losses (%) for IEEE 14-bus – Case 5.

Test Case	Reduction in Real Power Losses (%)	Reduction in Reactive Power Losses (%)
Case 5	0.84	88.56

The Real Power Losses have been reduced by 0.84 %. For the Reactive Power Losses, the total losses have been reduced by 88.56 %. The effect of the real power losses is observed from case 6. Tables 5.8 to 5.11 tabulate the power flow results for cases 1 and 6, analyzed at Line 12 (Branch 2 – 3).

Table 5.8 Voltage Magnitude, Voltage Phase, Real Power and Reactive Power Profiles at IEEE 14-bus – Bus 2.

Test Cases	$ V $	$\delta$	<i>P</i>	<i>Q</i>
Case 1	1.050000	0.025341	0.900000	0.314093
Case 6	1.050000	0.019411	0.900000	0.514209

Table 5.9 Line Flows at IEEE 14-bus – Line 12 (Branch 2 – 3).

Test Cases	<i>P</i> Flow (p.u.)	<i>Q</i> Flow (p.u.)	<i>P</i> Loss (p.u.)	<i>Q</i> Loss (p.u.)
Case 1	0.384531	0.165739	0.013598	-0.010230
Case 6	0.435688	-0.156067	0.000000	-0.453620

Table 5.10 Total Generation, Load and Losses for IEEE 14-bus – Cases 1 and 6.

Test Cases	Total Generation		Total Load		Total Losses	
	<i>P</i> (p.u.)	<i>Q</i> (p.u.)	<i>P</i> (p.u.)	<i>Q</i> (p.u.)	<i>P</i> (p.u.)	<i>Q</i> (p.u.)
Case 1	2.725808	1.088962	2.590000	0.814000	0.135808	0.274962
Case 6	2.692336	1.100657	2.590000	0.814000	0.102336	0.287094

From equation (5.33), it is observed that when the total losses ( $P_{LOSS}$ ) have been reduced, the total generation ( $P_G$ ) is also reduced; as the total load ( $P_L$ ) remains unchanged (no extra loads have been added to the network).

$$\therefore P_G \downarrow - P_L = P_{LOSS} \downarrow \quad (5.33)$$

Table 5.11 Reduction in Real and Reactive Power Losses (%) for IEEE 14-bus – Case 6.

Test Case	Reduction in Real Power Losses (%)	Reduction in Reactive Power Losses (%)
Case 6	24.65	4.41

The Real Power Losses have been reduced by 24.65 %. For the Reactive Power Losses, the total losses have been reduced by 4.41 %. Therefore, the objective of installing the UPFC has been achieved for both the real and reactive power, as the total losses have been reduced in all cases.

## 5.6 Simulation Results

The modified algorithm of SE is successfully tested on 5-bus, IEEE 14-bus, and IEEE 57-bus. In order to prove the validity of modified algorithm of SE, the test results are compared with the results obtained from power flow analysis. For all simulations, the tolerance specified for convergence is 0.001. Both these systems have been tested for two cases, i.e. case 1 without measurement errors and case 2 with measurement errors.



The parameters of the installed UPFC device are:

$X_p = 0.1$  p.u.,  $X_q = 0.1$  p.u.,  $V_{pmav} = 0.2$  p.u.,  $V_{qmax} = 1.1$  p.u.,  $P_{(target)} = 0.4$  p.u. and  $Q_{(target)} = 0.02$  p.u.,  $S_{pmax} = 1.0$  p.u.,  $S_{qmax} = 1.0$  p.u.

Available measurements for the three test systems are shown in Table 5.12.

Table 5.12 The summary of available measurements for all tested network.

System Bus	Measurements					Redundancy <i>m/n</i>
	<i>V</i>	<i>P</i>	<i>Q</i>	<i>p<sub>ij</sub> &amp; p<sub>ji</sub></i>	<i>q<sub>ij</sub> &amp; q<sub>ji</sub></i>	
5	5	4	2	12	11	3.77
IEEE 14	6	10	8	16	13	1.96
IEEE 57	45	33	30	93	35	2.09

### 5.6.1 5-bus system embedded with UPFC

A UPFC is installed on line 3 - 4 as shown in Figure 5.4. The developed software can be utilized in two different ways depending upon the purpose of study. It can be used as an estimator for the UPFC device parameters for a given set of measurements. The estimation will yield not only the system states but also the UPFC device parameters. It can also be utilized as a tool to estimate the required values for the parameters of the FACTS devices in order to maintain a specific level of flow through a specified line. The amount of desired power flow through line 3 - 4, which happens to have a UPFC device installed on it, can be maintained by the use of this program and estimating the required settings of the control variables of this UPFC device. This developed software is tested first by setting the power flow through line 3 - 4 equal to  $0.4 + j0.02$  p.u. In order to achieve this goal, the desired power flow is set as measurements. The SE result of this case is shown in Table 5.13. The average of errors as compared with the actual value is less than 1 % for the voltage magnitude and less than 2 % for the phase angle. Meanwhile the comparison between the actual power flow and estimated is shown in Figure 5.23 and 5.24 for active and reactive power, respectively.

Table 5.13 State estimation results.

Bus	Voltage magnitude			Voltage angle, deg		
	Power Flow	SE	% of error	Power Flow	SE	% of error
1	1.060	1.060	0	0.000	0.000	0.000
2	1.000	1.000	0	-1.769	-1.767	-0.136
3	1.000	1.000	0	-6.016	-6.006	-0.166
4	0.992	0.995	0.313	-3.191	-3.232	-1.298
5	0.975	0.976	0.144	-4.974	-4.974	-0.006

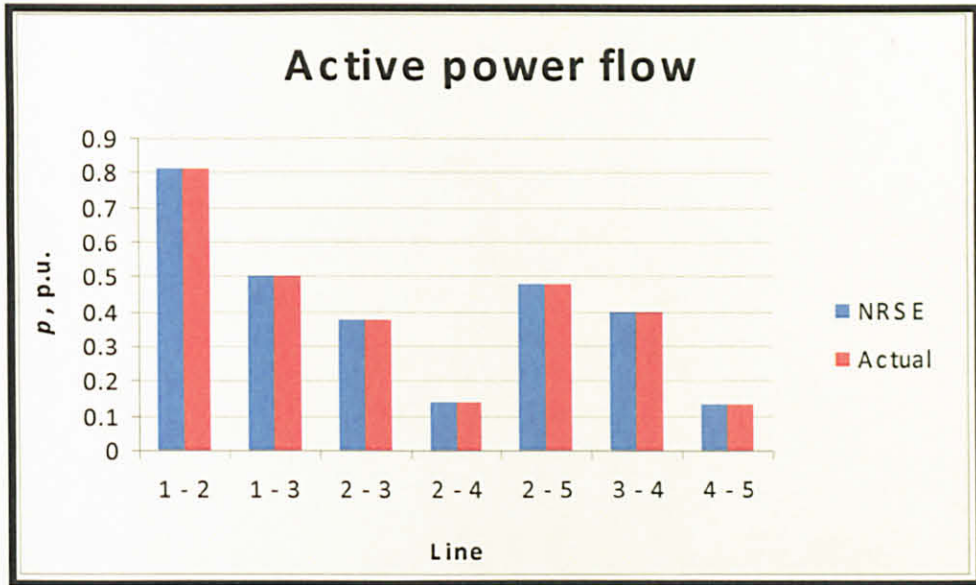


Figure 5.23 The comparison active power flow results between NRSE and power flow result.

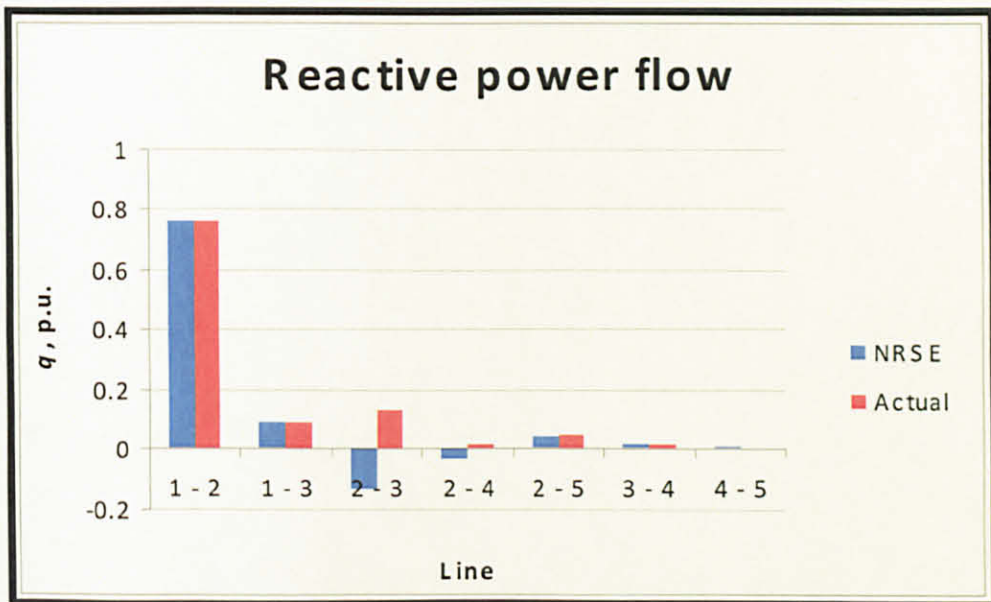


Figure 5.24 The comparison reactive power flow results between NRSE and power flow result.

The power flow in branch 3 - 4 is  $0.4 + j0.02$  p.u., which is the same as the desired set values. On the other hand, the estimated parameters of UPFC are shown in Table 5.14. From the Table 5.14, the constraint of  $P_p + P_q = 0$ , and  $V_p \leq 0.2$  p.u.,  $S_p \leq 1.0$  p.u.,  $V_q \leq 1.1$  p.u.,  $S_q \leq 1.0$  p.u., are met.

Now the software is tested without setting specific value of power flow. The result of SE is closely similar to the results tabulated in Table 5.13. However, the power flow through line 3 - 4 is changed to  $0.39976 + j0.04029$  p.u. The estimated UPFC variables are shown in Table 5.15 and seem to satisfy all the constraints.

Table 5.14 Estimated UPFC variables.

Variables	Actual value (p.u.)	Estimated value (p.u.)
$V_p \angle \delta_p$	$0.101 \angle -92.73^\circ$	$0.101 \angle -92.73^\circ$
$V_q \angle \delta_q$	$1.017 \angle -6.01^\circ$	$1.017 \angle -6.01^\circ$
$S_p$	$0.4 - j0.1779$	$0.4 - j0.1779$
$S_q$	$-0.4 - j0.02$	$-0.4 - j0.02$

Table 5.15 Estimated UPFC variables without setting any specific value.

Variables	Actual value (p.u.)	Estimated value (p.u.)
$V_p \angle \delta_p$	$0.04 \angle -87.12^\circ$	$0.04 \angle -87.12^\circ$
$V_q \angle \delta_q$	$1.014 \angle -5.07^\circ$	$1.014 \angle -5.07^\circ$
$S_p$	$0.2393 - j0.1102$	$0.2393 - j0.1102$
$S_q$	$-0.2393 - j0.038$	$-0.2393 - j0.038$

### 5.6.2 IEEE 14-bus system embedded with UPFC

After several cases are analyzed and discussed in section 5.5.2, the IEEE 14-bus system with a UPFC installed at Line 12 (Branch 2 - 3) is used as a reference to verify the modified algorithm of SE method. Table 5.16 shows the result of the modified SE as compared with power flow results obtained from the PSAT software. Similar analysis as 5-bus system, IEEE 14-bus system is successful to set the desired value of power flow through line 2 - 3, which is  $0.2 + j0.04$  p.u.

Table 5.16 State Estimation results.

Bus	Voltage magnitude			Voltage angle, deg		
	Actual	SE	% of error	Actual	SE	% of error
1	1.06	1.072	1.132075	0	0	0
2	1.05	1.045	0.47619	-5.15662	-5.21392	-1.11111
3	1.01	1.009	0.09901	-12.6051	-12.8916	-2.27273
4	1.01	1.011	0.09901	-10.3132	-10.2559	-0.55556
5	1.02	1.009	1.078431	-8.59437	-8.70896	-1.33333
6	1.07	1.061	0.841121	-14.3239	-14.0948	-1.6
7	1.05	1.053	0.285714	-13.178	-13.2353	-0.43478
8	1.09	1.085	0.458716	-13.178	-13.2353	-0.43478
9	1.03	1.039	0.873786	-14.8969	-14.6677	-1.53846
10	1.03	1.039	0.873786	-14.8969	-15.3553	3.076923
11	1.05	1.046	0.380952	-14.8969	-14.9542	0.384615
12	1.05	1.052	0.190476	-15.4699	-15.298	1.111111
13	1.05	1.047	0.285714	-15.4699	-15.3553	0.740741
14	1.04	1.052	1.153846	-16.0428	-17.7617	10.71429

The average of errors as compared with the actual value is less than 2 % for the voltage magnitude and less than 5 % for the phase angle. It shows that the modified NRSE method is acceptable. Meanwhile, the state and control variables for the UPFC device are estimated and the results are depicted in Table 5.17. The results show that the constraint given in equation (5.17) and equations (5.28) through (5.31) is met with.

Table 5.17 Estimated UPFC variables.

Variables	Actual value (p.u.)	Estimated value (p.u.)
$V_p \angle \delta_p$	$0.2 \angle -115^\circ$	$0.2 \angle -115^\circ$
$V_q \angle \delta_q$	$1.1 \angle -21.2^\circ$	$1.1 \angle -21.2^\circ$
$S_p$	$0.4 - j0.2185$	$0.4 - j0.2185$
$S_q$	$-0.4 - j0.02$	$-0.4 - j0.02$

## 5.7 SECJ Method Embedded With UPFC

The performance of SECJ method is also tested by integrating it with UPFC. It is already discussed in the Chapter 3, that SECJ method is significantly beneficial in terms of computer processing time especially when the size of network becomes

larger. Table 5.18 shows the summary of computational time for NRSE and SECJ methods when UPFC is installed in the tested networks. In this case, IEEE 57-bus system is discussed. For the sake of analysis, the tabulated data in Table 5.18 are represented by graphical as shown in Figure 5.25.

Table 5.18 Summary of computational time between NRSE and SECJ for IEEE 57 system.

System	SE method	Time, sec		
		<i>H</i>	<i>G</i>	Completed Process
IEEE 57	NRSE	0.0469	2.42	2.78
	SECJ	0.0469	1.86	2.30

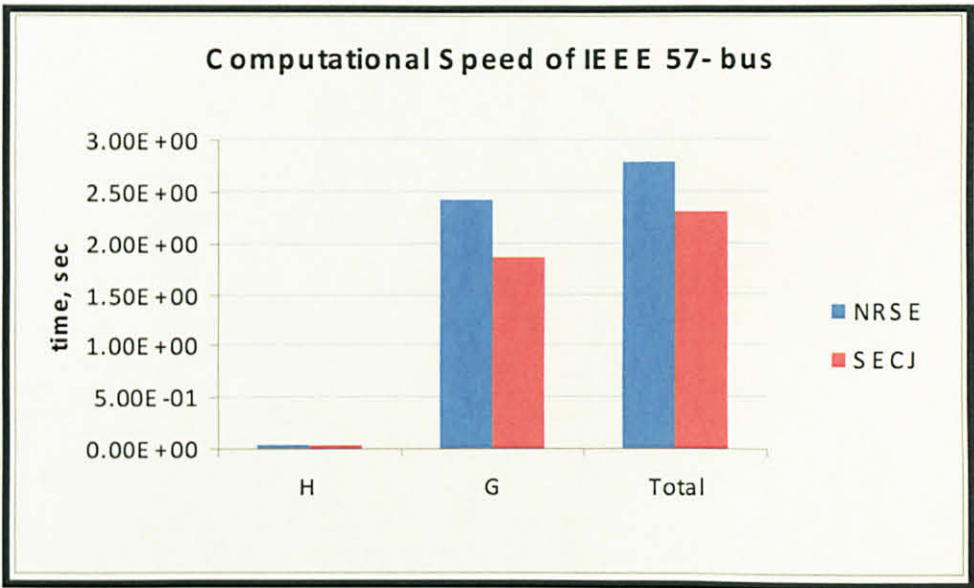


Figure 5.25 Comparison of NRSE and SECJ for IEEE 57-bus.

It has been illustrated from Figure 5.25 that the SECJ method again proved to be advantageous compared with NRSE method.

### 5.7.1 Bad data simulation

The capability of modified SE method is also tested by introducing bad measurements in the set of measurements. For each tested network a few true measurements randomly selected are made as bad measurements by either changing the power flow direction or increasing the value of voltage intentionally as shown in Table 5.19.

To analyze the process of the bad data, the 5-bus system is considered. Three of the 35 measurements are made as bad measurements. At the end of first run of estimation, the measurement with the largest normalized error ( $p_{1-2}$ ) was flagged as a gross error with the normalized residual  $r^N = 103.287$ . After removing  $p_{1-2}$  from the measurement system, a new estimate and  $r^N$  is obtained as shown in Table 5.20.

Table 5.19 List of bad measurements.

System Bus	Measurements	Measured value	Bad value
5	$p_{1-2}$	0.8114	-0.8114
	$P_2$	0.2	1.2
	$Q_5$	-0.1	0.1
IEEE 14	$p_{2-3}$	0.7345	-0.7345
	$q_{4-7}$	-0.0656	0.0656
	$V_2$	1.045	2.045
IEEE 57	$p_{24-26}$	-0.1018	0.1018
	$q_{30-25}$	-0.0453	0.0453
	$P_{33}$	-0.038	0.038

In the second run, the measurement  $P_2$  presenting the largest normalized residual was flagged as bad data since  $r^N > 4$ . The measurement  $P_2$  is deleted from the measurement system. The procedure is repeated and in the final run, the largest normalized residual  $q_{4-2}$  is equal to 2.955 is less than the threshold 4, meaning that all the bad data have already been eliminated. Once all the bad data are eliminated, the redundancy of the system is reduced to 2.91.

Table 5.20 Results of normalized residual test for 5-bus system.

1st. estimation			2nd. estimation			3rd. estimation			4th. estimation		
No	Mete	$r_i^N$	No	Mete	$r_i^N$	No	Mete	$r_i^N$	No	Mete	$r_i^N$
1	$V_1$	1.118570	1	$V_1$	0.331102	1	$V_1$	0.026545	1	$V_1$	0.088874
2	$V_2$	0.694232	2	$V_2$	0.330984	2	$V_2$	0.028106	2	$V_2$	0.096683
3	$V_3$	0.029589	3	$V_3$	0.455120	3	$V_3$	0.026904	3	$V_3$	0.095424
4	$V_4$	0.126712	4	$V_4$	1.266314	4	$V_4$	0.713026	4	$V_4$	0.498152
5	$V_5$	0.419716	5	$V_5$	0.008298	5	$V_5$	0.132891	5	$V_5$	0.043874
6	$P_2$	7.380413	6	$P_2$	<b>53.58851</b>	6	$P_4$	7.152E-	6	$P_4$	3.528E-
7	$P_4$	0.002451	7	$P_4$	0.016218	7	$P_5$	0.086830	7	$P_5$	0.005596
8	$P_5$	0.991004	8	$P_5$	6.073878	8	$Q_4$	0.000168	8	$Q_4$	0.002064
9	$Q_4$	9.475E-	9	$Q_4$	0.000854	9	$Q_5$	<b>9.205409</b>	9	$p_{1-3}$	0.008324
10	$Q_5$	9.188983	10	$Q_5$	8.854116	10	$p_{1-3}$	0.004306	10	$p_{2-3}$	0.002030
11	$p_{1-2}$	<b>103.2867</b>	11	$p_{1-3}$	2.807680	11	$p_{2-3}$	0.001766	11	$p_{2-4}$	0.060586
12	$p_{1-3}$	13.38425	12	$p_{2-3}$	15.577	12	$p_{2-4}$	0.035808	12	$p_{2-5}$	0.000941
13	$p_{2-3}$	13.72693	13	$p_{2-4}$	16.15406	13	$p_{2-5}$	0.145177	13	$p_{6-4}$	0.826573
14	$p_{2-4}$	2.426983	14	$p_{2-5}$	17.53630	14	$p_{6-4}$	1.260647	14	$p_{4-5}$	0.021041
15	$p_{2-5}$	2.710754	15	$p_{6-4}$	0.390007	15	$p_{4-5}$	0.046600	15	$p_{2-1}$	0.028322
16	$p_{6-4}$	0.160010	16	$p_{4-5}$	3.273472	16	$p_{2-1}$	0.024044	16	$p_{3-1}$	0.003761
17	$p_{4-5}$	0.459695	17	$p_{2-1}$	47.91090	17	$p_{3-1}$	0.004144	17	$p_{3-2}$	0.002224
18	$p_{2-1}$	101.1755	18	$p_{3-1}$	2.537955	18	$p_{3-2}$	0.008324	18	$p_{4-2}$	0.054396
19	$p_{3-1}$	12.36293	19	$p_{3-2}$	14.44941	19	$p_{4-2}$	0.030495	19	$p_{5-2}$	0.001829
20	$p_{3-2}$	12.76713	20	$p_{4-2}$	15.55357	20	$p_{5-2}$	0.144970	20	$p_{5-4}$	0.012898
21	$p_{4-2}$	2.365500	21	$p_{5-2}$	16.42688	21	$p_{5-4}$	0.044739	21	$q_{1-2}$	0.026751
22	$p_{5-2}$	2.585942	22	$p_{5-4}$	3.197884	22	$q_{1-2}$	0.000743	22	$q_{1-3}$	0.001708
23	$p_{5-4}$	0.446407	23	$q_{1-2}$	1.473480	23	$q_{1-3}$	0.000207	23	$q_{2-3}$	0.004197
24	$q_{1-2}$	3.689746	24	$q_{1-3}$	0.162437	24	$q_{2-3}$	0.003247	24	$q_{2-4}$	1.634063
25	$q_{1-3}$	1.736310	25	$q_{2-3}$	0.723888	25	$q_{2-4}$	1.095719	25	$q_{2-5}$	0.523177
26	$q_{2-3}$	0.801635	26	$q_{2-4}$	0.609075	26	$q_{2-5}$	3.461936	26	$q_{6-4}$	0.713263
27	$q_{2-4}$	1.028815	27	$q_{2-5}$	2.118625	27	$q_{6-4}$	0.743982	27	$q_{4-5}$	0.870590
28	$q_{2-5}$	3.313430	28	$q_{6-4}$	0.239576	28	$q_{4-5}$	0.795729	28	$q_{2-1}$	0.012386
29	$q_{6-4}$	0.669946	29	$q_{4-5}$	0.735122	29	$q_{2-1}$	1.035E-	29	$q_{3-1}$	0.020745
30	$q_{4-5}$	0.852859	30	$q_{2-1}$	1.626842	30	$q_{3-1}$	0.003557	30	$q_{4-2}$	2.954650
31	$q_{2-1}$	1.506374	31	$q_{3-1}$	0.869286	31	$q_{4-2}$	3.472506	31	$q_{5-2}$	0.491794
32	$q_{3-1}$	0.880558	32	$q_{4-2}$	2.723611	32	$q_{5-2}$	3.399027	32	$q_{5-4}$	0.881724
33	$q_{4-2}$	3.469060	33	$q_{5-2}$	4.428373	33	$q_{5-4}$	0.760483			
34	$q_{5-2}$	3.479354	34	$q_{5-4}$	0.551290						
35	$q_{5-4}$	0.721415									

## 5.8 Summary

Nowadays power systems embedded with FACTS controller are quite common. Hence, it is more appropriate to extend the SE algorithm to power systems with FACTS controllers.

The modification of Jacobian matrix presented in this Chapter 5 is proved to be successful when the constraints on the UPFC parameters are considered. Simulations are carried out on the 5-bus, IEEE-14-bus and IEEE 57-bus system in order to illustrate the algorithm's efficiency by numerical examples. From the results obtained on the small and medium scale networks, it is concluded that the developed program is suitable either to estimate the UPFC controllers parameters under normal power system operation or to estimate these parameter values in order to achieve the given control specifications, along with the power system state variables.

The SECJ method is also tested incorporating the UPFC. It shows a significant advantage in IEEE 57-bus system, where the total computational time reduces to about 25 % when compared with NRSE method. Thus, the strength of the developed program in the field of SE is established.



## CHAPTER 6

### CONCLUSIONS

#### 6.1 Conclusion

State estimation is a working tool employed to obtain the system state in a practical environment. The gain and Jacobian matrices of the classical normal equations in SE method are always claiming as a contributor for numerical stability problem for large scale power systems. Several methods have been proposed to overcome the problem. Among are those methods, Weighted Least Squares (WLS) algorithm is the most popular and finds applications in many fields. The basic Newton-Raphson WLS method, when used in power systems, has good convergence characteristic in addition to filtering and bad data processing properties, for a given observable meter placement with sufficient redundancy and yields correct estimates.

The modeling and the solution procedure for NRSE with some modifications are highlighted in this thesis. Bad data processing is a key issue in state estimation. The concept of bad data processing, which includes detection, identification and elimination, is also discussed. Hands-on experience with the SE software used by TNB on the Malaysian grid revealed certain drawbacks in the software. This motivated the author to develop a robust and more efficient SE package. The developed package is tested on several standard systems up to a size of IEEE 300-bus, and proved to be quite acceptable.

The Newton-Raphson State Estimation (NRSE) method using bus admittance matrix remains as an efficient and most popular method to estimate the state variables. In this method, elements of Jacobian matrix,  $H$  are computed from standard expressions which lack physical significance. The process of computing the elements of the Jacobian matrix is a significantly time consuming step which requires evaluation of

large number of trigonometric functions. It is significant, especially in large scale power system networks.

It is recognized that each element of the  $H$  matrix is contributed by the partial derivatives of the power flows in the network elements. The elements of the state estimation Jacobian matrix are obtained considering the power flow measurements in the network elements. The network elements are processed one-by-one based on the available measurements and the  $H$  matrix is updated suitably and simplifying the development of the Jacobian, which is one of the major contributions of this thesis. The final  $H$  matrix thus constructed is exactly the same as that obtained in available NRSE method, with less computational time.

The systematically constructed Jacobian matrix  $H$  is then integrated with the WLS method to estimate the state variables. The suggested procedure is successfully tested on IEEE standard systems, validated and proved to be efficient. The final estimates and time taken to converge are recorded and compared with the results obtained from NRSE method available in the literature. The results proved that the suggested method takes lesser computational time compared with the available NRSE method, particularly when the size of the network becomes larger.

The development of pre-estimation filter using autoregressive (AR) model to identify the gross measurement errors is also presented. The identification of the errors is accomplished by making a comparison between the measured value and the predicted value of measurements. If the difference exceeds 5 % error, the measured data is assumed to be grossly erroneous and is replaced by its predicted value in the measurement set.

Two methods of AR, namely, Burg and MC have been proposed. Both methods are used to calculate the one-step-ahead predicted values of the state variables. The simulation results show that those methods are able to accurately predict the behavior of the system variables given that the states of the system are within their normal variation.

The proposed AR model offers a measurement pre-screening ability that can complement other post-estimation detection/identification techniques by processing the raw measurements before estimation is performed. As shown in simulation results, it will always detect any gross errors existing in the measurement. The proposed method is also capable to deduct the bad measurements with high weighting factor. The AR method will also provide the necessary pseudo-measurements for those measurements that are identified as bad data. Thus, the strength of Burg and MC algorithm in the field of SE is established, in this thesis.

The development of SE algorithm suitable for a power system embedded with the FACTS controller, UPFC, is presented. Simulation studies are carried out on IEEE 14-bus and IEEE 57-bus systems together with the UPFC in order to illustrate the efficiency of the developed SE algorithm. From the results obtained on small and medium scale networks, it is concluded that the developed program is suitable either to estimate the UPFC controller parameters or to estimate these parameter values in order to achieve the given control specifications in addition to the power system state variables.

## **6.2 Summary of Contributions**

In conclusion, the main contributions of this dissertation are:

- i. After studying a SE software, a robust and more efficient SE package is developed and tested.
- ii. An algorithm to build a Jacobian matrix with a simplified procedure is developed and incorporated in SE algorithm in order to reduce the computational time for large scale networks.
- iii. Pre-screening process prior to SE computation is developed in order to ensure the accuracy of final estimate of SE.
- iv. Generation of high quality of pseudo-measurements is developed in order to solve the problem of unobservable system.
- v. The SE algorithm suitable for power systems with UPFC is developed and successfully tested.

### 6.3 Future Research

Some of the problems that have arisen for future investigation are outline below.

- i. The proposed methods/processes should be tested on real time application of power systems. Owing to lack of data from practical systems, all the proposed methods are tested only on simulated systems even for 103-bus system since the related local utility is in progress to install on-line SE. The Jacobian creating algorithm, the comprehensive method for pre-screening process and modification WLS method embedded with FACTS device are to be tested in real time systems before their real time application.
- ii. Any power system state estimator is sensitive to the presence of bad data and these erroneous data have to be deleted, identified and eliminated to obtain a reliable estimate. The bad data may be interacting or non-interacting type. The proposed method is developed for handling non-interacting type. However, bad data processing in the case of interacting type presents difficulties and requires further research.
- iii. Future research is necessary on SE of power systems embedded with other FACTS devices such as Static Var Compensators (SVCs), Thyristor Controlled Series Capacitors (TCSCs), Shunt and Series Static Synchronous Compensators (STATCOMs) and etc.

## REFERENCES

- [1] A. Monticelli, "Electric Power System State Estimation," *Proceedings IEEE*, vol. 88, no. 2, pp. 262-282, February 2002.
- [2] F.C. Schweppe, J. Wildes and D.B. Rom, "Power system static-state estimation, parts I, II and III," *IEEE Transactions on Power Apparatus and Systems*, vol. PAS-89, no. 1, pp.120-135, January 1970.
- [3] A. Abur and A. G. Exposito, *Power System Estimation: Theory and Implementation*, New York: Marcel Dekker, Inc., 2004.
- [4] M.M. Adibi and R. J. Kafka, "Minimization of Uncertainties in Analog Measurements For Use in State Estimation," *IEEE Transactions on Power Systems*, vol.5, no. 3, pp. 902-910, August 1990.
- [5] A. Bose and K. A. Clements, "Real-time Modeling of Power Networks," *Proceedings IEEE*, vol. 75, no. 12, pp. 1607-1622, December 1987.
- [6] M.B. Do Coutto Filho, A.M. Leite da Silva and D.M. Falcao, "Bibliography on power system state estimation (1968–1989)," *IEEE Transactions on Power Systems*, vol. 5, no. 3, pp 950-961, August 1990.
- [7] L. Holten, A. Gjelsvik, S. Aam, F.F. Wu and W.-H.E Liu, "Comparison of different methods for state estimation," *IEEE Transactions on Power Systems*, vol. 3, no 4, pp. 1798 – 1806, November 1988.
- [8] A. Garcia, A. Monticelli and P. Abreu, "Fast decoupled state estimation and bad data processing," *IEEE Transactions on Power Apparatus and Systems*, vol. PAS-98, n0. 5, pp.1645-1651, September/October 1979.
- [9] F. C. Schweppe and E. J. Handschin, "Static state estimation in electric power systems," *Proceedings IEEE*, vol. 62, no. 7, pp. 972-983, July 1974.
- [10] A. Monticelli and A. Garcia, "Fast decoupled state estimators," *IEEE Transactions on Power Systems*, vol. 5, no. 2, pp. 556-564, May 1990.
- [11] A. Simoes-Costa and V. H. Quintana, "A robust numerical technique for power system state estimation," *IEEE Transactions on Power Apparatus and Systems*, vol. PAS-100, no. 2, pp. 691-698, February 1981.

- [12] A. Simoes-Costa and V. H. Quintana, "An orthogonal row processing algorithm for power system sequential state estimation," *IEEE Transactions on Power Apparatus and Systems*, vol. PAS-100, no. 8, pp. 3791-3800, August 1981.
- [13] S. I.W. Vempatin and W.F. Tinney, "Orthogonal Sparse Vector Methods," *IEEE Transactions on Power Systems*, vol. 7, no. 2, pp. 926-932, May 1992.
- [14] B. Stott and O. Alsac, "Fast Decoupled Load Flow," *IEEE Transactions on Power Apparatus and Systems*, vol. PAS-93, pp. 859-867, May/June 1974.
- [15] A. Monticelli, *State Estimation in Electric Power Systems. A Generalized Approach*, New York: Kluwer Academic Publishers, 1999.
- [16] L. Mili, T. Van Cutsem and M. Pavella, "Bad Data Identification Methods in Power System Estimation. A Comparative Study," *IEEE Transactions on Power Apparatus and Systems*, vol. PAS 104, no. 11, pp 3037-3049, November 1985.
- [17] E. Handschin, F. C. Schweppe, J. Kohlas and A. Fiecher, "Bad data analysis for power system state estimation," *IEEE Transactions on Power Apparatus and Systems*, vol. PAS-94, no. 2, pp. 329-337, March/April 1975.
- [18] H. M. Merrill and F. C. Schweppe, "Bad data suppression in power system static-state estimation," *IEEE Transactions on Power Apparatus and Systems*, vol. PAS-90, no. 6, pp. 2718-2725, November 1971.
- [19] A. Monticelli and A. Garcia, "Reliable bad data processing for real-time state estimation," *IEEE Transactions on Power Apparatus and Systems*, vol. PAS-102, no. 5, pp. 1126-1139, May 1983.
- [20] M. Kezunovic, A. Abur, A. Edris and D. Sobajic, "Data integration/exchange, part 1: existing technical and business opportunities", *IEEE Power & Energy Magazine*, vol. 2, pp. 14-19, March/April 2004.
- [21] A.M. Leite da Silva, M.B. Do Coutto Filho and J.F. de Queiroz, "State forecasting in electric power systems," in *IEE Proceedings of Generation, Transmission and Distribution*, vol. 130, no. 5, pp.237-244, September 1983.
- [22] A. Abur, A. Keyhani and H. Bakhtiari, "Autoregressive Filters For the Identification and Replacement of Bad Data in Power System State Estimation," *IEEE Transactions on Power Systems*, vol. PWRS-2, no. 3, pp 552-558, August 1987.

- [23] M.B. Do Coutto Filho, A.M. Leite da Silva, J.M.C. Cantera and R.A. da Silva, "Information debugging for real-time power systems monitoring," in *IEEE Proceedings of Generation, Transmission and Distribution*, vol. 136, no. 3, pp. 145–152, May 1989.
- [24] G.R. Krumpholz, K.A. Clements and P.W. Davis, "Power System Observability: A Practical Algorithm Using Network Topology," *IEEE Transactions on Power Apparatus and Systems*, vol. PAS-99, no. 4, pp 1534-1542, July/August 1980.
- [25] A. Monticelli and F. F. Wu, "Network Observability: Theory," *IEEE Transactions on Power Apparatus and Systems*, vol. PAS-104, no. 5, pp. 1042-1048, May 1985.
- [26] J. Alber and M. Pöller., "Observability of Power Systems based on Fast Pseudorank Calculation of Sparse Sensitivity Matrices," in *Proceedings of IEEE PES Transmission and Distribution Conference*, pp. 127-132, May 2006.
- [27] F.F. Wu, K. Moslehi and A. Bose, "Power System Control Centers: Past, Present, and Future," *Proceedings IEEE*, vol. 93, no. 11, pp. 1890-1908, November 2005.
- [28] A.P. Sakis Meliopoulos, B. Fardanesh and S. Zelingher, "Power System Estimation: Modeling Error Effects and Impact on System Operation," in *Proceedings of the 34<sup>th</sup> Hawaii International Conference on Systems Science*, pp. 682-690, January 2001.
- [29] A.K. Al-Othman and M.R. Irving, "A Comparative study of two methods for uncertainty analysis in power system State estimation," *IEEE Transactions on Power Systems*, vol. 20, no 2, pp. 1181 – 1182, May 2005.
- [30] A. Simoes Costa, T.S. Piazza and A. Mandel, "Qualitative methods to solve qualitative problems in power system state estimation," *IEEE Transactions on Power Systems*, vol. 5, no 3, pp.941 – 949, August 1990.
- [31] F.F. Wu, "Power system estimation: a survey," *Electrical Power & Energy Systems*, vol. 12, no. 2, pp. 80-87, April 1990.
- [32] M. Shahidehpour and M. Marwali, "Role of Fuzzy Sets in Power System State Estimation," *International Journal of Emerging Electric Power Systems*, vol.1, issue 1, Article 1003, 2004.

- [33] J. Pereira, V. Miranda and J. Tome Saraiva, "Fuzzy Control of State Estimation Robustness," in *Proceedings of 14<sup>th</sup> PSCC*, Paper 5, June 2002.
- [34] S. Repo and J. Bastman, Applicability of Neural Network in Power System Computation, Report for Power Engineering Group, Tampere University of Technology, Tampere, Finland, 1996.
- [35] A. Papoulis, *Probability, Random Variables, and Stochastic Processes*, McGraw-Hill, New York, 1984.
- [36] Tenaga Nasional Berhad EMS Staff, "Network Analyst's Guide", ESCA Corporation, 1994.
- [37] K. A. Clements, G. R. Krumpholz and P. W. Davis, "Power system state estimation residual analysis: An algorithm using network topology", *IEEE Transactions on Power Apparatus and Systems*, vol. 100, pp. 1779-1787, April 1981.
- [38] J. W. Wang and V. H. Quintana, "A decoupled orthogonal row processing algorithm for power state estimation," *IEEE Transactions on Power Apparatus and Systems*, vol. PAS-103, no. 8, pp. 2337-2344, August 1984.
- [39] J. J. Grainger and W. D. Stevenson, Jr., *Power System Analysis*, McGraw-Hill International Editions, 1994.
- [40] G.W. Stagg and A.H. El-Abiad, *Computer Methods in Power System Analysis*, New York: McGraw-Hill, 1968.
- [41] R. Jegatheesan, N. M. Nor and M. F. Romlie, "Piecewise Power Flow Solution Using Impedance Parameters", *International Journal of Power, Energy and Artificial Intelligent*, vol. 1, no. 1, pp 50-55, August 2008.
- [42] R. Jegatheesan, N. M. Nor and M. F. Romlie, "Power Flow Solution Using Impedance Parameters", *International Journal of Power, Energy and Artificial Intelligent*, vol. 1, no. 1, pp 56-60, August 2008
- [43] N.D.R. Sarma, V. V. Raju and K.S. Prakasa Rao, "Design of telemetering configuration for energy management systems," *IEEE Transactions on Power Systems*, vol. 9, no. 1, pp. 381–387, February 1994.
- [44] A.M. Leite da Silva, M.B. Do Coutto Filho and J.M.C. Cantera, "An efficient dynamic state estimation including bad data processing," *IEEE Transactions on Power Systems*, vol. PWRS-2, no. 4, pp. 1050–1058, November 1987.



- [45] J.C.S. Souza, A.M. Leite da Silva and A.P. Alves da Silva, "Data debugging for real-time power system monitoring based on pattern analysis," *IEEE Transactions on Power Systems*, vol. 11, no. 3, pp. 1592–1599, August 1996.
- [46] J.C.S. Souza, A.M. Leite da Silva and A.P. Alves da Silva, "On-line topology determination and bad data suppression in power system operation using artificial neural networks," *IEEE Transactions on Power Systems*, vol. 13, no. 3, pp. 796–803, August 1998.
- [47] R. F. Bischke, "Power System State Estimation: Practical considerations," *IEEE Transactions on Power Apparatus and Systems*, vol. PAS-100, no. 12, pp. 5044-5047, December 1981.
- [48] A.S. Debs and R.E. Larson, "A dynamic estimator for tracking the state of a power system," *IEEE Transactions on Power Apparatus and Systems*, vol. PAS-89, no. 7, pp. 1670–1678, September/October 1970.
- [49] F. C. Schweppe and R. D. Masiello, "A tracking static state estimator," *IEEE Transaction on Power Apparatus and Systems*, vol. PAS-90, no. 3, pp. 1025-1033, May 1971.
- [50] M. H. Hayes, *Statistical Digital Signal Processing and Modeling*, John Wiley & Sons, Inc., 1996.
- [51] R. Bos, S. de Waele and P.M.T. Broersen, "Autoregressive Spectral Estimation by Application of the Burg Algorithm to Irregularly Sampled Data," *IEEE Transactions on Instrumentation and Measurement*, vol. 51, no. 6, pp 1989-1994, December 2002.
- [52] N. M. Nor, R. Jegatheesan and P. Nallagownden, "Pre-Screening Process in Power System State Estimation," in *Proceeding of 3<sup>rd</sup> International Power Engineering and Optimazation (PEOCO)*, Shah Alam, Malaysia, June 2009.
- [53] N. M. Nor and R. Jegatheesan, "Application of Burg's Algorithm in State Estimation," in *Proceedings of Fourth IASTED International Conference Power and Energy Systems (AsiaPES 2008)*, Malaysia, April 2008.
- [54] N. M. Nor and R. Jegatheesan, "Application of Modified Covariance in State Estimation," in *Proceedings of 6th International Conference on Electrical Engineering (ICEENG)*, Cairo Egypt, May 2008.

- [55] L. Jun-Yong, "Strategies for handling UPFC constraints in steady-state power flow and voltage control," *IEEE Transactions on Power Systems*, vol. 15, no. 2, pp. 566–571, May 2000.
- [56] M. Noroozian, L. Angquist, M. Ghandhari and G. Andersson, "Use of UPFC for Optimal Power Flow Control," *IEEE Transactions on Power Delivery*, vol. 12, no. 4, pp. 1629–1634, October 1997.
- [57] N. Mithulananthan, A Sode-Yome and Naresh Acharya, *Application of FACTS Controllers in Thailand Power Systems*, report of RTG Budget Joint Research Project Fiscal Year 2003, January 2005.
- [58] A. Sode-Yome, N. Mithulananthan and Y. Kwang Lee, "A Comprehensive Comparison of FACTS Devices for Enhancing Static Voltage Stability," in *report of IEEE Power Engineering Society General Meeting*, pp. 1-8, 24-28 June 2007.
- [59] L. Gyugyi, T. R. Rietman and A. Edris, "The unified power flow controller: a new approach to power transmission control," *IEEE Transactions on Power Delivery*, vol. 10, pp.1085-1092, April 1995.
- [60] K.K. Sen and E.J. Stacey, "UPFC – Unified power flow controller: theory, modeling and applications," *IEEE Transactions on Power Delivery*, vol. 13, no. 4, pp. 1453-1460, October 1998.
- [61] A. Nabavi-Niaki and M.R. Iravani, "Steady state and dynamic models of unified power flow controller (UPFC) for power system studies," *IEEE Transactions on Power Systems*, vol. 11, no. 4, pp. 1937-1943, November 1996.
- [62] X.P. Zhang, "Comprehensive modelling of the unified power flow controller for power system control," *Journal of Electrical Engineering*, vol. 88, no. 4, pp. 241-246, April 2006.
- [63] N.G. Hingorani and L. Gyugyi, *Understanding FACTS Concepts and Technology of Flexible AC Transmission Systems*, Institute of Electrical and Electronic Engineers, New York, 2000.
- [64] C.R. Fuerte-Esquivel and E. Acha, "The Unified Power Flow Controller: A Critical Comparison of Newton–Raphson UPFC Algorithms in Power Flow Studies," in *IEE Proceedings: Generation, Transmission and Distribution*, vol. 144, no. 5, pp. 437-444, September 1997.

- [65] F. Milano. (2002) PSAT, Matlab-Based Power System Analysis Toolbox. [Online] Available at: <http://thunderbox.uwaterloo.ca/~fmilano>.
- [66] E Acha, F. Esquivel, H Ambriz-Pérez and C Angeles-Camacho, *FACTS Modelling and Simulation in Power Networks*, John Wiley and Sons Ltd., England, 2004.

## LIST OF PUBLICATIONS

### i. International Journal:

- (1) R. Jegatheesan, **N. Mohd Nor** and M. F. Romlie, "Piecewise Power Flow Solution Using Impedance Parameters", *International Journal of Power, Energy and Artificial Intelligence*, vol. 1, no. 1, pp 50-55, August 2008.
- (2) R. Jegatheesan, **N. Mohd Nor** and M. F. Romlie, "Power Flow Solution Using Impedance Parameters", *International Journal of Power, Energy and Artificial Intelligence*, vol. 1, no. 1, pp 56-60, August 2008.
- (3) **N. Mohd Nor**, R. Jegatheesan and P. Nallagownden, "Autoregressive (AR) method in Power System State Estimation", **submitted** to *International Journal of Power, Energy and Artificial Intelligence*.

### ii. Chapter of Book:

- (1) **N. Mohd Nor**, R. Jegatheesan and P. Nallagownden, *Newton-Raphson State Estimation Solution Employing Systematically Constructed Jacobian Matrix*, pp XXX-XXX, Chapter X, Advanced Technologies, ISBN 978-953-7619-X-X, I-TECH Education and Publishing, Vienna, Austria, 2009. **(Accepted and ready to publish)**.

### iii. Paper Proceedings:

- (1) **N. Mohd Nor**, R. Jegatheesan and P. Nallagownden, "Pre-Screening Process in Power System State Estimation," in *Proceeding of 3<sup>rd</sup> International Power Engineering and Optimazation (PEOCO)*, Shah Alam, Malaysia, June 2009.

- (2) R. Jegatheesan, **N. Mohd Nor** and M. F. Romlie, "Newton-Raphson Power Flow Solution Employing Systematically Constructed Jacobian Matrix", in *Proceeding of IEEE 2<sup>nd</sup> International Power and Energy Conference (PECon2008)*, Malaysia, December 2008.
- (3) **N. Mohd Nor**, R. Jegatheesan and P. Nallagownden, "Newton-Raphson State Estimation Solution Employing Systematically Constructed Jacobian Matrix", in *Proceeding of International Conference on Computer, Electrical, and Systems Science, and Engineering, (CESSE 2008)*, Singapore, August 2008.
- (4) **N. Mohd Nor** and R. Jegatheesan, "Use of AR Block Processing for Estimating the State Variables of Power System", in *Proceeding of 2<sup>nd</sup> International Power Engineering and Optimization Conference (PEOCO2008)*, Malaysia, June 2008.
- (5) R. Jegatheesan, **N. Mohd Nor** and M. F. Romlie, "Piecewise Power Flow Solution Using Impedance Parameters", in *Proceeding of 2<sup>nd</sup> International Power Engineering and Optimization Conference (PEOCO2008)*, Malaysia, June 2008.
- (6) R. Jegatheesan, **N. Mohd Nor** and M. F. Romlie, "Power Flow Solution Using Impedance Parameters", in *Proceeding of 2<sup>nd</sup> International Power Engineering and Optimization Conference (PEOCO2008)*, Malaysia, June 2008.
- (7) **N. Mohd Nor** and R. Jegatheesan, "Application of Modified Covariance in State Estimation," in *Proceedings of 6th International Conference on Electrical Engineering (ICEENG)*, Cairo Egypt, May 2008.

- (8) **N. Mohd Nor** and R. Jegatheesan, "Application of Burg's Algorithm in State Estimation," in *Proceedings of Fourth IASTED International Conference Power and Energy Systems (AsiaPES 2008)*, Malaysia, April 2008.
  
- (9) **N. Mohd Nor** and R. Jegatheesan, "Power Systems State Estimation Embedded with FACTS Devices", in *Proceeding of International Conference on Electrical Engineering and Informatics (ICEEI2007)*, Indonesia, June 2007.

## APPENDICES

## APPENDIX A

### MATHEMATICAL TERMS AND NOTATIONS

To ensure common understanding and consistencies, all mathematical symbols, operators, notations and terminologies used are in compliance with the acceptable styles and conventions normally adopted worldwide.

A constant is denoted either as an italic lowercase *letter* (e.g.,  $k$ ,  $m$ , or  $n$ ) or an italic UPPERCASE *LETTER* (e.g.,  $K$ ,  $M$ , or  $N$ ). Moreover, any set of real and complex numbers will be designated by  $\mathfrak{R}$  and  $\mathfrak{C}$ , respectively. Italic lowercase **boldface letters** are used to denote *vectors* and matched *italic lowercase letters* are used for their *entries*. For example,  $\mathbf{x} \in \mathfrak{R}^M$  indicates an  $M$ -dimensional column vector  $\mathbf{x}$  with all elements in  $\mathfrak{R}$ . In this case, the matched *italic lowercase*  $x_i$  refers to the  $i$ th *component* of vector  $\mathbf{x}$ .

On the other hand, italic UPPERCASE **boldface LETTERS** are used to represent *MATRICES* and matched *italic lowercase letters* are used for their *entries*. For instance,  $\mathbf{X} \in \mathfrak{R}^{M \times N}$  denotes a set of  $M \times N$  matrix with elements in  $\mathfrak{R}$ . Therefore,  $x_{ij}$  refers to the entry (i.e., numerical quantity or scalar) in row  $i$  and column  $j$  of the matrix  $\mathbf{X}$ .

Moreover, since a matrix can be thought of as collections of column vectors, the  $j$ th column vector of a matrix  $\mathbf{X} \in \mathfrak{R}^{M \times N}$  can be represented by italic lowercase **boldface letters**  $\mathbf{x}_j$ . Explicitly, the pertinent representations are given by the following:

$$\mathbf{X} = [x_{ij}]_{M \times N} = [\mathbf{x}_j]_N = [\mathbf{x}_1, \mathbf{x}_2, \dots, \mathbf{x}_N] = \begin{bmatrix} x_{11} & x_{12} & \cdots & x_{1N} \\ x_{21} & x_{22} & \cdots & x_{2N} \\ \vdots & \vdots & \cdots & \vdots \\ x_{M1} & x_{M2} & \cdots & x_{MN} \end{bmatrix} \quad (\text{A.1})$$

where,



$$\mathbf{x}_1 = \begin{bmatrix} x_{11} \\ x_{21} \\ \vdots \\ x_{M1} \end{bmatrix}, \quad \mathbf{x}_2 = \begin{bmatrix} x_{12} \\ x_{22} \\ \vdots \\ x_{M2} \end{bmatrix}, \quad \dots, \quad \mathbf{x}_N = \begin{bmatrix} x_{1N} \\ x_{2N} \\ \vdots \\ x_{MN} \end{bmatrix} \quad (\text{A.2})$$

Further, the zero vector or matrix will be written as  $\mathbf{0}$ . Next, the identity matrix will be written as  $\mathbf{I}$ . The transpose of a matrix  $\mathbf{X}$  will be represented by  $\mathbf{X}^T$  and the inverse of  $\mathbf{X}$  is denoted as  $\mathbf{X}^{-1}$ . In complex number cases, conjugate transposition (i.e., Hermitian transposition) will be designated as  $\mathbf{X}^H$ .

Next, the following operators may be encountered throughout this documentation.

1.  $|\cdot|$  denotes the magnitude of a scalar enclosed within.
2.  $\text{diag}\{\cdot\}$  conveys two meanings—either extract or create symbolic diagonals. If  $\mathbf{x}$  is a vector with “ $N$ ” components, then  $\text{diag}\{\mathbf{x}\}$  creates an  $N$ -by- $N$  diagonal matrix having  $\mathbf{x}$  as its main diagonal. On the contrary, if  $\mathbf{X}$  is a matrix with  $N$ -by- $N$  components,  $\text{diag}\{\mathbf{X}\}$  extracts the main diagonal of  $\mathbf{A}$  producing a column vector with “ $N$ ” components.
3.  $\text{tr}\{\cdot\}$  represents the trace (i.e., the sum of the diagonal elements) of a matrix.
4.  $\text{rank}\{\cdot\}$  represents the rank of a matrix.
5.  $\text{det}\{\cdot\}$  represents the determinant of a matrix.
6.  $\text{range}\{\cdot\}$  represents the range of a matrix. For example,  $\text{range}(\mathbf{X})$  produces a row vector containing the range (i.e., the difference between the maximum and the minimum of a sample) of each column of  $\mathbf{X}$ .
7.  $\text{null}\{\cdot\}$  represents the null space of a matrix.

# APPENDIX B

## SABAH ELECTRICITY SDN. BHD.

### Introduction

Electricity started in Sabah as early as 1910 supplied by 3 separate organisations. In 1957 these three organisations combined to form North Borneo Electricity Board. When North Borneo joined Malaysia in 1963 and changed its name to Sabah, this entity was renamed Sabah Electricity Board. On 1st of September 1998 Sabah Electricity Board was privatised and became Sabah Electricity Sdn. Bhd (SESB). SESB is an 80% owned by subsidiary of Tenaga Nasional Berhad (TNB) and 20% by the State Government of Sabah.

The power system network in Sabah was divided into two grids known as West Coast Grid (WCG) and East Coast Grid (ECG) as shown in Figure B1. The installed capacity of the WCG which supplies electricity to Kota Kinabalu, Federal Territory Labuan, Keningau, Beaufort, Papar, Kota Belud, Kota Marudu and Kudat is 488.4MW and the maximum demand is 376.5MW. The ECG 132kV Transmission

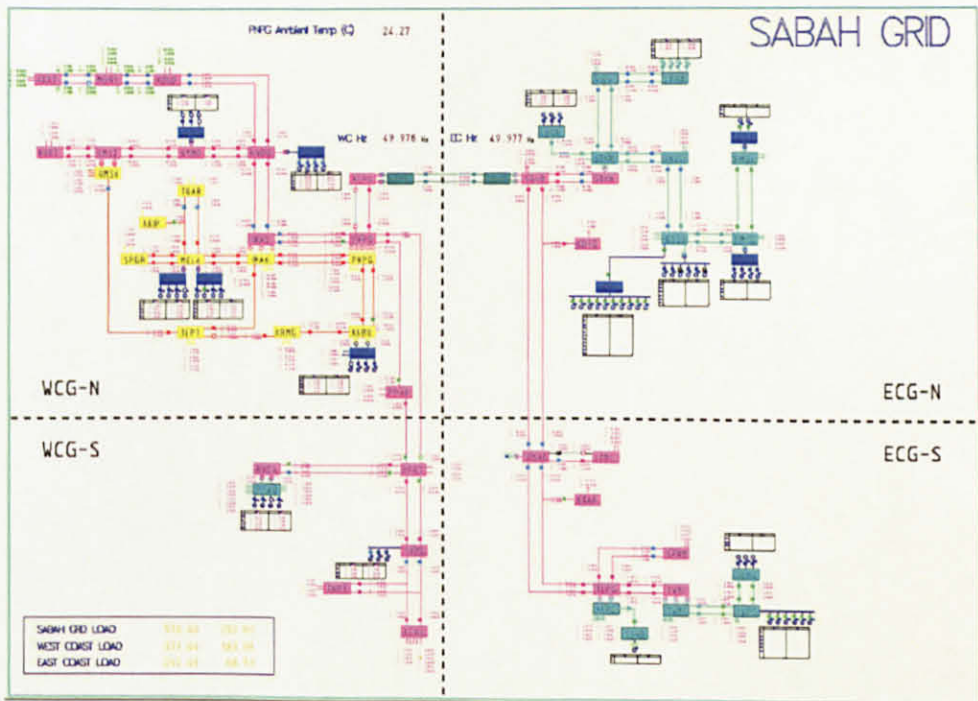


Figure B1 Schematic diagram of SESB captured from SCADA system.

Line connecting the major towns in the East Coast has an installed capacity of 333.02MW and the current demand is 196.2MW. Table B1 and B2 tabulate the system data and power flow results for SESB 103-bus system.

Table B1 Bus data and load flow results of 103-bus system.

Bus No.	Bus Voltage		Generation		Load	
	Magnitude per unit	Phase angle degrees	Real MW	Reactive MVAR	Real MW	Reactive MVAR
1	1.0439	0	0	0	32.3903	5.0257
2	0.9909	-5.6679	0	0	0	0
3	1.0293	-6.3249	15.4849	-43.5196	0	0
4	1.0687	0.2635	0	0	35.2085	24.6538
5	1.0312	-6.9271	2.5955	10.4262	0	0
6	1.0317	-5.9267	-3.6196	-9.6394	0	0
7	1.0292	-7.9590	41.6569	-4.5406	0	0
8	1.0029	-5.0347	0	0	0	0
9	1.0277	-6.6572	0	0	0	0
10	1.0425	-4.4170	0	0	19.2539	6.7280
11	1.0186	-7.1792	20.1485	10.8446	0	0
12	1.0304	-7.5693	29.6902	-8.5716	0	0
13	1.0258	-6.7512	11.8002	5.7388	0	0
14	0.9752	-3.7540	20.0268	0.9384	0.5460	-1.7240
15	1.0016	-6.1043	12.0000	5.9998	0	0
16	1.0114	-10.6690	0	0	0	0
17	1.0379	-4.8373	0	0	7.7733	2.2775
18	1.0544	-2.4330	0	0	18.3519	6.4733
19	1.0016	-6.7615	5.6000	2.7996	0	0
20	1.0027	-9.4303	0	0	0	0
21	0.9994	-5.6178	0	0	0	0
22	1.0015	-7.3270	18.0693	-1.9098	0	0
23	1.0309	-7.4450	0	0	0	0
24	1.0110	-10.6100	7.8288	-1.3968	0	0
25	0.9992	-9.5724	22.0944	12.0857	0	0
26	1.0119	-10.2428	0	0	0	0
27	1.0101	-6.4389	0	0	0	0
28	1.0148	-12.1358	14.5084	-4.4362	0	0
29	0.9743	-3.8069	8.8320	3.5634	0	0
30	1.0265	-9.5764	-2.9508	4.6651	0	0
31	0.9827	-3.3635	-2.1736	6.6077	0	0
32	1.0042	-2.9070	65.7270	2.8048	0	0
33	0.9736	-6.6079	0	0	0	0
34	1.0149	-7.1631	-14.8522	-36.7198	0	0
35	0.9756	-3.7248	14.8325	6.6366	0	0
36	1.0054	-2.8715	-20.1428	-20.8615	74.4800	62.7200
37	0.9840	-0.4445	0	0	25.9815	3.6927
38	1.0055	-2.0556	0	0	0.1565	13.0066
39	1.0054	-2.0450	0	0	14.1561	0.0122
40	0.9782	-2.9531	0	0	0	0
41	0.9782	-2.9530	0	0	0	0
42	0.9494	-6.6102	80.8162	74.0630	0	0
43	0.9951	-3.6746	-19.8719	-16.8739	0	0
44	1.0469	-0.0194	0	0	32.4004	6.1405
45	1.0472	0.0157	0	0	32.6349	6.2557

46	0.9935	-5.4748	0	0	0	0
47	0.9689	-6.1673	0	0	0	0
48	1.0367	-0.1730	0	0	32.5189	2.6904
49	1.0036	-4.6661	9.7455	-5.8804	0	0
50	1.0244	-6.8640	8.5089	3.9227	0	0
51	1.0308	-7.4639	28.3653	1.0170	0	0
52	0.9887	-5.6890	0	0	0	0
53	0.9788	-5.9255	0	0	0	0
54	0.9788	-5.9255	0	0	0	0
55	0.9988	-5.6908	14.1375	7.9590	0	0
56	0.9985	-3.9800	0	0	0	0
57	0.9986	-3.9797	0	0	0	0
58	0.9986	-3.9797	0	0	0	0
59	0.9986	-3.9797	0	0	0	0
60	1.0150	-0.1753	0	0	0	0
61	0.9995	-4.0963	0	0	0	0
62	0.9991	-3.9943	0.7813	-2.0508	0	0
63	0.9995	-4.0963	0	0	0	0
64	0.9991	-3.9941	0	0	0	0
65	1.0255	-6.7953	0	0	0	0
66	1.0019	-5.2825	0	0	0	0
67	1.0019	-5.2822	0	0	0	0
68	1.1856	-2.6333	19.3962	-11.4349	0	0
69	1.1822	0.6784	0	26.9742	0	-1.3847
70	1.2619	0.7397	0	30.3628	0	32.0333
71	1.1925	0.6861	0	32.8601	0	3.2381
72	1.1959	-2.6084	0	0.1259	0	2.2726
73	1.0141	-12.2057	0	0	0	0
74	1.0680	-10.0841	0	0	7.0330	7.8385
75	1.0658	-9.8738	0	0	7.5592	7.4197
76	1.0092	-12.2011	0	0	0.0054	-0.7351
77	1.0147	-12.3610	0	0	-0.4138	0.1037
78	0.9883	-13.8690	0	0	-4.4073	-3.6894
79	1.0140	-12.2069	12.9727	9.1917	0	0
80	1.0140	-12.2069	0	0	0	0
81	1.0303	-10.9538	0	0	3.4584	2.5050
82	0.9883	-13.8690	0	0	-4.4073	-3.6894
83	1.0118	-9.9276	0	0	0	132
84	1.0119	-9.9311	2.6154	-10.4675	0	0
85	1.0223	-8.8648	15.1878	-53.9276	0	0
86	1.0213	-8.8356	0	0	0	132
87	1.1839	-2.7034	0	0	0	0
88	1.1839	-2.7034	0	0	0	0
89	1.0402	-9.9317	0	0	0	0
90	1.0929	-9.9110	0	0	0.1730	8.6377
91	0.8921	3.1099	0	0	15.7020	-16.4490
92	0.9616	-0.7521	0	0	0	0
93	1.0147	-3.3805	1.3458	0.3178	24.8085	0.3645
94	1.0148	-3.4266	0	0	0	0
95	1.0148	-3.4266	0	0	0	0
96	0.9757	-3.7220	0	0	0	0
97	1.0054	-2.0557	4.7523	5.1475	0	0
98	0.9736	-6.6079	0	0	0	0
99	1.0054	-2.0557	0	0	0	0
100	1.0054	-2.0530	0	0	0	0

101	1.0140	-12.2069	0	0	0	0
102	1.0317	-5.9272	0	0	0	0
103	0.9996	-3.9989	0	0	0	0

Table B2 Line data and power flow results of 103-bus system.

Line No.	From Bus	To Bus	Line impedance		Half line charging per unit	Real Power Flow MW		Reactive Power Flow MVAR		Tap setting
			R per unit	X Per unit		From	To	From	To	
1	1	8	0.0108	0.2887	0	28.6640	-28.5510	17.9710	-14.9310	1
2	2	3	0.0208	0.3890	0	14.3910	-14.3380	8.8460	-7.8630	0.9375
3	2	3	0.0208	0.3890	0	12.9180	-12.8780	-5.5120	6.2660	0.9875
4	2	3	0.0208	0.3890	0	13.6250	-13.5890	1.2950	-0.6150	0.9625
5	2	3	0.0208	0.3890	0	13.6250	-13.5890	1.2950	-0.6150	0.9625
6	2	3	0.0208	0.3890	0	10.8240	-10.6490	-24.5650	27.8300	1.0750
7	2	42	0.0167	0.0712	0.0079	34.3120	-33.6380	52.3780	-51.0060	1
8	2	52	0.0016	0.0067	0	9.0790	-9.0740	15.1820	-15.1610	1
9	3	6	0.0192	0.0542	0.0006	-23.6420	23.7610	9.7950	-9.5860	1
10	3	6	0.0192	0.0542	0.0006	-23.6420	23.7610	9.7950	-9.5860	1
11	5	3	0.0328	0.0776	0.0011	0.7410	-0.7410	1.0580	-1.2900	1
12	5	3	0.0328	0.0776	0.0011	0.7410	-0.7410	1.0580	-1.2900	1
13	5	9	0.0530	0.1254	0.0008	-9.5640	9.6170	-3.7760	3.7290	1
14	5	9	0.0530	0.1254	0.0008	-9.5640	9.6170	-3.7760	3.7290	1
15	6	94	0.0230	0.3793	0	-11.7070	11.7420	4.6290	-4.0600	1
16	6	95	0.0230	0.3793	0	-11.7070	11.7410	4.6290	-4.0600	1
17	8	4	0.0108	0.2887	0	-34.8460	35.0350	-22.6410	27.6980	1
18	8	44	0.0108	0.2887	0	-32.1120	32.2510	-15.4510	19.1700	1
19	8	45	0.0108	0.2887	0	-28.6690	28.7870	-16.0560	19.2180	1
20	9	10	0.0143	0.4400	0	-19.1760	19.2250	-1.2250	2.7300	1
21	9	10	0.0143	0.4400	0	-19.1760	19.2250	-1.2250	2.7300	1
22	9	17	0.0143	0.4400	0	-7.7470	7.7550	0.1730	0.0720	1
23	9	18	0.0143	0.4400	0	-18.3630	18.4090	-2.8540	4.2610	1
24	9	13	0.0155	0.0368	0.0006	36.1000	-35.3370	63.2800	-61.5950	1
25	9	13	0.0155	0.0368	0.0006	36.1000	-35.3370	63.2800	-61.5950	1
26	9	65	0.0047	0.0170	0.0001	34.5280	-34.2590	70.7220	-69.7680	1
27	9	11	0.0305	0.1004	0	13.3570	-13.2630	12.5060	-12.1950	1
28	11	65	0.0258	0.0934	0.0007	-7.7220	7.7370	-1.0170	0.9240	1
29	12	51	0.0044	0.0150	0.0155	-10.1820	10.1900	7.9920	-11.2610	1
30	12	5	0.0055	0.0190	0.0169	-54.6610	54.8540	25.2920	-28.2190	1
31	12	7	0.0049	0.0168	0	38.5750	-38.4960	-15.4760	15.7480	1
32	15	8	0.0126	0.1042	0.0358	-33.8020	33.9760	12.3970	-18.0940	1
33	15	8	0.0126	0.1042	0.0358	-33.8020	33.9760	12.3970	-18.0940	1
34	15	19	0.0116	0.0955	0.018	23.5640	-23.4980	-6.2010	3.1060	1
35	15	19	0.0116	0.0955	0.018	23.5640	-23.4980	-6.2010	3.1060	1
36	16	26	0.0194	0.0771	0.0084	-18.1670	18.2370	5.3710	-6.8190	1
37	16	26	0.0194	0.0771	0.0084	-18.1670	18.2370	5.3710	-6.8190	1
38	16	28	0.0056	0.2778	0	18.8510	-18.8310	0.8220	0.1400	1
39	16	28	0.0056	0.2778	0	18.8510	-18.8310	0.8220	0.1400	1
40	20	25	0.0074	0.0153	0.0026	6.7520	-6.7200	-19.9930	19.5350	1
41	20	83	0.0094	0.0786	0.0143	13.9390	-13.8980	-16.9360	14.3710	1
42	20	86	0.0193	0.1621	0.0295	-22.3900	22.5690	-23.8080	19.1580	1
43	21	23	0.0038	0.1508	0	41.1100	-40.9790	-39.3050	44.5010	1.0334
44	21	23	0.0038	0.1508	0	41.1100	-40.9790	-39.3050	44.5010	1.0334
45	22	19	0.0194	0.1063	0.0117	-18.2650	18.3300	0.7860	-2.7960	1

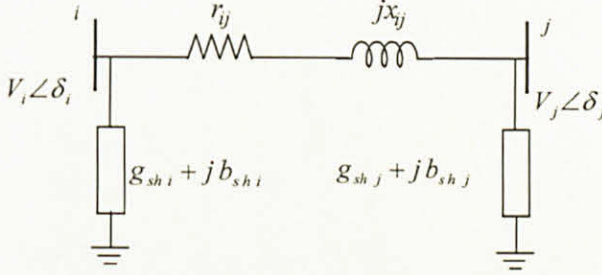
46	22	19	0.0194	0.1063	0.0117	-18.2650	18.3300	0.7860	-2.7960	1
47	23	51	0.0003	0.0008	0	33.3650	-33.3600	-26.3260	26.3390	1
48	26	30	0.0393	0.8327	0	-2.9810	2.9860	-1.8300	1.9290	1
49	26	24	0.0702	0.1442	0.0119	6.0300	-5.9780	-7.5270	5.1810	1
50	26	24	0.0702	0.1442	0.0119	6.0300	-5.9780	-7.5270	5.1810	1
51	26	20	0.0187	0.1571	0.0286	-12.6960	12.7380	5.4950	-10.9460	1
52	26	20	0.0187	0.1571	0.0286	-12.6960	12.7380	5.4950	-10.9460	1
53	26	30	0.0393	0.8327	0	-2.9810	2.9860	-1.8300	1.9290	1
54	26	83	0.0094	0.0786	0.0143	-11.6150	11.6280	-0.5640	-2.2670	1
55	27	31	0.0056	0.2778	0	-37.3890	37.5050	27.5940	-21.8360	1
56	27	31	0.0056	0.2778	0	-37.3890	37.5050	27.5940	-21.8360	1
57	28	79	0.0168	0.0642	0	1.5310	-1.5160	-9.3440	9.4000	1
58	28	79	0.0168	0.0642	0	1.5310	-1.5160	-9.3440	9.4000	1
59	29	14	0.0979	0.1881	0.0001	-2.6590	2.6780	-3.3090	3.3270	1
60	29	14	0.0979	0.1881	0.0001	-2.6590	2.6780	-3.3090	3.3270	1
61	30	89	0.0839	0.1724	0.0001	-0.4300	0.4910	-8.7670	8.8700	1
62	31	29	0.1131	0.2388	0.0001	3.6990	-3.6490	-5.1850	5.2730	1
63	31	29	0.1133	0.2388	0.0001	3.6950	-3.6440	-5.1860	5.2740	1
64	31	32	0.1131	0.0974	0.0028	-38.2070	40.4780	-19.3380	20.7490	1
65	31	32	0.1131	0.0974	0.0028	-38.2070	40.4780	-19.3380	20.7490	1
66	31	92	0.0839	0.1724	0.0001	-18.3370	18.8100	13.2450	-12.2910	1
67	32	36	0.0007	0.0020	0.0003	-59.9650	59.9900	8.1510	-8.1430	1
68	32	36	0.0007	0.0020	0.0003	-59.9650	59.9900	8.1510	-8.1430	1
69	33	34	0.0000	0.1537	0	12.6430	-12.6430	-53.4670	58.5060	1
70	33	34	0.0000	0.1537	0	12.6430	-12.6430	-53.4670	58.5060	1
71	33	47	0.0168	0.1014	0.3655	-12.3050	12.3410	-40.3920	-27.3570	1
72	33	47	0.0168	0.1016	0.3655	-12.2800	12.3160	-40.3830	-27.3670	1
73	33	98	0.0664	0.4997	0	-0.1590	0.1600	-1.1150	1.1220	1
74	34	27	0.0102	0.0624	0.0001	-34.2530	34.5740	47.5560	-45.6160	1
75	34	27	0.0108	0.0624	0.0001	-33.7540	34.0920	47.7990	-45.8650	1
76	34	20	0.0240	0.2015	0.0367	34.3830	-34.0420	15.2500	-20.0840	1
77	34	20	0.0240	0.2015	0.0367	34.3830	-34.0420	15.2500	-20.0840	1
78	34	86	0.0468	0.0392	0.0071	41.9270	-40.6030	-37.2770	36.8400	1
79	35	14	0.0036	0.0052	0.001	-26.1350	26.3230	-64.8210	64.9040	1
80	35	14	0.0036	0.0052	0.0001	-26.1350	26.3230	-64.7360	64.9890	1
81	38	99	0.0000	0.0010	0	0.1800	-0.1800	17.7380	-17.7340	1
82	39	100	0.0000	0.0010	0	14.1100	-14.1100	13.3840	-13.3800	1
83	40	35	0.0100	0.1000	0	13.0450	-13.0270	2.2600	-2.0730	1
84	40	37	0.0050	0.3250	0	-12.9890	12.9980	-1.6540	2.2460	1
85	41	37	0.0050	0.3250	0	-12.9880	12.9970	-1.6540	2.2460	1
86	41	35	0.0100	0.1000	0	13.0500	-13.0310	2.2600	-2.0730	1
87	42	43	0.0270	0.1153	0.0179	-47.0600	47.8600	-23.4280	23.4560	1
88	43	56	0.0188	0.0802	0.0089	8.7590	-8.6770	-19.6750	18.2440	1
89	43	56	0.0188	0.0802	0.0089	8.7590	-8.6770	-19.6750	18.2440	1
90	43	2	0.0437	0.1865	0.0418	17.2400	-17.0970	-9.2250	1.5630	1
91	43	60	0.0833	0.2057	0.0163	-56.8130	59.5760	5.2080	-1.7380	1
92	43	60	0.0833	0.2057	0.0163	-56.8130	59.5760	5.2080	-1.7380	1
93	46	5	0.0064	0.2427	0	22.1950	-22.1120	-26.6900	29.8490	1.0375
94	46	5	0.0064	0.2427	0	22.9970	-22.9420	-17.7040	19.8070	1.0125
95	46	5	0.0064	0.2427	0	20.3950	-20.2010	-45.6040	52.9570	1.1
96	46	8	0.0050	0.0245	0.0083	-55.2940	55.5050	33.2470	-33.8550	1
97	46	8	0.0050	0.0245	0.0083	-55.2940	55.5050	33.2470	-33.8550	1
98	46	2	0.0038	0.0185	0.0044	37.1360	-37.0830	3.9560	-4.5710	1
99	46	2	0.0038	0.0185	0.0044	37.1360	-37.0830	3.9560	-4.5710	1
100	47	53	0.0000	0.0640	0	-6.2700	6.2700	-13.2490	13.3950	1

101	47	54	0.0000	0.0640	0	-6.2700	6.2700	-13.2490	13.3950	1
102	49	63	0.0168	0.0914	0.0101	-9.9620	9.9830	4.1220	-6.0690	1
103	50	65	0.0047	0.0170	0.0001	-6.6750	6.6780	2.5150	-2.5280	1
104	53	52	0.0000	0.0640	0	-6.2900	6.2900	-26.3690	26.8610	1
105	54	52	0.0000	0.0640	0	-6.2900	6.2900	-26.3690	26.8610	1
106	55	21	0.0022	0.0094	0.1040	-14.9280	14.9340	-16.2610	-4.5530	1
107	56	57	0.0144	0.3673	0	15.9500	-15.9140	1.1730	-0.2470	1
108	56	59	0.0144	0.3673	0	15.9500	-15.9140	1.1730	-0.2470	1
109	56	58	0.0144	0.3673	0	15.9500	-15.9140	1.1730	-0.2470	1
110	56	63	0.0034	0.0183	0.0020	9.6200	-9.6140	-8.0590	7.6810	1
111	56	64	0.0034	0.0183	0.0020	0.6010	-0.6010	-4.1810	3.7780	1
112	60	87	0.4942	0.1317	0	-27.0060	31.8660	-17.9720	19.2670	1
113	60	88	0.4942	0.1317	0	-26.3750	31.0470	-17.7740	19.0190	1
114	61	63	0.0001	0.0001	0.0001	-68.4410	68.4500	-68.4560	68.4450	1
115	62	64	0.0001	0.0001	0.0001	-47.5640	47.5680	-44.0920	44.0760	1
116	66	48	0.0108	0.2887	0	-32.3370	32.4620	-10.3930	13.7360	1
117	66	67	0.0108	0.2887	0	-0.0440	0.0440	-1.0370	1.0400	1
118	66	8	0.0038	0.0229	0.0044	-18.2060	18.2440	25.4600	-26.1020	1
119	66	8	0.0038	0.2290	0.0044	-2.2120	2.2120	1.8860	-2.7340	1
120	66	21	0.0044	0.0229	0.0050	46.6980	-46.5780	-23.4720	23.0950	1
121	66	21	0.0044	0.0229	0.0050	46.6980	-46.5780	-23.4720	23.0950	1
122	68	69	0.0094	0.2997	0	-26.8950	26.9440	3.2340	-1.6730	1
123	68	70	0.0094	0.2998	0	-30.2150	30.3280	-28.0390	31.6540	1
124	68	72	0.0031	0.5445	0	-0.1070	0.1070	-2.0430	2.0590	1
125	68	71	0.0078	0.2499	0	-32.7660	32.8250	-0.9940	2.9000	1
126	68	87	0.0022	0.0061	0	22.5600	-22.5480	-15.7530	15.7860	1
127	73	74	0.0867	0.6670	0	-6.9050	6.9840	-6.8210	7.4270	1
128	73	79	0.0001	0.0002	0	-9.7430	9.7440	-37.4290	37.4320	1
129	73	75	0.0867	0.6670	0	-7.4300	7.5100	-6.3920	7.0110	1
130	79	76	0.0087	0.6667	0	-0.0130	0.0130	1.1410	-1.1330	1
131	79	77	0.0087	0.6667	0	0.4140	-0.4140	0.2980	-0.2960	1
132	79	78	0.0087	0.6667	0	4.4110	-4.4080	4.3360	-4.0900	1
133	79	80	0.0087	0.6667	0	-3.9530	3.9540	0.4920	-0.3900	1
134	79	81	0.0087	0.6667	0	-3.4580	3.4590	-1.9970	2.1000	1
135	79	82	0.0087	0.6667	0	4.4110	-4.4080	4.3360	-4.0900	1
136	84	83	0.0003	0.0012	0.0002	-8.2040	8.2050	-13.8080	13.7700	1
137	85	86	0.0004	0.0020	0.0029	-30.6530	30.6580	-18.9970	18.3930	1
138	88	68	0.0022	0.0061	0	-42.7440	42.7980	-40.4300	40.5810	1
139	89	90	0.0087	0.6667	0	-0.1640	0.1690	-7.7610	8.1290	1
140	92	91	0.0013	0.3666	0	-15.7250	15.7330	17.0590	-14.8560	1
141	94	93	0.0022	0.0061	0	-17.4740	17.4830	-10.7910	10.8160	1
142	95	93	0.0022	0.0061	0	-17.4840	17.4930	-10.8060	10.8310	1
143	96	35	0.0000	0.0010	0	9.2620	-9.2620	14.4950	-14.4920	1
144	96	35	0.0000	0.0010	0	9.2620	-9.2620	14.4950	-14.4920	1
145	96	97	0.0867	0.6670	0	-8.8100	8.9020	-4.6610	5.3700	1
146	96	97	0.0867	0.6670	0	-8.8100	8.9020	-4.6610	5.3700	1
147	99	97	0.0000	0.0010	0	-10.0730	10.0730	15.6750	-15.6720	1
148	99	97	0.0000	0.0010	0	-10.0730	10.0730	15.6750	-15.6720	1
149	99	97	0.0000	0.0010	0	-10.0730	10.0730	15.6750	-15.6720	1
150	100	97	0.0000	0.0010	0	14.2900	-14.2900	15.6710	-15.6660	1
151	100	97	0.0000	0.0010	0	14.2900	-14.2900	15.6710	-15.6660	1
152	100	97	0.0000	0.0010	0	14.2900	-14.2900	15.6710	-15.6660	1
153	101	79	0.0001	0.0002	0	-16.9420	16.9440	-33.8690	33.8720	1
154	102	6	0.0027	0.0092	0.0078	7.2970	-7.2800	24.4410	-26.0340	1
155	103	64	0.0168	0.0914	0.0101	-0.1590	0.1590	-2.2480	0.2000	1

## APPENDIX C

### REAL AND REACTIVE POWER FLOW IN A NETWORK ELEMENT

Consider the network element as shown below.



The line admittance  $= \frac{1}{r_{ij}^2 + jx_{ij}} = \frac{r_{ij}}{r_{ij}^2 + x_{ij}^2} - j \frac{x_{ij}}{r_{ij}^2 + x_{ij}^2} = g_{ij} + jb_{ij}$ . Thus,

$g_{ij} = \frac{r_{ij}}{r_{ij}^2 + x_{ij}^2}$  and  $b_{ij} = \frac{-x_{ij}}{r_{ij}^2 + x_{ij}^2}$ . The current flowing in the series impedance is  $I_{ij}$ .

Hence

$$\begin{aligned}
 I_{ij} &= (V_i \angle \delta_i - V_j \angle \delta_j)(g_{ij} + jb_{ij}) \\
 &= \{(V_i \cos \delta_i + jV_i \sin \delta_i) - (V_j \cos \delta_j + jV_j \sin \delta_j)\} \times (g_{ij} + jb_{ij}) \\
 &= \{(V_i \cos \delta_i - V_j \cos \delta_j) + j(V_i \sin \delta_i - V_j \sin \delta_j)\} \times (g_{ij} + jb_{ij}) \\
 &= (g_{ij}V_i \cos \delta_i - g_{ij}V_j \cos \delta_j - b_{ij}V_i \sin \delta_i + b_{ij}V_j \sin \delta_j) \\
 &\quad + j(g_{ij}V_i \sin \delta_i - g_{ij}V_j \sin \delta_j + b_{ij}V_i \cos \delta_i - b_{ij}V_j \cos \delta_j)
 \end{aligned} \tag{C.1}$$

The conjugate of  $I_{ij}$  is

$$\begin{aligned}
 I_{ij}^* &= (g_{ij}V_i \cos \delta_i - g_{ij}V_j \cos \delta_j - b_{ij}V_i \sin \delta_i + b_{ij}V_j \sin \delta_j) \\
 &\quad - j(g_{ij}V_i \sin \delta_i - g_{ij}V_j \sin \delta_j + b_{ij}V_i \cos \delta_i - b_{ij}V_j \cos \delta_j)
 \end{aligned} \tag{C.2}$$

The right hand side of the C.2 is represent as

$$I_{ij}^* = x + jy \tag{C.3}$$

Using equation C.3, the power flow from bus  $i$  to  $j$  is equal to

$$\begin{aligned}
 P_{ij} + jQ_{ij} &= (V_i \cos \delta_i + jV_i \sin \delta_i)I_{ij}^* \\
 &= (V_i \cos \delta_i + jV_i \sin \delta_i)(x - jy) \\
 &= V_i \cos \delta_i \cdot x + V_i \sin \delta_i \cdot y + j(V_i \sin \delta_i \cdot x - V_i \cos \delta_i \cdot y)
 \end{aligned} \tag{C.4}$$

Substitute equation C.2 into C.4, the power flows in the line not taking the shunt elements are equal to



$$\begin{aligned}
P_{ij} &= V_i \cos \delta_i (g_{ij} V_i \cos \delta_i - g_{ij} V_j \cos \delta_j - b_{ij} V_i \sin \delta_i + b_{ij} V_j \sin \delta_j) \\
&\quad + V_i \sin \delta_i (g_{ij} V_i \sin \delta_i - g_{ij} V_j \sin \delta_j + b_{ij} V_i \cos \delta_i - b_{ij} V_j \cos \delta_j) \\
&= V_i^2 g_{ij} - V_i V_j [g_{ij} (\cos \delta_i \cos \delta_j + \sin \delta_i \sin \delta_j) + b_{ij} (\sin \delta_i \cos \delta_j - \cos \delta_i \sin \delta_j)] \\
&= V_i^2 g_{ij} - V_i V_j (g_{ij} \cos \delta_{ij} + b_{ij} \sin \delta_{ij})
\end{aligned}$$

where  $\cos \delta_{ij} = \cos \delta_i \cos \delta_j + \sin \delta_i \sin \delta_j$  and  $\sin \delta_{ij} = \sin \delta_i \cos \delta_j - \cos \delta_i \sin \delta_j$

C.5

Similarly goes to reactive power flow from bus  $i$  to  $j$

$$\begin{aligned}
Q_{ij} &= V_i \sin \delta_i (g_{ij} V_i \cos \delta_i - g_{ij} V_j \cos \delta_j - b_{ij} V_i \sin \delta_i + b_{ij} V_j \sin \delta_j) \\
&\quad - V_i \cos \delta_i (g_{ij} V_i \sin \delta_i - g_{ij} V_j \sin \delta_j + b_{ij} V_i \cos \delta_i - b_{ij} V_j \cos \delta_j) \\
&= -V_i^2 b_{ij} - V_i V_j [g_{ij} (\sin \delta_i \cos \delta_j - \cos \delta_i \sin \delta_j) - b_{ij} (\sin \delta_i \sin \delta_j + \cos \delta_i \cos \delta_j)] \\
&= -V_i^2 b_{ij} - V_i V_j (g_{ij} \sin \delta_{ij} - b_{ij} \cos \delta_{ij})
\end{aligned}$$

where  $\cos \delta_{ij} = \cos \delta_i \cos \delta_j + \sin \delta_i \sin \delta_j$  and  $\sin \delta_{ij} = \sin \delta_i \cos \delta_j - \cos \delta_i \sin \delta_j$

If the shunt element is connected at bus  $i$ , the power flow from bus  $i$  to  $j$  will be equal to

$$P_{ij} + jQ_{ij} = (V_i \cos \delta_i + jV_i \sin \delta_i) I_{ij}^* + (V_i \cos \delta_i - jV_i \sin \delta_i) I_{sh_i} \quad \text{C.7}$$

$$\begin{aligned}
\text{where } I_{sh_i} &= (V_i \cos \delta_i + jV_i \sin \delta_i) (g_{sh_i} + jb_{sh_i}) \\
&= (g_{sh_i} V_i \cos \delta_i - b_{sh_i} V_i \sin \delta_i) + j(g_{sh_i} V_i \sin \delta_i + b_{sh_i} V_i \cos \delta_i)
\end{aligned} \quad \text{C.8}$$

Power flow in the shunt at bus  $i$ ,

$$P_{sh_i} - jQ_{sh_i} = (V_i \cos \delta_i - jV_i \sin \delta_i) I_{sh_i} \quad \text{C.9}$$

Substitute equation C.8 into C.9, the  $P_{sh_i}$  and  $Q_{sh_i}$  is equal to

$$\begin{aligned}
P_{sh_i} - jQ_{sh_i} &= (V_i \cos \delta_i - jV_i \sin \delta_i) \{ (g_{sh_i} V_i \cos \delta_i - b_{sh_i} V_i \sin \delta_i) + j(g_{sh_i} V_i \sin \delta_i + b_{sh_i} V_i \cos \delta_i) \} \\
&= g_{sh_i} V_i^2 \cos^2 \delta_i - b_{sh_i} V_i^2 \sin \delta_i \cos \delta_i + g_{sh_i} V_i^2 \sin^2 \delta_i + b_{sh_i} V_i^2 \sin \delta_i \cos \delta_i \\
&\quad - j(-g_{sh_i} V_i^2 \sin \delta_i \cos \delta_i - b_{sh_i} V_i^2 \cos^2 \delta_i + g_{sh_i} V_i^2 \sin \delta_i \cos \delta_i - b_{sh_i} V_i^2 \sin^2 \delta_i) \\
&= V_i^2 g_{sh_i} - jV_i^2 b_{sh_i}
\end{aligned} \quad \text{C.10}$$

Therefore, when shunt elements are included, total power flow can be obtained as

$$P_{ij} = V_i^2 (g_{sh_i} + g_{ij}) - V_i V_j (g_{ij} \cos \delta_{ij} + b_{ij} \sin \delta_{ij}) \quad \text{C.11}$$

$$Q_{ij} = -V_i^2 (b_{sh_i} + b_{ij}) - V_i V_j (g_{ij} \sin \delta_{ij} - b_{ij} \cos \delta_{ij}) \quad \text{C.12}$$